The development of pNIPAM-Laponite® hydrogels for dental applications

Abdusalam Saad Essa

A thesis submitted in partial fulfilment of the requirements

of Sheffield Hallam University

for the degree of Doctor of Philosophy

October 2018

Declaration

I hereby declare that the work described in this thesis was performed by the author, at Sheffield Hallam University between October 2014 and September 2018, and this thesis has not been submitted for higher degree to any other university or institute.

Author: Abdusalam Saad Essa

Director of study: Professor Chris Sammon

Dedication

To the spirit of my Father, who was my guidance of success, my Mother and her pray, to my beloved Wife and my children.

For all of you I present this work as a small gift.

Acknowledgement

First and foremost I would like to express my sincere gratitude to my supervisors: Professor Chris Sammon and Professor Christine Le Maitre, for their valuable guidance and unlimited support that they gave me during my PhD journey.

I would like to appreciate their wisdom throughout the four years of my study, which made a great difference in the quality of this work. I would appreciate their attention that they paid to my research to finish the work and gain good experience as a researcher.

Deep gratitude must go to all MERI PhD students, staff and technicians who were constantly of assistance.

Heartfelt thanks to my Mother, Wife and Children for their encouragements and patience.

Abstract

The impact of chemical composition on the mechanical and physical properties of Laponite® crosslinked pNIPAM hydrogels was investigated, and the implications of these changes on cell viability and behaviour were explored. A range of crosslink density was used, and two different hydrophilic comonomers (HEMA and HPMA) were incorporated into the reaction mixture at different ratios. Additionally, water dispersed hydroxyapatite nanoparticles (HAPna) was added to the hydrogel at a concentration of 0.5mg/ml, to promote osteogenic differentiation of hMSCs. Different compositions of novel pNIPAM based Laponite® hydrogels, were synthesised and characterised through this thesis.

Structural properties of the hydrogels were studied using SEM, and the influence of chemical composition on pore size was elucidated. The implications of structural changes on a host of properties including mechanical robustness and other physical behaviour such as swelling and deswelling ratios were observed. The physical water state, water diffusivity and water/polymer interactions within the hydrogels were explored by monitoring dehydration and rehydration behaviour, using ATR-FTIR. Cell viability within a range of chemical compositions of the hydrogels, was performed using Alamar blue assay, and histological and immunohistochemistry investigations were used to evaluate type of matrix deposition within the hydrogels.

Crosslink density was found to be a crucial factor to control, where changes in crosslink density influenced physical and mechanical properties of the hydrogels. Our findings showed increased crosslink density, lead to stiffer hydrogels as a result of a smaller pore size. Smaller pore size was also found to retard dehydration and rehydration rates. Furthermore, the free water fraction was reduced due to a decrease in pore size when crosslink density increased. In addition, cell viability varied as a result of using different crosslink density.

Incorporation of HEMA as a comonomer increased the pore size of Laponite® crosslinked pNIPAM hydrogels and hydrogel stiffness was reduced. The hydrophilicity of the hydrogel was increased when HEMA was added, and accordingly the dehydration rate decreased and rehydration rate increased, as the HEMA ratio was increased in systematic manner. Toxicity to hMSCs was observed needing further investigation to fully understand the mechanism.

Adding HPMA increased median pore size and decreased the mechanical stiffness of L-pNIPAM-co-HPMA hydrogels. The influence of HPMA on the hydrophilicity of the hydrogel was explored using water contact angle measurements. Dehydration and rehydration observations showed the influence of conflicting factors, including pore size, surface area of hydrogel droplet and hydrophilicity to affect dehydration and rehydration rates. L-pNIPAM$_{90}$-co-HPMA$_{10}$ (1) showed a significant increase ($P<0.05$) in cell viability of hMSCs when compared to L-pNIPAM (1). In addition, matrix deposition resembling that of cells undergoing osteogenic differentiation was promoted within L-pNIPAM$_{90}$-co-HPMA$_{10}$ (1).

When HAPna was added to L-pNIPAM$_{90}$-co-HPMA$_{10}$ (1) the mechanical properties were enhanced, the pore size was reduced and further increases of matrix deposition resembling that of cells undergoing osteogenic differentiation were observed.

Table of contents

List of Abbreviations

~	Approximately
˚	Degree
˚C	Degrees Celsius
˚Cmin^{-1}	Degrees Celsius per minute
µm	Micrometer
AF	Annulus Fibrosus
AFM	Tomic force microscopy
AIBN	Azobisisobutyronitrile
APS	Ammonium Persulfate
ATR-FTIR	Attenuated Total Reflection – Fourier Transform Infrared Spectroscopy
ATRP	Atom Transfer Radical Polymerisation
BHT	Butylated Hydroxytoluene
BIS	N, N'methylenebisacrylamide
cm	Centimetre
cm^{-1}	Wavenumber
D	Diffusion Coefficient
D_H	Z- Average Hydrodynamic Diameter
DLS	Dynamic Light Scattering
DMA	Dynamic Mechanical Analysis
DMAc	N,N-Dimethylacrylamide
DMF	Dimethylformamide
DSC	Differential Scanning Calorimetry

EBSD	Electron Backscatter Diffraction Detector
EDS	Energy Dispersive X-ray Spectrometry
EWC	Equilibrium Water Contents
FTIR	Fourier Transform Infrared Spectroscopy
G'	Storage Modulus (elastic properties)
G"	Loss Modulus (viscous properties)
GMAc	Glycedyl Methacrylate
GPC	Gel Permeation Chromatography
HEMA	Hydroxyethyl Methacrylate
HF	Hydrofluoric Acid
hMSC	Human Mesenchymal Stem Cells
HPMA	Hydroxypropyl Methacrylate
Hz	Hertz
IFM	Infinite focused microscope
IPN	Interpenetrating Polymer Network
IVD	Intervertebral Discs
Kg	Kilogram
KPS	Potassium Persulfate
Kpa	Kilopascal
LCST	Lower- Critical Solution Temperature
LVSEM	Low-Voltage Scanning Electron Microscopy
m	Metre
MALDI-TOF-MS	Matrix-Assisted Laser Desorption/ Ionisation Time-of-Flight Mass Spectrometry
MCR	Multivariate Curve Resolution

mg	Milligram
ml	Milter
mm	Millimetre
M_n	Number Average Molecular Weight
MPa	Megapascal
MSC	Mesenchymal Stem Cells
M_w	Molecular Weight
MWD	Molecular Weight Distribution
n	Number of experiments
NC	Nanocomposite
nm	Nanometre
NP	Nucleus Pulposus
Pa	Pascal
PCPH	Polymer/ Clay Precursor Hydrogel
PDMAc	*Poly*(N,N′-Dimethylacrylamide)
PTTNAG Gelation	Phase Transition-Triggered Nanoparticle Anchored
PNIPAM	*Poly*(N-isopropylacrylamide)
RAFT	Reversible Addition−Fragmentation Chain Transfer Polymerisation
R_h	Hydrodynamic Radius
RH	Relative humidity
rpm	Revolutions per minute
SD	Standard deviation
SEC	Size Exclusion Chromatography

SEM	Scanning Electron Microscopy
SRP	Stimuli Responsive Polymer
Tan δ	Tan Delta (loss tangent (G''/ G')
TEM	Transmission Electron Microscopy
TEMED	N’ N’tetramethylethylenediamine
TGA	Thermogravimetric Analysis
THF	Tetrahydrofuran
UV	Ultraviolet
w/v	Weight in volume
w/w	Weight in weight
XRD	X-ray Diffraction
ZPD	Point of Zero Path Difference
Δ	Change
δ	Bending vibration
v	Stretching vibration

Chapter - 1

Introduction and literature review

1.1 Polymers

Polymers are high molecular weight long sequences of molecules joined together, the way the molecules repeat in different ways depends on the polymer type. The simple molecules are referred to as monomers that are generally liquids or gases and during the polymerisation reaction convert to crystalline or amorphous solids(1). In some polymers, only one monomer type is used as the repeating units, others might be consisting of several different monomers. Polymers might be synthetic or could be found in nature; natural polymers include silk, wool and rubber. In addition there are many natural polymers in the living tissues in human, plants and animals, including proteins, glycogen and cellulose. Synthetic polymers such as: Nylon, polyester, polyurethane and acrylics. Synthetic polymers have a broad range of applications due to their variety in their physical properties and behaviour(2).

1.2 Polymer classification

Polymers can be classified in many different ways; they can be natural or synthetic, classified based on their structure, based on the polymerisation reaction from which they were produced or based on the source of the molecules joined together to make them(3) (Figure 1.1).

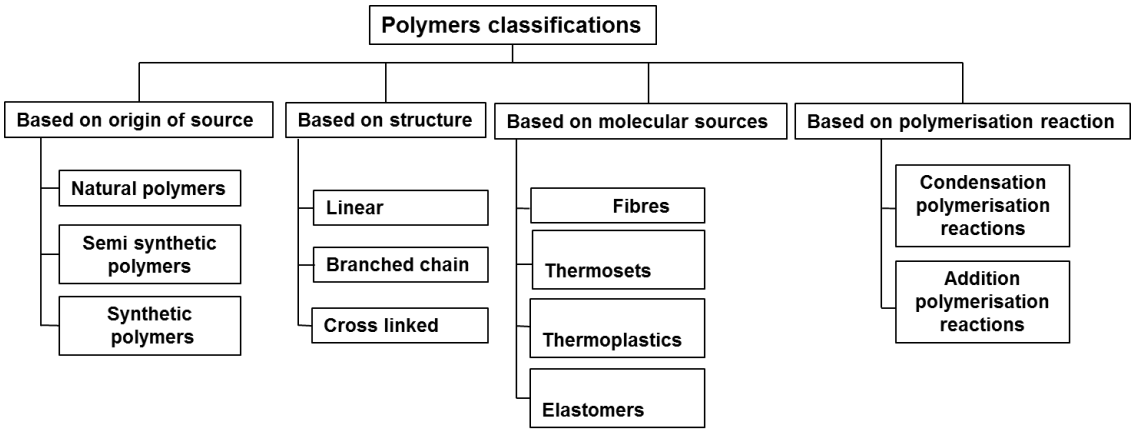

Figure 1.1: Classification of polymeric materials

1.2.1 Classification based on source

Natural polymers are the polymers found in nature in animals and plants; typical examples of this include proteins and natural rubber. There are some synthetic polymers that utilise natural sources such as cellulose triacetate and cellulose nitrate which are obtained from natural polymers by subjecting them to some form of chemical processing to produce different materials. These types of polymers are known as semi-synthetic polymers. The final classification of polymers based on the source are synthetic polymers, which are produced by different polymerisation reactions of synthetic monomers(3,4). Common examples of synthetic polymers include commodity polymers such as Nylon, poly (methyl methacrylate) and polyesters.

1.2.2 Classification based on polymer structure

Polymer classification based on structure has sub-divisions of linear, branched or crosslinked polymers (Figure 1.2 a, b and c).

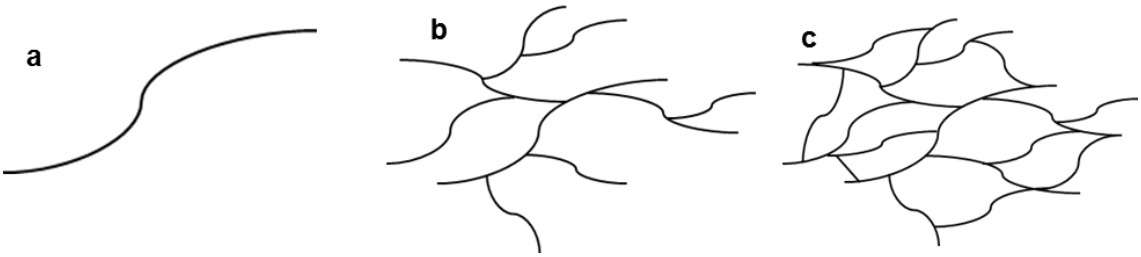

Figure 1.2: a) Linear, b) branched and c) cross linked polymers

Within these three different structures, it is possible to have polymers that are based on a single monomeric unit or homopolymer and more than one monomeric unit or copolymer(s) (3,5,6). In the case where there is more than one monomer type, the arrangement of the monomers in the polymeric chains can also be different and might be one of the following sub-classifications:

1) Alternating copolymer: where the monomer units arranged in an alternating system(5).

Figure 1.3: Alternating copolymer

2) Block copolymer: where the monomer units arranged in blocks (5).

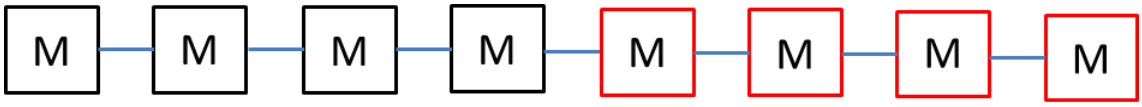

Figure 1.4: Block copolymer

3) Random copolymer: with a random arrangement of the monomer units in the polymeric chains(5).

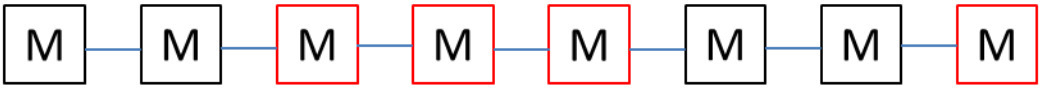

Figure 1.5: Random copolymer

1.2.3 Classification of polymers based on molecular forces

Depending on the forces between the polymeric chains, polymers can be classified into the following categories:

1.2.3.1 Elastomers

In this type of polymer, the polymeric chains are held together by relatively weak intermolecular forces, resulting in a stretchable polymer with elastic behaviour due to few crosslinks between the chains. These crosslinks allow the

polymer to retract to its original shape when forces are released. Examples of elastomeric polymers: natural rubber and synthetic poly isoprene(4,6).

1.2.3.2 Fibres

Fibres are solid polymeric materials consisting of threats, these polymers retain a high tensile strength and modulus; due to strong intermolecular forces for example hydrogen bonding. Cellulose is the best example for natural fibre polymer. In addition Nylon 6, 6 and polyesters are examples of synthetic fibre polymers that used widely in industry.

1.2.3.3 Thermoplastic polymers

Thermoplastic polymers can be softened by heating and hardened by cooling; therefore they have the possibility to be recycled and used multiple times. The polymeric chains in these polymers would be either in linear or branched structures(4,6). Typical examples of these polymers include polythene and PVC.

1.2.3.4 Thermosetting polymers

Thermosetting polymers can only be shaped once by heating; if they are heated again, they will not soften because the polymeric chains have become interlinked. These polymers are crosslinked or heavily branched molecules(4,6). Examples this type include polyester resin, epoxy resin and urea formaldehyde.

1.2.4 Classification of polymers based on polymerisation reactions

Polymers can be divided into two groups, based on the type of polymerisation reaction as follows:

1.2.4.1 Polymers formed via condensation reactions

In this type of polymer two different moieties are added together and a small molecule is produced as a side product such as water or ethanol. Polyesters and polyamides are examples of condensed polymers(4,6).

1.2.4.2 Polymers formed via addition reactions

These polymers are formed by joining monomeric units to make long chains, typically adding across a carbon carbon double bond. Addition polymers formed using one monomeric type is known as homopolymer, a polymer that is formed by joining different types of monomers is referred to as a copolymer(4,6).

1.3 Mechanism of Addition Polymerisation

There are numerous mechanisms that describe polymerisation reactions, including chain-growth (addition polymerisation) and step-growth (condensation polymerisation). The polymers used in this thesis were all manufactured using free radical addition polymerisation, so this section will only describe this reaction mechanism(2).

In chain-growth polymerisation the reaction occurs by successive addition of monomer molecules to the reactive end (e.g. a radical end) of a propagating polymer chain. The added units could be the same or different monomers. The monomers normally employed in this type of polymerisation contain carbon-carbon double bonds that can participate in a chain reaction. The addition reaction consists of three stages; initiation, propagation and termination and will be discussed(2).

Initiation: initiation occurs when an initiator (I), a compound with an easily broken covalent bond (by light energy or heat), fragments to form radicals (I^{*}) that can induce a radical chain reaction.

Propagation: is the rapid chemical reaction of monomer molecule with another monomer, and the subsequent repetition to elongate the repeating chain of the polymer.

Termination: This step occurs when a free radical reacts in a way that avoids further propagation. The most common procedure of termination is by coupling, where two radicals react together forming a single molecule(4).

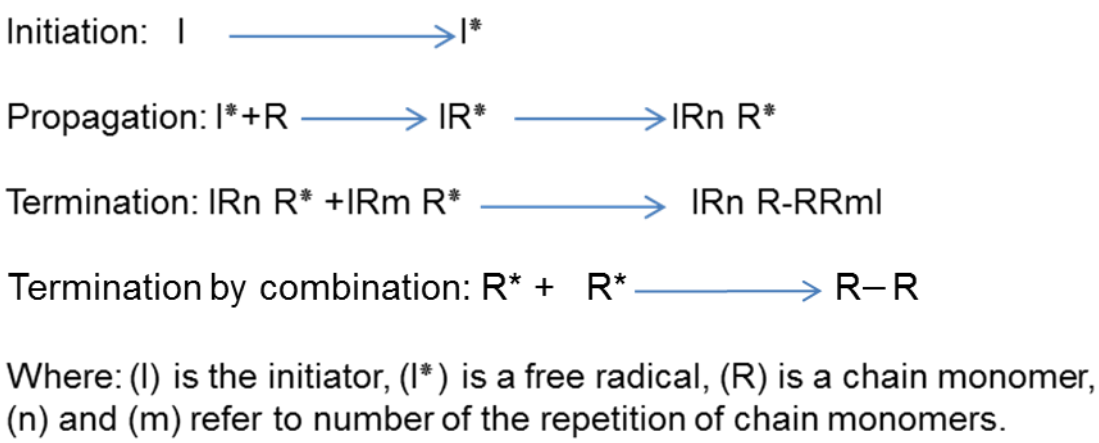

Figure 1.6: Illustration of the three stages of 'free radical' polymerisation

In polymeric chemistry, precipitation polymerization is a heterogeneous polymerization process which starts as a homogeneous system, where the monomer and initiator are totally soluble. However during propagation at some point the produced polymer becomes insoluble and therefore precipitates(3)

1.4 Poly (N-isopropyl) acrylamide (PNIPAM)

Poly (N-Isopropylacrylamide) was first synthesised in 1956(7–9) and, the first study on its phase diagram was published in 1968 by Heskins and Guillet(10). Subsequently, poly (N-Isopropylacrylamide) (pNIPAM) has been extensively studied by researchers as it is a thermoresponsive polymer with conformational transitions occurring close to the body temperature(11–13). The investigation of lower critical solution temperature (LCST) for free pNIPAM dates back to 1967, when Scarpa et al, have presented a study describing a precipitation and resolving of pNIPAM from the solution as an "inverse temperature coefficient of solubility"(14).

A thermally responsive polymer is one that undergoes changes in solubility at a specific temperature known as the critical solution temperature(12,15). The lower critical solution temperature (LCST) is defined as the temperature at which coil-to-globule conversion of the polymer network happens as a result of sufficient disruption of hydrogen bonding between the amide groups and the water molecules, creating hydrophobic interactions to be formed between the non-polar domains of the system(16,17). Polymers can be also responsive to a change in pH(18,19). Aqueous pNIPAM solutions become opaque and insoluble in water if heated above the LCST which is between 30°C (20) and 35°C (21). This a reversible transition, because if the turbid suspension is cooled down, it will fully recover its optical clarity.

Over the last two decades, pNIPAM based hydrogels have been of special interest to researchers due to their precise and modifiable stimuli-responsive properties and large numbers of studies have been conducted on different applications such as absorbed on surfaces(5), microgels (23,24) and coatings(22). Other potential uses of pNIPAM have been investigated in many fields including biology(25–27), physics(28–30) and medicine(31–33). In Figure 7 the 2D structure of pNIPAM and its amphiphilic nature are shown.

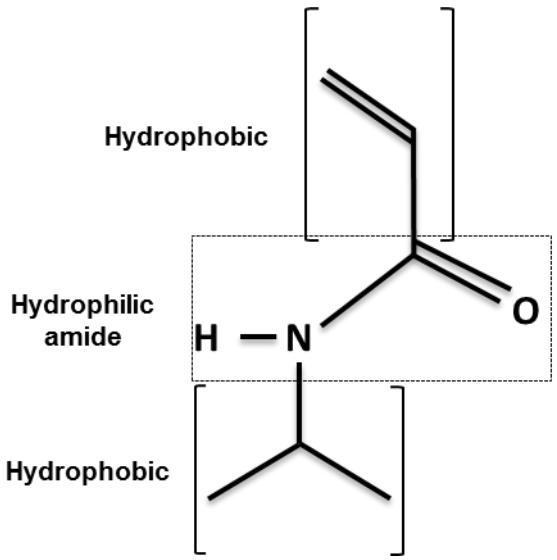

Figure 1.7: 2D structure of N-isopropyl acrylamide (NIPAM) with functional group indicated

1.5 Clays

Clays are naturally existing material composed primarily of fine-grained minerals, which become plastic when wet and harden if dried or fired(34), the grain size of clays is ranging from a few µm to hundreds of a µm. There are many clay types including common ones such as mica, chlorite and smectite, they mostly consist of SiO_4, Al, Mg and Si; arranged in layered structures.
The use of clays dates back to 7800 years BC, when Greeks and Romans built their houses using clay due to the low cost of these materials(35). Since then, the use of clays has escalated and they are used in varied application such as oil drilling, construction, sealants and cosmetics (35,36). In addition, clays are used in water purification, due to their ability to remove heavy metallic ions from waste water(35,37,38).

Each clay type has different range of properties; therefore they could be used in different applications. In health and medical applications clays have been used in curing and therapeutic purposes since prehistoric periods(39–41). Furthermore, Clays are used nowadays as anti-diuretics (42). In the pharmaceutical industry clays have being used as flavour correctors, lubricants and as drug delivery vehicles(43).

Clay structure consists of silica tetrahedral sheets and octahedral sheets; the principal atom in the tetrahedral sheets is the Si^{4+} cation, although this can be replaced by the Al^{3+} cation. Exchange Si^{4+} cation for Al^{3+} cation causes an imbalance of the charge, which must be counteracted in the clay layer structure by having positively-charged material (and H_2O) between the layers(34). This region is called the "interlayer" space (Figure 8).

Both sheets are fused by the sharing of oxygen atoms, and these fused sheets collectively create a clay layer. The layers form regular stacks, with a large interlayer area and a high aspect ratio.

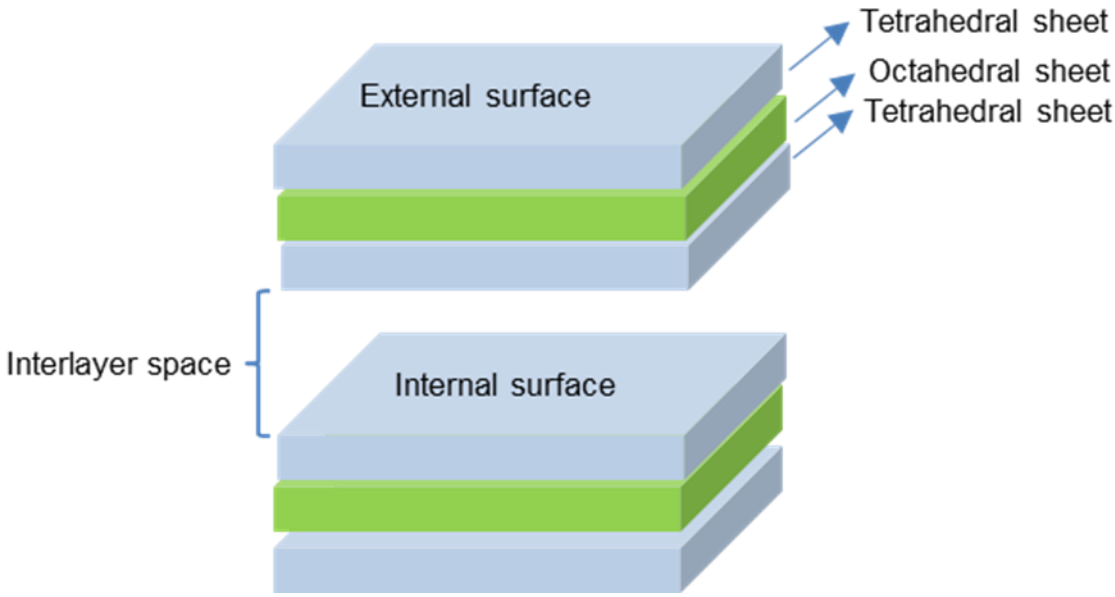

Figure 1.8: General structure of clays adapted from (44)

The importance of the interactions between cations in solution and the interlayer spaces has been well understood since the last century(45,46), where in high humidity, clay swells and these spaces increase(47) (Figure 9). The magnitude of the increase in the interlayer space depends on the amount of water absorbed into clay's structure(46), and the swellability of the clay depends on the strength of the bonding between the cations and the clay layers.

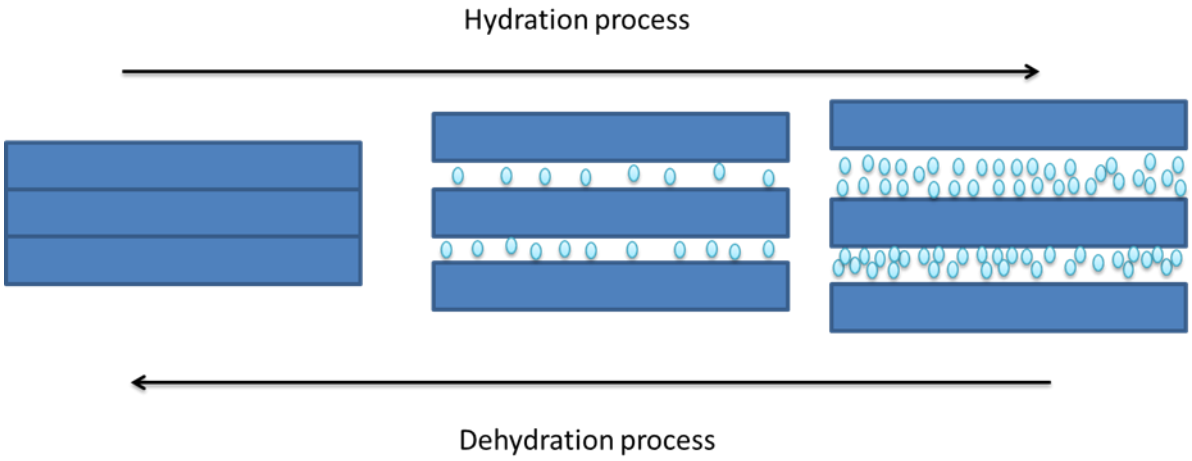

Figure 1.9: Increasing interlayer space by absorbing water

When clay is used as a crosslinker in clay/polymer composites, the interlayer spaces are crucial for bonding polymer molecules. Over the last decade, it was

reported that swelling and mechanical behaviour of nanocomposite hydrogels consisting of exfoliated clay can be controlled by modifying their chemical compositions(48–50). These studies explored the effects of changing chemical compositions of Poly (N-Isopropylacrylamide) - based Laponite® Hydrogel on a range of different physical and mechanical properties. Where, increase clay concentration increase the stiffness of pNIPAM based Laponite® hydrogel and decrease both swelling ratio and transparency of the hydrogel.

1.5.1 Laponite®

Laponite® is synthetic clay, manufactured by Rockwood in Widnes, UK(51) and it incorporates Na, Mg and Li in its structure. Laponite® RD (used in this work) has a layered structure with platelets thickness of 0.92nm and ~25nm in diameter(52,53). This specific structure becomes beneficial when we incorporate Laponite® into the polymer matrix in an exfoliated manner and polymer chains connect with layers of the clay(48). Laponite® is one of the most common clays has being used as crosslinker with polymeric materials to produce composites for different purposes, most likely because it is cheap and easy to exfoliate in water as a suspension at room temperature(54).

1.6 Composite materials

Composites are composed of two or more individual components, which are combined to obtain the ideal properties of each component, resulting in better properties than those of the individual components used alone, to end up with unique behaviour and properties. The most accepted definition of composite material has been declared by Jartiz(55–57) “Composite is a multifunctional material system that provide characteristics not obtainable from any distinct material." The use of composites dates back to 2500 years ago, where the Egyptians have used straw and clay in composite combination to build their houses(58,59). The name of composites came from their matrix phase (ceramic-metal or polymer)(60).

1.6.1 Composites in biological systems

Since 1980 when Bonfield *et al*. introduced the possibility of using composite materials in bone grafts(60,61). Consequently, composites have been used in many applications such as household appliances, aerospace and medical devices(62). A polymer composite is a composite material in which one of its components is polymer, to produce new material that is relatively cheap with unique properties for many engineering applications such as house goods, construction materials and medical instruments.

Bone is a natural composite material consisting of a hard but brittle material called hydroxyapatite (inorganic component) and a soft and flexible material called collagen (organic component), this combination gives the bones the unique properties that are needed to support the body and protect organs such as brain and lungs(63). In recent years there have been several studies investigating the possibility of using composite materials in medical applications(60,64–66), one of the most attractive and promising composite in biomedical and tissue culture fields was polymer/inorganic composite, because often enhancement is needed for mechanical properties and this can be obtained by incorporating nanoparticles into polymeric materials(49,67–73), where nanoparticles improve tensile strength (48–50,74,75), increase stiffness (76,77) and elongation at break (49,50,69,74,78) when compared to that of the pure polymer.

Several types of inorganic nanoparticle material can be used such as hydroxyapatite (HA), layered silicates, carbon nanotubes and clays. These nanoparticles will enhance and improve different properties, according to several studies conducted in the field, incorporation of nanoparticles enhance transparency (50,79–82), electrical conductivity (73,83–85) and thermal stability (70,86–88). Although incorporating nanoparticles enhances the properties of nanocomposite materials, in the case of polymer - clay nanocomposite it is only a few weight percent of clay can be added (<10 wt. % max)(52), because there are difficulties in preparation of nanocomposite when in organic particles increase (52,89,90). In this thesis Laponite® nanoparticles have been used as crosslinker with Poly (N-Isopropylacrylamide) to produce pNIPAM based Laponite® hydrogels, and the influence of Laponite® has been studied. In addition, synthetic hydroxyapatite nanoparticles (HAPna) was incorporated into

pNIPAM based Laponite® hydrogels, to promote osteogenic differentiation of human mesenchymal stem cells (hMSC)

1.6.2 Nanocomposite materials

Nanocomposite material is a composite in which one of its components has dimensions on the nanometre scale (< 100nm). Nanocomposite hydrogels have being increasingly studied to produce a new advanced material(64,91–94). Since 1989, when Toyota has improved the properties of Nylon-6 by mixing pure polymer with nano clay minerals to develop new heat resistant and tough improved composite materials(95,96), that had incredible usability in different areas. Consequently, researchers have conducted many studies in order to understand these materials and their applicability, and many different inorganic nanoparticles such as clay minerals; have been used in combination with polymers, to produce nanocomposite hydrogels (52).

In this study Laponite® RD was incorporated to poly (N-isopropylacrylamide), hydroxypropyl methacrylate and hydroxyethyl methacrylate, to produce pNIPAM based Laponite® hydrogels with a range of comonomer types and concentrations.

1.6.3 Polymer/ clay nanocomposites

Polymer nanocomposite (NCs) is a combined of polymers with clay minerals, by which we get new composite material that own both polymers' properties such as stiffness, elasticity and toughness, and inorganic materials' behaviour (e.g., hardness, resistance to ignition) which improves the final products properties as well as reducing the cost(97,98). The advent of clay/polymer nanocomposites began with Toyota, developing clay/Nylon-6 nanocomposites in the end of 1980s and the beginning of 1990s(95,99–101). Much work has followed to investigate polymer/ clay nanocomposite properties and their possible applications(48,49,67,74,87,102) and some have shown appreciable improvements in certain properties, such as permeability, modulus and stiffness(52).

1.7 Hydrogels

Hydrogels are three dimensional crosslinked polymeric networks with high water contents and are able to absorb a huge amount of water and swell without dissolving at physiological pH, temperature and ionic strength(103,104). Due to having a huge amount of water in their structures, they possess a high degree of flexibility which is very similar to the nature of natural tissue (105). The research of hydrogel dates back to 1960, when, Wichterle and Lim initially proposed the utilization of hydrophilic systems of 2-hydroxyethyl methacrylate (PHEMA) in contact lenses applications(104,106). Since then workers have extensively studied hydrogel materials, due to their possible applications in regenerative medicine and drug delivery(106–109). Hydrogels have been studied with investigations regarding their physical(110–115), mechanical properties(50,102,116) and their possible applications(66,93,117,118) in different engineering and industrial areas. To date hydrogels have been used in a range of commercial applications which include hygienic products(119), agriculture(120), artificial snow(119) and medical applications such as drug delivery(106,121–123), wound healing, cell culture and cell encapsulation, coating material for implants and contact lenses (63,103,124–126). In recent years, many studies have been conducted in the medical field, utilising hydrogels as tissue culture biomaterials (64,77,117,127,127,128).

1.7.1 Hydrogel Classification

Hydrogel classifications generally divide them based on their physical properties, preparation method, ionic charge, crosslinking types and responsive behaviour to environmental changes(121). Hydrogels have been classified in the literature based on polymer source in three different ways; natural, synthetic or hybrid hydrogels. Natural polymers such as natural polypeptides, collagen, alginate and gelatine have been employed for hydrogel preparations. Hydrogels based on naturally derived polymers usually possess innate biocompatibility and biodegradability. In contrast these polymers from nature are frequently saddled with high batch-to-batch variability and conceivable immunogenic reactions. However, Hydrogels based on synthetic polymers such as synthetic polypeptide, poly (2-hydroxypropyl methacrylamide) and poly(hydroxyethyl methacrylate), offer incredible flexibility in controlling polymer structure and building design,

which is vital to create hydrogels with tailorable system and mechanical qualities(129).

According to structural features, hydrogels can be classed as having semi-crystalline, amorphous, or hydrogen-bonded structures. They can also be classified based on their method of preparation, ionic charge, or physical structure features. In this system of classification hydrogels may be: 1) homopolymer hydrogels, 2) copolymer hydrogels, 3) multipolymer hydrogels, or 4) interpenetrating polymeric hydrogels. Homopolymer hydrogels are crosslinked systems of one sort of hydrophilic monomer unit, while copolymer hydrogels are created by crosslinking of two comonomer units, no less than one of which must be hydrophilic to render them swellable. Multipolymer hydrogels are created from three or more comonomers combined together. Finally interpenetrating polymeric hydrogels are created by setting up a first system that is then swollen in a monomer. It is also possible to subdivide hydrogel materials according to their response to the environmental changes such as temperature, pH and light. Another category has been added recently to Stimuli-responsive polymers is biochemical responsive polymers(130), that might be used in hydrogel synthesis to get hydrogel responsive to changing in bio - environmental conditions, such as enzyme, antigen and ligand, which could be beneficial in medical applications.

The general classification of hydrogel materials based on their physical and chemical properties, behaviour, preparations and sources, along with details for each main class is shown in Figure 9.

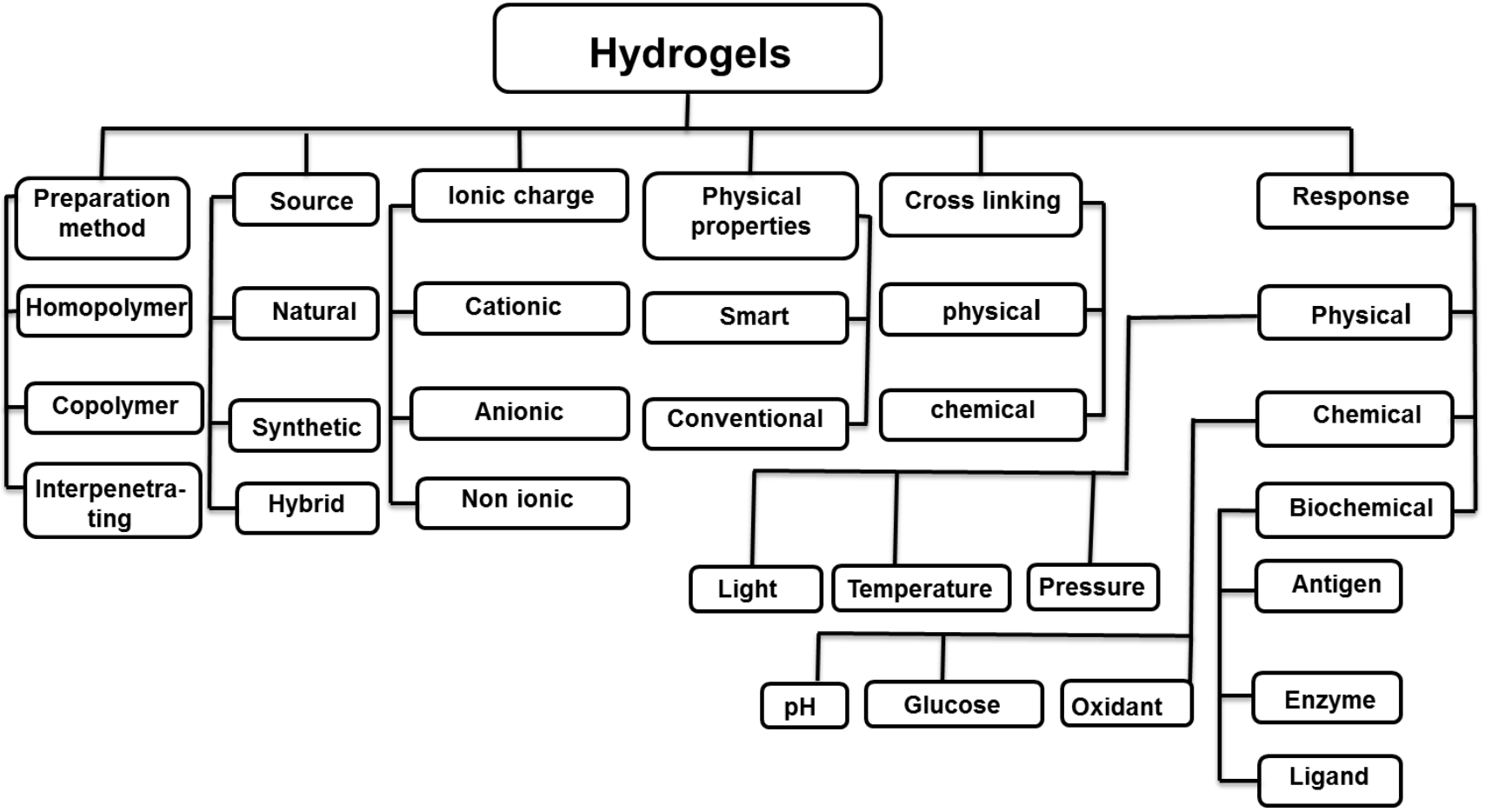

Figure 1.10: Classification of hydrogel materials adapted from(105)

1.7.2 Medical and dental applications of hydrogels

Over the last decade, hydrogels have been proposed as potential choices for tissue engineering, tissue culture and drug delivery; currently the following applications have all used hydrogel as a biomaterial:

- Soft contact lenses (131)
- Drug delivery (pills/capsules)(132)
- Wound Healing(107,125)
- Implant Coatings : where hydrogels used to improve surface properties of peacemaker and orthopaedic devices (133,134)
- Tissue Engineering and tissue culture(77,128,135)

The tuneable properties of hydrogels allow these materials to be used for different proposes; such as contact lenses(109), as a filler in aesthetical surgery(136) and drug delivery(137,138).

In dentistry, hydrogels have been reported as a promising solutions in several applications, such as to recreate soft and hard normal tissue and deliver bioactive molecules into the oral cavity(139,140).

The formation the secondary palate in mammals is complex, and includes different stages of cell development such as proliferation, migration, differentiation, and finally programmed cell death(141). However, in some cases this process is interrupted and the palate or/and the lip remain not fully developed. In 1998, Peters *et al*, reported that the uncompleted development of the human palate could be the result of abnormal characteristics of the palatal shelves in early stage of gestation (142).

The cleft palate is still the most prevalent major facial malformation, that affecting the ability of new-borns to feed and impairing speech development, it occurs in about 1.7 per 1000 live born babies(143,144).

One example of the potential dental applications of hydrogels is to regenerate hard or soft tissue around cleft palate by injecting these materials with suspended cells. Martinez A. *et al*, in 2013 proposed that if bone morphogenetic protein-2 (BMP-2) was injected using an appropriate carrier into the periosteum of the cleft palate borders, the border volume would increase and connective tissue cells would be activated to produce extra bone. They used an injectable hyaluronic acid-based hydrogel containing hydroxyapatite as the carrier; this study was conducted using dog pups with congenital cleft palates. Four weeks

after the hydrogel injection, the palatal cleft margins had reached the midline, and cultured bone had enlarged the palatal bones(143).

According to a study conducted in field of surgical dentistry, keratin hydrogel promoted earlier osteo-integration around titanium dental implants(145). This study investigated the applicability of a range of different compositions of pNIPAM based Laponite® hydrogels to be used as cell carrier in surgical dentistry.

1.8 Poly (N-isopropylacrylamide) - Based clay Hydrogels

In 2002 Haraguchi et al, developed pNIPAM / clay nanocomposites (48), and documented their swelling, mechanical and optical properties(49,102,146). As mentioned earlier, the main purpose of producing composite materials is improving their general properties as well as reducing the cost. In the same context, incorporating inorganic particles such as clays to Poly (N-isopropylacrylamide) may improve several properties as mentioned earlier in 1.5.

Poly (N-isopropylacrylamide) has interesting properties, such as thermal response (20), the ability to absorb large volumes of water(103) and biocompatibility(77,117,147) that make it such a promising material for different applications, such as artificial soft tissues(148–151) and drug delivery(111). Poly (N-isopropylacrylamide) has Lower critical solution temperature at ~32^{o}C, but it can be modified by the addition of a comonomer to to meet a wide range of different applications' requirements(152)

The thermoresponsive behaviour of PNIPAM can be modified to be used as an injectable scaffold, where cells could suspend in the hydrogel in liquid state above lower critical solution temperature (LCST), then either injected *in vivo* or *in vitro* depending on the application and the gel will encapsulate the cells within its structure when temperature is decreased below the (LCST)(117).

1.8.1 Mechanical properties of Poly (N-isopropylacrylamide) - Based Hydrogels

Consideration of the mechanical behaviour of biomaterials used as cell scaffolds in tissue regeneration or in tissue engineering is crucial (84), where biomaterials should enhance and support cells mechanically to offer an appropriate environment for cell proliferation and development.

Mechanical properties can be influenced by several parameters, such as the monomer type and concentration, crosslink density, polymerization method and temperature, swelling degree at the time of the measurement and the technique that used to test the sample(49,103,118,122,153,154). Crosslink density of hydrogel materials, due to its importance in controlling the mechanical properties of viscoelastic networks(72) has received significant attention over the last decade. In previous studies Haraguchi *et al* and Djonlagic *et al* have reported that increasing the crosslink density was shown to increase the stiffness of hydrogel materials(76,146). Hence, mechanical properties of hydrogel materials can be tuned to meet different application requirements. In the current study, the influence of composition on the mechanical properties of pNIPAM based hydrogels has been studied.

1.8.2 State of water within Poly (N-isopropylacrylamide) - Based Hydrogels

As stated earlier, hydrogels are 3d polymeric network structures containing water , and have ability to absorb a huge amount of water or biological fluids in their structures(155). For biomedical applications, high water contents are very important for hydrogel's biocompatibility. Hence, it is crucial to understand the behaviour of the water within hydrogel materials that are used as biomaterials when attempting to develop better materials.

Water in hydrogels is classified into three different states(156–159):

1) Free water (Freezable water): This is not bound to the polymeric chains and therefore possesses behaviour like pure water, such as freezing at 0 °C.

2) Bound water (non-Freezable water): This water is strongly bound to the polymeric chains; either through hydrophilic groups or via hydrogen bonds and therefore dose not behaves like pure water.

3) Freezable bound water: in this state, water is weakly bound to the polymeric chains, having transitional properties between those of bound and free water, such as freezing at temperature lower than 0 °C(124,160).

Differential scanning calorimetry (DSC) is the most informative procedure that used semi-routinely by researchers, to study water binding in polymers(156,161). However, different techniques can be used; such as Nuclear magnetic resonance spectroscopy (NMR)(143), Fourier transform infrared spectroscopy (FTIR)(146) and X-ray diffraction (XRD)(163,164).

Differential scanning calorimetry (DSC) was used frequently to determine water state in hydrogel materials and to understand water polymer - interaction within these materials(156,165–168), based on different behaviour of each state. Absorbed water in hydrophilic polymer molecules has thermodynamic behaviour different from pure water; such as freezing temperature(169). Higuchi et al. have conducted a study on Water states in Poly (Vinyl Alcohol) Membranes using DSC, they have shown that the endotherm for melting the point of water in PVA is 9% higher than of pure water crystallisation, in in the water content of this material was more than 60 wt. %(170).

Other techniques such as Fourier Transform Infrared spectroscopy has been used to distinguish between different water states, by investigating hydrogen bonding between water and polymer molecules(162,169,171).

In the present study Fourier Transform Infrared spectroscopy was used to determine state of water within series of different composition of pNIPAM based Laponite® hydrogel and DSC has been used to corroborate these results.

1.8.3 Swelling and de-swelling behaviour of Poly (N-Isopropylacrylamide) - Based Hydrogels in distilled water

Since water is the largest component of hydrogels(50), and they have a propensity to absorb large volumes of water in their structures(103), as well as the applicability of their use in the body (70% water), it is important to investigate the response of these materials in an aqueous environment. Many studies have reported the swelling and swelling characterisation of Poly (N-Isopropylacrylamide) Hydrogels. Yucel D. *et al*. have studied the influence of

the composition on swelling behaviour of Poly (N-Isopropylacrylamide) in distilled water at 25 °C for swelling and at 48 °C for deswelling. They found that increased crosslink density decreased both swelling and deswelling rates of hydrogel, due to the reduction in mesh size(111). Haraguchi K. *et al.* have revealed the same effect of crosslink density of pNIPAM hydrogels on the swelling/deswelling behaviours(142). For different hydrogels, Djonlagic et al. and Yacob N. *et al*. have shown that crosslink density decreases both swelling and deswelling rates as a result of the decrease in the hydrogel pore size(76,114). Here, in this work swelling and deswelling behaviour of pNIPAM based Laponite® hydrogels were studied and the effect of composition was investigated.

1.8.4 Structural properties of Poly (N-Isopropylacrylamide) - Based Hydrogels

Structural properties and their influence on the behaviour of pNIPAM based hydrogels, has been widely studied over the last two decades(173–175). It was well reported that morphological and structural properties of pNIPAM based hydrogels were impacted by crosslink density(76,146,176), polymerisation conditions(177) and comonomer type and concentration(154). Similarly, it was documented for different hydrogel materials, where Jang J, *et al*. have found that increased crosslink density decreased average pore size of alginate hydrogels(127). Modifying the pore size of hydrogel materials is very important when used in tissue culture, to improve fluid and nutrition transportation through the hydrogel rapidly and effectively. In addition, structural and morphological properties influence other properties, such as the mechanical behaviour(76,116) and swelling degree(114,116). The current study focused on influences of crosslink density, co-monomer type and concentrations on the morphology and structure of pNIPAM based Laponite® hydrogels. In addition the correlation between changing hydrogel structure and the influence on a range of properties including mechanical properties, swelling/deswelling, dehydration/rehydration rates and water states has been reported, as well as cell viability within these materials.

1.8.5 Biocompatibility and cell viability of Poly (N-Isopropylacrylamide) - Based Hydrogels

Biomedical and regenerative medicine applications of hydrogel materials have being studied prodigiously since the last decade(175), due to their biocompatibility and similarities to natural tissue (151,178–180). In addition, many hydrogel materials have proven their nontoxicity to cells and they promoted cell growth(64,77). Biocompatibility of pNIPAM based Laponite® hydrogels has been well reported(77,117,147). In this study the biocompatibility of pNIPAM based hydrogels was shown to be varied, depending on the comonomers that were used. Moreover, cell viability was shown to be affected by composition of the hydrogel.

1.9 Poly hydroxyethyl methacrylate hydrogels

Poly (2-hydroxyethyl methacrylate) (pHEMA) is a polymer that reported in many studies to be used in drug delivery and tissue engineering, due to its good biocompatibility and can be easily synthesised and its mechanical and physical behaviour can be controlled (181,182). PHEMA was used with stimuli responsive copolymer to enhance the mechanical and physical properties of the hydrogel (183,184). In the current study HEMA was added at concentration of 5, 10 and 12wt. % to some composition as copolymer, and influence of incorporation of HEMA on physical and mechanical properties was investigated. In addition, effect of HEMA as comonomer on cell viability was assessed.

1.10 Poly hydroxypropyl methacrylate hydrogels

Hydroxypropyl methacrylate (HPMA) copolymers were used in pharmaceutical applications since 1970 (185,186). Subsequently, using of HPMA in tissue engineering was reported by researchers due to its flexibility which was shown to be similar to soft tissue, also its hydrophilicity and biocompatibility which found to be important for cell growth (187). In this thesis, HPMA was used as comonomer at concentration of 5, 10 and 17wt. % and effect of HPMA on physical and mechanical properties was explored and relevant cell behaviour was addressed.

1.11 Aims and Objectives of This Study

This work aimed generally to improve a previously synthesised pNIPAM based Laponite® and to investigate the effects of a range of different chemical compositions, on mechanical, structural, dehydration/rehydration and swelling/deswelling behaviour. In addition, the influence of each composition on cell viability and growth was assessed.

The importance of water content in hydrogels has been stated in this chapter, and a complete understanding of water/polymer interaction within hydrogel, is needed in order to exploit this in practice. For more and sufficient understanding, this research focused on:

Dehydration behaviour of pNIPAM based Laponite® hydrogel and the influence of chemical composition has been investigated.

Rehydration behaviour and diffusion rate of water through different compositions of pNIPAM based Laponite® hydrogels was explored, to investigate the influence of chemical composition on these characteristics.

Dehydration and rehydration studies were conducted using Fourier Transform Infrared spectroscopy (FTIR), collected data were analysed and used to determine dehydration and rehydration rates, diffusion coefficient, bound and free water content.

Swelling and deswelling behaviour of hydrogels in aqueous media were also examined. Dehydration and rehydration data were compared to swelling and deswelling observations and the agreement between them was explained and documented.

The correlation between water behaviour in different compositions and the applicability of this material to be used in cell culture was addressed.

Due to the importance of structural features of hydrogels and their influence on different properties have been conducted(76,114,116). This research also aimed to explore the morphology of pNIPAM based Laponite® using Scanning electron microscopy (SEM) and find links between morphology and mechanical properties.

1.12 References

1. John M, and Angus W,. Applied dental materials. 9th edn. Blackwell Publishing Ltd; 2008.

2. David T,. Polymer chemistry introduction to an Indispensable science. Arlington: NSTA Press; 2004. 1-286 p.

3. Fried J. Polymer Science and Technology. 2nd edn. Upper Saddle River: Prentice Hall Professional Technical Reference; 2003. 608 p.

4. Charles E, and Carraher J,. Polymer Chemistry. 2nd edn. Polymer Chemistry. Prentice Hall Professional Technical Reference; 2003. 850 p.

5. Michael M, and Coleman P,. Fundamentals of Polymer Science: An Introductory Text, 2nd edn. CRC Press.; 1998.

6. Fried JR. Polymer Science and Technology, 3rd edn Prentice Hall. 2014. 637.

7. Specht, E. H.; Neuman, A.; Neher HT. Acrylamides. U. S. pat. 2,773,063, 1956.

8. Zoppe JO, Osterberg M, Venditti R a, Laine J, Rojas OJ. Surface interaction forces of cellulose nanocrystals grafted with thermoresponsive polymer brushes. Biomacromolecules. 2011;12(7):2788–2796.

9. Halperin A, Kröger M, Winnik FM. Poly(N-isopropylacrylamide) Phase Diagrams: Fifty Years of Research. Angew Chemie - Int edn. 2015;54(51):15342–15367.

10. Heskins M and Guillet J E . Solution Properties of Poly (N-isopropylacrylamide), Journal of Macromolecular Science: Part A - Chemistry. 1968; 2(8): 1441-1455.

11. Pelton R. Temperature-sensitive aqueous microgels. Advanced Colloid Interface Science. 2000;85(1):1–33.

12. Gil ES, Hudson SM. Stimuli-reponsive polymers and their bioconjugates. Progress in Polymer Science. 2004;29(12):1173–1222.

13. Cole MA, Voelcker NH, Thissen H, Griesser HJ. Stimuli-responsive interfaces and systems for the control of protein-surface and cell-surface interactions. Biomaterials. 2009;30(9):1827–1850.

14. Scarpa JS, Mueller DD, Klotz IM. Slow Hydrogen-Deuterium Exchange in a Non-α-helical Polyamide. Journal of the American Chemical Society. 1967;89(24):6024–6030.

15. Nechifor CD, Dorohoi DO, Ciobanu C. The influence of gamma radiations on physico-chemical properties of some polymer membranes. Romanian Reports in Physics. 2009;54(3–4):349–359.

16. Okada Y, Tanaka F. Cooperative hydration, chain collapse, and flat LCST behavior in aqueous Poly(N-isopropylacrylamide) solutions. Macromolecules. 2005;38(10):4465–4471.

17. Haraguchi K. Synthesis and properties of soft nanocomposite materials with novel organic/inorganic network structures. Polymer Journal. 2011;43(3):223–241.

18. Bignotti F, Penco M, Sartore L, Peroni I. Synthesis, characterisation and solution behaviour of thermo- and pH-responsive polymers bearing l-leucine residues in the side chains : Polymer Journal. 2000;41:8247–8256.

19. Pinkrah VT, Snowden MJ, Mitchell JC, Seidel J, Chowdhry BZ, Fern GR. Physicochemical properties of poly(N-isopropylacrylamide-co-4-vinylpyridine) cationic polyelectrolyte colloidal microgels. Langmuir. 2003;19(3):585–590.

20. Yim H, Kent M, Mendez S, Balamurugan S, Balamurugan S, and Lopez G,. Temperature-Dependent Conformational Change of PNIPAM Grafted Chains at High Surface Density in Water. Macromolecules. 2004;37(5):1994–1997.

21. Huber DL. Programmed Adsorption and Release of Proteins in a Microfluidic Device. Polymer Science (80-). 2003;301(5631):352–354.

22. Vickie Pan Y, Wesley RA, Luginbuhl R, Denton DD, Ratner BD. Plasma polymerized N-isopropylacrylamide: Synthesis and characterization of a smart thermally responsive coating. Biomacromolecules. 2001;2(1):32–36.

23. Hu T, Wu C. Grafting density induced stretching and collapse of tethered poly(ethylene oxide) chains on a thermally sensitive microgel. Macromolecules. 2001;34(19):6802–6805.

24. Zhang G, Wu C. The water/methanol complexation induced reentrant coil-to-globule-to-coil transition of individual homopolymer chains in extremely dilute solution. Journal of the American Chemical Society. 2001;123(7):1376–1380.

25. Ohya S, Matsuda T. Poly(N-isopropylacrylamide) (PNIPAM)-grafted gelatin as thermoresponsive three-dimensional artificial extracellular matrix: Molecular and formulation parameters vs. cell proliferation potential. Journal of Biomaterials Science Polym Edn. 2005;16(7):809–827.

26. Naha PC, Bhattacharya K, Tenuta T, Dawson KA, Lynch I, Gracia A, *et al.* Intracellular localisation, geno- and cytotoxic response of polyN-isopropylacrylamide (PNIPAM) nanoparticles to human keratinocyte (HaCaT) and colon cells (SW 480). Toxicology Letters journal. 2010;198(2):134–143.

27. Deka SR, Quarta A, Di Corato R, Riedinger A, Cingolani R, Pellegrino T. Magnetic nanobeads decorated by thermo-responsive PNIPAM shell as medical platforms for the efficient delivery of doxorubicin to tumour cells. Nanoscale. 2011;3(2):619–629.

28. Budhlall BM, Marquez M, Velev OD. Microwave , Photo- and Thermally Responsive PNIPAm Gold Nanoparticle Microgels Microwave , Photo- and Thermally Responsive PNIPAm - Gold Nanoparticle Microgels. Journal of the American Chemical Society.2008;(8):11959–11966.

29. Riskin M, Tel-Vered R, Willner I. Thermo-switchable charge transport and electrocatalysis using metal-ion-modified pNIPAM-functionalized electrodes. Advanced Functional Materials. 2009;19(15):2474–2480.

30. Tagit O, Tomczak N, Jafarpour A, Jańczewski D, Han MY, Vancso GJ, et al. Influence of the length and grafting density of PNIPAM chains on the colloidal and optical properties of quantum dot/PNIPAM assemblies. Nanotechnology. 2011;22(26).

31. Niazov T, Pavlov V, Xiao Y, Gill R, Willner I. DNAzyme-functionalized Au nanoparticles for the amplified detection of DNA or telomerase activity. Journal of the American Chemical Society (Nano Letters). 2004;4(9):1683–1687.

32. Ohya S, Sonoda H, Nakayama Y, Matsuda T. The potential of poly(N-isopropylacrylamide) (PNIPAM)-grafted hyaluronan and PNIPAM-grafted gelatin in the control of post-surgical tissue adhesions. Biomaterials. 2005;26(6):655–659.

33. Zintchenko A, Ogris M, Wagner E. Temperature dependent gene expression induced by PNIPAM-based copolymers: Potential of hyperthermia in gene transfer. Bioconjugate Chemistry. 2006;17(3):766–772.

34. Lavikainen L. The structure and surfaces of 2 : 1 phyllosilicate clay minerals The structure and surfaces of. (Dissertation) University of Eastern Finland Vol. 137. 2016.

35. Savic I, Stojiljkovic S, Savic I, Gajic D. Industrial Application of Clays and Clay Minerals. Clays and Clay Minerals : Geological Origin, Mechanical Properties and Industrial Applications. 2014. 379-402 p.

36. Croker J, Poss R, Hartmann C, Bhuthorndharaj S. Effects of recycled bentonite addition on soil properties, plant growth and nutrient uptake in a tropical sandy soil. Plant Soil. 2005;267(1–2):155–163.

37. XianJin WSDYHMCLY. Characterization of GMZ bentonite and its application in the adsorption of Pb(II) from aqueous solutions. Applied Clay Science. 2009;43(2):164–171.

38. Al-Qunaibit MH, Mekhemer WK, Zaghloul AA. The adsorption of Cu(II) ions on bentonite - A kinetic study. Journal of Colloid Interface Science 2005;283(2):316–321.

39. Carretero MI. Clay minerals and their beneficial effects upon human health. A review. Applied Clay Science 2002;21(3–4):155–1563.

40. Carretero MI, Gomes CSF, Tateo F. Chapter 11.5 Clays and Human Health. Development in Clay Science 2006;1(C):717–741.

41. Dawson JI, Oreffo ROC. Clay: New opportunities for tissue regeneration and biomaterial design. Advanced Materials. 2013;25(30):4069–4086.

42. Carretero MI, Pozo M. Clay and non-clay minerals in the pharmaceutical and cosmetic industries Part II. Active ingredients. Applied Clay Science

2010;47(3–4):171–81.

43. Carretero MI, Pozo M. Clay and non-clay minerals in the pharmaceutical industry. Part I. Excipients and medical applications. Applied Clay Science 2009;46(1):73–80.

44. M. Ghadiri, W. Chrzanowski and R. Rohanizadeh. Biomedical applications of cationic clay minerals. The Royal Society of Chemistry. 2015; 5: 2967-81.

45. Hendricks SB, Nelson RA, Alexander LT. Hydration Mechanism of the Clay Mineral Montmorillonite Saturated with Various Cations. Journal American Chemistry Society. 1940;62(6):1457–64.

46. Truhlar DG. Valence Bond Theory for Chemical Dynamics. Journal of Computitional Chemistry. 2009;28(1):73–86.

47. Fanning, DS, Rabenhorst, MC, Burch, SN, Islam, KR, Tangren SA. Sulfides and sulfates. In Dixon, J.B., Schulze, D.G., Daniels, W.I. (Eds.), Soil Mineralogy with Environmental Application. Soil Science of America Society. 2002;323–66.

48. Haraguchi, K, Takehisa K. Nanocomposite hydrogels: A unique organic-inorganic network structure with extraordinary mechanical, optical, and swelling/de-swelling properties. Advanced Materials. 2002;14(16):1120–4.

49. Haraguchi K, Robin F, Akira O, and Toru T. Compositional effects on mechanical properties of nanocomposite hydrogels composed of poly(N,N-dimethylacrylamide) and clay. Macromolecules. 2003;36(15):5732–41.

50. Haraguchi K, Li HJ. Mechanical properties and structure of polymer-clay nanocomposite gels with high clay content. Macromolecules. 2006;39(5):1898–905.

51. BYK Additives & Instruments. Laponite : performance additives. LAPONITE Perform Additives (Technical Information Report). 2014;22.

52. Haraguchi K, Ebato M, Takehisa T. Polymer-clay nanocomposites exhibiting abnormal necking phenomena accompanied by extremely large reversible elongations and excellent transparency. Advanced Materials 2006;18(17):2250–4.

53. Min J, Braatz RD, Hammond PT. Tunable staged release of therapeutics from layer-by-layer coatings with clay interlayer barrier. Biomaterials. 2014;35(8):2507–17.

54. Ashby NP, Binks BP. Pickering emulsions stabilised by Laponite clay particles. Physical Chemistry Chemical Physics . 2000;2(24):5640–6.

55. Jartiz AE. Design. US Patent. 1965. p. 18.

56. Shukla SP. (2011). Investigation in to tribo potential of rice husk (RH) char reinforced epoxy composite. (2011). MSc. (Thesis) Deemed University.

57. Verma D, Gope PC, Maheshwari MK, Sharma RK. Bagasse fiber

composites-A review. Journal of Material Environmental Science. 2012;3(6):1079–92.

58. Brouwer, W. (2000). *Natural Fiber Composites in Structural Components: Alternative Applications for Sisal*. (2000). PhD. (Thesis). Delft University.

59. Vimla (2015). *Synthesis and Characterization of a Biocomposite Derived From banana plants*. (2015). PhD. (Thesis) Durban.

60. Wang M. Developing bioactive composite materials for tissue replacement. Biomaterials. 2003;24(13):2133–2151.

61. Bonfield W, Charnley Journal of Composites. 1988;I:522–526.

62. Aleksendrić D, Carlone P. Introduction to composite materials. Soft Computing in the Design and Manufacturing of Composite Materials. 2015. 1-5.

63. Ramakrishna S, Mayer J, Wintermantel E, Leong KW. Biomedical applications of polymer-composite materials : Composite Science and Technology Journal. 2001;61.

64. Haraguchi K. Development of soft nanocomposite materials and their applications in cell culture and tissue engineering. Journal of Stem Cells Regenenerative Medicine. 2012;8(1); 2-11.

65. Craciunescu O, Moldovan L. Designing Bio-Inspired Composite Materials for Medical Applications. Nanocomposites Polymer with Analalytical Methods. 2011;309–34.

66. H.E. Davis and J.K. Leach, H. (2008). *Hybrid and Composite Biomaterials in Tissue engineering*. 2nd edn. New york: N Ashammakhi, pp.2-17.

67. Tsivintzelis I, and Marras S,. Porous Poly(llactic acid) nanocomposite scaffolds prepared by phase inversion using supercritical CO_2 as antisolvent. Polymer Journal. 2007;48(8):6311-6318.

68. Okamoto M, John B. Synthetic biopolymer nanocomposites for tissue engineering scaffolds. Progress in Polymer Science. 2013;38(10–11):1487–1503.

69. Tien YI, Wei KH. High-tensile-property layered silicates/polyurethane nanocomposites by using reactive silicates as pseudo chain extenders Macromolecules. 2001;34(26):9045–9052.

70. Wang S, Long C , Wang X, Li Q, Qi Z. Synthesis and properties of silicone rubber organomontmorillonite hybrid nanocomposites. Journal of Applied Polymer Science, 1998;69(8):1557–1561.

71. Liu, L.M. et al. Studies on Nylon 6 clay nanocomposites by melt-intercalation process. Applied Polymer Science 1999;71(7):1133–1138.

72. Koenigs MME, Pal A, Mortazavi H, Pawar GM, Storm C, Sijbesma RP. Tuning cross-link density in a physical hydrogel by supramolecular self-sorting. Macromolecules. 2014;47(8):2712–2717.

73. Wichmann MHG, Sumfleth J, Gojny FH, Quaresimin M, Fiedler B, Schulte K. Glass-fibre-reinforced composites with enhanced mechanical and electrical properties - Benefits and limitations of a nanoparticle modified matrix. Engineering Fracture Mechanics. 2006;73(16):2346–59.

74. Ray, S.S., et al. New polylactide-layered silicate nanocomposites. 2. Concurrent improvements of material properties, biodegradability and melt rheology. Polymer Journal. 2003;44(3):857–66.

75. Tien T, and Wei K,. High-tensile-property layered silicates/polyurethane nanocomposites by using reactive silicates as pseudo chain extenders. Macromolecules. 2001;34(26):9045–52.

76. Djonlagic, J, Lancuski A, S, Jelena R, Sanja O, and Zoran P, . Hydrogels reinforced with nanoclays with improved response rate. Journal of Applied Polymer Science 2016;134(9):1–14.

77. Dosh RH, Essa A, Jordan-Mahy N, Sammon C, Le Maitre CL. Use of hydrogel scaffolds to develop an in vitro 3D culture model of human intestinal epithelium. Acta Biomaterialia 2017;62:128–43.

78. Ou, Y.C., Yang, F., Yu, Z. New conception on the toughness of Nylon 6/silica nanocomposite prepared via in situ polymerization . Journal of Polymer Science, Part B-Polymer Physics. 1998;36(5):789–95.

79. Sun, J, William W, and Lorraine F,. Electrical and optical properties of ceramic-polymer nanocomposite coatings. Journal of Polymer Science, Part B-Polymer Physics. 2003;41(14):1744–1761.

80. Lu, C, Cui Z, Wang Y, Li Z, Guan C, Yang B, and Shen J. Preparation and characterization of ZnS-polymer nanocomposite films with high refractive index. Journal of Materials Chemistry, 2003;13(9):2189–2195.

81. Hsiue, G.H. . Microstructural and morphological characteristics of PS-SiO2 nanocomposites. Polymer Science. 2000;41(8):2813–2825.

82. Caseri WR. Nanocomposites of polymers and inorganic particles: preparation, structure and properties. Materials Science and Technolology. 2006;22(7):807–817.

83. Ging H, Kuo W, Huang Y, and Jeng R,. Evaluation and identification of electrical and thermal conduction mechanisms in carbon nanotube/epoxy composites. Polymer Journal. 2006;47(6):2036–2045.

84. Du, F.M., et al. Nanotube networks in polymer nanocomposites: Rheology and electrical conductivity. Macromolecules. 2004;37(24):9048–9055.

85. Jiang B, Liu C, Zhang C, Wang B, Wang Z. The effect of non-symmetric distribution of fiber orientation and aspect ratio on elastic properties of composites. Composites Journal, Part B Engineering. 2007;38(1):24–34.

86. Leroux, F, and Besse J. Polymer interleaved layered double hydroxide: A new emerging class of nanocomposites, (10):Chemical Materials 2001;13(10):3507–3515.

87. Luo, J, Daniel, I. Characterization and modeling of mechanical behavior of

polymer/clay nanocomposites. Composite Science Technology 2003;63(11):1607–1616.

88. Zhu J, Fawn M, Laexander B, and Charles A. Studies on the mechanism by which the formation of nanocomposites enhances thermal stability. Chemical Materials, 2001;13(12):4649–4654.

89. Usuki A, Kojima Y, Kawasumi M, Okada Y, and Kurauchi T . Journal of Materials Research 1993;8:1179.

90. E. P. Giannelis. , 8, 29. Advanced Materials 1996;8:29.

91. Huang Y, Zhang X, Wu A, Xu H. An injectable nano-hydroxyapatite (n-HA)/glycol chitosan (G-CS)/hyaluronic acid (HyA) composite hydrogel for bone tissue engineering. Royal Society of Chemistry Advances. 2016;6(40):33529–33536.

92. Shi Z, Huang X, Cai Y, Tang R, Yang D. Size effect of hydroxyapatite nanoparticles on proliferation and apoptosis of osteoblast-like cells. Acta Biomaterialia. 2009;5(1):338–345.

93. Wang X., Grogan S.P., Rieser F., Winkelmann V., Maquet V. BML& M-VP. Tissue engineering of biphasic cartilage constructs using various biodegradable scaffolds: an in vitro study. Biomaterials. 2004;25:3681–3688.

94. Chen Y.S. KSM& YCH. A review for gelatin used for artificial nerve and bone implants. Biomedical Engineering Basis and Communication. 2009;21:233–238.

95. Usuki, A, Kojima Y, Kawasumi M, and Okada A. Synthesis of Nylon 6-clay hybrid Journal of Materials Research Cambridge Core. Journal of material research. 1993;8(5):1179–1184.

96. Usuki, A, Kojima Y, Kawasumi M, and Okada A. Mechanical properties of Nylon 6-clay hybrid. . Journal of Material research 1993;8(5):1185–1189.

97. Nanomaterials Synthesis, Properties and Applications, 2nd edn - CRC Press Book.

98. Brunier B, Sheibat-Othman N, Chniguir M, Chevalier Y, Bourgeat-Lami E. Investigation of Four Different Laponite Clays as Stabilizers in Pickering Emulsion Polymerization. Langmuir. 2016;32(24):6046–6057.

99. Okada, A. Fukushima Y, Kawasumi M, Inagaki S, Usuki, ASugiyama S, Kurauchi T, and Kamigaito O,. US Patent. 1988. p. 4,739,007.

100. Kawasumi, M, Kohazaki M, Kojima Y, Okada A, and Kamigaito O,. US Patent. 1989. p. 4,810,734.

101. Kojima, Y, Usuki A, Kawasumi M, and Kamigaito O,. Mechanical properties of nylon 6-clay hybrid Journal of Materials Research Cambridge Core. Journal of Materials Research. 1993;8((5)):1185–1189.

102. Haraguchi, K., Li H. Mechanical properties and structure of polymer-clay nanocomposite gels with high clay content. Macromolecules.

2006;39(5):1898–1905.

103. Hoffman AS. Hydrogels for biomedical applications. Advanced drug Delivery Review . 2012;64(SUPPL.):18–23.

104. Distefano MD. NIH Public Access. 2015;61(5):213–223.

105. Bocchiaro P, Zamperini A. Thermoresponsive hydrogels in biomedical applications - a review - a review. European Journal of Pharmaceutics and Biopharmaceutics Journal. 2008; 68(1): 34–45

106. Rizwan M, Yahya R, Hassan A, Yar M, Azzahari AD, Selvanathan V, et al. pH sensitive hydrogels in drug delivery: Brief history, properties, swelling, and release mechanism, material selection and applications. Polymers (Basel). 2017;9(4).

107. Yannas I V, Lee E, Orgill DP, Skrabut EM, Murphy GF. Synthesis and characterization of a model extracellular matrix that induces partial regeneration of adult mammalian skin. Proceedings of the National Academy of Sciences of the USA. 1989;86(3):933–937.

108. Helle B, and Jindich K . Polyelectrolyte Gels. 1992;480:285–304.

109. Nanomaterials S. NIH Public Access. Journal Polymer Science 2009;47(22):5929–5946.

110. Ren H, Zhu M, Haraguchi K. Characteristic Swelling Deswelling of Polymer / Clay Nanocomposite Gels. Macromolecules 2011;8516–8526.

111. Dogu Y, Okay O. Swelling-deswelling kinetics of poly(N-isopropylacrylamide) hydrogels formed in PEG solutions. Journal of Application Polymer Science 2006;99(1):37–44.

112. Omidian H, Hasherni S, Askari F, Nafisi S. Swelling and Crosslink Density Measurements for Hydrogels. Iran Journal of Polymer Science Technology 1994;3(2):115–119.

113. Cates RS. Influence of Crosslink Density on Swelling and Conformation of Surface-Constrained Poly(n-isopropylacrylamide) Hydrogels. 2010;84.

114. Yacob N, Hashim K. Morphological effect on swelling behaviour of hydrogel. AIP Conference Proceedings. 2014;1584:153–159.

115. Haraguchi K, Li H, Okumura N. Hydrogels with Hydrophobic Surfaces : Abnormally High Water Contact Angles on PNIPA Nanocomposite Hydrogels. Macromolecules 2007; 40: 2299-2302.

116. Lanasa SM, Hoffecker IT, Bryant SJ. Presence of pores and hydrogel composition influence tensile properties of scaffolds fabricated from well-defined sphere templates. Journal Biomedical Materials Research - Part B Applied Biomaterials 2011;96 B(2):294–302.

117. Thorpe AA, Dougill G, Vickers L, Reeves ND, Sammon C, Cooper G, et al. Thermally triggered hydrogel injection into bovine intervertebral disc tissue explants induces differentiation of mesenchymal stem cells and

restores mechanical function. Acta Biomaterialia. 2017;54:212–226.

118. Nguyen W, and KT J,. Photopolymerizable hydrogels for tissue engineering applications. Biomaterials. 2002;23(October 2001):4307–4314.

119. Singh A, Sharma P, Garg V, and Garg G,. HYDROGELS : A REVIEW. 2010;4(2).

120. Saxena A,. Synthetic biodegradable hydrogel (PleuraSeal) sealant for sealing of lung tissue after thoracoscopic resection. Journal of Thoracic and Cardiovascular Surgery. 2010;139(2):496–497.

121. Qiu Y, Park K. Environment-sensitive hydrogels for drug delivery. Advanced Drug Delivery Review. 2012;64:49–60.

122. Lin CC, and Metters A,. Hydrogels in controlled release formulations: Network design and mathematical modeling. Advanced Drug Delivery Review 2006;58(12–13):1379–1408.

123. Kumar A, Pandey M, Koshy M, and Saraf S,. Synthesis of fast swelling superporous hydrogel: effect of concentration of crosslinker and acdisol on swelling ratio and mechanical strength. International Journal of Drug Delivery. 2010;2(2):135–140.

124. Omidian, H.; Park K. Introduction to Hydrogels. In Biomedical Applications of Hydrogels. Handbook; London: Springer; 2010. 1-16 p.

125. Sikareepaisan P, Ruktanonchai U, Supaphol P. Preparation and characterization of asiaticoside-loaded alginate films and their potential for use as effectual wound dressings. Carbohydrate Polymers Journal, 2011;83(4):1457–1469.

126. Ramon S, Blaney PG, Creek W, Ramon S. US Patent. 1981;(19).

127. Jang J, Seol YJ, Kim HJ, Kundu J, Kim SW, Cho DW. Effects of alginate hydrogel cross-linking density on mechanical and biological behaviors for tissue engineering. Journal of mechanical behaviour of biomedical Materials. 2014;37:69–77.

128. Drury JL, Mooney DJ. Hydrogels for tissue engineering: Scaffold design variables and applications. Biomaterials. 2003;24(24):4337–4351.

129. Horbett, T., Ratner, B. and Stayton P. Polymer Edition. Journal of Biomaterials Science 2004;15(9):1081–1083.

130. Hoffman AH, Stayton · Patrick S. StaytonPatrick S., Bulmus · Volga BulmusVolga, Authors · Show 25 more, Miyata · Takashi MiyataTakashi. Really smart bioconjugates of smart polymers and receptor proteins. · Journal of Biomedical Materials Research. 2000;52(4):577–586.

131. Stefan T, Mihai T, Stefano G, and Rajiv S, . A Brief History of Contact Lens Materials. Human and Veterinary Medicine International Journal of the Bioflux Society. 2011; 3(1), 33-37.

132. Sahu NK, Gils PS, Ray D, Sahoo PK. Biodegradable Hydrogels in

Controlled Drug Delivery. An Introduction Journal 2013;3(2):22–30.

133. Trzaskowski M, Butruk B, Ciach T. Hydrogel coatings for arti fi cial heart implants Biomedical Engineering. 1863;1–4.

134. Malizos K, Blauth M, Danita A, Capuano N, Mezzoprete R, Logoluso N,. Fast-resorbable antibiotic-loaded hydrogel coating to reduce post-surgical infection after internal osteosynthesis: a multicenter randomized controlled trial. Journal of Orthopedic Traumatology 2017;18(2):159–169.

135. Zhu J, Marchant RE. Design properties of hydrogel tissue-engineering scaffolds. Expert Review Medical Devices. 2011;8(5):607–626.

136. Delorenzi C. Complications of injectable fillers, Part 2: Vascular complications. Aesthetic Surgery Journal. 2014;34(4):584–600.

137. T. Okano, Y. H. Bae, H. Jacobs SWK. Thermally on-off switching polymers for drug permeation and release. Journal of Control Release. 1990;11(1–3):255–265.

138. Sutton C. Adhesions and their prevention. Obstetrics Gynecology Journal. 2005;7(3):168–176.

139. Toh WS, Spector M, Lee EH, Cao T. Biomaterial-mediated delivery of microenvironmental cues for repair and regeneration of articular cartilage. Molecular Pharmaceutics. 2011;8(4):994–1001.

140. Toh WS. Injectable Hydrogels in Dentistry : Advances and Promises. Austin Journal of Dentistry. 2014;1(1):1–2.

141. Ferguson MW. Palate development. Development. 1988;103 Suppl:41–60.

142. Peters H, Neubüser A, Kratochwil K, Balling R. Pax9-deficient mice lack pharyngeal pouch derivatives and teeth and exhibit craniofacial and limb abnormalities. Genes Development. 1998;12(17):2735–2747.

143. Martínez-Álvarez C, González-Meli B, Berenguer-Froehner B, Paradas-Lara I, López-Gordillo Y, Rodríguez-Bobada C, et al. Injection and adhesion palatoplasty: A preliminary study in a canine model. Journal of Surgical Research. 2013;183(2):654–662.

144. Mossey PA, Little J, Munger RG, Dixon MJ, Shaw WC. Cleft lip and palate. Lancet. 2009;374(9703):1773–1785.

145. Campbell DI, Duncan WJ. The Effect of a Keratin Hydrogel Coating on Osseointegration: An Histological Comparison of Coated and Non-coated Dental Titanium Implants in an Ovine Model. Journal of Maxillofacial and Oral Surgery. 2014;13(2):159–164.

146. Haraguchi K, Takehisa T, Fan S. Effects of Clay Content on the Properties of Nanocomposite Hydrogels Composed of Poly(N - isopropylacrylamide) and Clay. Macromolecules. 2002;35(27):10162–10171.

147. Thorpe AA, Creasey S, Sammon C, Le Maitre CL. Hydroxyapatite nanoparticle injectable hydrogel scaffold to support osteogenic

differentiation of human mesenchymal stem cells. European Cells and Materials Journal. 2016;32:1–23.

148. Osada, Y.; Okuzaki, H.; Hori H. Electroactive Polymer Actuators as Artificial Muscles,. 1992. p. 245,355.

149. Yoshida R, Takahashi T, Yamaguchi T, Ichijo H. Self-oscillating gel. Journal of American Chemistry Society. 1996;118(21):5134–5135.

150. Liang L, Liu J, Gong X. Thermosensitive poly(N-isopropylacrylamide)-clay nanocomposites with enhanced temperature response. Langmuir. 2000;16(25):9895–9899.

151. Zhang C-H, Luo Y-L, Chen Y-S, Wei Q-B, Fan L-H. Preparation and Theophylline Delivery Applications of Novel PMAA/MWCNT-COOH Nanohybrid Hydrogels. Journal of Biomaterials Science, Polymer edn. 2009;20(7–8):1119–1135.

152. Jain K, Vedarajan R, Watanabe M, Ishikiriyama M, Matsumi N. Tunable LCST behavior of poly(N-isopropylacrylamide/ionic liquid) copolymers. Journal of Polymer Chemistry. 2015;6(38):6819–6825.

153. Takigawa T, Yamawaki T, Takahashi K, and Masuda T,. Change in Young's modulus of poly(N-isopropylacrylamide) gels by volume phase transition. Polymer Gels Networks. 1997;5(6):585–589.

154. Fauze A. Aouada, 1, 2 Bor-Sen Chiou, 3 William J. Orts 3 Luiz H.C. Mattoso2. Physicochemical and Morphological Properties of Poly(acrylamide) and Methylcellulose Hydrogels: Effects of Monomer, Crosslinker and Polysaccharide Compositions. Polymer Engineering Science. 2009;49:2467–2474.

155. Hamidi M, Azadi A, Rafiei P. Hydrogel nanoparticles in drug delivery. Advanced Drug deliv Review. 2008;60(15):1638–1649.

156. Ostrowska-Czubenko J. State of water in noncrosslinked and crosslinked hydrogel chitosan membranes–DSC studies. Progess Chemistry 2011;:147–156.

157. Hyon S, Cha W, and Ikada Y. Polymer Bulletin 9. Polymer Bulletin 1987;29(3):119–126.

158. Hodge R, Edward G, and Simon G. Water absorption and states of water in semicrystalline poly(vinyl alcohol) films. Polymers. 1996;37(8):1371–1376.

159. Müller-Plathe F. Different States of Water in Hydrogels. Macromolecules. 1998;31(19):6721–6723.

160. Pasqui D, De Cagna M, and Barbucci R. Polysaccharide-based hydrogels: The key role of water in affecting mechanical properties. Polymers (Basel). 2012;4(3):1517–1534.

161. Corkhill PH, Jolly AM, Ng CO, and Tighe BJ. Synthetic hydrogels: 1. Hydroxyalkyl acrylate and methacrylate copolymers - water binding studies. Polymers. 1987;28(10):1758–1766.

162. Black SB, Chang Y, Bae C, and Hickner M,. FTIR characterization of water-polymer interactions in superacid polymers. Journal of Physical Chemistry B. 2013;117(50):16266–16274.

163. Gun'ko V, Savina I, Mikhalovsky S,. Properties of Water Bound in Hydrogels. Gels. 2017;3(4):37.

164. Naohara R, Narita K, Ikeda-Fukazawa T. Change in hydrogen bonding structures of a hydrogel with dehydration. Chemical Physics Letters. 2017;670:84–88.

165. Khalid MN, Agnely F, Yagoubi N, Grossiord JL, Couarraze G. Water state characterization, swelling behavior, thermal and mechanical properties of chitosan based networks. European Journal of Pharmaceutical Sciences. 2002;15(5):425–432.

166. Hatakeyama T, Ueda C, Hatakeyama H. Structural change of water by gelation of curdlan suspension. Journal of Thermal Analaysis and Calorimetry. 2006;85(3):661–668.

167. Yudianti R, Karina M, Sakamoto M, Azuma J-I. DSC analysis on water state of salvia hydrogels. Macromol Research. 2009;17(12):1015–1020.

168. Mu F. Different States of Water in Hydrogels Macromolecules. 1998;9297(98):6721–6723.

169. Ping Z, Nguyen Q, Chen S, Zhou J, Ding Y. States of water in different hydrophilic polymers — DSC and FTIR studies. Polymers. 2001;42(20):8461–8467.

170. Higuchi, A. and Iijima T. DSC Investigation of the States of Water in Poly (Vinyl Alcohol) Membranes. Polymer. 1985;26:1207–1211.

171. Gierszewska-Druzyńska M, Ostrowska-Czubenko J, and Kwiatkowska A. Effect of ionic crosslinking on density of hydrogel chitosan membranes. Progress of chemical applications. 2013;18:49–58.

172. Djonlagic J, Lancuski A, Nikolic MS, Rogan J, Ostojic S, and Petrovic Z. Hydrogels reinforced with nanoclays with improved response rate. Journal of Applied Polymer Science. 2017;134(9):1–14.

173. You Han Bae, Teruo Okano SWK. Temperature dependence of swelling of crosslinked poly(N,N′-alkyl substituted acrylamides) in water. Journal of Polymer Science Part B Polymer Physics. 1990;28(6).

174. Feil H, Bae YH, Kim SW, Feijen J. Mutual Influence of pH and Temperature on the Swelling of Ionizable and Thermosensitive Hydrogels. Macromolecules. 1992;25(20):5528–5530.

175. Jeong B, Wan S, Han Y. Thermosensitive sol – gel reversible hydrogels. Advanced Drug Delivery Review. 2002;54:37–51.

176. Xia LW, Xie R, Ju XJ, Wang W, Chen Q, Chu LY. Nano-structured smart hydrogels with rapid response and high elasticity. National Community. 2013;4:1–11.

177. Nigmatullin R, Bencsik M, Gao F. Influence of polymerisation conditions on the properties of polymer/clay nanocomposite hydrogels. Soft Materials. 2014;10(12):2035–2046.

178. Hunt JA, Chen R, van Veen T, Bryan N. Hydrogels for tissue engineering and regenerative medicine. Journal of Materials Chemistry, part B. 2014;2(33):5319–5338.

179. Smith EL, Kanczler JM, Gothard D, Roberts CA, Wells JA, White LJ, et al. Evaluation of skeletal tissue repair, Part 2: Enhancement of skeletal tissue repair through dual-growth-factor-releasing hydrogels within an ex vivo chick femur defect model. Acta Biomaterialia. 2014;10(10):4197–4205.

180. Smith EL, Kanczler JM, Gothard D, Roberts CA, Wells JA, White LJ, et al. Evaluation of skeletal tissue repair, Part 1: Assessment of novel growth-factor-releasing hydrogels in an ex vivo chick femur defect model. Acta Biomaterialia . 2014;10(10):4186–4196.

181. Haraguchi K, Farnworth R, Ohbayashi A, Takehisa T. Compositional effects on mechanical properties of nanocomposite hydrogels composed of poly(N,N-dimethylacrylamide) and clay. Macromolecules. 2003;36(15):5732–5741.

182. Paula Andrade-Vivero 1, Elena Fernandez-Gabriel 1, Carmen Alvarez-Lorenzo 1 AC. Improving the Loading and Release of NSAIDs from pHEMA Hydrogels by Copolymerization with Functionalized Monomers. Journal of Pharmaceutical Science. 2007;96(4):802–813.

183. El-Din HMN. Characterization and Caffeine Release Properties of N-isopropylacrylamide/Hydroxypropyl Methacrylate Copolymer Hydrogel Synthesized by Gamma Radiation. Journal of Applied Polymer Science. 2011;119:577–585.

184. Mohammad M. Fares AAO. Lower Critical Solution Temperature Determination of Smart, Thermosensitive N–Isopropylacrylamide-alt-2–Hydroxyethyl Methacrylate Copolymers: Kinetics and Physical Properties. Journal of Applied Polymer Science. 2008;110:2815–2825.

185. Ina G. US Patent (1970), (19).

186. Enzymes P. US Patent (1980);96(19):62–6.

187. Whiteman KR, Subr V, Ulbrich K, and Torchilin VP. Poly(HPMA)-coated liposomes demonstrate prolonged circulation in mice. Journal of Liposome Research. 2001;11(2–3):153–164.

Chapter - 2

Experimental work

2. Overview

This chapter outlines the materials and methods used in this thesis and include relevant information about the instrumentation and data analysis.

2.1 Materials used in hydrogel synthesis

N-Isopropylacrylamide 99% (NIPAM), hydroxyethyl methacrylate (HEMA) and hydroxypropyl methacrylate (HPMA) monomers and 2-2'-azobisisobutyronitrile (AIBN) initiator were purchased from SIGMA-Aldrich and used without further purification. Inorganic clay, the synthetic hectorite Laponite RD®, was supplied by BYK Additives Ltd, Cheshire UK and used without any further treatment. Hydroxyapatite nano particles (<200 nm) 10 wt. % in water (HAPna), was purchased from sigma-Aldrich and mixed homogenously with hydrogels directly without further purification. All water was 18 MΩ, distilled and deionised prior to use.

2. 2 Hydrogel synthesis

Laponite® (1g) was dispersed in deionised water (90g) by continual stirring for 24 hours. N-Isopropylacrylamide 99% (NIPAM) (2.34g) and 2-2'-azobisisobutyronitrile (AIBN) (0.0234g) were added to the Laponite® \water suspension (23.66g) and left to stir. After one hour, the suspension was filtered using 5-8 µm pore filter paper and the liquid was placed in a sealed glass vial with no headspace to minimise oxygen content. Polymerisation was initiated by heating to 80±2 °C in an oil bath and allowed to propagate for 24 hours. The final product was a milky low viscosity injectable hydrogel with a composition of 1% wt. Laponite®, 9% wt. pNIPAM and 90% wt. water (referred to as L-pNIPAM (1)).

2.2.1 Modification of hydrogel composition

This study investigated the effect of comonomers and Laponite® concentrations on the morphological, mechanical and influence on cellular behaviour of the hydrogels. Specifically: hydroxyethyl methacrylate (HEMA) and hydroxypropyl

methacrylate (HPMA) were incorporated as comonomers at different concentrations (5, 10, 12 and 17 wt. %) of total monomer. Four Laponite® concentrations were used in this study (0.5, 1, 1.5 and 2%), where water content was 90% for all chemical compositions. After polymerisation reaction was finished, initial observation was performed on each composition to evaluate injectability of the hydrogels, where the highest Laponite® concentration was found not injectable due to exist of sediments. Similarly, was found in the hydrogels contained 12 wt. % HEMA and 17 wt. % HPMA, hence no further characterisations were performed on these compositions.

In some hydrogel compositions, synthetic hydroxyapatite nanoparticles (HAPna) was incorporated, at concentration of 0.5mg/ml, as this concentration was optimised by Thorpe A. *et al*(1). In all synthesised hydrogel compositions no additional purification steps, to remove the possible residual monomer units, were taken prior to use.

Sample codes and corresponding chemical compositions of all hydrogels synthesised and examined are given in table 2.1.

Table 2.1: Formulations of all pNIPAM based Laponite® hydrogels used in this study.

Sample code	Overall composition w/w	
	Laponite®	monomer
L-pNIPAM (0.5)	0.5%	9.5% NIPAM
L-pNIPAM (1)	1%	9% NIPAM
L-pNIPAM (1.5)	1.5%	8.5% NIPAM
L-pNIPAM (2)	2%	8% NIPAM
L-pNIPAM$_{95}$-co- HPMA$_5$(0.5)	0.5%	9.025%NIPAM, 0.475%HPMA
L-pNIPAM$_{90}$coHPMA$_{10}$(0.5)	0.5%	8.55%NIPAM, 0.95%HPMA
L-pNIPAM$_{83}$-co-HPMA$_{17}$(0.5)	0.5%	7.885%NIPAM,1.615%HPMA
L-pNIPAM$_{95}$-co-HEMA$_5$(0.5)	0.5%	9.025%NIPAM,0.475%HEMA
L-pNIPAM$_{90}$-coHEMA$_{10}$(0.5)	0.5%	8.55%NIPAM, 0.95%HEMA
L-pNIPAM$_{88}$-coHEMA$_{12}$(0.5)	0.5%	8.36%NIPAM,1.14%HEMA
L-pNIPAM$_{95}$-co- HPMA$_5$(1)	1%	8.55%pNIPAM,0.45%HPMA
L-pNIPAM$_{90}$-co- HPMA$_{10}$(1)	1%	8.1%pNIPAM, 0.9%HPMA
L-pNIPAM$_{83}$-co-HPMA$_{17}$(1)	1%	7.47%pNIPAM, 1.53%HPMA
L-pNIPAM$_{95}$-co-HEMA$_5$(1)	1%	8.55%pNIPAM, 0.45%HEMA
L-pNIPAM$_{90}$-co- HEMA$_{10}$(1)	1%	8.1%pNIPAM, 0.9%HEMA
L-pNIPAM$_{88}$-co- HEMA$_{12}$(1)	1%	7.92%pNIPAM, 1.08%HEMA
L-pNIPAM (0.5) hap	0.5%	9.5% NIPAM
L-pNIPAM (1) hap	1%	9% NIPAM
L-pNIPAM (1.5) hap	1.5%	8.5% NIPAM
L-pNIPAM$_{90}$coHPMA$_{10}$(1) hap	1%	8.55%NIPAM, 0.95%HPMA

2.3 Characterisation techniques and instrumentation

2. 3.1 Dynamic Mechanical Analysis (DMA)

Dynamic mechanical analysis (DMA) is a characterisation technique used to test the mechanical properties of a material as a function of temperature, time, frequency and stress(2). This technique applies a small sinusoidal force, to a sample of known geometry. The response and deformation to the applied force is recorded and the modulus of elasticity (E) calculated according to the following equations:

σ (stress) = F (force) / A(cross section area) (2.1)

ε (strain) = Δ L / L (2.2)

E = slope = σ/ε (2.3)

Where L and Δ L are the original Length and changing in length respectively.

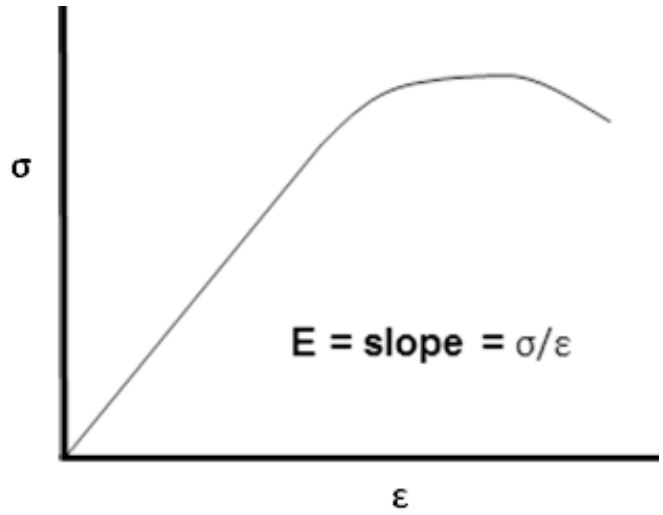

Figure 2.1: Stress - strain curve relate applied force to deformation

Moduli calculate using DMA are not exactly the same as elastic moduli that calculated using stress-strain curves (Figure 2.1). Dynamic mechanical analysis calculates different moduli: a complex modulus (E*), storage modulus (E') and loss modulus (E''). Storage modulus (E') is defined as the energy that is stored during a loading cycle, whereas loss modulus (E'') represents the dissipated energy(3).

The ratio of loss modulus to storage modulus is referred to as the tan delta (tan δ), which is the energy dissipated by the measured sample. DMA instrumentation consists of a displacement sensor, such as a linear variable differential transformer, that measures the changes in voltage as a result of the instrument probe moving through a magnetic core, a temperature control system, a drive motor which is a linear motor for probe loading, which provides load for the applied force (Figure 2.2). Depending on the geometry and nature of the measurement, samples will be prepared and handled differently(2,3), e.g. for compression measurements, the sample is prepared in a cylindrical shape, whilst for tensile testing samples would have a dog bone shape.

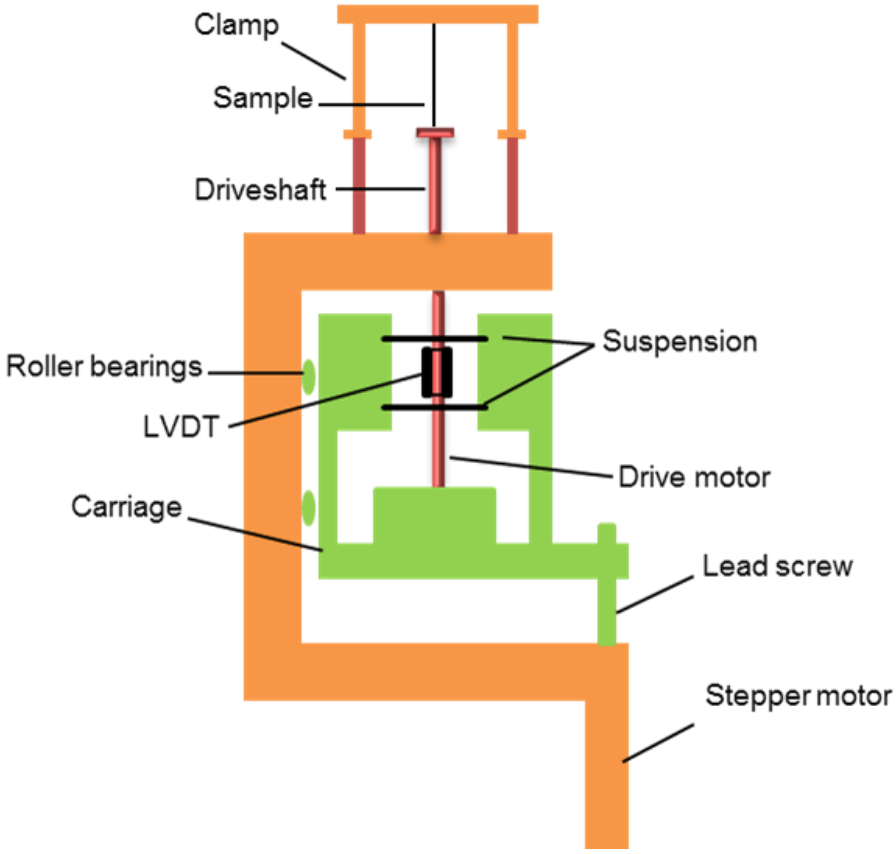

Figure 2.2: General schematic of the primary components of DMA instrument adapted from(4)

2. 3.1.1 Dynamic Mechanical Analysis (DMA) experimental parameters and method

DMA was used to explore the viscoelastic behaviour of pNIPAM based Laponite® hydrogels, with a range of chemical compositions which were studied, using (PerkinElmer DMA 8000) with frequency testing type (0.063 - 10 Hz), in compression mode at 25 ˚C. Hydrogel samples were freshly prepared and pipetted in the liquid state directly into an in-house designed sample holder, which is ~ 3 mm in depth and 5 mm diameter (Figure 2.3). Subsequently, the hydrogel was allowed to solidify for 2 hours at RT and 98% relative humidity (RH). Sinusoidal force was applied with 0.02 mm displacement. Six replicates for each sample were measured.

The standard method of Measuring storage Young's modulus is to apply unconfined compression force between two parallel compression plates. In the current work confined compression test set-up was employed for DMA does not strictly measure storage Young's modulus due to the triaxial stress condition

imposed by the walls of the sample holder when axial compression is applied (Figure 2.3). However, for the purposes of this thesis, the term storage Young's modulus is employed.

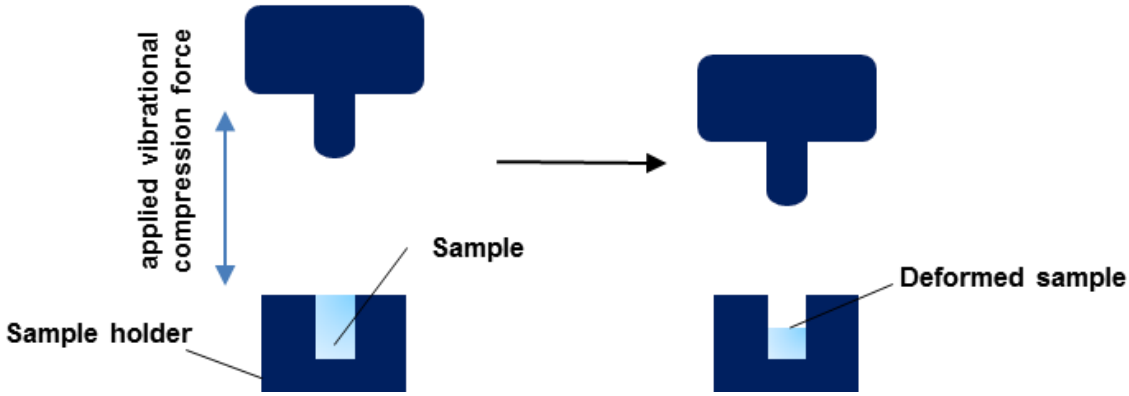

Figure 2.3: A simple schematic illustration of compression test of hydrogel sample.

2.3.2 Scanning electron microscopy

High resolution topographical 3D images can be obtained by focusing a primary electron beam, which has an intrinsically short wavelength, at a particular point on the sample's surface and then measuring the resulting secondary or back scattered electrons with suitable detectors(5).

Incident electron collisions with the sample's surface result in removal of an inner shell electron from one of the elements of the sample. The removed electron's energy emission as X-ray scatters from the sample surface. The amount of this energy depends on the element that has been scanned by the primary electron beam, and the size, shape and texture of the sample. The rest of the primary electron beam scatters from the sample into different ways; including: auger, cathodeluminescence, backscattered and the secondary electron beam, which provides information about the samples topography and chemical composition. The secondary electron beam is backscattered and collected by detectors which generate three dimensional surface image (Figure 2.4).

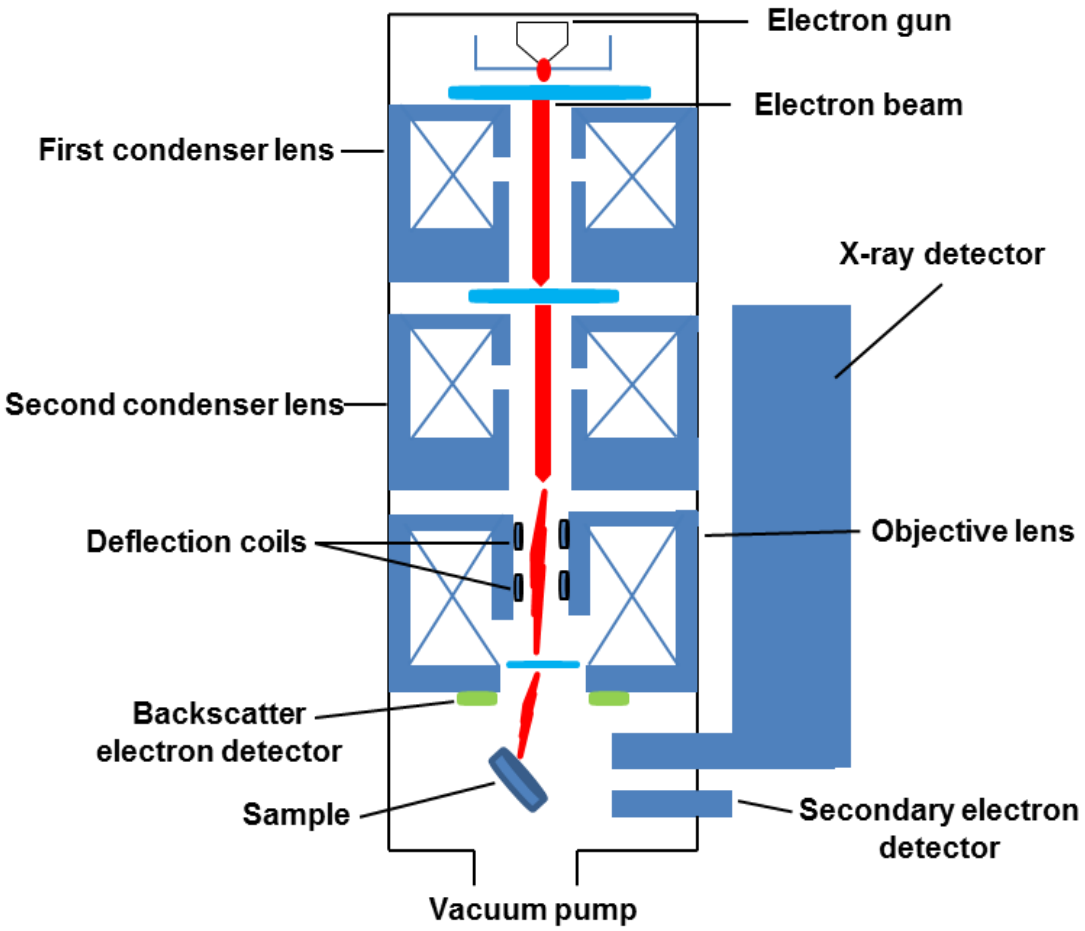

Figure 2.4: A Schematic of scanning electron microscopy method adapted from(6)

2.3.2.1 Scanning electron microscopy (SEM) parameters and method

All samples were flash frozen in liquid nitrogen for 5 minutes and subsequently freeze dried overnight using (FD-1A-50) and fractured into two or more pieces to obtain cross-sectional edges, where scanned piece of sample's diameter ≈ 5 mm.

Samples were then mounted onto aluminium stubs and gold coated using (Q150T-ES sputter coater (Quorum, UK) (10lA sputter current for 190 s with a 2.7 tooling factor).

Scanning electron microscope (FEI NOVA nano SEM 200), was used to capture images of hydrogel samples in low vacuum mode, with an operational water vapour pressure of 0.8-1 Torr, accelerating voltage of 5-7KV, spot size of 4 and magnification between 100 - 20000 X.

2.3.3 Fourier Transform Infrared (FTIR) Spectroscopy

FTIR is widely used in organic and inorganic chemistry, polymer science, and the pharmaceutical industry to provide information about chemical composition. It is a characterisation technique that provides information based on the ability of each different chemical compound to absorb infrared radiation at different frequencies, which correlates to vibrational energy levels of functional groups of different compounds within the sample(7).

In the electromagnetic spectrum, infrared radiation has a wavelength of 700 nm -1mm; which can be divided into near IR 0.78- 2.5 µm, mid-IR 2.5 – 50µm and far-IR 50-1000 µm. This wavelength is presented as wavenumber in infrared spectroscopy with cm^{-1} unit and wavenumber equal to $1/\lambda$ (cm^{-1})(3). However, the most applicable range for chemical analysis is mid-infrared 2.5 µm and 25 µm (4000 to 400 cm^{-1}), which include the frequencies correlated to the vibrations of nearly all of the functional groups of organic molecules(7,10).

2. 3.3.1 FTIR working theory:

FTIR spectrometers are based on the Michelson interferometer, which works as follows.

1) A broad band infrared beam is emitted from a source, typically a globar. The beam goes to a beam splitter which splits the beam into two parts. The first part is transmitted to a moving mirror, the other part to a stationary mirror.

2) The recombined wavelengths combine constructively and destructively making an interference pattern, known as an interferogram.

3) The recombined infrared beam is directed onto the sample. The components of the sample absorb some energy and the rest is transmitted or reflected depending on the sampling geometry of any sampling accessory used e.g. attenuated total reflectance (ATR).

4) After interaction with the sample any remaining energy goes to the detector, these are typically mercury cadmium telluride (MCT) or deuterated triglycine sulfate (DTGS) detector elements, the information about each wavelength is read by the detector in the infrared range.

5) The detector sends the information as signals to the computer that is connected with the FTIR instrument where it can be processed (Figure 2.5). The output of an interferogram is an interference pattern with an imposed time signal. By performing a Fourier transform on this data a single beam spectrum is generated. The instrument specific response can be removed from the single beam spectrum by ratioing the sample single beam by the blank single beam.

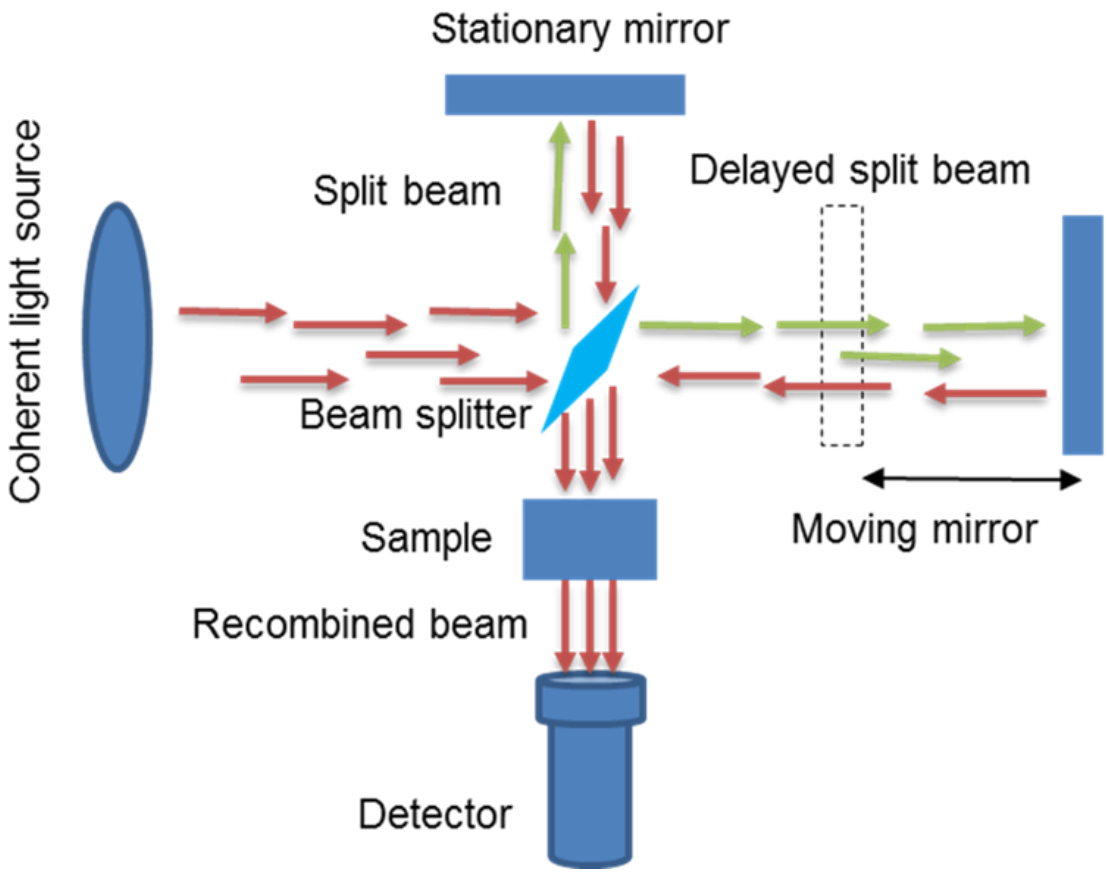

Figure 2.5: Simple schematic scheme illustrating ATR - FTIR spectroscopy, adapted from (9)

2.3.3.2 Attenuated Total Reflectance - Fourier Transform Infrared Spectroscopy (ATR -FTIR)

When light propagates through a material with a high refractive index (n_1), at an angle (θ_{inc}) bigger than the critical angle (θ_c), then it will be totally internally reflected at the interface of a material with a lower refractive index (n_2). Upon reflection an evanescent wave will be created, which decays exponentially with

distance from the surface into the sample. The depth that the evanescent wave penetrates into the sample is known as the depth of penetration (d_p) and is given by equation 2.4.

$$dp = \frac{\lambda_1}{2\pi\left(sin^2\,\theta_{inc} - n_{21}^2\right)^{1/2}} \qquad (2.4)$$

Where: θ_{Inc} is angle of incidence, λ_1 is wavelength of radiation in high RI medium ($\lambda 1 = \lambda / n1$).

n_{21} is the ratio of the RI of the sample (n_2) and the RI of ATR crystal (n_1).

Real penetration depth is approximately 3Dp (effective sample thickness).

This technique is used when there is a sample which is difficult to be analysed by transmission, due to excessed thickness or high ability of absorption (Figure 2.6). However, good contact with crystal is needed due to a limited ability of IR to transmit through the sample (few micrometres).

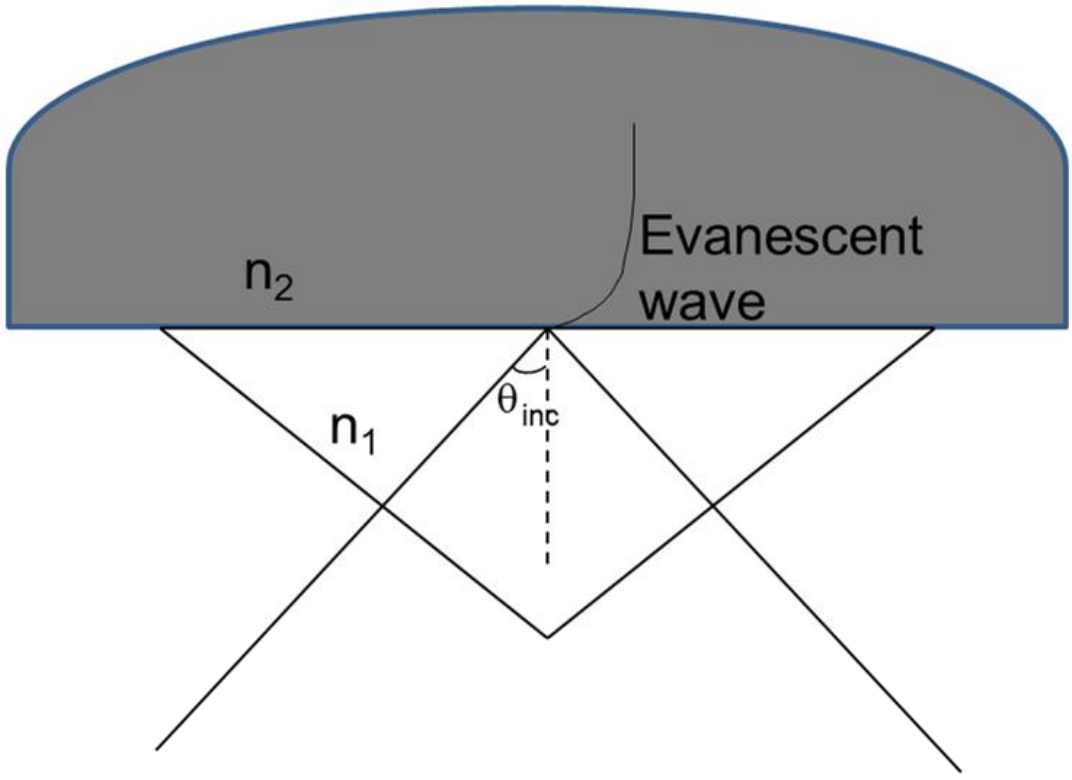

Figure 2.6: Schematic of ATR measurement of polymer samples

2.3.3.3 Dehydration and rehydration methods

All samples were investigated using a Nexus FTIR instrument (Thermo Nicolet Corp., USA) coupled to a Graseby single reflection diamond ATR cell to analyse the chemical composition of each sample and the dehydration-Rehydration behaviour of pNIPAM hydrogel samples. Each FTIR spectrum was recorded between 500 and 4000 cm^{-1}. Samples were prepared by pipetting 30µl of liquid hydrogel directly onto the diamond ATR crystal and allowing it to dry.

Data collection was immediately started by collecting one spectrum every 30 second for up to 800 minutes, with 8 scans per spectrum at a resolution of 8 cm^{1} on a Thermo Nicolet Nexus instrument, using a series setup, decrease in intensity of ν (OH) band between 3600-3100 cm^{-1}, increase in NH band at 1550 cm^{-1} were being monitored in real time during hydrogel drying (Figure 2.7). Both bands represent water contents and polymer concentration respectively. ν(OH) band intensity was plotted as function of time to display dehydration rate of hydrogel sample (Figure 2.8). Three samples of each different composition were used in this experiment, to analyse dehydration behaviour of pNIPAM based Laponite® hydrogel.

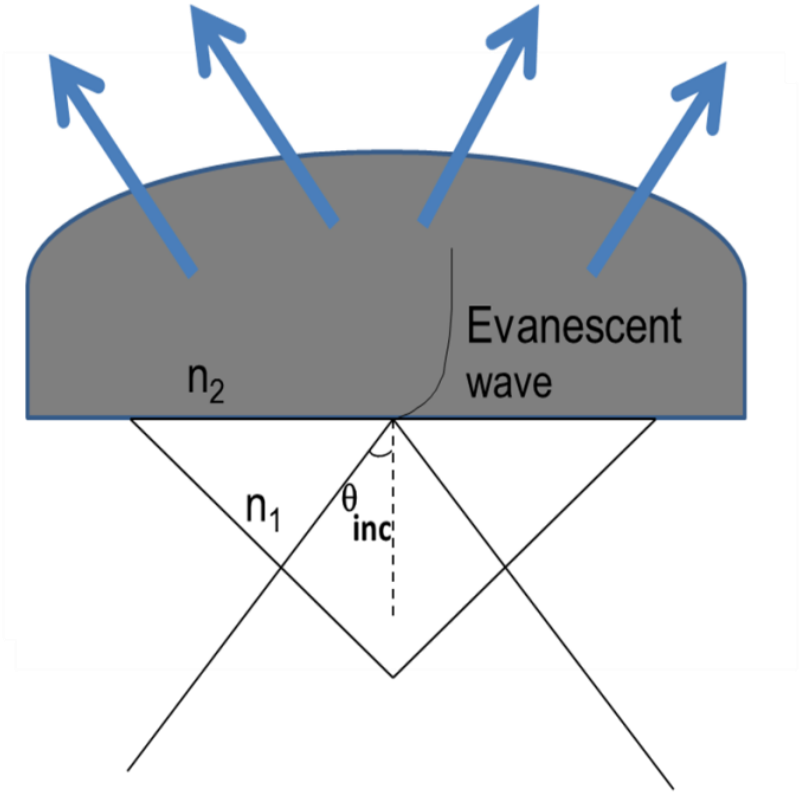

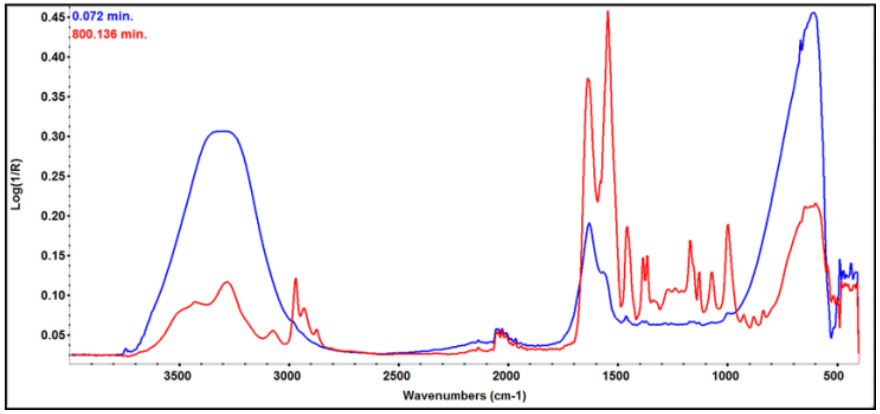

Figure 2.7: Dehydration experiment schematic of L-pNIPAM (1) hydrogel at 25˚C, showing first and last spectrum.

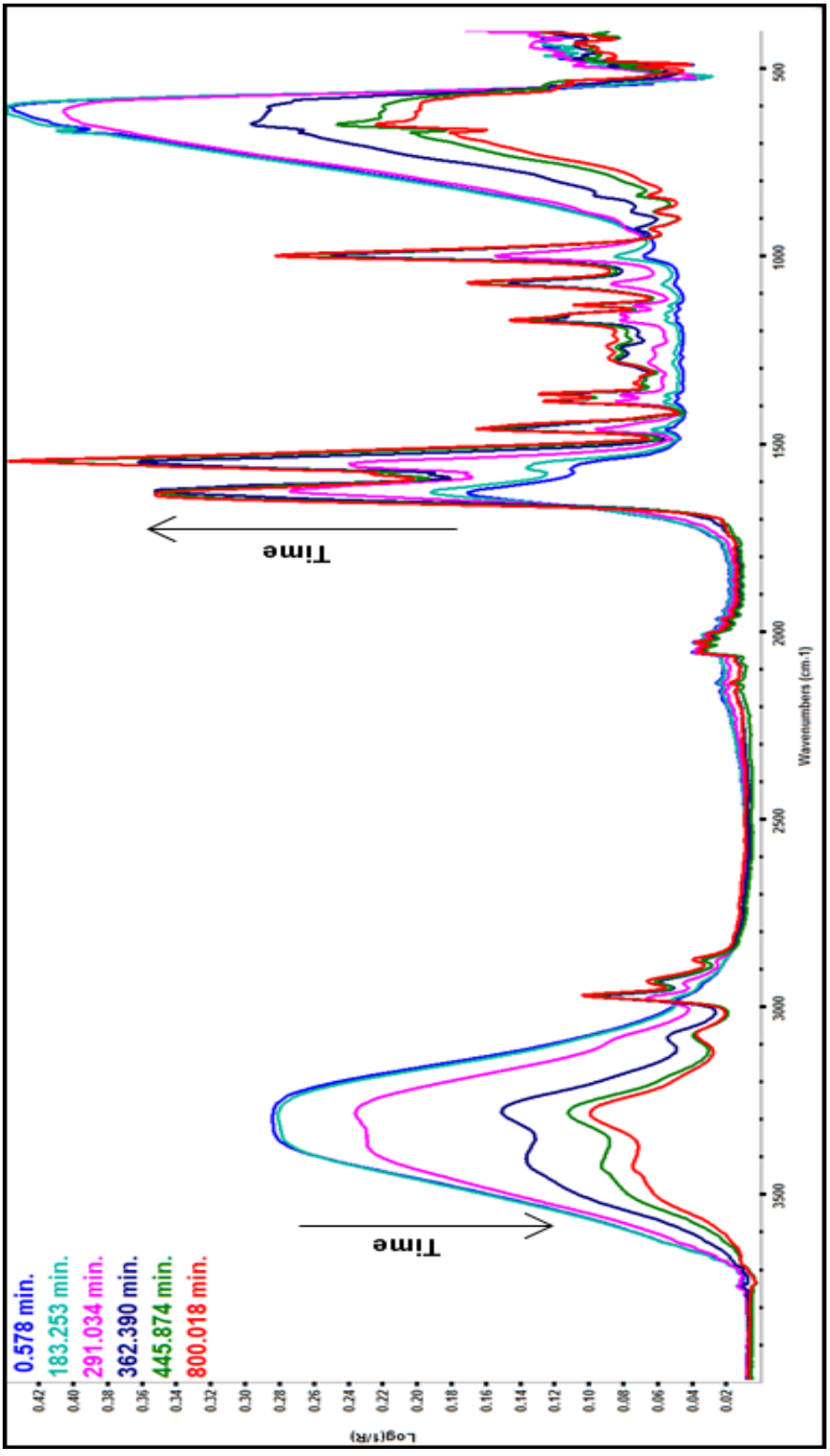

Figure 2.8: Full spectra of water evaporating from L-pNIPAM (1) hydrogel at 25˚C.

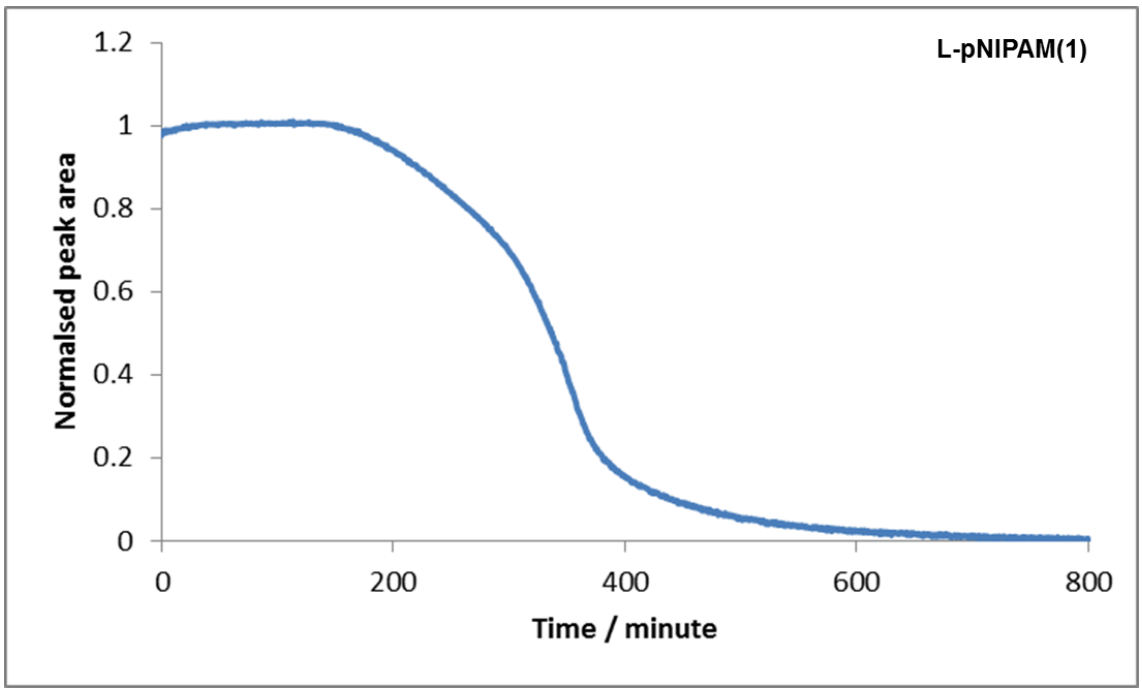

Figure 2.9: Intensity of ν (OH) during dehydration of hydrogel samples

Rehydration was performed by putting deionised water into contact with a previously dried sample using a liquid cell holder. Spectra were collected every 30 seconds for up to 240 minutes, and the same bands were monitored to observe changes in ν(OH) and NH bands. All experiments were conducted using 8 scans at a resolution of 8 cm^{-1}.

FTIR-ATR can successfully be used as a method to determine the dehydration and rehydration rates of polymeric samples. When the polymer sample (*l*) is thicker than dp (equation 2.4) water will only be observed when it enters or leaves the evanescent field. This means that by monitoring the few microns closest to the ATR crystal one can relate these changes to hydration/dehydration processes. During these processes one also observed the polymer therefore swelling/deswelling and interactions between the water and polymer can all be monitored simultaneously. However it is critical to maintain intimate contact between the sample and the ATR crystal to ensure the quality of results. If the sample loses contact with the ATR crystal during an experiment, then this will result in anomalous data being recorded.

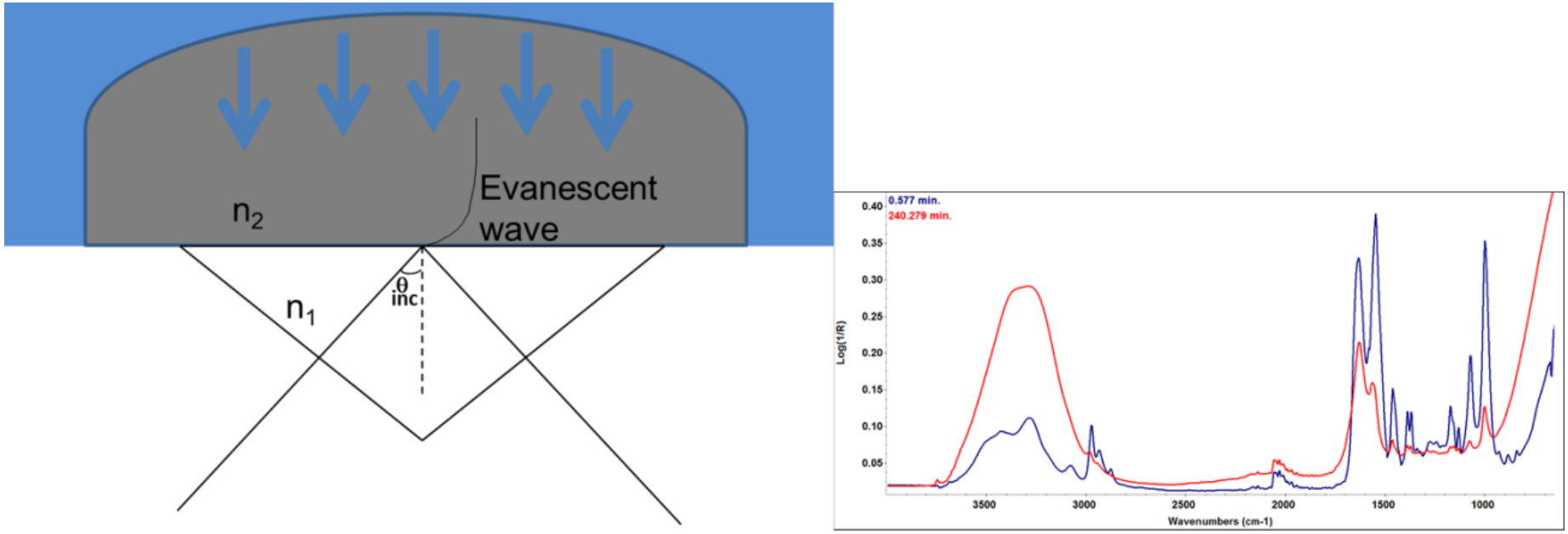

Figure 2.10: Rehydration experiment schematic of L-pNIPAM (1) hydrogel at 25˚C, showing first and last spectrum.

2.3.4 Differential scanning calorimetry

Differential scanning calorimetry (DSC) is a technique used to investigate thermal energy changes of materials(11). DSC consists of two separate chambers with two pans: one for the sample and one for a reference, liquid nitrogen tank for cooling, heater for heating and PC unit with installed software to monitor and control the experiments (Figure 2.7).

Differential thermal analysis (DTA) is a principal by which DSC can compare the amount of energy required to change sample's phase, with reference that has a known thermal behaviour. The working theory of DSC uses the fact that to heat or cool the sample and the reference at the same rate, it is necessary to adjust the heat flow that is required to keep the temperature of both pans the same when the material is undergoing a phase/state change(12).

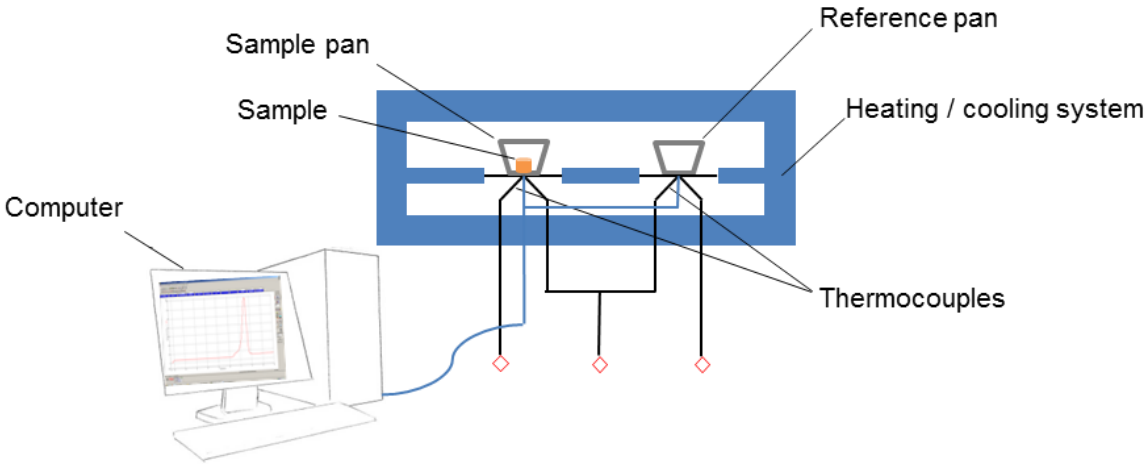

Figure 2.11: A schematic drawing of Differential scanning calorimetry adapted from(11)

2.3.4.1 Differential scanning calorimetry parameters and method

The state of water in L-pNIPAM hydrogel with different crosslink densities was determined using differential scanning calorimetry (Perkin Elmer DSC 8000), equipped with a liquid nitrogen cooling accessory. The DSC cell was calibrated using deionized water. Three to 10 mg of hydrogel was poured into a DSC aluminium hermetic pan and sealed firmly using an aluminium pan cover to prevent water loss during the experiment. The sample in the pan was firstly cooled to -63°C, and subsequently heated to 30°C, at a rate of 10 °C/min. The

phase transition of the water in the hydrogel sample during heating was recorded as the endothermic peak, which integrated later using commercial software (Pyris series-DSC 8000). The freezable water fraction was then calculated using equation 2.5:

$$X_{BW} = X_{TW} - \left(\frac{Q_{endo}}{Q_f}\right) \quad (2.5)$$

Where: X_{BW} is the bound water fraction in the hydrogel, X_{TW} is the total water fraction in the hydrogel, Q_{endo} is the heat of fusion for freezable water in hydrogel that obtained from the DSC-thermogram (J/g) and Q_f is the heat of fusion of pure water (333 J/g).

2.3.5 Contact angle measurements

Contact angle on glass slides (Leica Microsystem Milton Keynes, UK) and water contact angle of different hydrogel compositions were determined using a Data Physics OCA 15EC contact angle instrument. A drop of hydrogel (30 µl) was placed on a dry clean microscope slide, an image was immediately captured via CCD camera and the hydrogel contact angle was measured using (Dataphysics instruments GmbH, 2007, Germany). Four measurements of each composition were recorded and the average value calculated.

For hydrogel wettability, the water contact angle (WCA) of hydrogel was conducted as follows: Spin coated samples for different L-pNIPAM based compositions were prepared. To make L-pNIPAM films, 60 µl of hydrogel was placed on a glass slide (Leica Microsystem Milton Keynes, UK) at 50°C. Using spin coating system (Electronic Micro Systems (EMS), England, Quorum, Q300T T) hydrogel was spin coated at 1000 rpm onto the surface of the glass slide, forming a homogenous polymer composite film.

A drop of distilled water (20 µl) was placed on the spin-coated hydrogel surface, four contact angle measurements (tensile drop method) of each composition were recorded and the average determined.

2.3.6 Raman spectroscopy

In 1928 Chandrasekhar Venkata Raman discovered the phenomenon which takes his name; using sunlight as the source and his eyes as the telescope and collector(13). Raman spectroscopy can most simply be described as the inelastic scattering of light. Photons scattered by a molecule can either be scattered elastically (Rayleigh scattering), lose energy to the molecule (Stokes scattering) or gain energy from the molecule (anti-Stokes scattering). Modern Raman spectrometers use a laser as the source, holographic filters to remove the Rayleigh light and have one or more gratings to separate the inelastically scattered light into its constituent wavelengths(14). The magnitude of the shifts observed in the Raman experiment equates to changes in the vibrational energy levels of the molecule and the output is analogous to infrared spectroscopy.

Raman spectroscopy can be used to investigate structure and the physical state of organic and inorganic molecules.

In medical and biological studies Raman spectroscopy is used by researchers to diagnose diseases in cells, by investigating changes in their molecular composition(15). In addition, Raman has been used to observe the major components of bone such as matrix collagen and mineral phosphate to help in understanding the pathogenesis of bone diseases such as osteoporosis and osteosclerosis(16,17), and to compare between natural bone to synthetic substitutes such as hydroxyapatite and tricalcium phosphate(18).

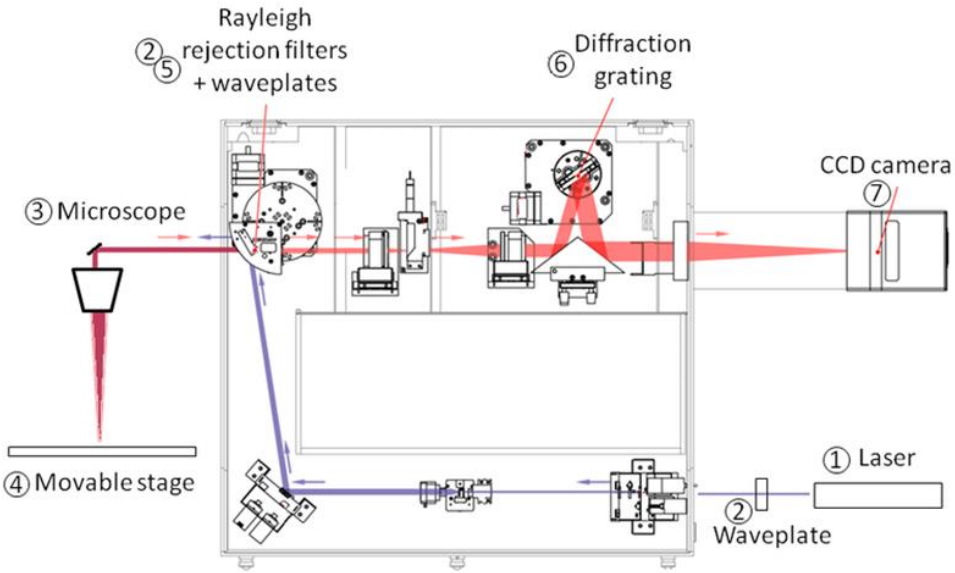

Figure 2.12: Schematic of Renishaw InVia Raman microscope(19)

2.3.6.1 RAMAN spectroscopy parameters and method

Samples were mapped using Raman microscopy was performed using a Thermo Fisher Scientific DXR™ 2 Raman Microscope. In order to distinguish between free calcium and calcium phosphate, in hydrogel samples contained hMSCs and acellular hydrogels, 4 µm sections were mounted onto quartz microscope slides (Alfa Aesar, USA). Sections were allowed to dry for 24 hours at 37°C, then Raman microscopy was used to perform mapping for each section, Raman microscope conditions and parameters were as follow:

10 X objective lens was used, 500 x 500 µm mapped area, 10 µm spacing between points (step size), collect exposure time of 5 seconds, laser power 10mw,sample exposure time of 5 seconds, wavenumber (spectrum range) was 50 - 350 cm^{-1} and number of collection 10 x 10.

2.3.7 Swelling ratio measurement

The determination of the swelling capacity of hydrogel samples was performed gravimetrically. Three replicates of pre-weighed dry hydrogel discs (~0.5mg), 10 mm ø x 20 mm length from each different composition were studied. Samples were stored in glass vials under 10 ml of distilled water at 25°C and at pre-determined time intervals, over a period of up to 24 hours, the change in mass was determined. Swollen hydrogels were removed and excess water was

blotted from the samples surfaces, by using meshing tissue to facilitate transfer of the swollen samples from water to weighing scales. The change in sample mass was subsequently recorded and the gravimetric time-dependent swelling ratio was calculated according to equation 2.6.

$$\text{Percentage Swelling } (\%) = \frac{W_t - W_0}{W_0} \times 100 \quad (2.6)$$

Where W_t is the weight of swollen gel at time t, and W_0 is the initial weight of initial Hydrogel sample(20).

2.3.8 Deswelling measurement

A deswelling experiment was performed using graduated glass cylinders, where exactly 2ml of each hydrogel composition was measured using a suitable pipet, and poured into prewashed and dried graduated glass cylinders and allowed to set for 10 minutes, at room temperature. Hydrogel samples were then covered with deionised water (2ml) at 62 °C and maintained at 62 °C for 24 hours, images were captured at 10, 30, 60, 120, 240, 360, 480 and 1440 minutes. The captured images were analysed using ImageJ version number 150 software to measure the outer dimensions of each sample at different time points.

Dimensional time-dependent deswelling ratio was determined for each composition according to equation 2.7.

$$\text{Percentage deswelling } (\%) = \frac{D_i - D_t}{D_i} \times 100 \quad (2.7)$$

Where D_t is the outer dimensions of de-swollen gel at time t, and D_i is the initial outer dimensions of control sample.

2.4 Lower critical solution temperature measurements

Lower critical solution temperature is an important characteristic for thermoresponsive polymers such as pNIPAM, where the polymer chains undergo coil to globule conformation changes during sol to gel transformation around the LCST which is ~32°C as mentioned previously in Chapter 1.4. Thermally responsive polymers are applicable in different fields, one of which is tissue regeneration, where injectable hydrogels potentially used to deliver cells/drugs into human body. Therefore, LCST is crucial to be understood and consider when development for this material is needed. In the current study LCST was measured using digital thermometer with ultra-thin needle probe

(Ø1.1 x 60 mm) (Sous Vide Thermapena, UK). Three millilitre of each hydrogel composition was poured into glass vial at 55°C, needle probe was immersed immediately into the liquid hydrogel and changes in sample temperature was observed until solidification was detected, by either transparency or increase the hydrogel viscosity.

2.5 Surface roughness measurements

Surface roughness is a crucial characteristic for scaffold materials, due to its correlation to other properties such as; surface biocompatibility, fluid adhesion (23). In the current work surface roughness of pNIPAM based Laponite® hydrogels was measured using atomic force microscopy (AFM) and infinite focus microscopy (IFM).

2.5.1 Atomic force microscopy measurements (AFM)

Spin coated samples for different L-pNIPAM based compositions were prepared. To make L-pNIPAM films, 60 µl of hydrogel was placed on a glass slide (Leica Microsystem Milton Keynes, UK) at 50°C. Using a spin coating system (Electronic Micro Systems (EMS), England, Quorum, Q300T T) the hydrogel was spin coated at 1000 rpm onto the surface of the glass slide, forming a flat polymer composite film. AFM Bruker multimode was used to identify the topography of L-pNIPAM films, using tapping mode with a scanning range of 2 X 2 μm^2.

2.5.2 Infinite focus microscopy measurements (IFM)

Hydrogel samples were prepared by pipetting 60 ml of each different hydrogel composition on a glass slide (Leica Microsystem Milton Keynes, UK) at 50°C, and allowed to solidify overnight at room temperature. 3-D images of each L-pNIPAM film with different crosslink density was used to measure average surface roughness, using infinity focus microscope with measurement settings as follows: exposure time of 2.85 ms, magnification at 50x, estimated vertical resolution at 11.991 nm and estimated lateral resolution at 5.0096 µm.

2.6 Cell culture within Poly (N-Isopropylacrylamide) - Based Laponite® Hydrogels

Rat stem cells were used initially to screen cytocompatibility of the different pNIPAM based Laponite® hydrogels. Once cytocompatibility was confirmed, further cell studies were conducted using human mesenchymal stem cells (hMSCs).

2.6.1 Cell culture

Rat stem cells (extracted in the lab and supplied by Dr. Abbey Thorpe) and human mesenchymal stem cells (Lonza) were maintained in DMEM media (Life Technologies, Paisley UK) supplemented with 10% v/v heat inactivated foetal calf serum (FCS)(Life Technologies, Paisley UK), 100U/ml Penicillin (Life Technologies Paisley UK), 100 µg /ml Streptomycin (Life Technologies Paisley, UK), 250 ng/ml amphotericin (Sigma, Poole UK), 2 mM glutamine (Life Technologies, Paisley UK) and 10 µg/ml ascorbic acid (Sigma, Poole UK) (complete cell culture media). Cells were expanded in monolayer culture upto passage 9 to ensure sufficient cells were available.

Subsequently, cells were seeded at density of 1 X 10^6 cells / ml either layered on or suspended into different compositions of Poly (N-Isopropyl acrylamide) - Based Laponite® Hydrogel (L-pNIPAM (0.5),L-pNIPAM (1), L-pNIPAM (1.5), L-$pNIPAM_{90}$-co- HPA_{10}(1) and L-$pNIPAM_{90}$-co- $HEMA_{10}$(1)) with and without hydroxyapatite incorporated into the hydrogel as differentiation factor(21).

To prepare layered cultures, 300µL of hydrogel was added to each well of the 48 well plates and allowed to solidify at room temperature for 10 minutes. Subsequently, 300 µL of cells at a cell density of 1 X 10^6 cells/ml in complete media was applied to the surface of each well and further 100 µL of media was added. Then, the plates were incubated at 37 °C and 5% CO_2 and maintained in culture up to 14 days.

To prepare cells/hydrogel suspension, cells were suspended into the hydrogel at cell density of 1 X 10^6 cells/ml and temperature of 37°C. Thereafter, cells/hydrogel suspension was mixed homogeneously, and 300 µL of cells/hydrogel was added into each to each well of the 48 well plates and allowed to solidify at room temperature for 5 minutes. 100 µL of complete

media was added. Subsequently, the plates were incubated at 37 °C and 5% CO_2 and maintained in culture up to 14 days.

2.6.2 Cytocompatibility assessment of hydrogel scaffolds

Metabolic cell activity of L-pNIPAM hydrogels was determined following 0, 2 and 7 days of culture in normal media, cultured in 5% O_2 at a density of 1 x 10^6 cells/ml were assessed using Alamar blue assay (Life Technologies, Paisley UK), where the manufacture's protocol was followed. Fluorescent intensity was recorded using a fluorescence microplate reader (CLARIOstar, BMG LABTECH), with fluorescence excitation wavelength of 590 nm. Corresponding units of fluorescence were recorded and normalised to acellular control hydrogels and used to determine cytocompatibility. Alamar blue is an assay reagent for cell viability, which contains fluorescent nontoxic blue dye. The dye works as an oxidation-reduction indicator, which exhibits varied colorimetric responses to cellular metabolic reduction. The fluorescence intensity is proportional to the live cells number(22).

2.6.3 Matrix deposition within hydrogel's structure

Matrix deposition was investigated in different compositions of L-pNIPAM hydrogel, with and without cells following 48 hours, 2 and 4 weeks incubation. For each composition, triplicate samples were removed from culture and fixed in paraformaldehyde/PBS (4% w/v) overnight. Samples were then washed in PBS prior to embedding in paraffin wax using TP1020 tissue processor (Leica Microsystems, Milton Keynes, UK). Subsequently, 4 µm sections were mounted onto positively charged slides (Leica Microsystems, Milton Keynes, UK). All sections were transferred to Sub-X (Leica Microsystems, Milton Keynes, UK) (3 X 5 min) for dewaxing. Then, rehydrated using IMS (Fisher, Loughborough, UK) (3 X 5 min) before washing in distilled water for 5 minutes.

Sections were directly stained using different histological staining as follows:

1. For cell morphology Haematoxylin and Eosin (H&E) was used, where sections stained with Mayer's Haematoxylin (Leica) for 2 minutes, rinsed in water for 5 minutes and transferred to Eosin (Leica) for 2 minutes.
2. Proteoglycan deposition was assessed using 1% w/v Alcian Blue (pH 2.5) which detects glycosaminoglycans (Sigma Aldrich, Poole UK), where sections were firstly covered with 3% v/v acetic acid (Sigma Aldrich, Poole

UK), stained in 1% w/v Alcian Blue (pH 2.5) for 5 minute, washed with acetic acid for 1minute and distilled water for 2 minutes and covered with 1% Neutral Red (Sigma Aldrich, Poole UK) for 5 minutes.

3. Calcium deposition was assessed using Alizarin Red (Sigma Aldrich, Poole UK) at concentration of 2% w/v in distilled water (pH 4.2), where sections were covered with Alizarin Red for 5 minutes and subsequently washed with acetone for 30 seconds.
4. Collagen deposition was assessed using Masson's Trichrome (Bio-Optica, Miller & Miller (Chemicals) Ltd, Hainault UK), according to the manufacturer's instructions.

Subsequently, stained sections were immersed in IMS (4 X 5 minutes) to dehydrate and then transferred to Sub-X (3 X 5 minutes) to clear and mounted in Pertex (Leica Microsystems, Milton Keynes UK).

An Olympus BX51 microscope was used to study all slides and collect images of different hydrogel compositions, both with and without cells, following 48 hours, 2 and 4 weeks incubation. Olympus BX51 microscope was used to visualise all slides and images captured by digital camera and capture PRO OEM v8.0 software (Olympus 1.17 cellSens standard, UK).

Images were captured using digital camera and Capture Pro OEM v8.0 software (Olympus 1.17 cellSens standard, UK). The matrix staining intensity of all slides was evaluated using line profile analysis on Capture Pro OEM v8.0 software; ten randomly selected fields for each image were used to conduct line profile analysis. The resultant intensity measurements of each different composition were compared to each relevant and control sample, to investigate the influence of composition on differentiation of hMSC.

2.6.4 Immunohistochemistry assessment of apoptosis and phenotypic characteristics

Caspase 3 as a marker of apoptosis was used to assess the potential induction of controlled cell death as an indication of cellular viability, collagen type I and osteopontin were selected for immunohistochemistry to determine the phenotypic characteristics of NP tissue explants and delivered hMSCs. Immunohistochemistry was performed as follow:

4 µm paraffin sections were de-waxed in Sub-X, and rehydrated in industrial methylated spirits (IMS) prior to rehydrate in distilled water. Sections were subjected in Sub-X and IMS overnight, where 12 baskets filled with different

concentrations of Sub-X and IMS, and sections were immersed in each basket for 1.5 hour. After that, endogenous peroxidase blocked using hydrogen peroxide (Sigma, Aldrich Poole UK). From this, sections were washed in tris-buffered saline (TBS; 20 mM tris, 150 mM sodium chloride, pH 7.5). Sections were then subjected to antigen retrieval protocols (Table 2.2). Following this, sections were washed with TBS and nonspecific binding sites were blocked at RT for 90 minutes in 25% w/v serum (Abcam, Cambridge,UK) (Table 2.2) and 1% w/v bovine serum albumin in TBS. Primary antibody was applied (Table 2.2) and sections incubated overnight at 4 °C. Negative controls in which mouse or rabbit IgGs (Abcam Cambridge UK) replaced the primary antibody at an equal protein concentration were used (Table 2). Sections were washed in TBS and incubated for 30 mins in 1:500 biotinylated secondary antibody (Table 2.2). Disclosure of secondary antibody binding was by the HRP-streptavidin biotin complex (30 minutes incubation) (Vector Laboratories, Peterborough, UK), TBS washing, followed by application of 0.08% v/v hydrogen peroxide in 0.65 mg/ml 3,30 diaminobenzidine tetrahydrochloride (Sigma Aldrich, Poole UK) in TBS (20 min incubation). Sections were then counterstained with Mayer's haematoxylin, dehydrated in IMS, cleared in Sub-X and mounted in Pertex. Olympus BX51 microscope was used to visualise all slides and images captured by digital camera and capture PRO OEM v8.0 software (Olympus 1.17 cellSens standard, UK). Evaluation of IHC staining was performed by Professor Le Maitre by counting immuno positive and immuno negative cells for all cells within each hydrogel section and immunopositive cells expressed as a percentage of total count.

Table 2.2: Target antibodies used for IHC and their optimal concentrations and antigen retrieval methods.

Target antibody	Clonality	Dilution	Antigen retrieval	Secondary antibody	Serum block
Caspase 3	Rabbit polyclonal (ab39012)	1:400	None	Goat anti rabbit	Goat
Collagen type I	Mouse monoclonal (ab34710)	1:200	Enzyme	Rabbit anti mouse	Rabbit
Osteopontin	Mouse monoclonal (ab8448)	1:400	None	Rabbit anti mouse	Rabbit

2. 7 References

1. Thorpe AA, Creasey S, Sammon C, Le Maitre CL. Hydroxyapatite nanoparticle injectable hydrogel scaffold to support osteogenic differentiation of human mesenchymal stem cells. European Cells and Materials. 2016;32:1–23.
2. PerkinElmer I,. Dynamic Mechanical Analysis (DMA) - A Beginner's Guide. Introduction to DMA. 2008;1–23.
3. Menard K,. Dynamic mechanical analysis a practical introduction. 2nd edn. Boca Raton, London, Newyork: CRC Press. Copyright. Taylor & Francis Group; 2008. 1-12 p.
4. https://commons.wikimedia.org/wiki/File:Schematic_of_DMA.png.
5. Vernon K,. Scanning electron microscopy: an introduction. III-Vs Review. 2000;13(4):40–4.
6. Choudhary O, Priyanka A,. Scanning electron microscope. Advantages and disadvantages in imaging components and applications. Introduction Journal Current Microbial Application Science. 2017;6(5):1877–82.
7. Stuart B,. Infrared Spectroscopy: Fundamentals and Applications. Vol. 8, Methods. 2004. 224 p.
8. Struve W, Mills I,. Fundamentals of Molecular Spectroscopy. Vol. 1, Vibrational Spectroscopy. 1990. 103-104 p.
9. Doyle W,. Principles and Applications of Fourier Transform Infrared (FTIR) Process Analysis. Technical Notes (AN–906 Revision).
10. Duygu D, Baykal T, Açikgöz İ, and Yildiz K,. REVIEW Fourier Transform Infrared (FT-IR) Spectroscopy for Biological Studies. Gazi University Journal of Science. 2009;22(3):117–21.
11. Paper C, Universitat LFC, Consultant HM, Technology PCM, Pe C. Standardization of PCM Characterization via DSC. 2015;(MAY).
12. Kodre K V., Attarde SR, R. YP, Patil RY, Barge VU. Differential Scanning Calorimetry: A Review. Research Review, Journal of Pharmacutical Analysis. 2014;3(3):11–22.
13. Raman, C. V. KKS. A new class of spectra due to secundary radiation. Indian Journal of Physics. 1928;2:399–419.
14. Ferraro JR, Nakamoto K, Brown CW. Introductory Raman Spectroscopy: 2nd edn. Introductory Raman Spectroscopy: 2nd edn. 2003. 1-434 p.

15. Downes A, Elfick A. Raman spectroscopy and related techniques in biomedicine. Sensors. 2010;10(3):1871–89.
16. Bachmann L, Gomes ASL, Zezell DM. Collagen absorption bands in heated and rehydrated dentine. Spectrochimica Acta - Part A Molecular and Biomolecular Spectroscopy. 2005;62(4–5):1045–9.
17. Yeni YN, Yerramshetty J, Akkus O, Pechey C, Les CM. Effect of fixation and embedding on Raman spectroscopic analysis of bone tissue. Calcified Tissue International Journal. 2006;78(6):363–71.
18. Khan AF, Awais M, Khan AS, Tabassum S, Chaudhry AA, Rehman IU. Raman spectroscopy of natural bone and synthetic apatites. Applied Spectroscopic Review. 2013;48(4):329–55.
19. Nataf, G,. (2016). New approaches to understand conductive and polar domain walls by Raman spectroscopy and low energy electron microscopy. PhD. (Thesis) Paris-Saclay.
20. Ren H, Zhu M, and Haraguchi K,. Characteristic SwellingÀDeswelling of Polymer / Clay Nanocomposite Gels. Macromolecules. 2011;8516–26.
21. Dhivya S, Saravanan S, Sastry T, and Selvamurugan N. Nanohydroxyapatite-reinforced chitosan composite hydrogel for bone tissue repair in vitro and in vivo. Journal Nanobiotechnology. 2015;13(1):1–13.
22. Rampersad S,. Multiple applications of alamar blue as an indicator of metabolic function and cellular health in cell viability bioassays. Sensors (Switzerland). 2012;12(9):12347–60.
23. V. dos Santos. Biomaterials: Characteristics and Properties. In: Engineering of Biomaterials. Springer; 2017. p. 5–15.

Chapter - 3

Influence of crosslink density on physical and mechanical properties of L-pNIPAM hydrogel

3.1 Introduction

The crosslink density of hydrogels and its effect on different properties such as mechanical properties(1), swelling and deswelling behaviour(2–5) and structural properties(2,6) has been studied intensively over the last few decades. However, in all cases of using clays as a crosslinker to produce polymer - clay nanocomposites, only a limited weight percent of inorganic clay is typically utilised (< 10 wt. % as the highest). This is because incorporating higher percentages of clay causes high structural heterogeneity of the nanocomposites (NCs), as a result of incomplete dispersion of the clay, which affects the properties of NCs negatively(7).

Haraguchi *et al.* conducted studies using pNIPAM, which was initiated with free radical polymerisation, using potassium peroxodisulfate (KPS) as initiator. Polymerisation reaction temperature was at 20°C and polymer chains crosslinked by Laponite® XLG, to determine the effect of changing crosslink density on physical and mechanical properties of the hydrogels. They found that tensile modulus and tensile strength increased with increased clay content. In addition, swelling and deswelling behaviours also changed dramatically by changing crosslink density, where both swelling and deswelling rates were significantly decreased as crosslink density was increased(8). In 2016, Djonlagic *et al.* reported similar results for pNIPAM based hydrogels containing clay, prepared with different initiator and polymerisation method, where Ammonium persulfate (APS) used as initiator. They concluded that higher crosslink densities resulted in stiffer hydrogels with slower swelling and deswelling rates(5). Different hydrogel materials have shown significant mechanical and structural differences as a function of crosslink density, in 2014 Jang *et al,* studied the influence of crosslink density on the mechanical, morphological and biological behaviour of alginate as a scaffolding material. Calcium carbonate ($CaCO_3$) was used as crosslinker, at different concentrations; they demonstrated that crosslink density affected the mechanical properties and morphology of alginate as well as cellular response within this material. They found that stiffer alginate hydrogel was shown to enhance differentiation of Primary chondrocytes, where collagen type II and aggrecan, was enhanced in the smaller pore size alginate(6).

In 2015 Wong *et al,* investigated the effects of pentaerythritol tetra-acrylate (PETRA) as a crosslinking agent on polyethylene oxide (PEO) hydrogels. They concluded that mesh size and swelling rate were decreased when PETRA concentration increased. Whilst tensile strength increased by increasing crosslink agent(2).

In this chapter the potential effects of crosslink density on the physical and mechanical properties of pNIPAM hydrogel was investigated, together with determination of cell behaviour within different crosslink density hydrogels. Dynamic mechanical analysis was used to explore the influence of using different crosslink densities on the viscoelastic properties of pNIPAM based Laponite® hydrogel. Additionally, the structural and morphological properties were explored using scanning electron microscopy, by which the surface morphology and pore sizes of each composition were obtained. As mentioned earlier, swelling and deswelling behaviours were investigated, in order to explore the impact of using different crosslink densities on both swelling and deswelling ratio. Fourier transform infrared (FTIR) was used to explore the influence of crosslink density on dehydration and rehydration behaviour of the hydrogels. The data collected from the dehydration and rehydration studies used to calculate bound/free water states and the diffusion rate respectively. Historically, differential scanning calorimetry (DSC) has been used semi-routinely to investigate the physical water state in the hydrogels(9–11). Since DSC was the standard technique to calculate water states(12,13), in the current study DSC has been used to validate the results obtained by using Fourier Transform Infrared.

Water contact angle has been measured for pNIPAM Laponite® dried films with different crosslink densities, because wettability is a crucial property of all biomaterials, as it relates to many other properties such as biocompatibility (14–17). Spin coated samples on glass microscope slides were used to measure the water contact angle for different crosslink density of pNIPAM based Laponite® films, to consider the potential different surface roughness for different samples, that has a strong influence on the surface water contact angle(18) . In other studies(5,19), swollen hydrogel samples and "as prepared" hydrogel were investigated using water contact angle, where contact angle increased as crosslink density increased, despite the hydrophilic nature of the clay. This

abnormal hydrophobicity was considered to be the result of other factors such as hydrogel water content and surface roughness(19) which was considered in this work by using spin coated samples and examination of surface roughness for each sample.

It is extremely difficult to consider the actual geometry of the surfaces(20,21), where even the smooth surfaces exhibit a complex mix of geometric aspects. However, different techniques provide qualitative and quantitative characterisation that help to judge whether the surface is smooth or rough, also the degree of the roughness. Atomic surface roughness (AFM) gives precise information on the surface characterisation(21–23). It is an effective tool for the high resolution examination of the surface, where it avoids artefacts due to dehydration and coating(24). In the current work scanning electron microscopy and atomic force microscopy were used to explore the surface morphology and surface roughness in micro and nanoscale respectively.

3.2 Methods

3.2.1 Synthesis of pNIPAM Laponite® hydrogels with different crosslink densities

Methods of hydrogel synthesis and experimental work were detailed in Chapter 2.2. Hydrogels containing pNIPAM and Laponite® alone will be referred to as L-pNIPAM, with the numbers 0.5, 1 and 1.5 etc. in parentheses used to distinguish between formulations with different crosslink densities. When no number is shown (e.g. L-pNIPAM) then the crosslink density is 1% by weight.

3.3 Results

3.3.1 Morphological study and pore size determination

Typical SEM images of L-pNIPAM hydrogels with crosslink densities of 0.5, 1 and 1.5% by weight respectively allow an insight into their internal structure (Figure 3.1). A honeycomb like structure was observed within the hydrogels which was affected by crosslink density, where the shape, size and the number of the pores was shown to be dependent on the crosslink density (Figure 3.1).

In previous studies, the pore size of hydrogels was shown to play an important role and affected properties such as mechanical properties(6,8), swelling and

deswelling(25) and cell behaviour(26). Since the pore size of a hydrogel is crucial for cell viability and proliferation, the pore size distribution was selected in this study to explore the morphological changes, related to the use of different crosslink densities. Where the diameter of each pore was measured (μm) manually using the Capture Pro OEM v8.0 software (Media Cybernetics, Buckinghamshire, UK).

Plotting the pore size distribution from six such SEM images of each hydrogel composition, with their medians as a function of crosslink density (Figure 3.2), facilitates the determination of the impact that crosslink density has on the hydrogel internal structure. Measured pore sizes were in the range of 1.5 to 42 μm (Figure 3.2).

The pore size of the hydrogel was shown to significantly decrease systematically when the crosslink density was increased ($p \leq 0.05$) (Figure 3.2), indicating a direct link between the internal structure of the hydrogels and crosslink density. Where the median of the hydrogel pore size was found to be 16, 13 and 8 μm for L-pNIPAM (0.5), L-pNIPAM (1) and L-pNIPAM (1.5) respectively. Furthermore, with an increase in crosslink density of the hydrogels, pore size was more uniform (Figure 3.2).

Jang *et al* (6) and Wong, R. *et al* (2) have shown that increasing crosslink density of hydrogel materials decreases pore sizes. Jang *et al* investigated the effect of crosslink density on structural properties calcium carbonate as crosslinker on the pore sizes of sodium alginate hydrogel material, which is commonly used in tissue engineering. Within this study average pore sizes were evaluated through geometrical measurements on SEM images. In the current study, scanning electron microscopy images were analysed in a similar way and the findings were similar, increasing crosslink density led to a decrease in average pore size.

In 2015 Wong, R. *et al*, investigated the effect of the concentration of pentaerythritol tetra-acrylate (PETRA) as the crosslinking agent on the morphology of polyethylene oxide (PEO) hydrogels. They used two different methods to estimate and calculate the pore sizes. Firstly, they visually estimated the pore sizes using SEM images. Then they calculated the pore sizes based on equilibrium swelling ratio of PEO hydrogel. Both procedures

have showed comparable results, where pore sizes decreased with the increase in PETRA concentration.

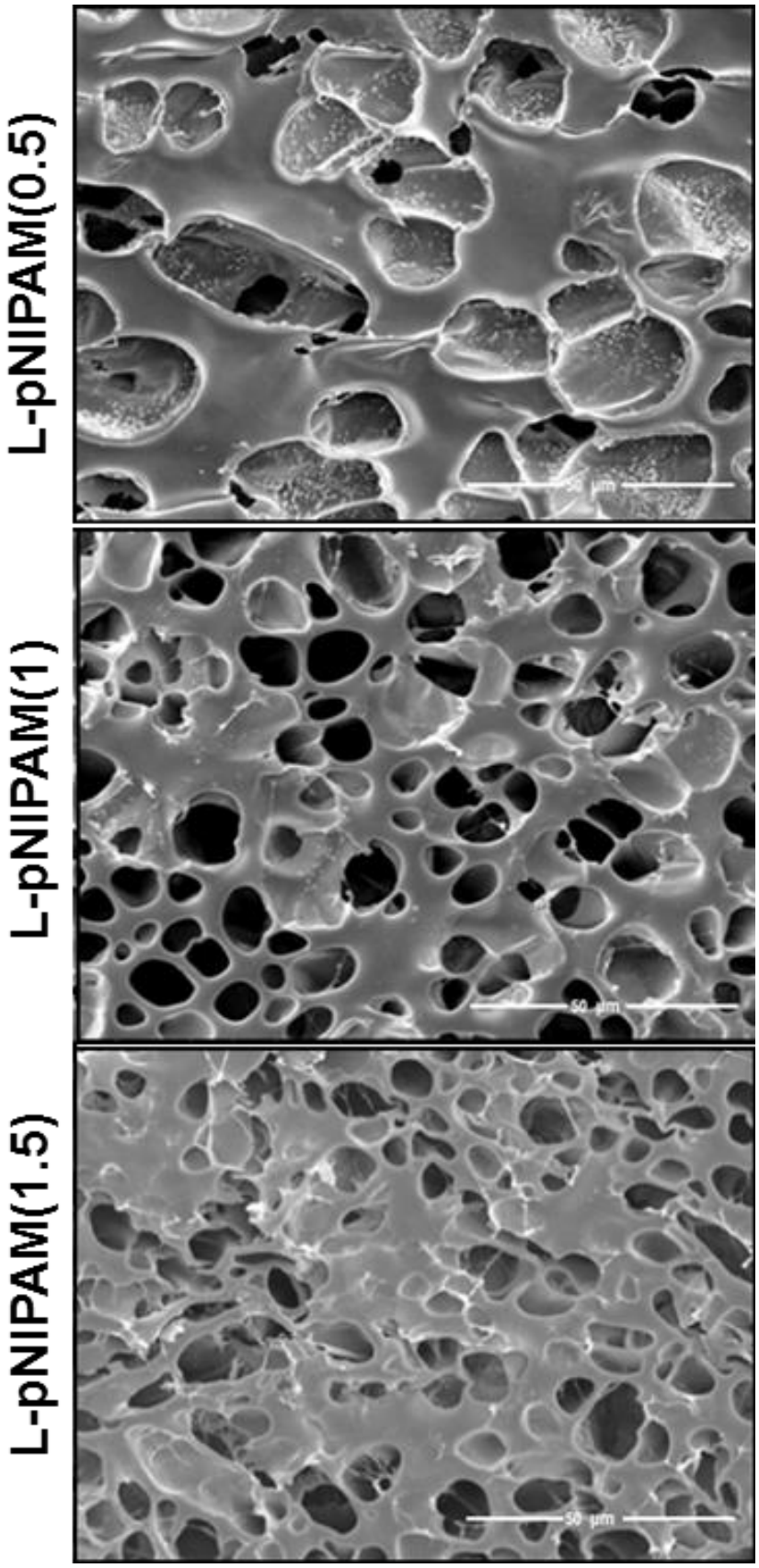

Figure 3.1: Scanning electron microscopy images of L-pNIPAM hydrogels with crosslink densities of 0.5, 1 and 1.5%. Scale bars = 50 µm.

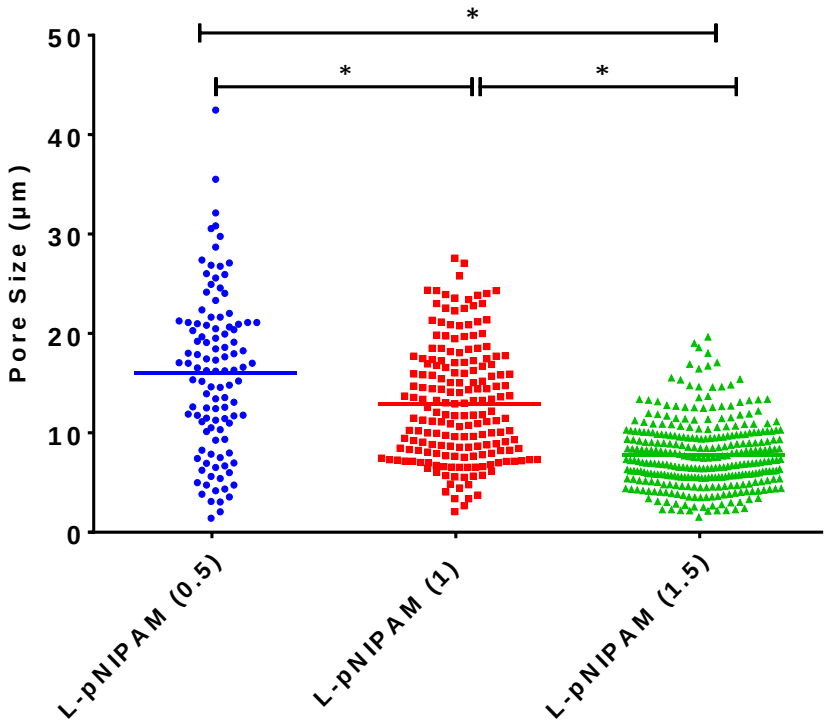

Figure 3.2: Statistical analysis of pore size of L-pNIPAM hydrogels with crosslink densities of 0.5, 1 and 1.5% w/w. *=P<0.05.

3.3.2 Dynamic Mechanical Analysis (DMA) frequency scan data of PNIPAM based Laponite®

The storage modulus of L-pNIPAM hydrogels with different crosslink densities was determined using DMA in frequency compression mode. The storage modulus (E') values, for all hydrogel samples studied, did not increase as a function of increasing frequency (Figure 3.3), meaning L-pNIPAM with different crosslink density did not exhibit viscoelastic behaviour. As the storage modulus (E') for all formulations was frequency independent, 10 Hz was selected to compare potential differences in the mechanical properties between each different crosslink density of hydrogel samples (Figure 3.4). The hydrogel with the lowest crosslink density, L-pNIPAM (0.5), showed the lowest storage modulus values with a range of 7.7 X 10^5 - 3.5 X 10^6 pascal. For L-pNIPAM (1) the range was 5.8 X10^6 - 3.2 X 10^7 pascal, and for the hydrogel with the highest crosslink density, L-pNIPAM (1.5), it was 2.2 X 10^7 - 6 X 10^7 pascal. It is clear that the variation between storage modulus values of each composition decreased as hydrogel stiffness increases, meaning stiffer hydrogels were more

reproducible in this experiment (Figure 3.4), due to difficulty in handling the weaker gels.

Increasing the crosslink density was shown to significantly increase the storage modulus systematically in a linear manner ($p \leq 0.05$) (Figure 3.4).

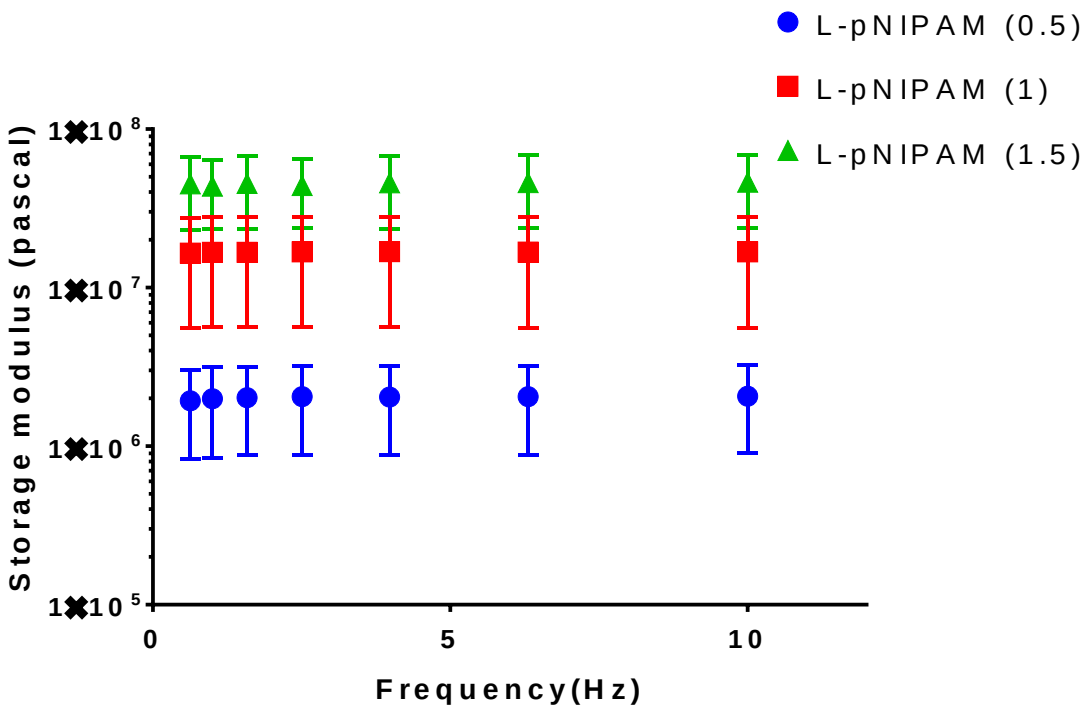

Figure 3.3: Dynamic Mechanical Analysis (E' values) of pNIPAM based Laponite® hydrogels with different crosslink density. n=6.

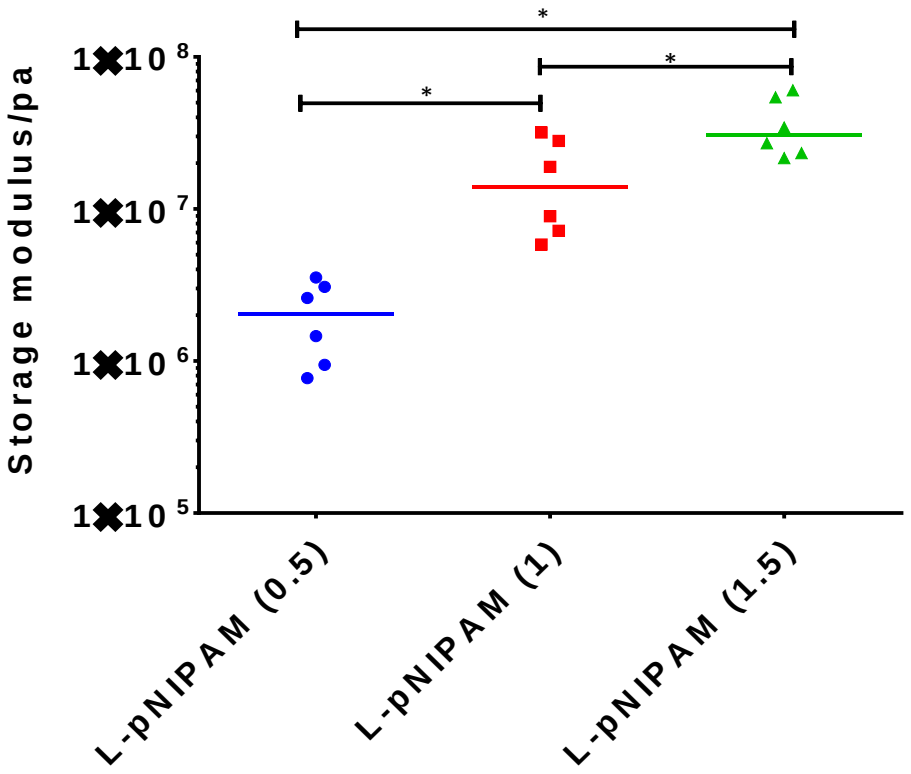

Figure 3.4: Influence of crosslink density on storage modulus determined by DMA in compression mode at 10Hz. *=P<0.05. n=6.

These findings are in full agreement with Haraguchi *et al*(27), Kumar *et al*(28) and Djonlagic *et al* (25), who all demonstrated that an increase in crosslink density of pNIPAM based hydrogels increased the mechanical stiffness.

For different hydrogel systems Jang *et al* (6), Lee k. *et al*(29) and Wong, R. *et al* (2) showed that the highest crosslink density hydrogel is mechanically the stiffest, for alginate and polyethylene oxide respectively. Jang *et al* investigated the effect of the concentration of calcium carbonate as a crosslinker on the mechanical stiffness of sodium alginate. They used $CaCO_3$ concentrations of 36, 72 and 144 mM and the relevant average compressive modulus were 4.647, 16.187 and 36 kPa respectively(6).

Lee k. *et al,* showed that mechanical properties of sodium alginate hydrogels can be controlled using different kinds of crosslinking molecules and varied crosslink densities. They used Ca^{2+} and Poly- (ethylene glycol) with different

molecular weights. Where they found that the shear modulus of alginate varied depending on the crosslinker type and crosslink density(29).
According to Wong, R. *et al,* (Year) whom investigated effects of crosslink densities of polyethylene oxide (PEO) hydrogel films, on mechanical properties. Pentaerythritol tetra-acrylate (PETRA) was used as a crosslinker with concentrations of 1% w/w, 2.5% w/w, 5% w/w, and 10% w/w. With increases in tensile strength seen with increasing crosslink density (2).

In 2006 Metz, J. *et al* studied the influence of crosslink density on the compressive strength of hydrogel contain poly (e-caprolactone) maleic acid with molecular weight of 900 (PCLTMA) and poly (ethylene glycol) diacrylate macromer (PEGDA) with molecular weight of 400. The studied hydrogel was generated using chemical photo crosslinking with three different ratios of PEGDA to PCLTMA: 25/75, 50/50 and 75/25, where 75/25 hydrogel was stiffer than the other compositions(30).

In this pNIPAM based Laponite® hydrogel system, it was also observed that increasing the crosslink density significantly increases the stiffness ($p \leq 0.05$) in a systematic manner (Figure 3.4), with a decrease in the average pore sizes of the hydrogels, playing a part in this phenomenon.

Generally, L-pNIPAM hydrogels possess mechanical strength less than those observed in natural tissue, which is not ideal if this material is to be used as a scaffold to regenerate natural tissue. However, the mechanical properties of L-pNIPAM hydrogels were improved, when synthetic hydroxyapatite was incorporated within this hydrogel(31), and further enhancement was observed when human mesenchymal stem cells (hMSC) were seeded in their structure(31,32). These findings will be followed up in subsequent chapters.

3.3.3 Determination of swelling and de-swelling kinetics

3.3.3.1 Swelling behaviour

The determination of swelling ratio of 0.5, 1 and 1.5% by weight L-pNIPAM hydrogels at 25°C, in distilled water was performed to explore the effect of Laponite® concentration on the swelling behaviour. All hydrogel samples show typical swelling behaviour of hydrogel materials, where the swelling ratio of

pNIPAM hydrogels at all Laponite® concentrations increased with time and reached the equilibrium state in the first 12 hours (Figure 3.5), with significant differences ($p \leq 0.05$) in the amount of water that can be held in their internal structures after reaching the equilibrium swelling state at the end of the experiment (t=1440minutes)(Figure 3.6). Higher concentrations of Laponite® resulted in significantly lower swelling percentages due to increased numbers of crosslinks restricting the movement of polymer chains(3). Thus the expansion of the hydrogel structure became more difficult as crosslink density increased, due to increased hydrogel stiffness.

Wong, R. *et al*, Ren H. *et al*, and Cates, R. S. *et al* (2–4), demonstrated that increasing crosslink density of hydrogels decreased the percentage swelling ratio in PEO, Laponite® crosslinked pNIPAM and organically crosslinked pNIPAM hydrogel systems respectively.

In a previous study by Yacob N. *et al,* the effect of irradiation dose on pore size and swelling behaviour of hydrogels prepared from natural and synthetic polymers using irradiation electron beams of 0 kGy, 5 kGy 25 kGy and 40 kGy was investigated. Concluding that changes in internal structure of Polyvinyl pyrolidone / carrageenan hydrogels altered the swelling ratio of this material in distilled water (33)

The current study has shown similar results in the influence of crosslink density on swelling characteristics, where changes in hydrogel's structure on raising the crosslinker content, reduced the ability of the hydrogel to absorb water, thereby decreasing the interconnected pore channels as paths that water can diffuse through. In addition mechanical properties could be a factor to impact on the degree of swelling, where stiffer hydrogels prevent expansion and absorption of water.

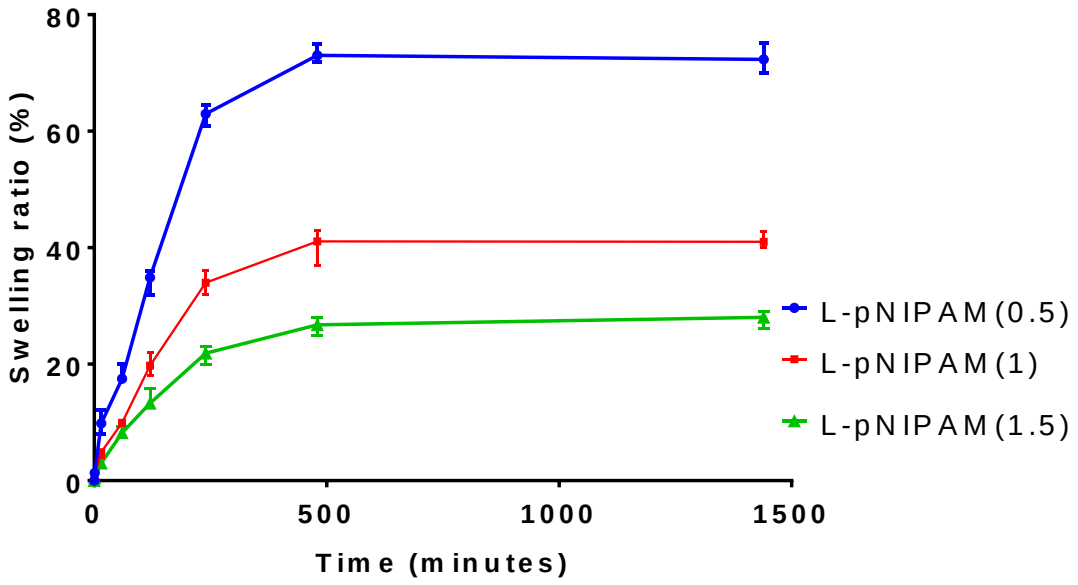

Figure 3.5: Swelling ratio of L-pNIPAM hydrogels with crosslink densities of 0.5, 1 and 1.5% w/w (n=3).

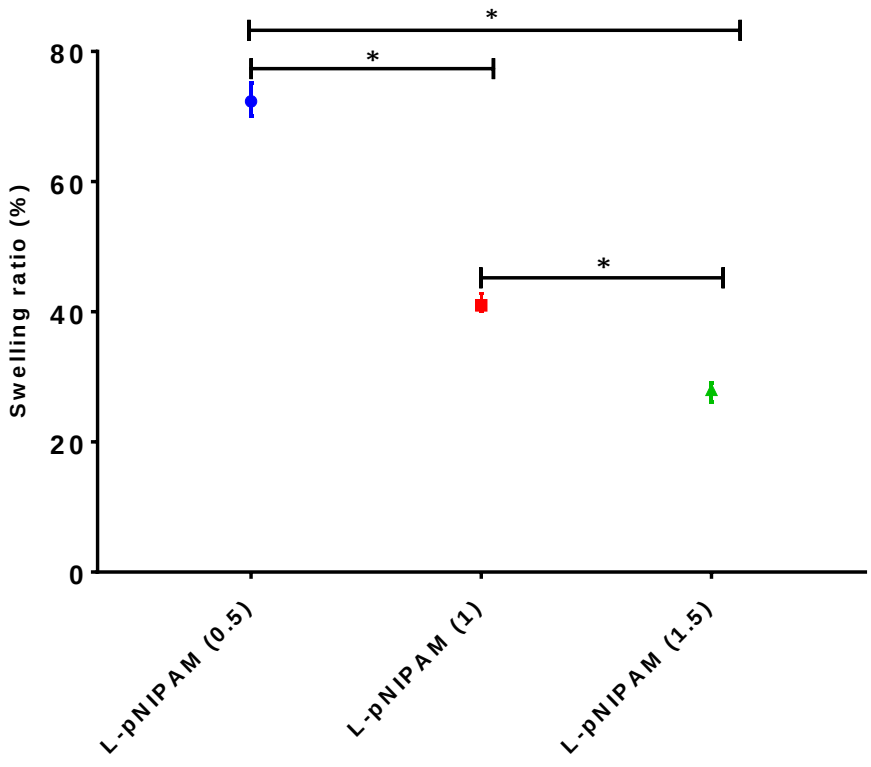

Figure 3.6: Equilibrium swelling state of L-pNIPAM hydrogels with crosslink densities of 0.5, 1 and 1.5% w/w at 1440 minutes, shows Statistical differences between each composition. *=P<0.05. n=3.

3.3.3.2 Deswelling behaviour

L-pNIPAM hydrogels possess a lower critical solution temperature at ~ 32°C, as pNIPAM, is a thermally responsive polymer. Thermally responsive hydrogels could be used in wide range of biomedical applications, including drug delivery where the shrinkage these materials undertake in response to thermal changes can expel drugs held within them. Therefore, it is important to investigate the influence of crosslink density on hydrogel shrinkage as a response to thermal changes.

In this study deswelling as a response to thermal changes from 25 °C to 62 °C varied, depending on the crosslink density, where an increase in crosslink density, resulted in a decrease in deswelling response rate. This reduction was thought to be due to changes in internal structure of pNIPAM based Laponite® hydrogel that affected the diffusion of water out of the hydrogel during thermal shrinkage (Figure 3.7 & 3.8). In addition, an increase in the amount of Laponite® resulted in more non-thermosensitive moiety into pNIPAM backbone, which restricted the water flow from the interior hydrogel structure as a result of impermeable nature of the collapsed surface layer(34). Also increased crosslink density was shown to increase hydrogel stiffness, which may affects the degree in which the hydrogel shrank as a response to thermal changes. These results are in good agreement with previous studies investigated effect of crosslinker on deswelling of pNIPAM based hydrogels (27,34,35).

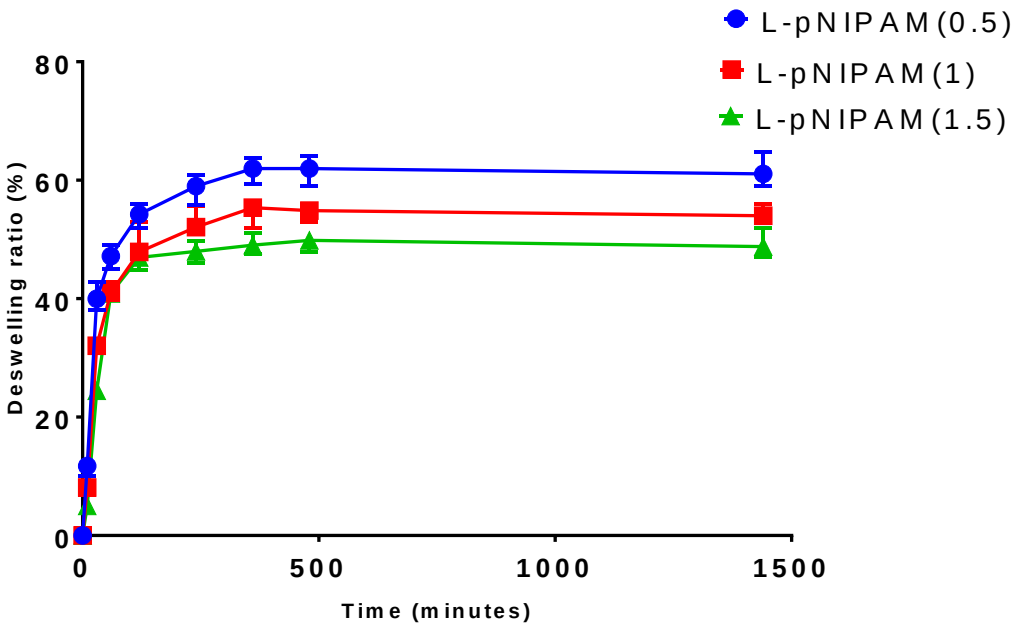

Figure 3.7: Deswelling ratio of L-pNIPAM hydrogels with crosslink densities of 0.5, 1 and 1.5% w/w (n=3).

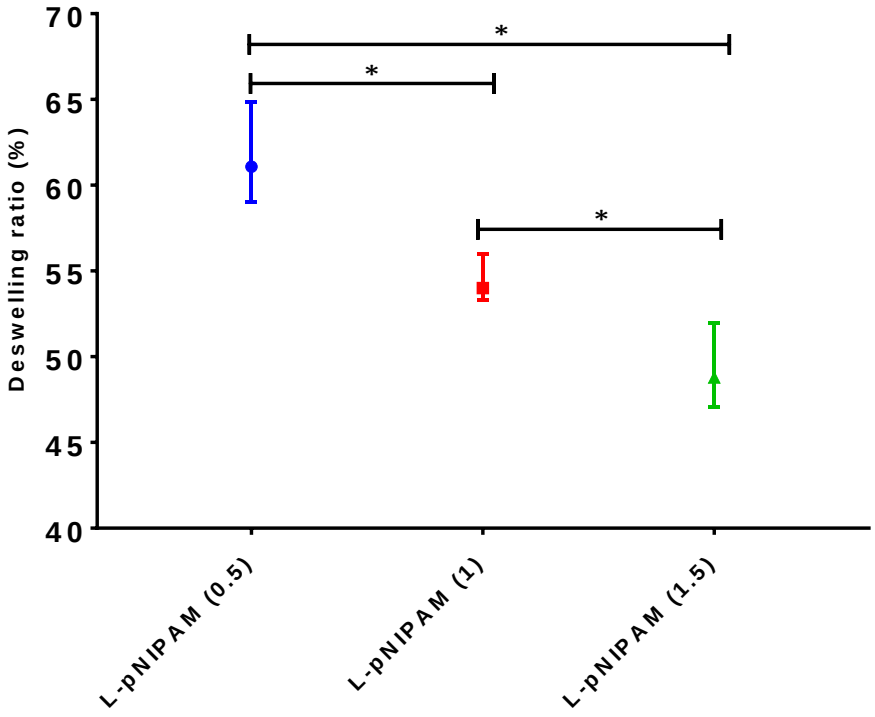

Figure 3.8: Maximum deswelling degree of L-pNIPAM hydrogels with crosslink densities of 0.5, 1 and 1.5% w/w at 1440 minutes, shows statistical differences between each composition. *=P<0.05. n=3.

3.3.4 Water states and water/polymer interactions

A good understanding of water/ polymer interactions or water dynamics within polymeric systems is very important for the development of such systems, and the water state existing in, evaporating from, and being absorbed into or interacting with such systems has received numerous attention (36–39). In this work dehydration and rehydration behaviour, water/polymer interactions and water states within different formulations of pNIPAM based Laponite® hydrogel were investigated.

3.3.4.1 Dehydration study

Real-time Fourier transform infrared attenuated total reflectance (FTIR-ATR) spectroscopy is a convenient and accurate method to study diffusion and absorption kinetics in polymers(39,40). Barbari *et al* determined diffusion coefficients for polymers measured from FTIR-ATR spectroscopy were in agreement with those measured gravimetrically(41).

Hydrogel samples were synthesized as described in Chapter 2.2; 30µl of each different formula was pipetted directly onto the ATR crystal which had been pre-set to 25˚C. Data collection was immediately begun with 8 scans per spectrum at a resolution of 8cm^{-1} on a Thermo Nicolet Nexus instrument, using a series setup, a spectrum was taken automatically every 30 sec for 800m (13.3h). For clarity, selections of spectra at different time intervals during drying of L-pNIPAM (1) have been chosen, to facilitate the monitoring of the drying of hydrogel samples in real time by tracking the decrease in intensity of the ν(OH) band between 3600-3100 cm^{-1} (Figure 3.9). Expansions of these spectra are shown in Figure 3.10 and 3.11, to highlight the observable peak intensity and peak shifts changes during the drying process (Figure 3.10 and 3.11). The ν(OH) band between 3600-3100 cm^{-1} shows the amount of water within the hydrogel during the drying of the sample, and the δ(NH) band (1550cm^{-1}) was selected to represent polymer concentration during dehydration. The intensity of the ν(OH) band between 3600-3100 cm^{-1} was used to observe changes in hydrogel states, as the water being lost.

The integrated intensity of the ν(OH) band over the duration of the 800 minutes experiment was plotted as a function of time (Figure 3.12). Hydrogel samples exhibited reorganisation in structure, with a small degree of shrinkage when the sample changed from liquid to gel, due to the decrease the temperature around lower critical temperature (LCST) of pNIPAM, causing a slight increase in intensity of this band (Figure 3.12), Due to the reduction in hydrogel temperature between 50˚C and 25˚C. This observation was also made by Boyes, V. *et al,* when the influence of temperature on intensity of ν(OH) band in L-pNIPAM, where a range of temperature between 40-24 ˚C was used. Where an increase in intensity of ν(OH) was observed as temperature reduced from 40 to 24˚C. This increase in intensity of ν(OH) band was suggested to be due to less interactions between water- water and water-polymer in a relatively high energy system (39). Thereafter more water evaporated from the system and one can observe a decrease in the ν(OH) band intensity (Figure 3.12).

Plotting the intensity of ν(OH) band between 3600-3100 cm^{-1} as a function of time for different Laponite® concentrations of pNIPAM based Laponite® hydrogel samples (Figure 3.13) allows the influence of crosslink density on dehydration rate to be elucidated.

Dehydration rates for different crosslink density pNIPAM based Laponite® hydrogel are shown in Figure 3.13, where an increase crosslink density decreased dehydration rate (Figure 3.13). This could be due to multiple factors, one of which is the reduction of the interconnected pore channels that allow water to diffuse through. In addition, an increase crosslink density was shown to reduce flexibility of L-pNIPAM hydrogels which negatively impacted on the water diffusivity through the sample. Also, the hydrophilicity of the clay could be an additional factor that may affect the way in which water behaves within the hydrogel matrix. Whereas limited difference in dehydration rate, between L-pNIPAM (0.5) and L-pNIPAM (1), was observed, when crosslink density increased to 1.5, a reduction in dehydration rate was observed (Figure 3.13).

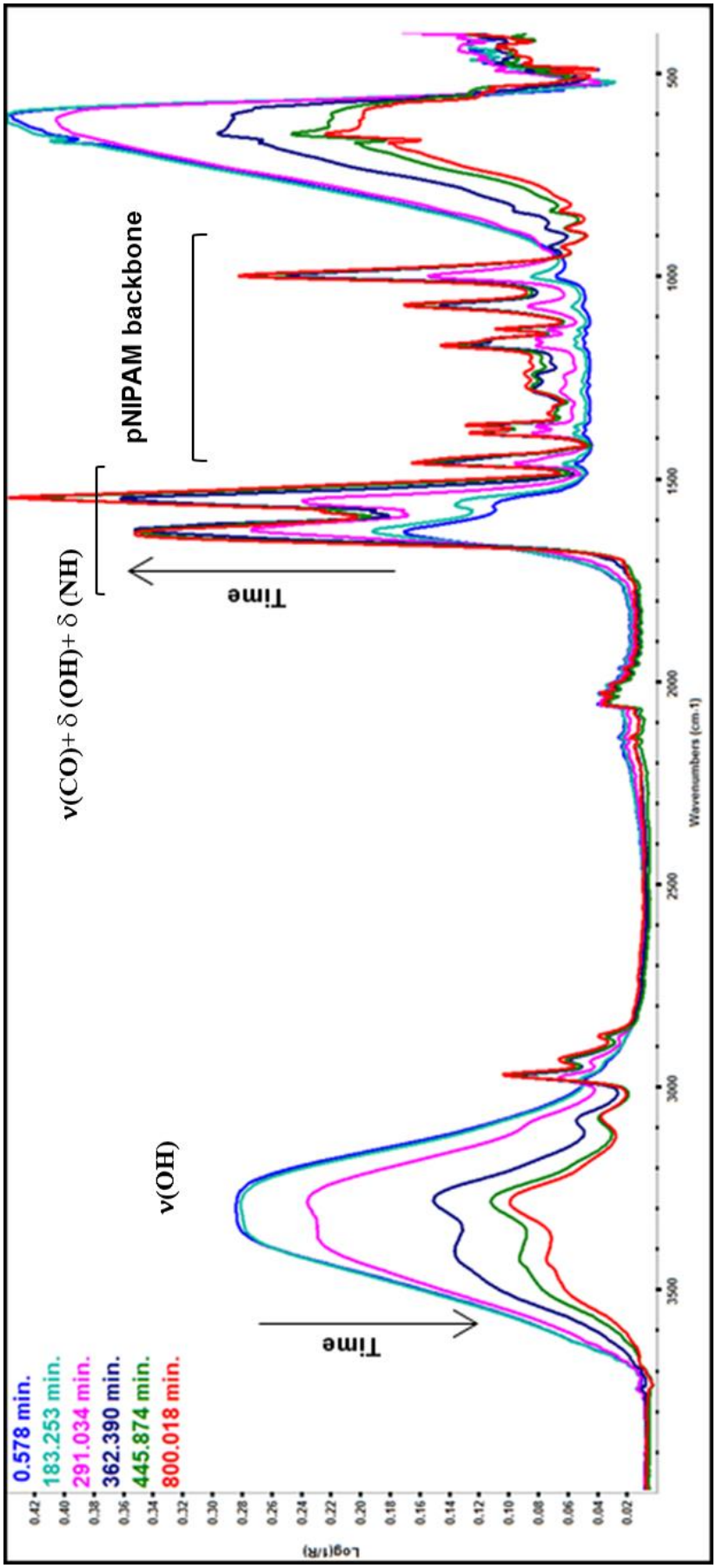

Figure 3.9: Full spectra of water evaporating from L-pNIPAM (1) hydrogel at 25˚C.

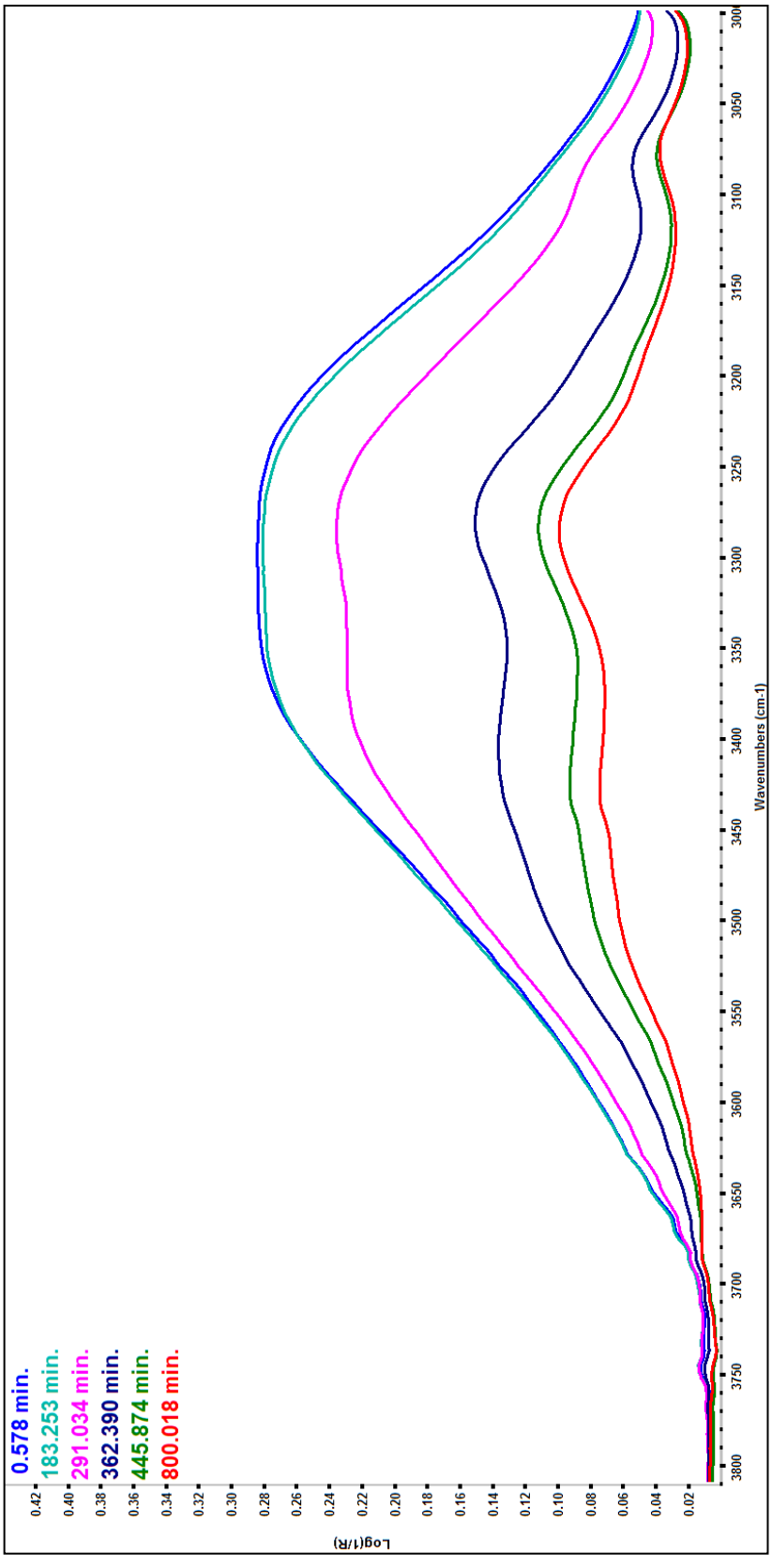

Figure 3.10: *v* (OH) (3700-300cm-1) taken during the drying of L-pNIPAM (1) hydrogel at 25˚C.

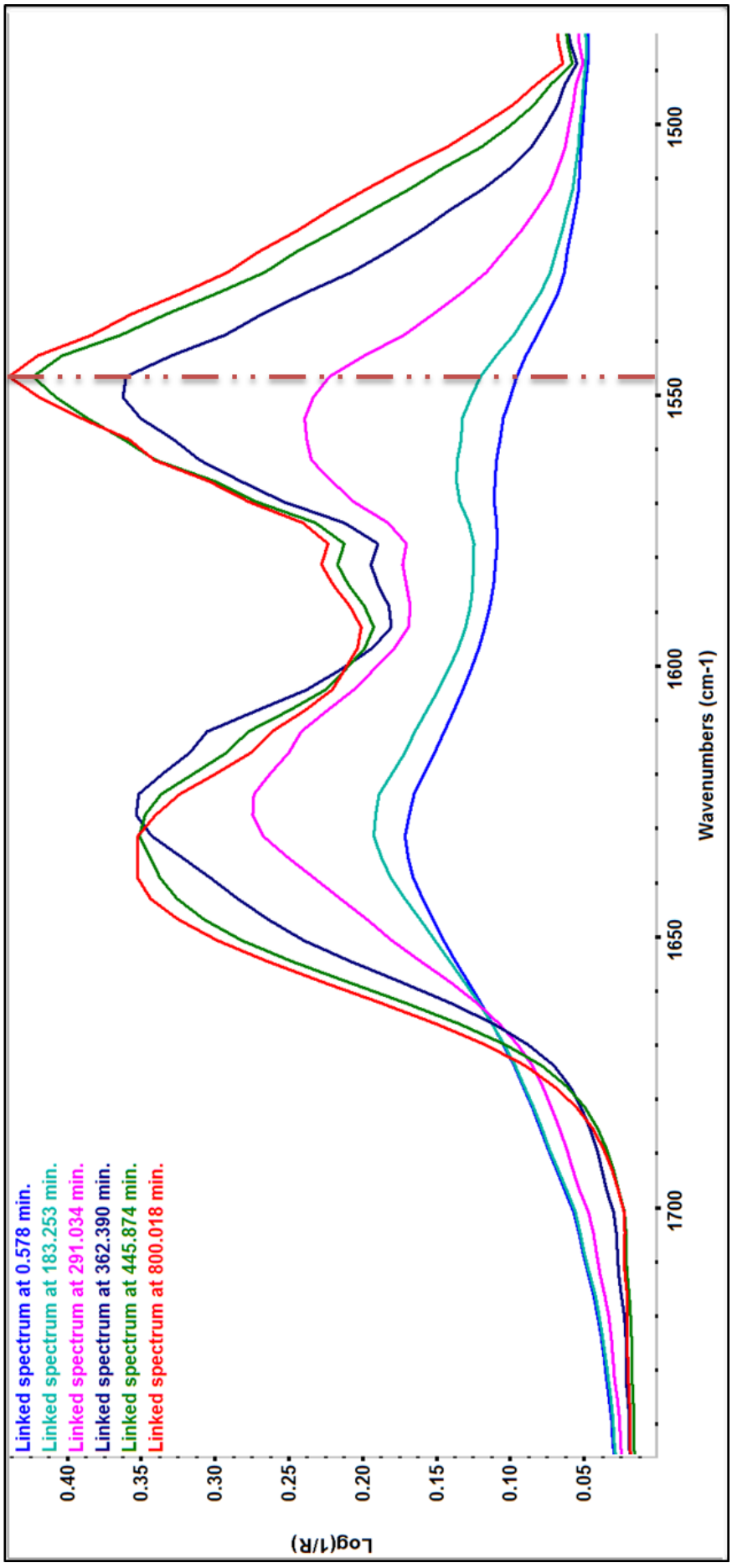

Figure 3.11: δ (NH) band (1550cm^{-1}) taken during the drying of L-pNIPAM (1) hydrogel at 25˚C.

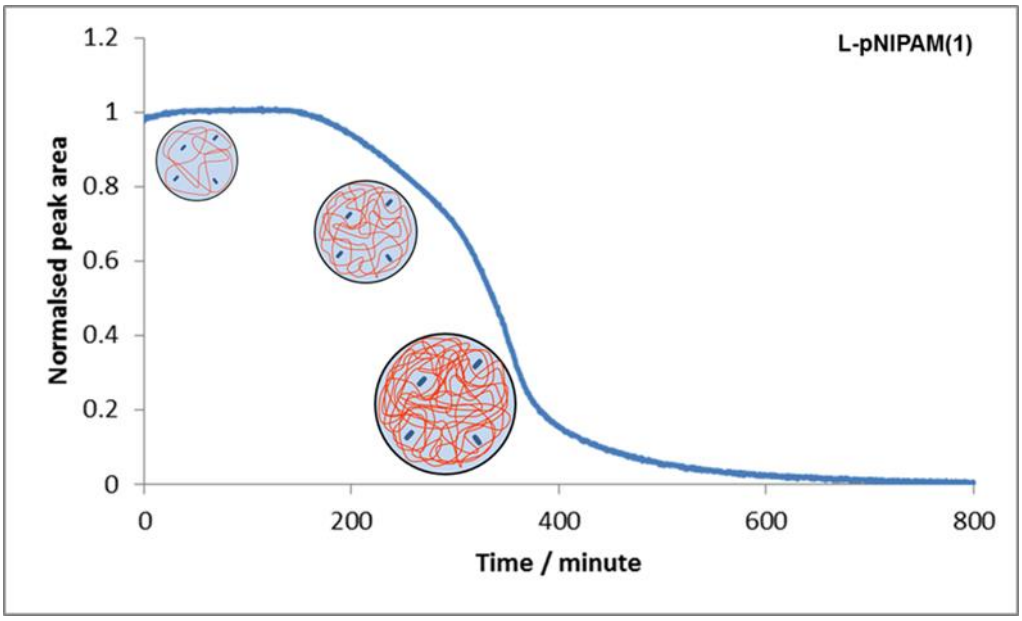

Figure 3.12: Kinetic profile of water evaporation from L-pNIPAM (1) hydrogel into the atmosphere as a function of time, with structural changes during dehydration.

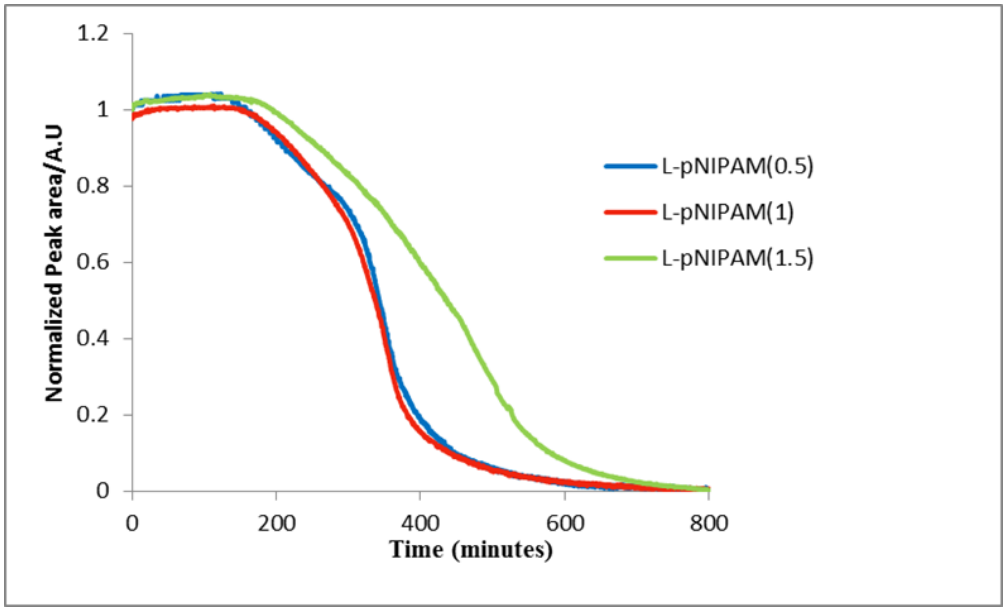

Figure 3.13: water profiles for different cross link density hydrogels during dehydration (n=3).

Shifts in the position of δ(NH) band observed with time, during dehydration allow us to determine interactions between water and the polymer chains (Figure 3.14). The change in δ(NH) band position during water loss is plotted in Figure 3.14, along with the dehydration profile. This illustrates the link between the water content and the δ(NH) band position during the drying of hydrogel sample. Changes in δ(NH) band position shifts are a clear indication of a reduction of the number of H-bonds between polymer chains and water molecules as the water content was reduced. Recognising that there are three phases to the dehydration profile, it is proposed that the different phases can be explained as follows. The initial phase (first 60 minutes) shows a subtle increase in intensity of the ν(OH) and a shift in theδ(NH) band, indicating a decrease in temperature of the system and a reorganisation from the globule to the coil conformation of the pNIPAM as the system goes through the LCST(42). The next phase in the diagram (60 minutes to 300 minutes), shows a decrease in the intensity of the ν(OH) band and very subtle shifts in theδ(NH) band, which is proposed to be derived from the loss of free water from the system. The final phase in the diagram, the second phase of dehydration, shows a further decrease in the intensity of the ν(OH) band and greater shifts in the position of the δ(NH) band. The greater changes in δ(NH) band position when compared to the first dehydration phase are much more marked during the second phase of dehydration, suggesting that bound water is being lost from the system (Figure: 3.14).

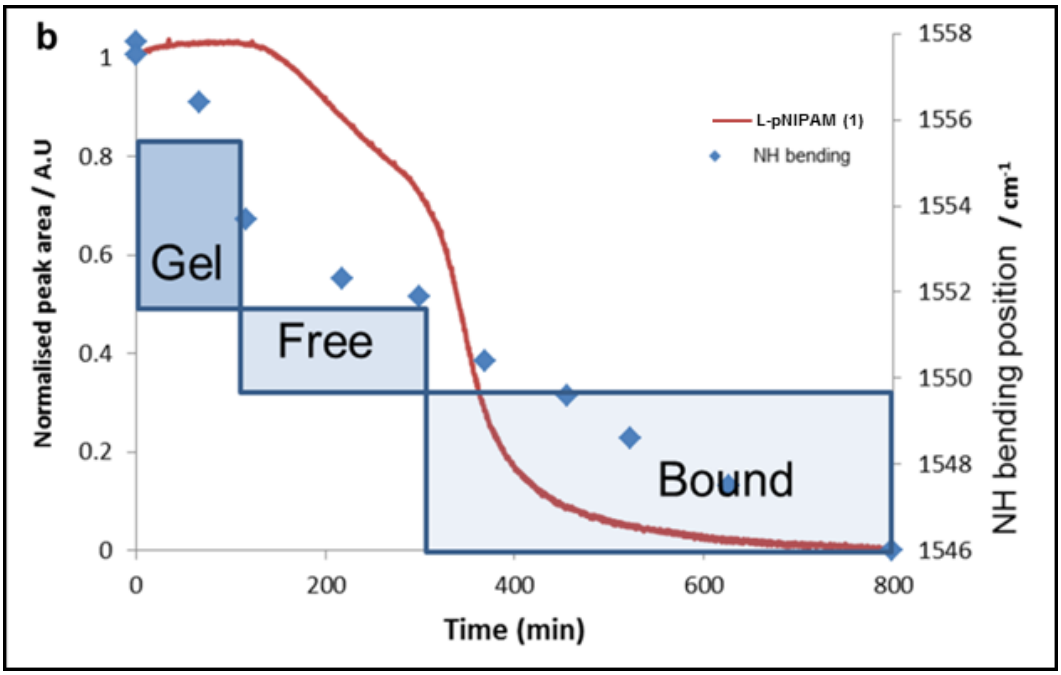

Figure 3.14: water profiles and δ (NH) band shift during dehydration of L-pNIPAM (1), including three stages of the hydrogel during dehydration: gel, free and bound water lost.

By drawing a straight line between the two different phases in which water has been lost (Figure 3.15), the quantity of the two different water states were estimated using dehydration data that were collected using Fourier transform infrared attenuated total reflectance (FTIR-ATR).

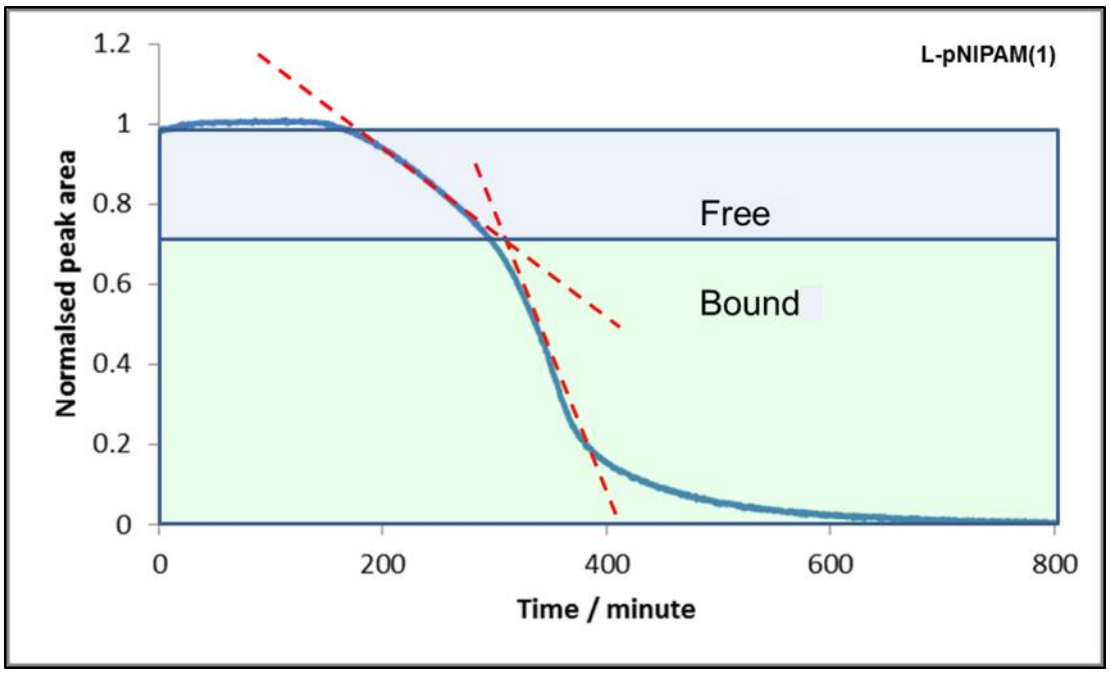

Figure 3.15: Water profiles with two different phases of water lost.

Based on the hypothesis that water is lost during the drying process(43), free and bound water were estimated using profile of water evaporating from hydrogel samples. Where two different phases can be identified (Figure: 3.15). Bound water percentage calculated for different crosslink density of pNIPAM based Laponite® hydrogels (Figure: 3.16). Where higher crosslink density hydrogel with smaller pore size having greater proportion of bound water (Figure: 3.16). The proportion of bound and free water within the hydrogels was verified using the 'gold standard' method of Differential scanning calorimetry with a good agreement observed between the two methods (Figure: 3.17).

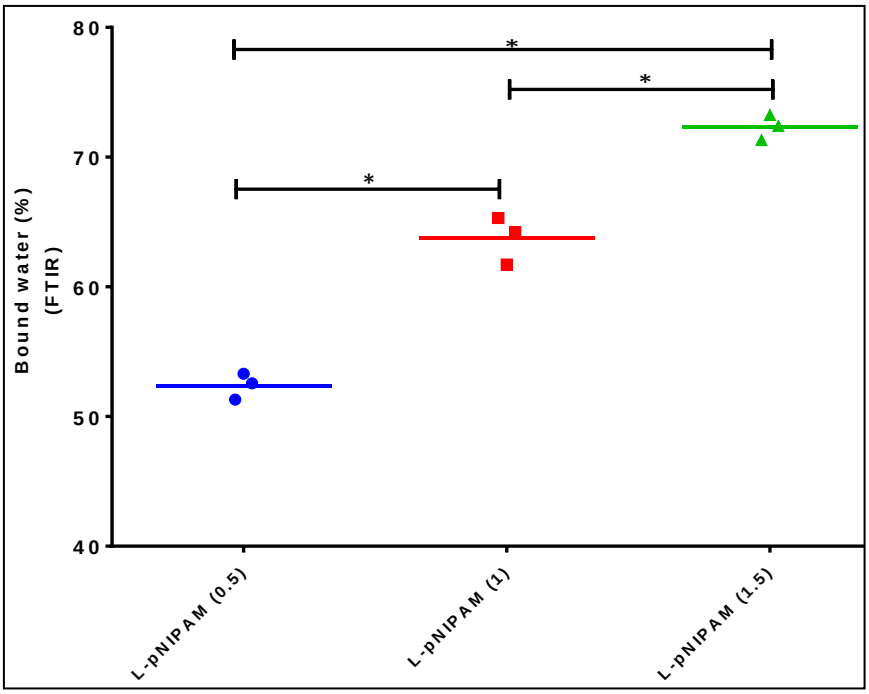

Figure 3.16: Bound water content of pNIPAM based Laponite® hydrogel with different crosslink densities, calculated using FTIR. *=P<0.05.

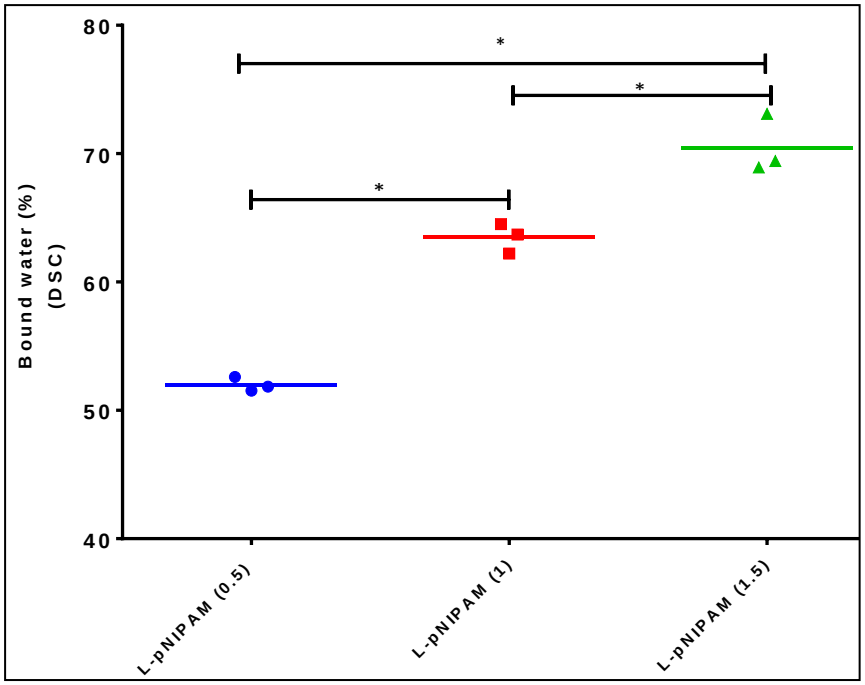

Figure 3.17: Bound water content of pNIPAM based Laponite® hydrogel with different crosslink densities, calculated using DSC. *=P<0.05. n=3.

3.3.4.2 Rehydration study

Following complete dehydration, hydrogel samples were fully dried and adhered to the ATR crystal. A rehydration experiment was then performed by putting deionised water in contact with dried sample using liquid cell holder, with the same setting that used in dehydration experiment except using a shorter time (240m). A range of spectra at different time intervals were chosen (Figure 3.18), to show changes in different bands within these spectra of L-pNIPAM during rehydration (Figure 3.18). Once more, the ν(OH) band between 3600-3100 cm^{-1} was selected to monitor the water content of hydrogel sample, and the δ(NH) band at ~1550 cm^{-1} was used to monitor polymer concentration during rehydration (Figure 3.18). An increase in intensity of ν(OH) band between 3600-3100 cm^{-1} was observed with time, whilst the intensity of δ(NH) band at ~ 1550 cm^{-1} was shown to decrease (Figure 3.18) indicating swelling of the polymer film. In addition, the δ(NH) band was shown to shift to higher wavenumber as water was being absorbed (Figure 3.18). To highlight these observable changes in peak intensity and position, expansions of these spectra are shown (Figure 3.19 and 3.20).

Absorption of water by L-pNIPAM samples was observed as an increase in intensity of the ν(OH) band between 3600-3100 cm^{-1} (Figure 3.18 and 3.19). In addition, increased numbers of H-bonds between the sorbet water and the NIPAM polymer chains were indicated by shifts to higher wavenumber of the δ(NH) band ~ 1550 cm^{-1}, as water absorbed into the sample (Figure 3.20).

The intensity of ν(OH) band between 3600-3100 cm^{-1} over 240 minutes (Figure 3.19) was plotted as function of time during rehydration, and rehydration rates of L-pNIPAM hydrogels calculated for different crosslink densities (Figure 3.21). The rate at which water was absorbed into the hydrogel samples was shown to be influenced by the crosslink density, where increasing the crosslink density decreased the rate of rehydration of L-pNIPAM films at 25˚C.

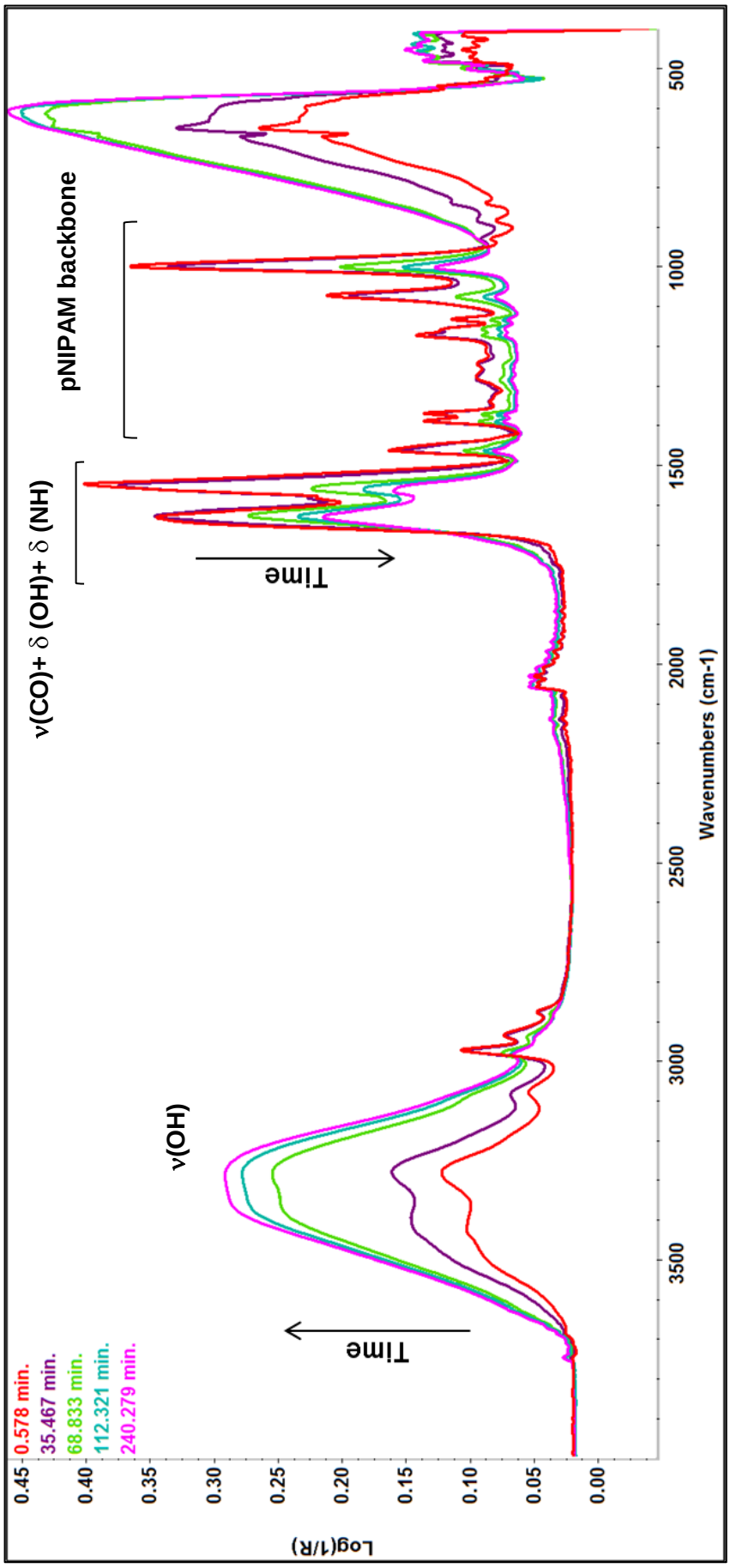

Figure 3.18: Full spectra of water absorbing into L-pNIPAM (1) hydrogel at 25˚C.

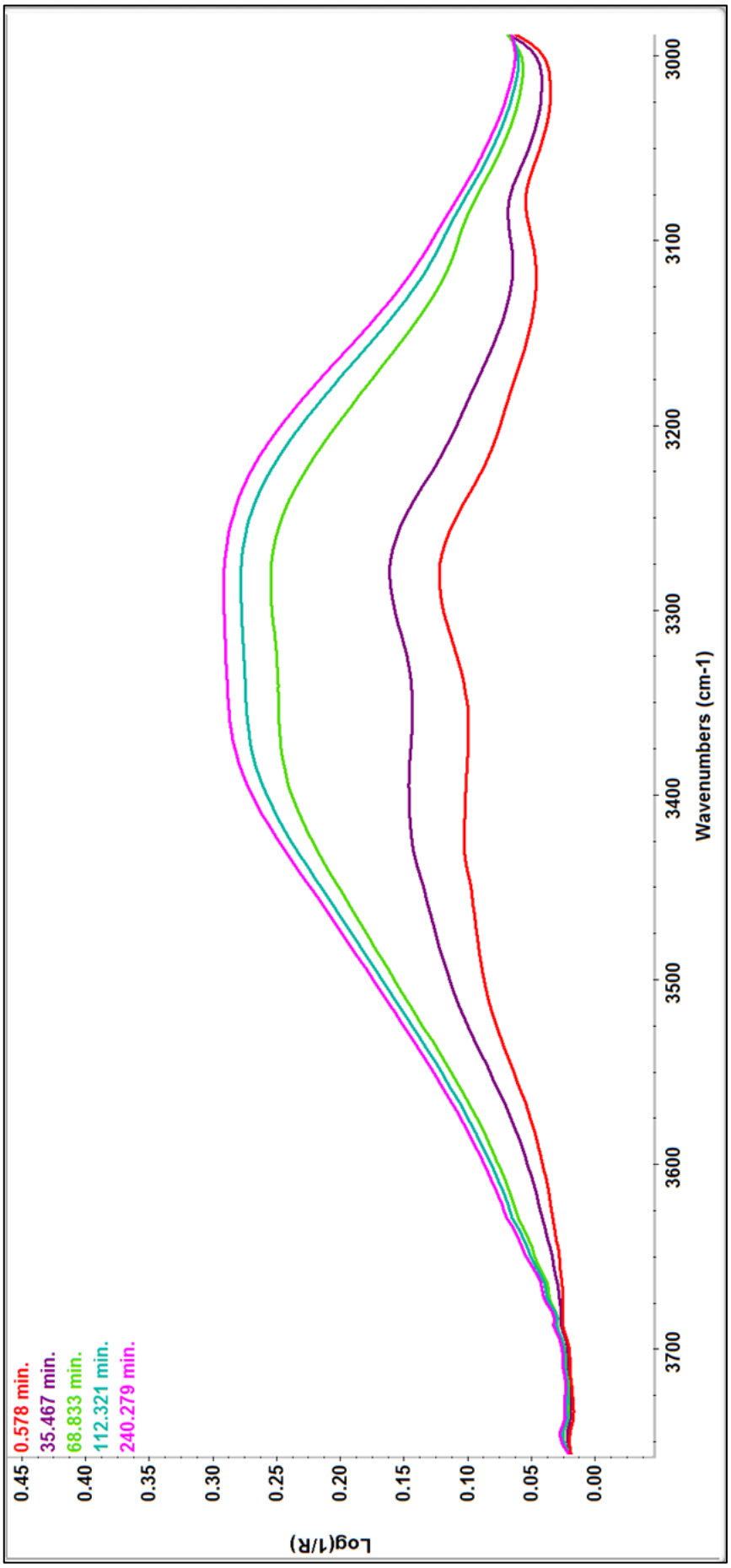

Figure 3.19: *v* (OH) (3700-300cm-1) taken during the drying of L-pNIPAM (1) hydrogel at 25˚C.

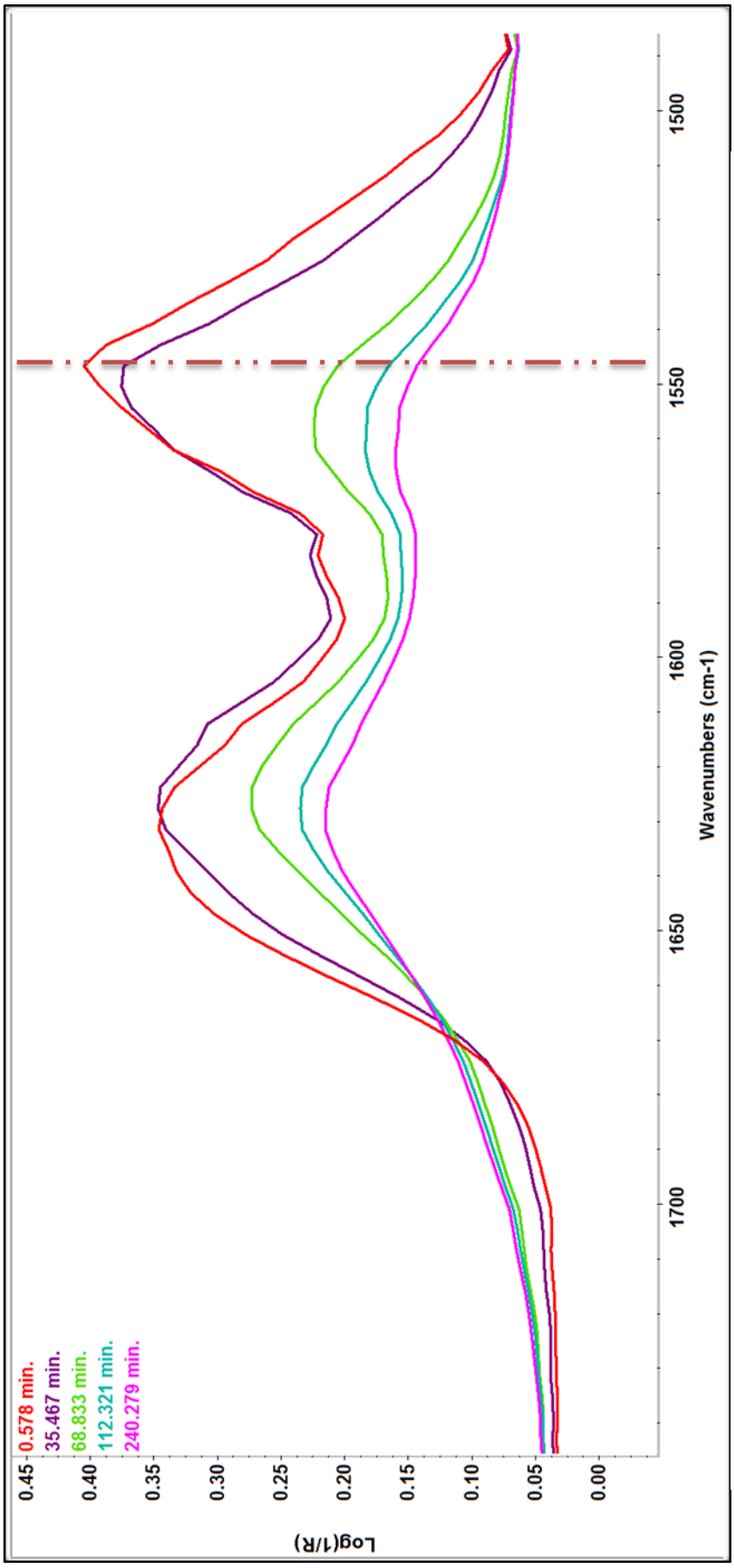

Figure 3.20: δ (NH) band (1550cm^{-1}) taken during the rehydrating of L-pNIPAM (1) hydrogel at 25˚C.

Due to the reduction in pore size of L-pNIPAM and increase hydrogel stiffness, when crosslink density increased, water diffusion through the sample was reduced. Narrower interconnected paths were observed in hydrogels with high crosslink density, which inhibited water diffusivity through the hydrogel structure. In addition, an increase in stiffness of the hydrogel adversely impacted the capacity of internal structure by decreasing its expansion, during water absorption (Figure 3.21).

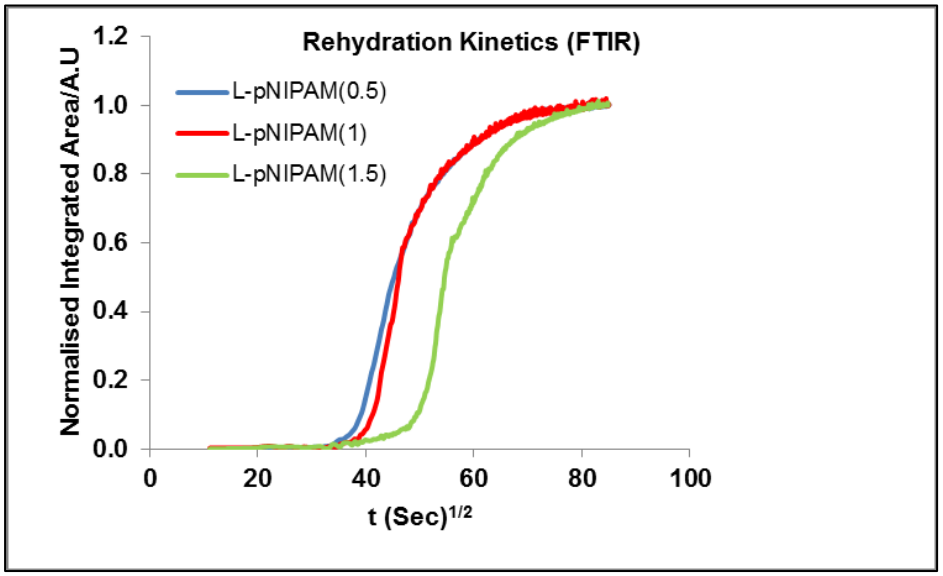

Figure 3.21: Water profiles for different cross link density hydrogels during rehydration (n=3).

Diffusion coefficient of water through hydrogel samples was calculated according to Fieldson equation (44,45) (equation 3.1).

$$\frac{Mt}{M\infty} = \frac{2}{L}\sqrt{\frac{D}{\pi}}\ \sqrt{t} \qquad \text{Equation 3.1}$$

Where (M_t) is the mass sorbet at specific time t, (M_∞) is the mass sorbet at equilibrium, (D) is the diffusion coefficient and (L) is sample thickness.

The relationship between the slope of the linear trend line, sample thickness and diffusion coefficient D is given by:

$$M = \frac{2}{L}\sqrt{\frac{D}{\pi}}$$ Equation 3.2

In order to calculate D value equation 3.2 was rewritten as:

$$D = \pi\left(\frac{ML}{2}\right)^2$$ Equation 3.3

This equation was applied to calculate diffusion coefficient of water through pNIPAM based Laponite® hydrogel samples during rehydration process. Water profiles for different crosslink density were plotted as a function of square root of time per second, and slope of the linear proportion of the curves (< 0.5) was calculated using a linear trend line (44) (Figure 3.22).

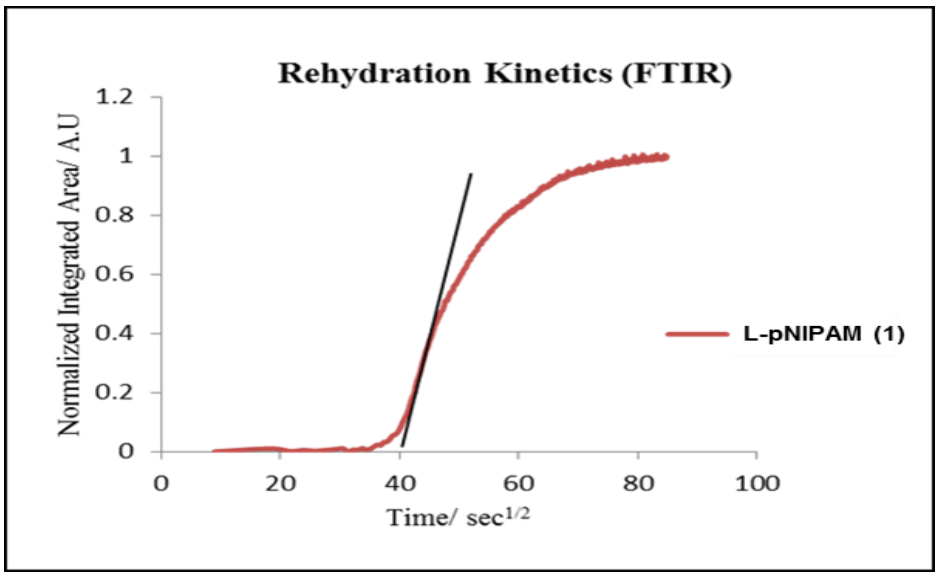

Figure 3.22: Water profile for L-pNIPAM (1), showing the slope of the linear portion.

The diffusion coefficient (D) of L-pNIPAM (0.5), was calcualted to have a median value of $1.4X10^{-5}$ cm^2/s and decreased when the crosslink density was doubled to median of $4.6X10^{-6}$ cm^2/s. A further reduction in D value was observed when the crosslink density increased to 1.5%, where the calculated median of diffusion coefficient of L-pNIPAM (1.5) was $4.6X10^{-6}$ cm^2/s (Figure 3.23).

The diffusion coefficient for water through L-pNIPAM samples during rehydration process was shown to be impacted by crosslink density, where water diffusivity significantly decreased as crosslink density increased due to smaller pore sizes for higher crosslink density hydrogels. Furthermore, a high degree of crosslinking between polymeric chains inhibited the mobility of these chains, which reduced the ability of the water to diffuse through hydrogel matrix at high crosslink density (Figure 3.23). Sample thickness (l) is also an additional factor that affects the shape of the profile from which one can calculate the D value (equation 3.3). As it was not possible to measure sample thickness prior to conducting the experiment, the hydrogel sample thickness was measured 24 hours after the rehydration experiment was finished, using digital callipers. The hydrogel formulation with the lowest crosslink density showed the highest average thickness (0.66mm). When the crosslink density doubled to 1wt. % the average thickness was reduced to 0.61mm, and further reduction in hydrogel sample thickness to 0.58mm was observed when the crosslink density was increased to 1.5wt.% (Table 3.1).

Table 3.1: Average sample thickness with different crosslink density.

Sample code	Average sample thickness (mm), n=3
L-pNIPAM(0.5)	0.66±0.04
L-pNIPAM(1)	0.61±0.02
L-pNIPAM(1.5)	0.58±0.02

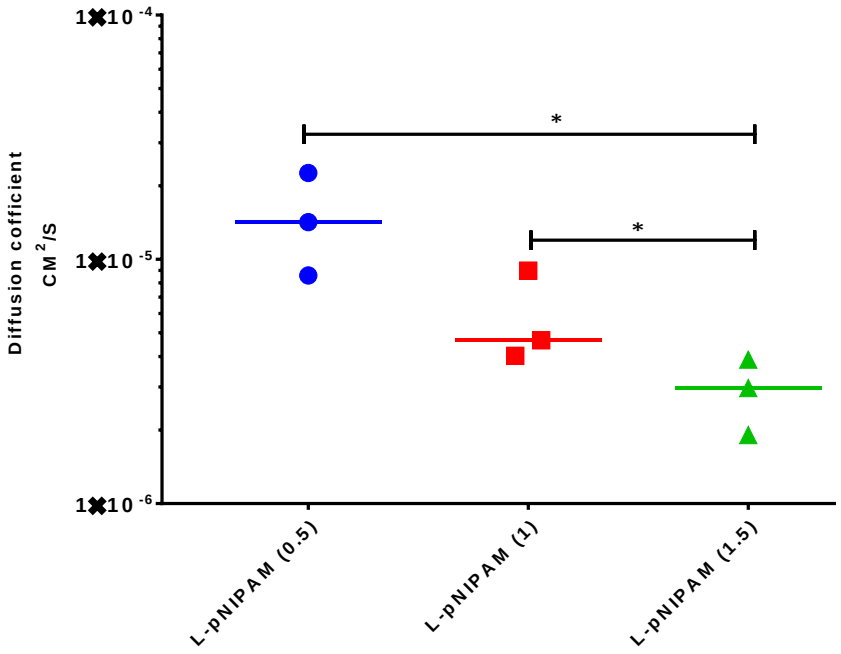

Figure 3.23: Diffusion coefficient of pNIPAM base d Laponite® hydrogel with different crosslink density. *=P<0.05.

Diffusion coefficients of L-pNIPAM samples, calculated in this study were in agreement with values obtained in previous studies for similar hydrogel systems(46–50), where D value for different hydrogel systems were in range of 0.3 $X10^{-5}$ to $1X10^{-7}$ cm^2/sec. In addition, Yanbin W. *et al,* studied the effect of crosslink density on photo initiated PEG hydrogels. They used molecular weights of the chains ranging from 572 to 3400 Daltons, and the influence of increased crosslink density was explored. They found that an increase in crosslink density decreased water diffusivity within PEG hydrogel structure(50).

3.3.5. Wettability measurements

There are many vital properties of hydrogel materials, such as biocompatibility, adhesion and release of molecules as well as their possible applications related to their surface properties, it is very important to explore the surface wettability of these materials(51). In Figure 3.24(D), the water contact angle of L-pNIPAM spin coated films, with crosslink densities of 0.5, 1 and 1.5% by weight respectively is given, showing the impact of crosslink density on surface wettability. It is a clear that an increase in crosslink density decreased water contact angle systematically and dramatically ($p \leq 0.05$), meaning that the wettability characteristics of pNIPAM based Laponite® spin coated films

gradually improved by increasing Laponite® concentration as crosslinker. Water contact angle of hydrogel materials was intensively studied, due to the importance of surface/water interactions of these materials especially for medical applications. Several studies conducted using either hydrogel in gel state or swollen samples(5,19), to investigate the influence of crosslink density on the wettability of the hydrogel materials, have shown that water contact angle increased with increases in clay content. The changes in wettability of the hydrogel could be caused by many factors, such as water content, network structure and topological roughness(19). In this study, spin coated hydrogel samples were used to determine the effect of Laponite® content, on the water contact angle. SEM images of spin coated samples with various Laponite® contents are shown in Figure 3.24(a-c), illustrating that they all have same surface morphology. Water contact angle from four such spin coated samples of each hydrogel composition are plotted (Figure: 3.24(d)), indicating the impact of crosslink density on wettability of L-pNIPAM films, where an increase in crosslink density was shown to decrease water contact angle significantly ($p \leq 0.05$), meaning that film wettability has increased.

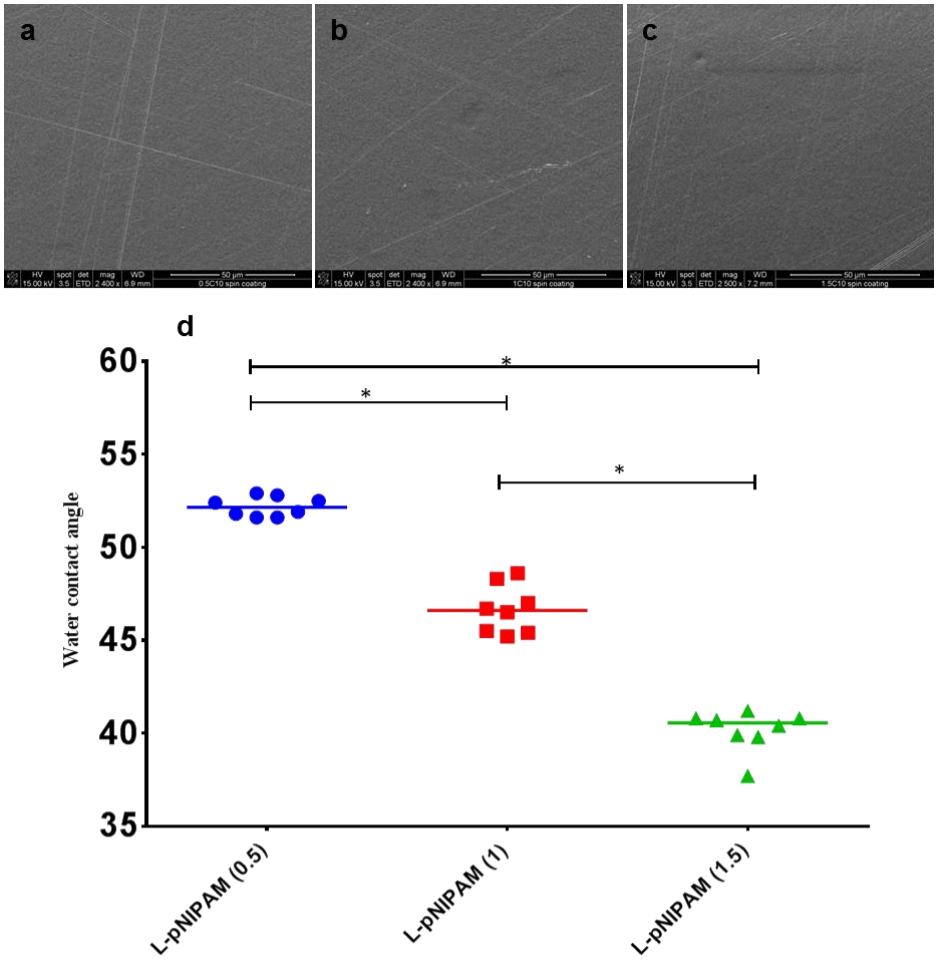

Figure 3.24: a) SEM image of spin coated film of L-pNIPAM (0.5), b) SEM image of spin coated film of L-pNIPAM (1), d) SEM image of spin coated film of L-pNIPAM (1.5). Scale bar = 50 µm. d) Water contact angle of pNIPAM based Laponite® hydrogel with various cross link density. *=P<0.05. n=4.

3.3.6 Surface roughness study

Surface properties of biomaterials are crucial to be considered when new materials are being engineered or existing ones developed. They are related to many other properties; such as biocompatibility, cell adhesion and wettability(52). In this work surface roughness was studied using different tools due to the possible impact on wettability of L-pNIPAM and to explore the influence of crosslink density on the surface roughness.

3.3.6.1 Surface roughness measurements using atomic force microscopy

The corresponding 3-D image of spin coated samples of L-pNIPAM with crosslink densities of 0.5, 1 and 1.5% per weight (Figure 3.25) were investigated for surface roughness using AFM tapping mode with scanning range of 2 X 2 μm^2.

Both root mean square (RMS) roughness (Rq) and roughness average of the surface were taken from the images produced by the software (Figure 3.25). Where, Rq is represent the root mean square average of the roughness profile, and Ra represents roughness Average of the surfaces measured microscopic peaks and valleys.

The hydrogel with the lowest crosslink density exhibits a relatively smooth surface with roughness of: (Ra = 0.690 nm, Rq = 0.856 nm). Whilst the other two crosslink density samples exhibit significantly rougher surfaces ($p \leq 0.05$), while roughness average (Ra) and the root mean square roughness (Rq) were (Ra =1.06 nm, Rq = 1.31 nm) and (Ra =1.15 nm, Rq =1.42 nm) for L-pNIPAM (1) and L-pNIPAM (1.5) respectively (Figure 3.25). Whilst this failed to reach significance, surface roughness appeared to increase with increased crosslink density. Therefore, increase surface roughness increased wettability of L-pNIPAM, when the crosslink density increased.

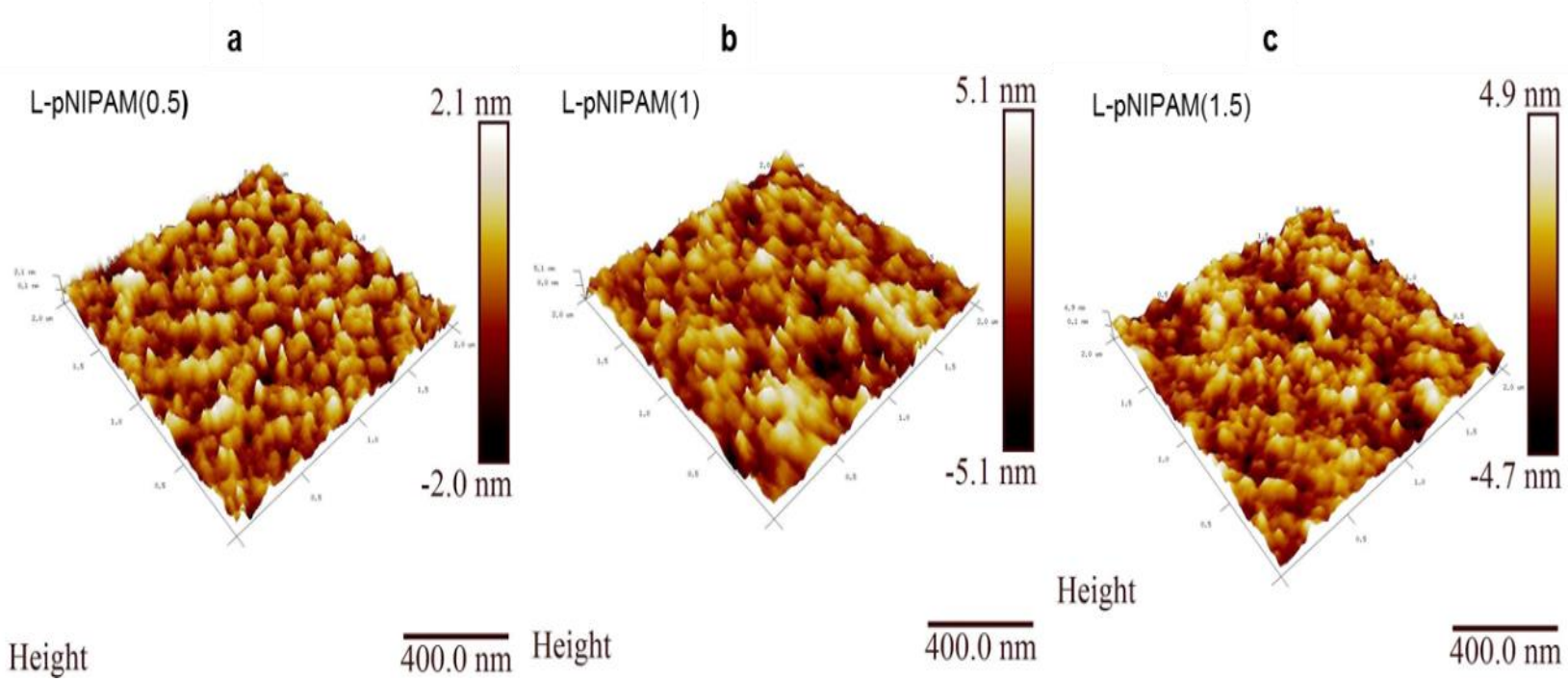

Figure 3.25: Three-dimensional images generated by the AFM analysis of a 4 μm2 area of: a) a) L-pNIPAM (0.5), b) L-pNIPAM (1), c) L-pNIPAM (1.5)

3.3.6.2 Surface roughness measurements using infinite focus microscopy (IFM)

3-D images of each L-pNIPAM film with different crosslink density was used to measure average surface roughness, using infinity focus microscope with measurement settings as follows: exposure time of 2.85 ms, magnification at 50x, estimated vertical resolution at 11.991 nm and estimated lateral resolution at 5.0096 µm.

Average surface roughness of hydrogel samples was shown to increase linearly by increasing crosslink density (Table 3.2). As fully dried samples were used to measure surface roughness, an increase in Laponite® platelets could have resulted in a rougher surface as they moved to the surface during the film drying stage. According to these results, surface roughness enhanced the wettability of the hydrogel when the crosslink density increased. Compared to AFM results the surface roughness values obtained using IFM were much higher, due, perhaps, to using different sample preparation methods. For AFM, spin coated films were used, whilst in IFM samples were pipetted directly on glass slides and left to dry overnight at room temperature. Therefore, surface roughness became higher as a result of shrinkage of the samples during drying.

Table 3.2: Roughness average of different crosslink density L-pNIPAM films.

	Roughness average (Ra)
L-pNIPAM(0.5)	38.757nm
L-pNIPAM(1)	48.146nm
L-pNIPAM(1.5)	61.736nm

3.3.7 Influence of crosslink density on cell behaviour

Rat stem cells were used initially to explore cell viability within pNIPAM based Laponite® injectable hydrogel with different crosslink density. Where Alamar

Blue assay was used as a measure of metabolic cell activity and thus representative of the total number of viable cells, was assessed over 7 days in culture (Figure 3.26). A significant decreased in metabolic cell activity was detected in day zero samples between L-pNIPAM (1.5) compared to cells cultured in L-pNIPAM (0.5 and 1) (Figure 3.26). This could be as a result of smaller pore size for L-pNIPAM(1.5), meaning less space for cells to occupy (Figure 3.26), where cells normally fill the pores of the hydrogel when cultured within this material(53).

Annabi N. *et al*, studied effects of pore size of α - elastin hydrogels, where they succufully produced high porous crosslinked α - elastin hydrogels, by using high pressure of CO_2 at 60 bar(54). Hydrogel synthesised with this method was less dense than α - elastin that produced at atmosphere pressure. They found that highly porous hydrogel promoted cellular penetration and growth of human skin fibroblast cells throughout the α - elastin hydrogel matrix(55).

From zero to two days in culture a significant decrease in metabolic cell activity was observed in all crosslink densities hydrogels, before a significant increase on day 7 in all composition that studied in this chapter (Figure 3.26). Interestingly, on day 7 a significant decreased was detected in metabolic cell activity within L-pNIPAM (0.5), when compared to other two crosslink densities hydrogels (Figure 3.26). This could be as a result of very big pore size that observed in L-pNIPAM (0.5), where stem cells grow as cell clusters.

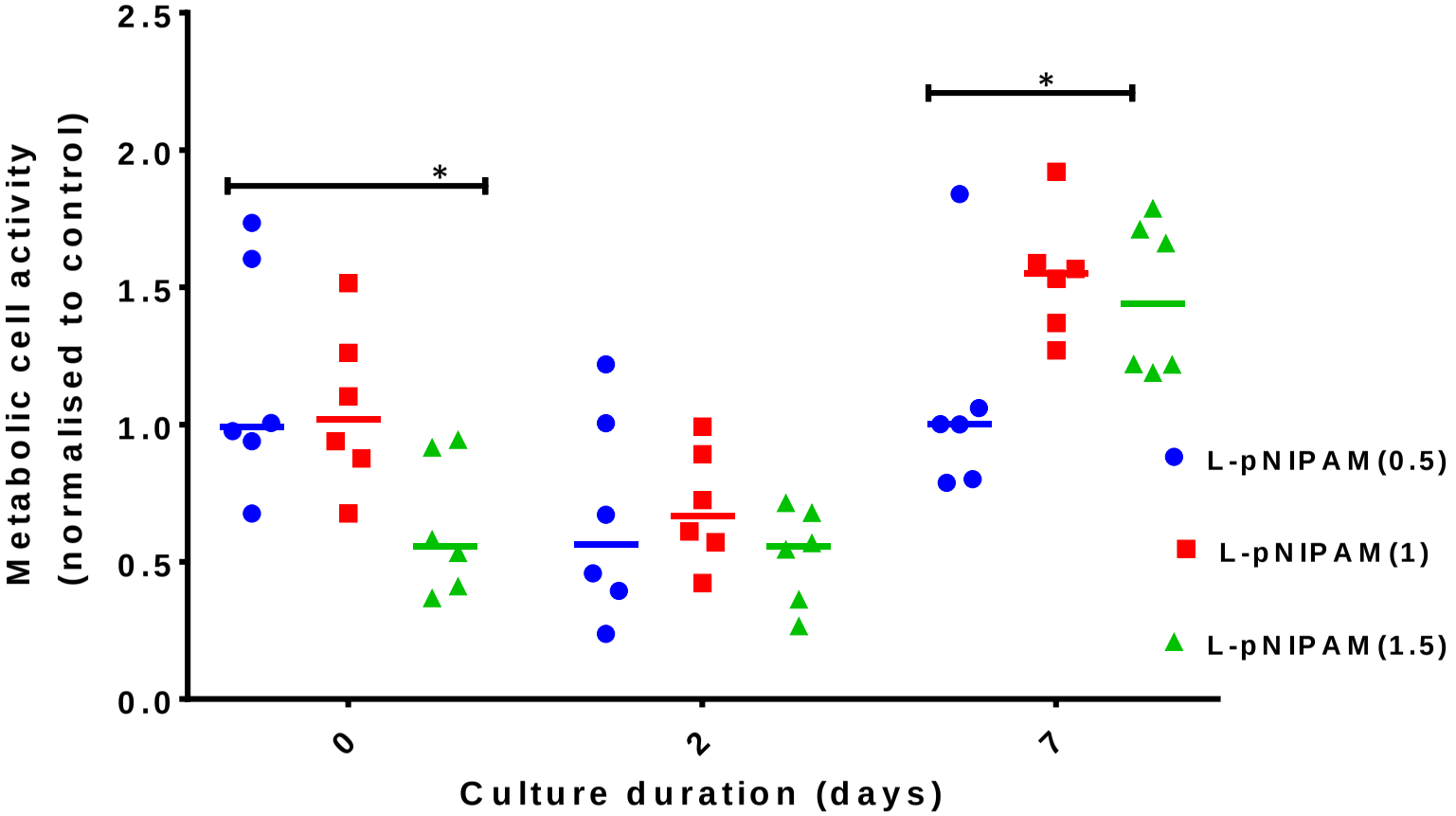

Figure 3.26: *In vitro* cell proliferation using Alamar blue assay of rat stem cells incorporated into L-pNIPAM(0.5), L-pNIPAM(1) and L-pNIPAM(1.5). *=P<0.05.

Metabolic cell activity level and total number of viable cells, within pNIPAM based Laponite® injectable hydrogel with different crosslink densities, were verified using human mesenchymal stem cells (hMSC). Results showed that the lowest metabolic cell activity level on day 0 was observed in highest crosslink density that has the smallest pore size (Figure 3.27). This result could also be due to a lack of water diffusivity, which will affect nutrient transfer to cells.

Similar results were obtained to those seen in rat stem cells; metabolic cell activity was decreased on day 2 within all compositions, due to changing in surrounding environment of cells, where they transferred from monolayer culture to hydrogel matrix (Figure 3.27). On day 7 significant increases were detected in metabolic cell activity within all compositions (Figure 3.27). On day 7 cells cultured within L-pNIPAM (1) showed slightly higher metabolic cell activity (Figure 3.27), suggesting an ideal pore size for maintance of cells.

Pore size and hydrogel stiffness influenced the cell viability within pNIPAM based Laponite® injectable hydrogel, where those two factors affected water diffusivity which is a crucial for cells, as this responsible for nutrition, oxygen diffusion and waste removal.

Tiantian G. *et al* explored the influence of pore size on viability of HepG2 cells, cultured for 21 days within poly (N-isopropylacrylamide-co-2-hydroxyethyl methacrylate) (p(NIPAM-HEMA)) microgel. They found that the reduction in pore size of hydrogel decreased the number of live cells(56).

Their result was in agreement with our findings. However, pore size was not affected the cell viability in linear manner in the current study. As the highest number of live cells was recorded within pNIPAM (1), due to two factors that affected cell viability within pNIPAM based Laponite® injectable hydrogels, where very small pores constricted diffusion of oxygen and nutrients to the cells, as well as reduced waste removal. In contrast the biggest pores were observed to negatively influence the number of life cells, as a result of very big spaces that need to be covered with cells to grow, and very big pores decreased hydrogel stiffness which affected cell behaviour within the hydrogel.

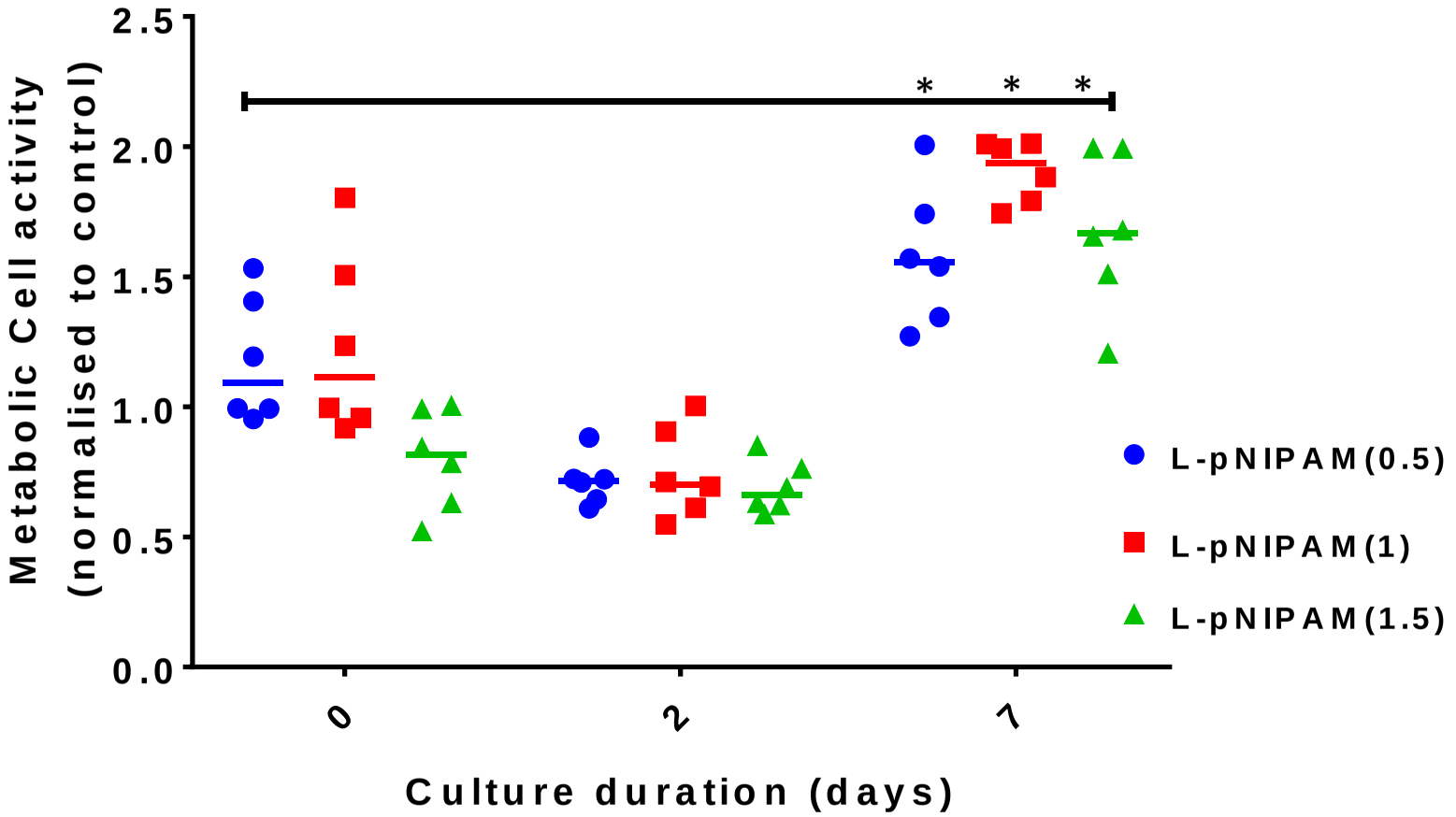

Figure 3.27: *In vitro* cell proliferation using Alamar blue assay of hMSC incorporated into L-pNIPAM (0.5), L-pNIPAM (1) and L-pNIPAM (1.5). *=P<0.05.

Cell viability and the number of live cells, were shown that the previous hypothesis of bigger pore size hydrogels increase the cell viability within their structures(57,58), is not always correct, where in this pNIPAM based Laponite® injectable hydrogel, bigger pores decrease hydrogel stiffness, that negatively affected cell behaviour.

3.3.7.1 Scanning electron microscopy investigation

Hydrogel samples with human mesenchymal stem cells (hMSC), either layered or suspended in hydrogel for two weeks, were examined with SEM at different magnification to explore the influence of crosslink density on cell migration within hydrogel structure.

3.3.7.1.1 Scanning electron microscopy investigation of human mesenchymal stem cells (hMSC) layered on hydrogel samples surface.

Scanning electron microscopy images of hMSC cells cultured on the surface of L-pNIPAM with different crosslink density, are shown in Figure 3.28 and 29, where cells cultured on hydrogel surface after 10 minutes of solidification. Cells can be seen to occupy the pores of honeycomb like structure of hydrogels with spherical morphology (Figure 3.28 and 29). This is visibly influenced by hydrogel porosity, where denser structures were observed in hydrogel with cultured cells, when compared to no cell controls. Since SEM images were taken of fractured hydrogels to show surface as well as inside the hydrogel, to explore whether the culture cells were migrated within the hydrogel or not. It is clear that all hydrogels with different crosslink density have cells migrated within their structures (Figure 3.28 and 29).

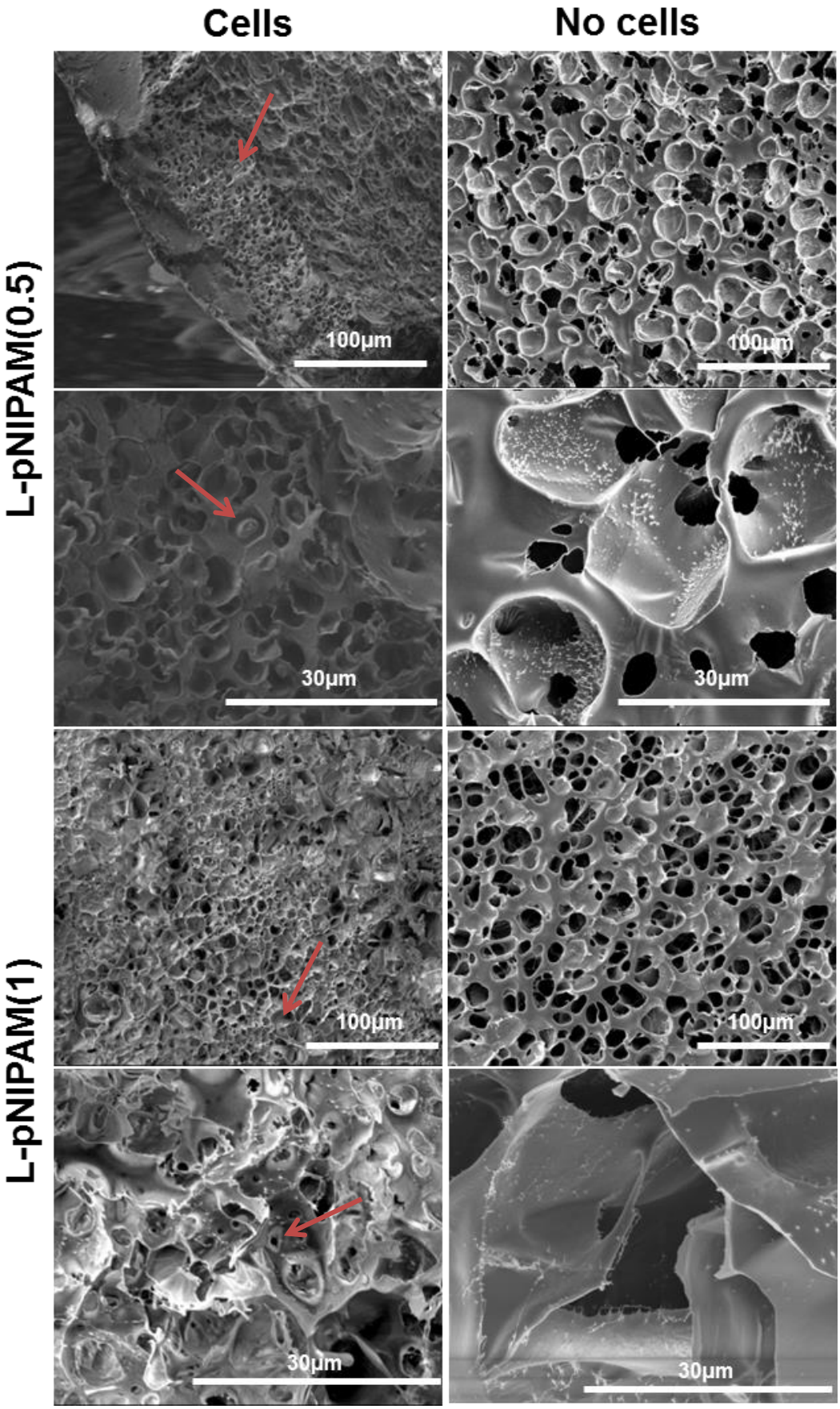

Figure 3.28: Scanning electron microscopy (SEM) of hMSC layered on hydrogel surfaces for 2 weeks and acellular hydrogels with crosslink density of 0.5 and 1wt. %. Red arrows show cells within the pores. Scale bar = 100 and 30 µm.

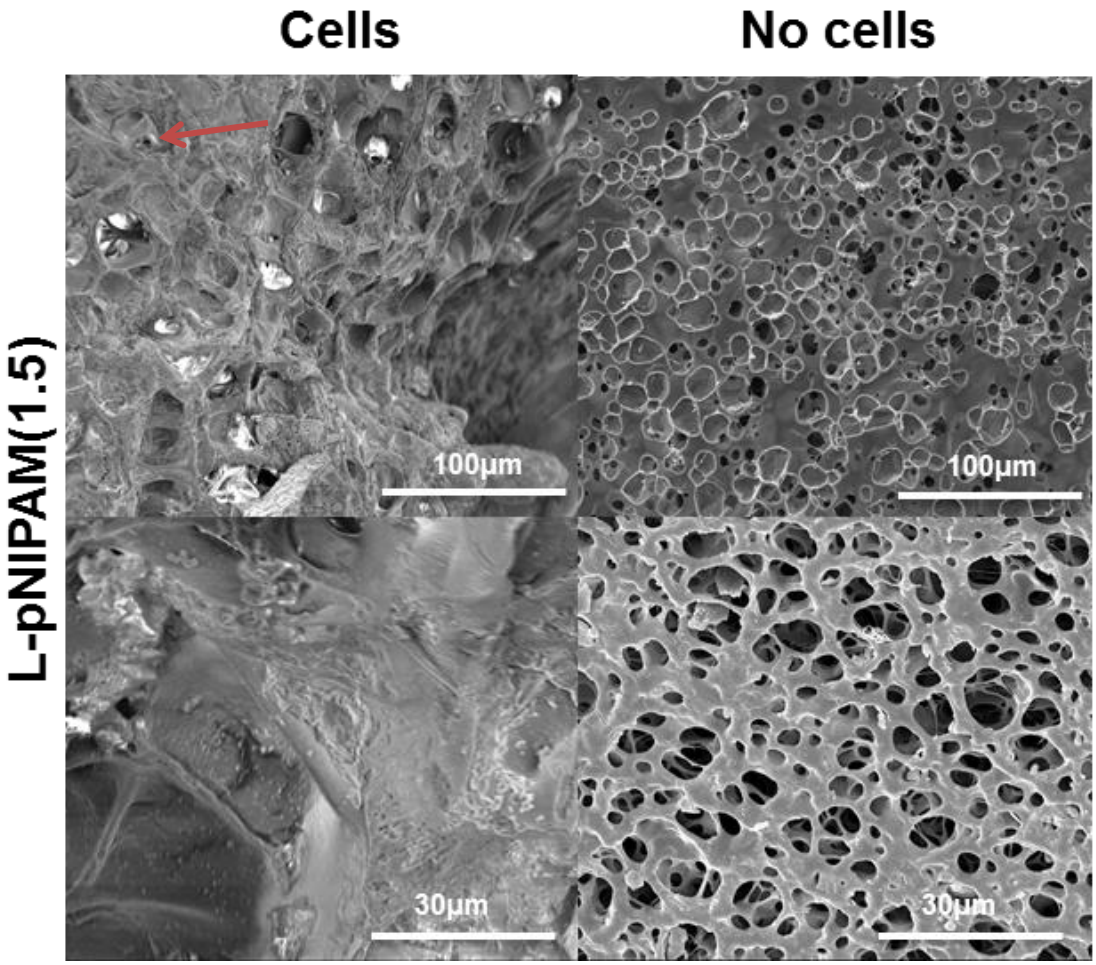

Figure 3.29: Scanning electron microscopy (SEM) of hMSC layered on hydrogel surfaces for 2 weeks and acellular hydrogels with crosslink density of 1.5wt. %. Red arrows show cells within the pores. Scale bar = 100 and 30 µm.

3.3.7.1.2 Scanning electron microscopy investigation of human mesenchymal stem cells (hMSC) suspended in hydrogel samples.

Hydrogel samples were synthesised with crosslink density of 0.5, 1 and 1.5wt. %, as described in Chapter 2.2. Samples were mixed with cell suspension at a density of $1x10^6$ cells/ml and images were taken using scanning electron microscope (SEM). Images were visually analysed and their structure was compared to each relevant and control samples. The honeycomb like structure of pNIPAM based Laponite® injectable hydrogel was shown to be deformed by cells suspended within its structure, and interconnected pores were decreased as cells were detected to occupy the pores and growing through them (Figure 3.30 and 3.31). Similar observations were found by Thorpe A. *et al,* where they cultured hMSC cells within pNIPAM based Laponite® injectable hydrogel for up to 6 weeks, and cells were observed to grow within the pores(53).

Cells were found to cover the pores of hydrogel samples in all compositions that were studied (Figure 3.30 and 3.31), despite slight differences that found between each composition, when Alamar blue protocol was used as indication of the number of live cells. Metabolic cell activity of hMSC cultured within L-pNIPAM (1) was slightly higher than two different crosslink density hydrogel. These findings lead to conclude that smaller pore size of hydrogel retarded the diffusion of oxygen and nutrients to the cells within pNIPAM based Laponite® injectable hydrogel. On other hand, bigger pore size was adversely affected cell behaviour, where cells cultured in L-pNIPAM (0.5) were shown the lowest number of live cells. Meaning that, even with lack of oxygen and nutrients in the hydrogel with smallest pore size (L-pNIPAM (1.5)), the number of live cells in this formulation was higher than that in L-pNIPAM (0.5). Within the lowest crosslink density it is possible that cells were lost through the hydrogel as they would be able to migrate through the hydrogel and fall onto the culture plate below.

In this study changing crosslink density and thereby the inherent pore size of L-pNIPAM hydrogel and its dependant properties, was shown to influence cell viability within this material.

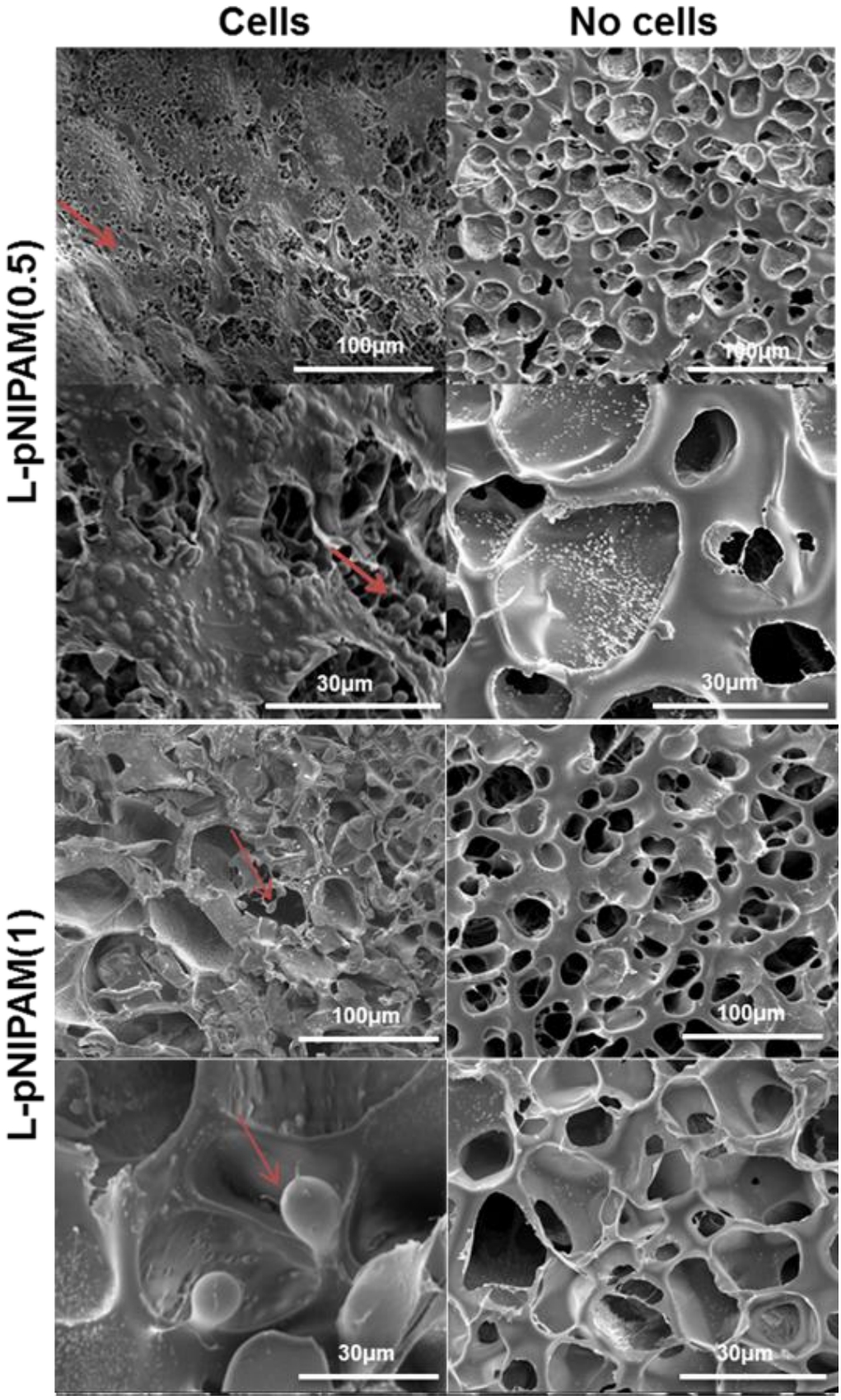

Figure 3.30: Scanning electron microscopy (SEM) of hMSC suspended into hydrogel for 2 weeks and acellular hydrogels with crosslink density of 0.5, and 1wt. %. Red arrows show cells within the pores. Scale bar = 100 and 30 µm. n=3.

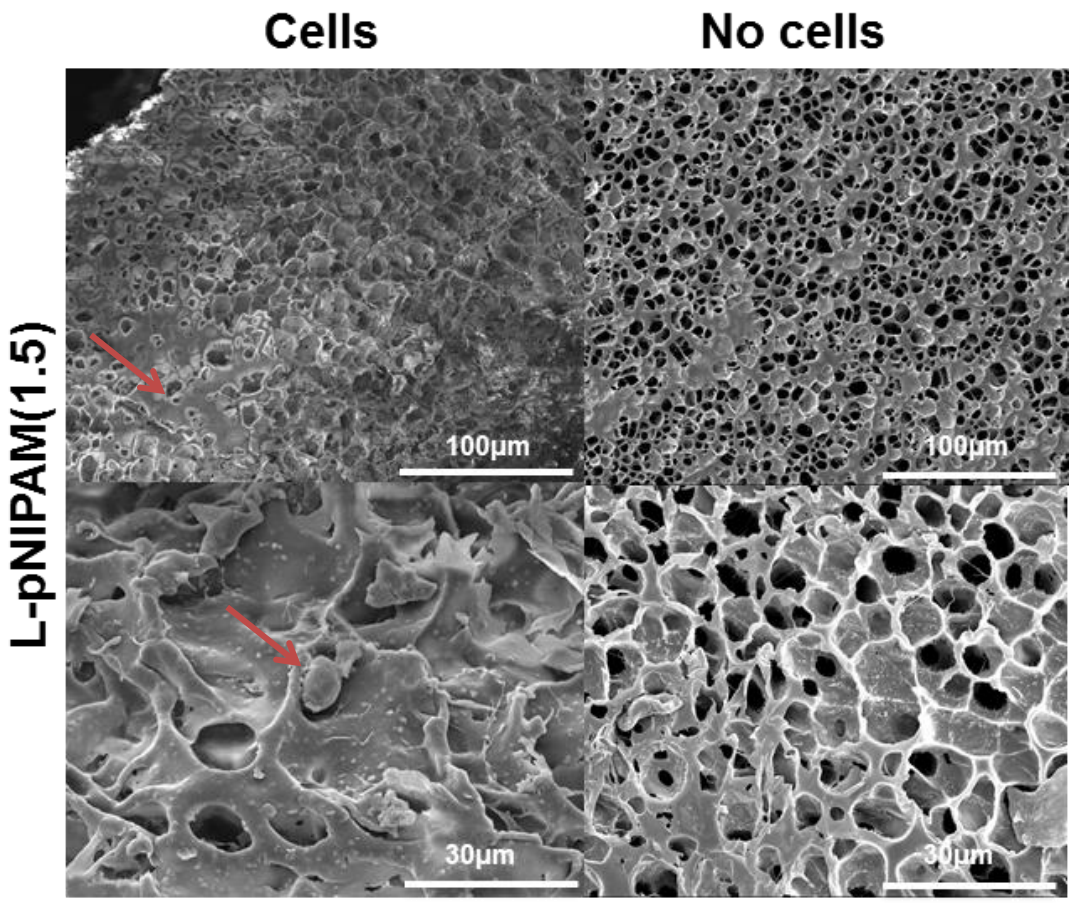

Figure 3.31: Scanning electron microscopy (SEM) of hMSC suspended into hydrogel for 2 weeks and acellular hydrogels with crosslink density of 1.5wt. %. Red arrows show cells occupy the pores. Scale bar = 100 and 30 µm. n=3.

L-PNIPAM hydrogel with crosslink density of 1wt. % was found to be the most optimal formulation for cells, due to number of live cells that were observed within its structure, up to 7 day of culture, due to sufficient oxygen and nutrients that can diffuse through its structure.

3.4 Summary

In this chapter, the effects of using different crosslink density on physical and mechanical properties of pNIPAM based Laponite® hydrogel have been investigated in depth. Structural properties were found to be key for function and behaviour of the hydrogels, where pore size was linked to other physical and mechanical properties. For mechanical behaviour, smaller pore sizes resulted in stiffer hydrogel materials, where storage modulus (G') increased linearly with increase crosslink density. Swelling - deswelling rates were also decreased when the pore sizes decreased in higher crosslink density hydrogels. Dehydration and rehydration rates were decreased with decrease pore sizes. In addition, Dehydration and rehydration data allowed calculation of bound water content and diffusion coefficient respectively, for L-pNIPAM hydrogel with different crosslink densities. Pore size was also shown to affect the state of water and diffusion rate within this material.

Wettability of L-pNIPAM hydrogel was enhanced by increasing crosslink density as expected(19). Surface topography was explored using different approaches with two different sample preparation methods. The measured surface roughness values varied depending on the preparation method and technique. Surface roughness for L-pNIPAM hydrogels measured using AFM, showed lower values, due to the preparation method used, with spin coating leading to smoother films. Generally, both techniques showed that increasing crosslink density increased surface roughness.

Cell behaviour was affected by using different crosslink density, where cell viability results for rat and human mesenchymal stem cells (hMSC) showed different metabolic cell activity levels when cells were cultured in L-pNIPAM hydrogels with different crosslink densities. The morphology of the hydrogels and pore size of each crosslink density could be one of the possible factors that impacted cell viability within this material, where L-pNIPAM (1.5) with the smallest pore size negatively influenced diffusion nutrients. Whereas, L-pNIPAM (0.5) with the biggest pore size showed lowest cell numbers after 7 days in culture, where cell clusters were observed. SEM images of cultured cells within different crosslink density hydrogels also showed cells within all hydrogel formulations that studied, in either layered or suspended cells, with the highest populations seen in L-pNIPAM (1).

Crosslink density is a crucial factor that affects a range of properties of pNIPAM based Laponite® hydrogel as well as cell behaviour. Therefore, it is essential to consider the crosslink density during optimisation of materials.

3.5 References

1. Koenigs M, Pal A, Mortazavi H, Pawar GM, Storm C, and Sijbesma RP. Tuning cross-link density in a physical hydrogel by supramolecular self-sorting. Macromolecules. 2014;47(8):2712–2717.

2. Wong R, Ashton M, and Dodou K. Effect of crosslinking agent concentration on the properties of unmedicated hydrogels. Vol. 7, Pharmaceutics. 2015.

3. Ren H, Zhu M, and Haraguchi K. Characteristic Swelling Deswelling of Polymer / Clay Nanocomposite Gels. Macromolecules. 2011;8516–8526.

4. Cates, R. (2010). *Influence of Crosslink Density on Swelling and Conformation of Surface-Constrained Poly (n-isopropylacrylamide) Hydrogels*. PhD (Thesis). University of South Florida.

5. Djonlagic, J. et al. Hydrogels reinforced with nanoclays with improved response rate. Journal applied Polymer Science. 2016;134(9):1–14.

6. Jang J, Seol YJ, Kim HJ, Kundu J, Kim SW, Cho DW. Effects of alginate hydrogel cross-linking density on mechanical and biological behaviors for tissue engineering. Journal Mechanical Behavaviour of Biomedical Materials. 2014;37:69–77.

7. Haraguchi K, Ebato M, Takehisa T. Polymer-clay nanocomposites exhibiting abnormal necking phenomena accompanied by extremely large reversible elongations and excellent transparency. Advanced Materials. 2006;18(17):2250–2254.

8. Haraguchi K, Takehisa T, Fan S. Effects of Clay Content on the Properties of Nanocomposite Hydrogels Composed of Poly(N - isopropylacrylamide) and Clay. Macromolecules. 2002;35(27):10162–10171.

9. Khare AR, Peppas NA. Investigation of hydrogel water in polyelectrolyte gels using differential scanning calorimetry. Polymer. 1993;34(22):4736–4739.

10. Mu F. Different States of Water in Hydrogels. Macromolecules.1998;9297(98):6721–6723.

11. Ostrowska-Czubenko J. State of water in noncrosslinked and crosslinked hydrogel chitosan membranes–DSC studies. Progess of Chemistry. 2011:147–156.

12. Corkhill PH, Jolly AM, Ng CO, Tighe BJ. Synthetic hydrogels: 1. Hydroxyalkyl acrylate and methacrylate copolymers - water binding studies. Polymer. 1987;28(10):1758–1766.

13. Gierszewska M, Ostrowska J, and Kwiatkowska A,. Effect of ionic crosslinking on density of hydrogel chitosan membranes. Progress on Chemistry and Application of Chitin and its Derivatives Journal. 2013;18:49–58.

14. Sun J, William W, Geberich, and Lorraine F. Electrical and optical

properties of ceramic-polymer nanocomposite coatings. Journal of Polymer Science, Part B-Polymer Physics. 2013;41(14):1744–1761.

15. Yabu H, Takebayashi M, Tanaka M, Shimomura M. Superhydrophobic and lipophobic properties of self-organized honeycomb and pincushion structures. Langmuir. 2005;21(8):3235–3237.

16. Allcock HR, Steely LB, Kim SH, Kim JH, Kang B-K. Plasma surface functionalization of poly[bis(2,2,2-trifluoroethoxy)phosphazene] films and nanofibers. Langmuir. 2007;23(15):8103–8107.

17. Haraguchi K, Li HJ, Song L, Murata K. Tunable optical and swelling/deswelling properties associated with control of the coil-to-globule transition of poly(N-isopropylacrylamide) in polymer - Clay nanocomposite gels. Macromolecules. 2007;40(19):6973–6980.

18. Kubiak K, Wilson M, Mathia T, and Carval P. Wettability versus roughness of engineering surfaces. Wear Journal. 2011;271(3–4):523–528.

19. Haraguchi K. Hydrogels with Hydrophobic Surfaces: Abnormally High Contact Angles for Water on PNIPA Nanocomposite Hydrogels. Macromolecules. 2007: 93-95.

20. Gadelmawla E, Koura M, Maksoud T, Elewa I, Soliman H. Roughness parameters. Journal of Materials and Process Technology. 2002;123(1):133–145.

21. Giraldez M, and Yebra-Pimentel E. Hydrogel Contact Lenses Surface Roughness and Bacterial Adhesion. 2012:99-103.

22. Guryča V, Hobzová R, Přádný M, Širc J, Michálek J. Surface morphology of contact lenses probed with microscopy techniques. Contact Lens Anterior Eye. 2007;30(4):215–222.

23. González-Méijome JM, Löpez-Alemany A, Almeida JB, Parafita MA. Surface AFM microscopy of unworn and worn samples of silicone hydrogel contact lenses. Journal of Biomedical Materials Research - Part B: Applied Biomaterials. 2009;88(1):75–82.

24. Kim SH, Opdahl A, Marmo C, Somorjai GA. AFM and SFG studies of pHEMA-based hydrogel contact lens surfaces in saline solution: Adhesion, friction, and the presence of non-crosslinked polymer chains at the surface. Biomaterials. 2002;23(7):1657–1666.

25. Djonlagic J, Lancuski A, Nikolic MS, Rogan J, Ostojic S, Petrovic Z. Hydrogels reinforced with nanoclays with improved response rate. Journal of Applied Polymer Science. 2017;134(9):1–14.

26. Leal-Egaña A, Dietrich-Braumann U, Díaz-Cuenca A, Nowicki M, Bader A. Determination of pore size distribution at the cell-hydrogel interface. Journal of Nanobiotechnology. 2011;9(1):24.

27. Haraguchi K, Takehisa T, Fan S. Effects of Clay Content on the Properties of Nanocomposite Hydrogels Composed of Poly(N -

isopropylacrylamide) and Clay. Macromolecules. 2002;35(27):10162–10171.

28. Kumar A, Pandey M, Koshy MK, Saraf SA. Synthesis of fast swelling superporous hydrogel: effect of concentration of crosslinker and acdisol on swelling ratio and mechanical strength. Introduction of Journal Drug Delivery. 2010;2(2):135–140.

29. Lee KY, Rowley JA, Eiselt P, Moy EM, Bouhadir KH, Mooney DJ. Controlling mechanical and swelling properties of alginate hydrogels independently by cross-linker type and cross-linking density. Macromolecules. 2000;33(11):4291–4294.

30. Metz J, Gonnerman K, Chu A, Chu T-MG. Effect of crosslinking density on swelling and mechanical properties of PEGDA400/PCLTMA900 hydrogels. Biomedical Science Instrumentation. 2006;464:389–394.

31. Thorpe AA, Creasey S, Sammon C, Le Maitre CL. Hydroxyapatite nanoparticle injectable hydrogel scaffold to support osteogenic differentiation of human mesenchymal stem cells. European Journal of Cells Materials. 2016;32:1–23.

32. Ahearne M, Yang Y, Liu K. Mechanical Characterisation of Hydrogels for Tissue Engineering Applications. Tissue Engineering. 2008;4:1–16.

33. Yacob N, Hashim K. Morphological effect on swelling behaviour of hydrogel. AIP Confress Process. 2014;1584(2014):153–159.

34. Zhang XZ, Wu DQ, Chu CC. Effect of the crosslinking level on the properties of temperature-sensitive poly(N-isopropylacrylamide) hydrogels. Journal of Polymer Science, Part B Polymer Physics. 2003;41(6):582–593.

35. Dogu Y, Okay O. Swelling-deswelling kinetics of poly(N-isopropylacrylamide) hydrogels formed in PEG solutions. Journal of Applied Polymer Science. 2006;99(1):37–44.

36. Muthudoss, P. (2011). Application of FTIR imaging and spectroscopy to solid dosage formulations. PhD.(Thesis) Sheffield Hallam University.

37. Sammon C, Deng C, Mura C, Yarwood J. Vibrational spectroscopic studies of the dynamics and perturbation of water in polymeric films. Journal of Molecular Liquids. 2002;101(1–3):35–54.

38. Sammon C, Deng C, and Yarwood J. Polymer-water interactions. Origin of perturbed infrared intensities of water in polymeric systems. Journal of Polymer. 2003;44(9):2669–2677.

39. Boyes, V. (2012). *The Synthesis and development of novel, easily processable poly (N- Isopropylacrylamide) - based hydrogels*. PhD.(Thesis) Sheffield Hallam University.

40. Elabd YA, Baschetti M, and Barbari TA. Time-resolved Fourier transform infrared/attenuated total reflection spectroscopy for the measurement of molecular diffusion in polymers. Journal of Polymer Science. Part B.

2003;41(22):2794–807.

41. Guo J, and Barbari TA. Unified dual mode description of small molecule sorption and desorption kinetics in a glassy polymer. Macromolecules. 2009;42(15):5700–8.

42. Sammon C, Li C, Armes SP, and Lewis AL. ATR-FTIR studies of a thermo-responsive ABA triblock copolymer gelator in aqueous solution. Polymer. 2006;47(17):6123–6130.

43. Sammon C, Mura C, Yarwood J, Everall N, Swart R, Hodge D. FTIR−ATR Studies of the Structure and Dynamics of Water Molecules in Polymeric Matrixes. A Comparison of PET and PVC. Journal of Physical Chemistry. Part B. 1998;102(18):3402–3411.

44. Duda L. Molecular diffusion in polymeric systems. 1985;57(1):1681–90.

45. Karimi M. Diffusion in Polymer Solids and Solutions. Mass Transfer in Chemical Engineering Processes. 2011; 17-40.

46. Chen J, Park H, Park K. Synthesis of superporous hydrogels: Hydrogels with fast swelling and superabsorbent properties. Journal of Biomedical Materials Research. 1999;44(1):53–62.

47. George KA, Wentrup-Byrne E, Hill David DJT, Whittaker AK. Investigation into the diffusion of water into HEMA-co-MOEP hydrogels. Biomacromolecules. 2004;5(4):1194–1199.

48. Tanaka T, Fillmore DJ. Kinetics of swelling of gels. Journal of chemical Physics. 1979;70(3):1214–1218.

49. Schuster J, Cichos F, Wrachtrup J, Von Borczyskowski C. Diffusion of Single Molecules Close to Interfaces. Single molecules. 2000;1(4):299–305.

50. Wu Y, Joseph S, Aluru NR. Effect of Cross-Linking on the Diffusion of Water , Ions , and Small Molecules in Hydrogels Effect of Cross-Linking on the Diffusion of Water , Ions , and Small Molecules in Hydrogels. Journal of Physical Chemistry B. 2009;3512–3520.

51. Haraguchi K, Li H, Okumura N. Hydrogels with Hydrophobic Surfaces : Abnormally High Water Contact Angles on PNIPA Nanocomposite Hydrogels. Macromolecules 2007; 40 (7):2299–2302.

52. V. dos Santos. Biomaterials: Characteristics and Properties. In: Engineering of Biomaterials. Springer; 2017; 5–15.

53. Thorpe AA, Dougill G, Vickers L, Reeves ND, Sammon C, and Cooper G,. Thermally triggered hydrogel injection into bovine intervertebral disc tissue explants induces differentiation of mesenchymal stem cells and restores mechanical function. Acta Biomaterialia. 2017;54:212–226.

54. Annabi N, Mithieux SM, Weiss AS, and Dehghani F. The fabrication of elastin-based hydrogels using high pressure CO2. Biomaterials. 2009;30(1):1–7.

55. Annabi N, Mithieux SM, Boughton EA, Ruys AJ, Weiss AS, and Dehghani F. Synthesis of highly porous crosslinked elastin hydrogels and their interaction with fibroblasts in vitro. Biomaterials. 2009;30(27):4550–4557.

56. Gan T, Guan Y, and Zhang Y. Thermogelable PNIPAM microgel dispersion as 3D cell scaffold: Effect of syneresis. Journal of Materials Chemistry. 2010;20(28):5937–5944.

57. Kim HJ, Kim UJ, Vunjak-Novakovic G, Min BH, Kaplan DL. Influence of macroporous protein scaffolds on bone tissue engineering from bone marrow stem cells. Biomaterials. 2005;26(21):4442–4452.

58. Mygind T, Stiehler M, Baatrup A, Li H, Zou X, and Flyvbjerg A,. Mesenchymal stem cell ingrowth and differentiation on coralline hydroxyapatite scaffolds. Biomaterials. 2007;28(6):1036–1047.

Chapter 4

Incorporation of hydroxyethyl methacrylate into pNIPAM based Laponite hydrogel

4.1 Introduction

Poly(2-hydroxyethyl methacrylate) (pHEMA) is a useful polymer in drug delivery and tissue engineering, as it can be easily synthesised and its mechanical and physical behaviour can be manipulated(1,2). In 1960 pHEMA was the first hydrophilic polymer to be used in hydrogel synthesis by Wichterle and Lim(3,4). Since then, researchers have studied this polymer intensively due to its physiochemical behaviours and similarity to living tissues(5–7). Poly(HEMA) has also been used in the synthesis of stimuli responsive copolymer hydrogels(8). Copolymers which may have lower critical solution temperature (LCST) were the most attractive, due to their importance in many applications including biomedical and pharmaceutical fields(9). Therefore, N-Isopropylacrylamide was a favourable monomer to be used in conjunction with HEMA, to create a copolymer hydrogel that has a tuneable LCST. Enhancing physical and mechanical properties were the main goal for researchers who synthesised and studied the properties and applicability of (pNIPAM-HEMA) hydrogels(10–12). Berna Y. *et al* studied the influence of incorporated different ratio of NIPAM and HEMA on hydrogels synthesised by radical redox polymerization at 4°C. They used N,N`-methylenebisacrylamide (MBAAm) was used as crosslinker agent and potassium persulphate (KPS) as initiator. The synthesised PNIPAM-co-HEMA hydrogels in their study were non-injectable, where blocks of hydrogels were washed with distilled water for 24 hours to remove any potential unreacted monomers. The authors found that the equilibrium swelling ratio of the copolymeric gels decreased as HEMA content increased(12).

In the current work influence of adding HEMA as comonomer to pNIPAM based Laponite® injectable hydrogels, was studied, where physical and mechanical behaviour of a series of fully injectable pNIPAM-co-HEMA hydrogels were investigated, and cell viability within different pNIPAM-co-HEMA compositions were explored.

4.2 Methods

All materials and methods of hydrogel synthesis, experimental work and characterisation techniques were detailed in Chapter 2.2

4.3 Results and Discussion

4.3.1 Influence of incorporation of hydroxyethyl methacrylate (HEMA) on lower critical solution temperature of pNIPAM hydrogel

Hydroxyethyl methacrylate (HEMA) was incorporated into pNIPAM based Laponite® injectable hydrogel with a ratio of 5 and 10 wt. % of total monomers used. As previously mentioned in chapter 2, section 2.2 a range of HEMA concentrations was used (5, 10 and 12wt. %), where the highest concentration of HEMA was found to be not fully injectable, hence no further characterisations were performed on this composition.

Literature has shown that adding more hydrophilic monomer into pNIPAM hydrogels raises LCST(13,14). However, it is also known that "changes in LCST when comonomers are incorporated are due to changes in overall hydrophilicity and are not due to comonomer hydrophilicity or hydrophobicity"(15). Due to differences in hydrophilicity between hydroxyethyl methacrylate (HEMA) and N-Isopropylacrylamide (NIPAM), where HEMA is more hydrophilic than NIPAM (Figure 4.1).

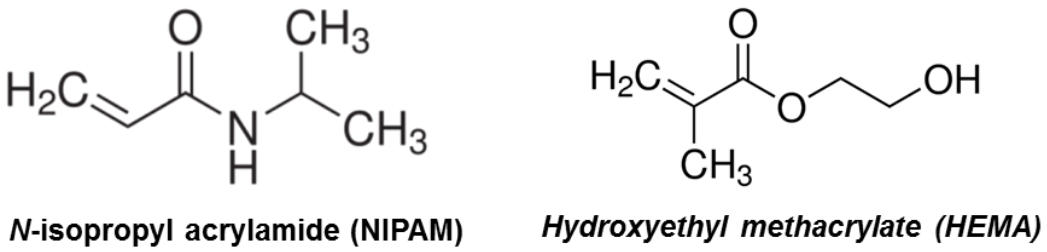

N*-isopropyl acrylamide (NIPAM)** ***Hydroxyethyl methacrylate (HEMA)

Figure 4.1: Chemical structures of N-isopropyl acrylamide (NIPAM) and Hydroxyethyl methacrylate (HEMA).

Hence, in the current study changes in LCST were expected when HEMA was added into L-pNIPAM, as a result of copolymerisation of HEMA and NIPAM. The influence of HEMA on the LCST of HEMA was determined by measuring the LCST using the method described in Chapter 2.4 of a number of systems where the HEMA content was systematically modified (5 and 10 wt. %). Interestingly no changes in LCST were observed when HEMA was incorporated into L-pNIPAM (Figure 4.2). Increasing the HEMA concentration in L-pNIPAM$_{95}$-

co-$HEMA_5$ and L-$pNIPAM_{90}$-co-$HEMA_{10}$ had no impact on the measured setting temperature (believed to be linked to the LCST) compared to L-pNIPAM, which was somewhat counterintuitive, as the perceived wisdom is that increasing the hydrophilicity of an amphiphilic copolymer system should raise the LCST (16). It was postulated that the pendant OH groups on the HEMA units could be interacting with the polar groups of the Laponite® platelets effectively shielding their hydrophilicity and negating the anticipated impact on the setting temperature. Changes in phase transition behaviour of copolymer systems from their single polymer counterparts is good evidence of copolymerisation of NIPAM and HEMA(16).

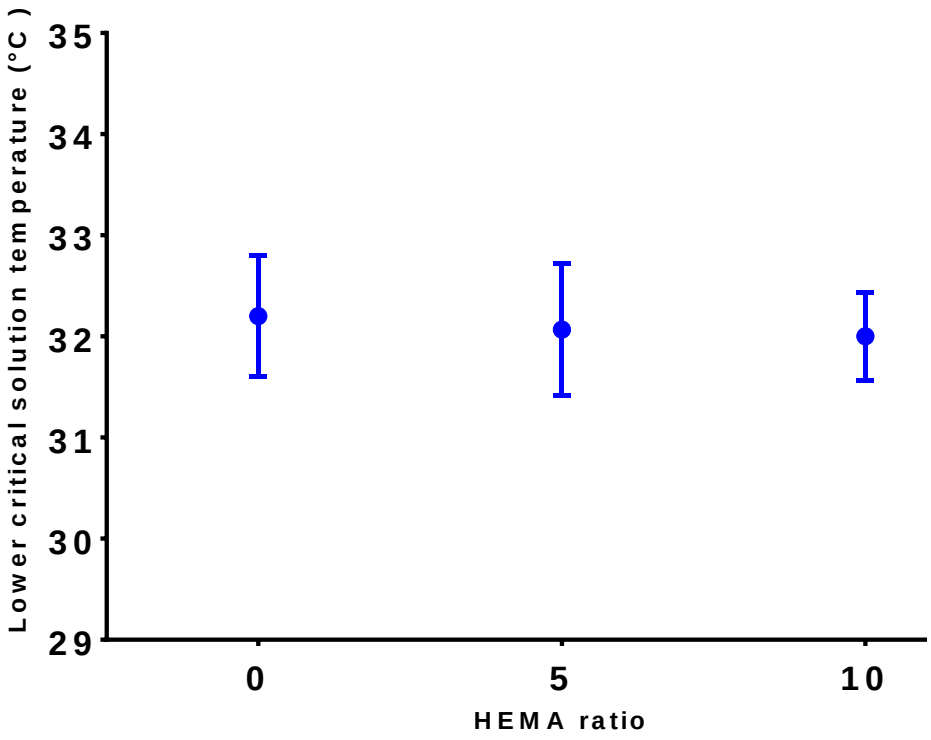

Figure 4.2: Lower critical solution temperature (LCST) of pNIPAM/HEMA based Laponite® hydrogel with different HEMA ratios.

4.4 Morphological study and pore size measurement of L-pNIPAM-co-HEMA

Influence of incorporation of HEMA on the structural properties of L-pNIPAM-co-HEMA hydrogels, was investigated using SEM and the pore size of each composition was measured as described in Chapter 2.3.2. SEM images showed limited differences in morphology between L-pNIPAM and L-pNIPAM-co-HEMA

(Figure 4.3). Pore sizes of different compositions were measured using six images of each composition; demonstrating no effect on pore size within the hydrogel with or without HEMA (Figure 4.4). However, heterogeneity was noticeably increased at 10 wt. % HEMA concentration, and the average pore size was slightly increased (Figure 4.3 and 4.4). An increase in heterogeneity supports the scenario in which NIPAM and HEMA polymerised separately, either by crosslinking or free radical polymerisation.

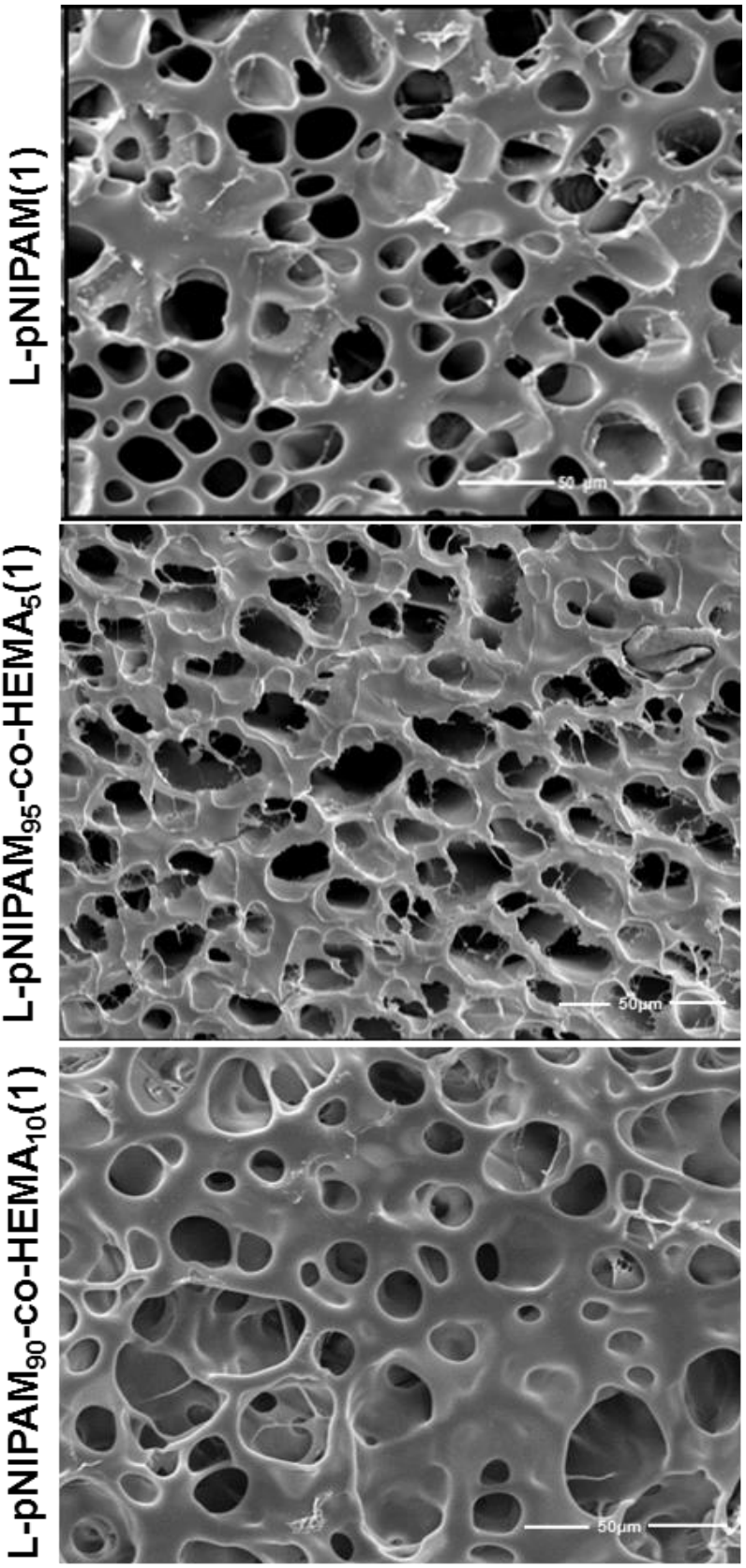

Figure 4.3: Scanning electron microscopy images of L-pNIPAM, L-pNIPAM$_{95}$-co-HEMA$_5$ and L-pNIPAM$_{90}$-co-HEMA$_{10}$. Scale bars=50 µm, n=6.

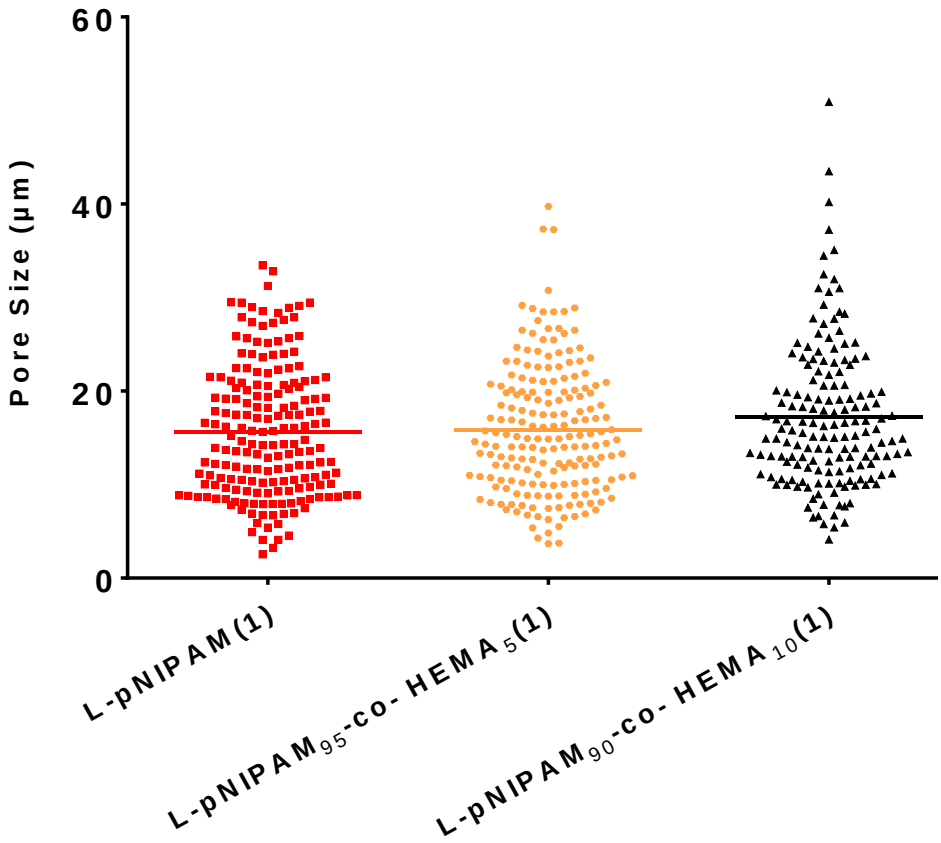

Figure 4.4: Statistical analysis of pore size of L-pNIPAM, L-pNIPAM$_{95}$-co-HEMA$_5$ and L-pNIPAM$_{90}$-co-HEMA$_{10}$. n=6.

4.5 Dynamic Mechanical Analysis (DMA) frequency scan data of PNIPAM based Laponite®

Viscoelastic properties of L-pNIPAM-co-HEMA were studied and the influence of HEMA concentration on the storage modulus was investigated. Dynamic mechanical analysis, in a frequency compression mode was used. Six samples for each composition were analysed to determine the effect on mechanical properties of incorporation of HEMA into L-pNIPAM (Figure 4.5). In all samples studied there were no changes in storage modulus as a function of frequency. Hence, 10 Hz was used to compare possible differences in the mechanical properties between each composition (Figure 4.6).

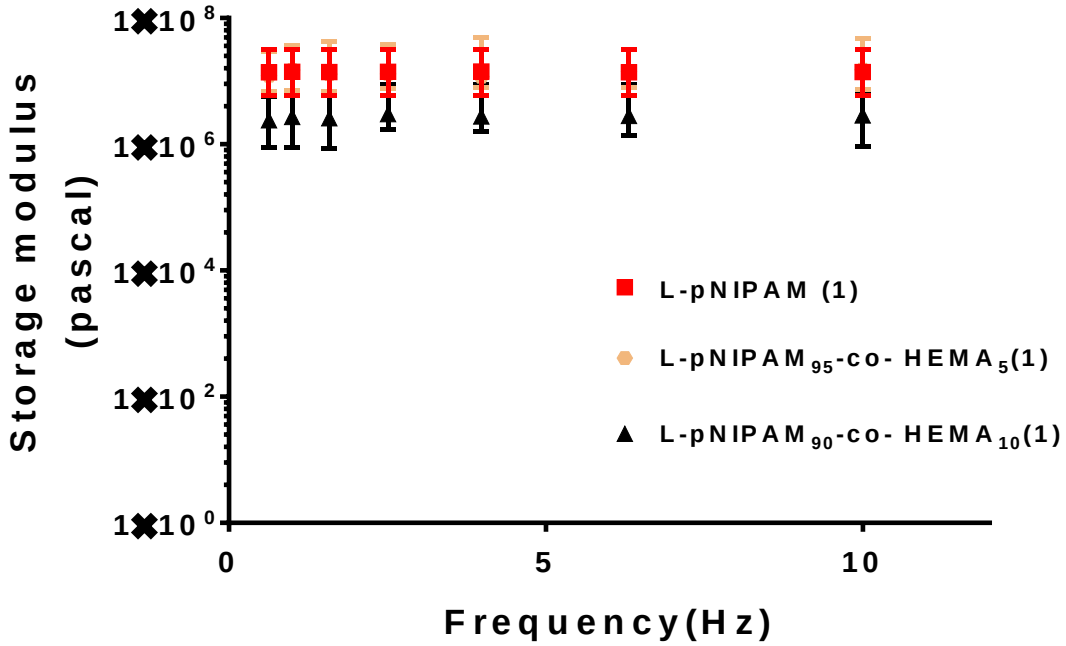

Figure 4.5: Dynamic Mechanical Analysis (E' values) of L-pNIPAM, L-pNIPAM$_{95}$-co-HEMA$_5$ and L-pNIPAM$_{90}$-co-HEMA$_{10}$. n=6.

Results showed that an increase HEMA concentration to 10 wt. % significantly decreased storage modulus of pNIPAM/HEMA based Laponite® injectable hydrogel (Figure 4.6). A decrease in storage modulus was thought to be due to the slight increase seen in average pore size, when HEMA concentration increased to 10 wt. %. In addition, an increase the number of pHEMA molecules, influenced the mechanical properties of the pNIPAM/HEMA hydrogel. These results were in good agreement with Yan L. et al(17) and Tuncel et al(16), where both studies have shown that HEMA concentration increased the elasticity of pNIPAM based hydrogels when incorporated.

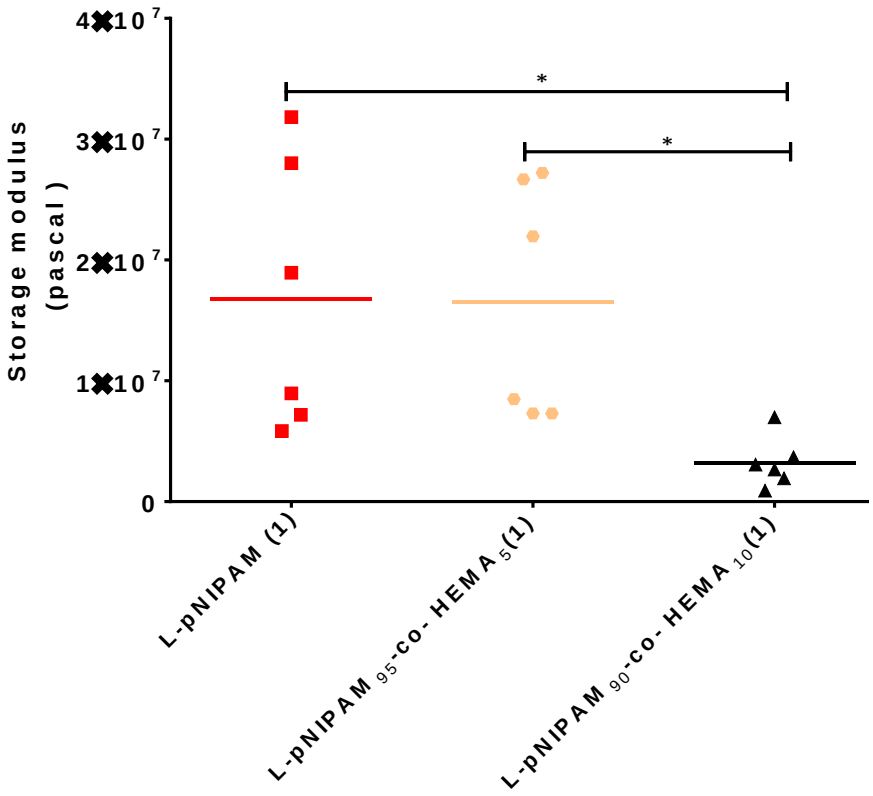

Figure 4.6: Influence of HEMA concentration on storage modulus of L-pNIPAM-co-HEMA determined by DMA in compression mode at 10Hz. *=P<0.05. n=6.

4.6. Swelling and deswelling kinetics of L-pNIPAM-co-HEMA

4.6.1 Swelling kinetics

Swelling kinetics in distilled water at 25°C as a function of time up to 24 hours, for L-pNIPAM-co-HEMA hydrogels was investigated, to determine the effect of incorporating HEMA on the swelling ratio and maximum equilibrium swelling degree. When HEMA was incorporated, the hydrogel exhibited a slightly higher degree of swelling coinciding with a higher equilibrium swelling degree (Figure 4.7 and 4.8). Faster swelling after the first two hours (120 minutes) was observed (Figure 4.7), due to an increase in the hydrophilic polymeric molecules that are able to interact with water. Also, pore size was shown an increase when 10 wt. % HEMA was incorporated, which enhances water permeability.

Jianquan et al have studied swelling ratio and equilibrium water content of a series of hydrogels based on 2-hydroxyethyl methacrylate HEMA and epoxy methacrylate (EMA). They have found that an increase in EMA concentration

decreased equilibrium water content due to its hydrophobicity(19). Yan et al, have shown same effect of HEMA concentration on pNIPAM based hydrogel on swelling ratio, where a range of NIPAM: HEMA ratios of 0:10, 1:9, 2:8, 3:7, 4:6, and 5:5, v/v) were used. Their results have shown that increase HEMA ratio increase swelling ratio of hydrogel at temperature lower than the LCST of NIPAM(17).

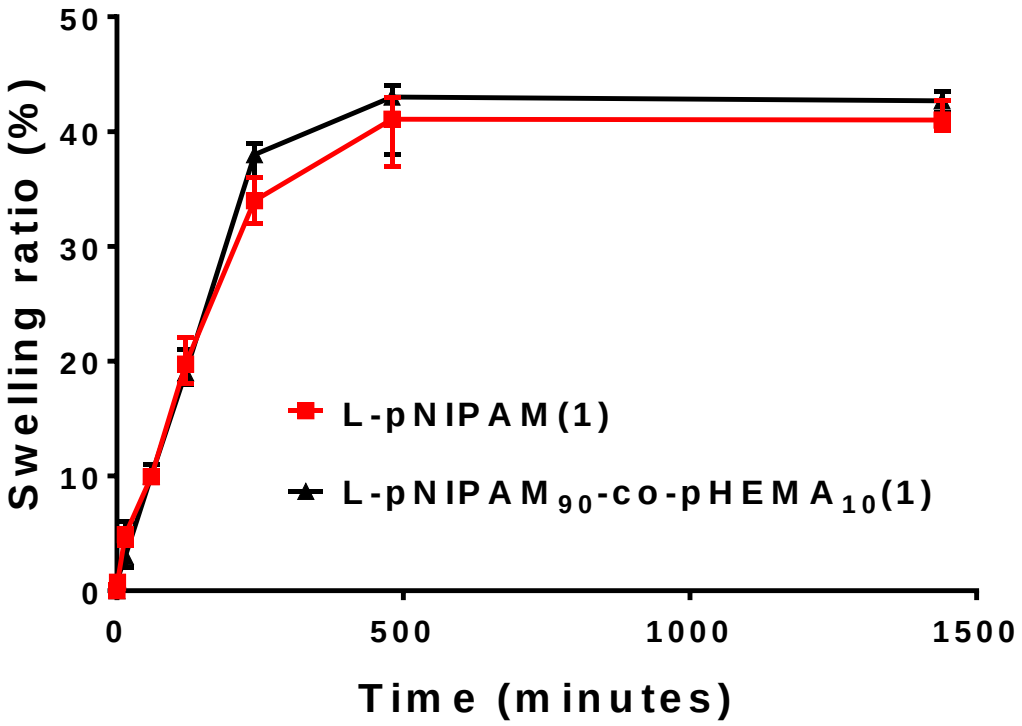

Figure 4.7: Swelling ratio of L-pNIPAM hydrogels with and without HEMA incorporated.

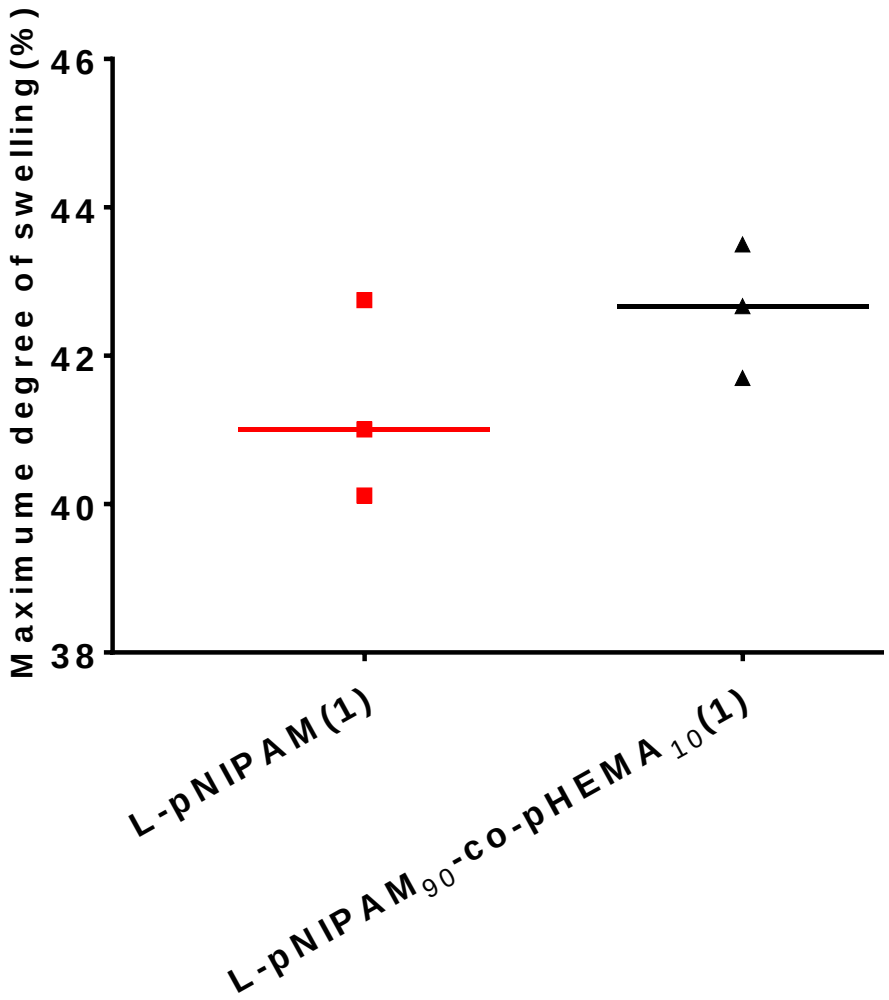

Figure 4.8: Equilibrium swelling degree of L-pNIPAM hydrogels with and without HEMA incorporated.

4.6.2 Deswelling kinetics of L-pNIPAM-co-HEMA

Deswelling behaviour of L-pNIPAM-co-HEMA hydrogels was observed from 25°C to 62°C. When 10 wt. % HEMA was incorporated, the hydrogel displayed a lower degree of deswelling (Figure 4.9), and a significant reduction in the maximum degree of deswelling was observed (Figure 4.10). The reduction in deswelling could be due to presence of pHEMA molecules, which inhibit thermal response of pNIPAM molecules around their LCST temperature. Due to non-thermal responsive nature of pHEMA molecules, they obstructed thermal response of pNIPAM molecules(16). Similiar results were obtained by Yan et al, when they studied thermal response behaviour of pNIPAM-co-HEMA hydrogel, at 37°C. They have shown that incorporation of HEMA into pNIPAM hydrogel inhibited the thermal response of pNIPAM hydrogel, due to p(NIPAM-HEMA) chains can easily provide fast relaxation to coil to globule transition(20).

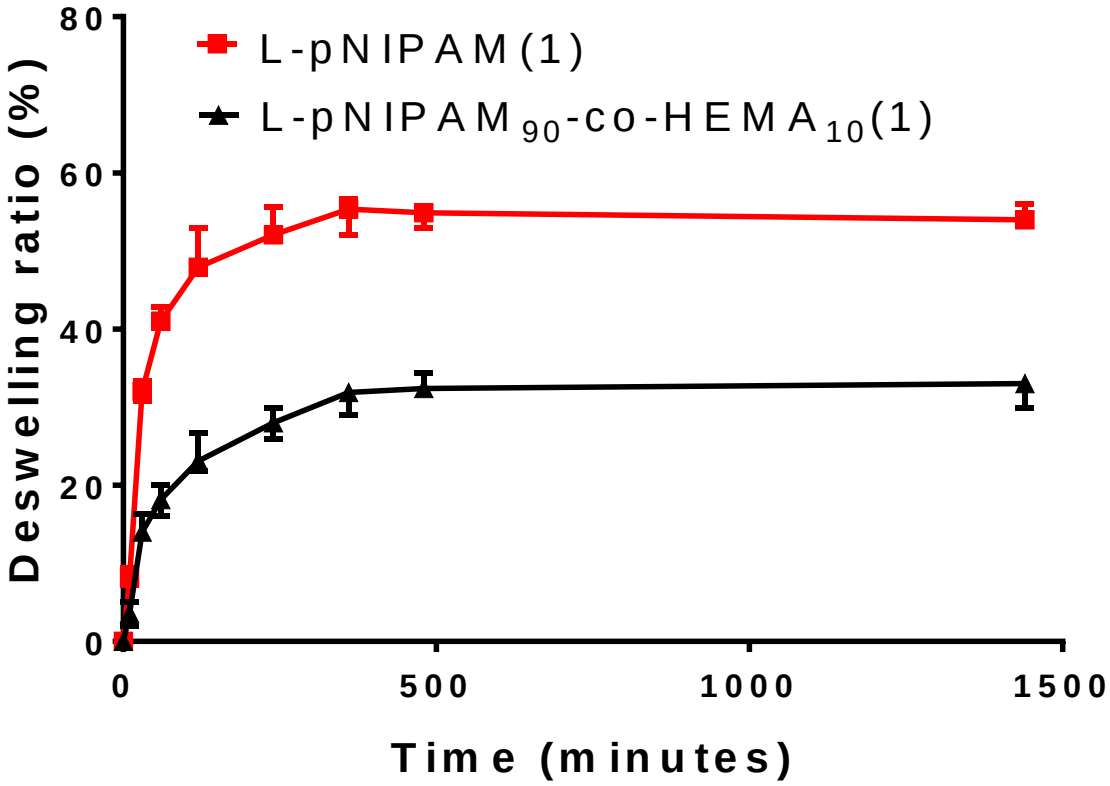

Figure 4.9: Deswelling ratio of L-pNIPAM hydrogels with and without HEMA incorporated.

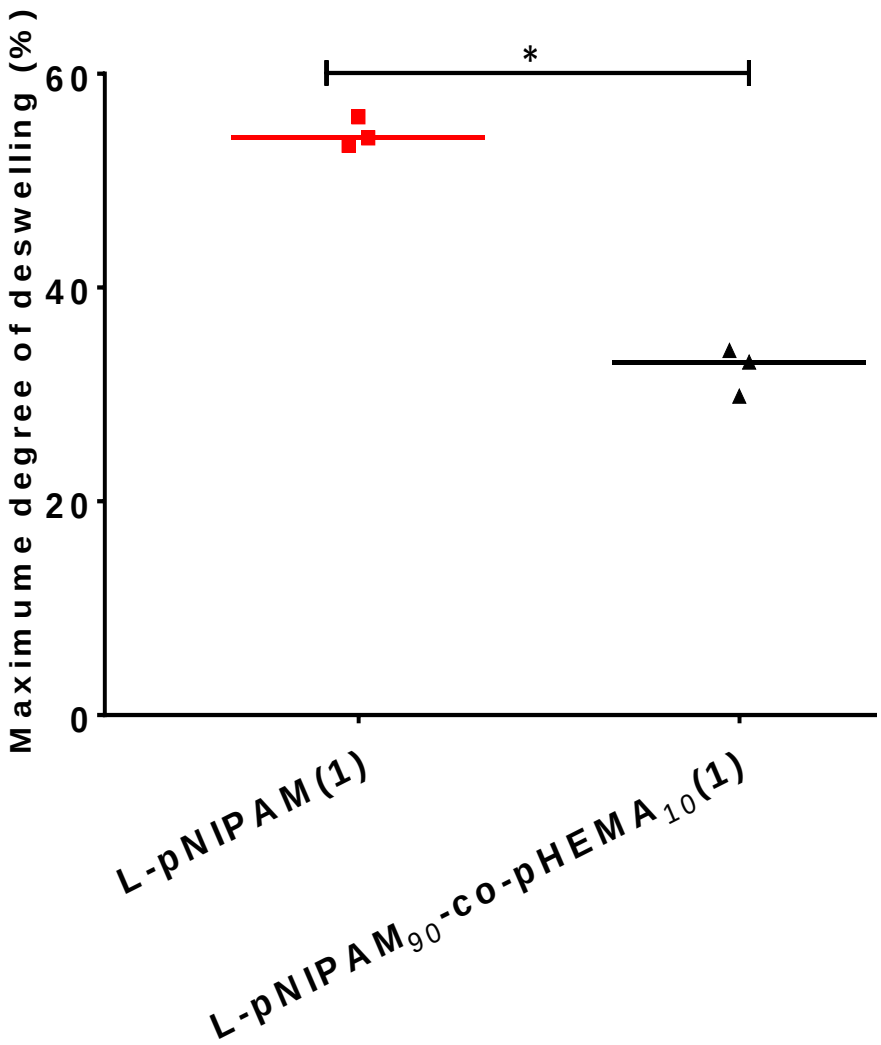

Figure 4.10: Maximum degree of deswelling of L-pNIPAM hydrogels with and without HEMA incorporated.

4.6 Water states and water/polymer interactions in L-pNIPAM-co-HEMA

Poly (N-Isopropylacrylamide) based Laponite® injectable hydrogel consist of 90% water, and have shown promising results as potential scaffolds for biomedical field(13,21). Thorpe A. *et al* were studied applicability of L-pNIPAM-co-DMAc in tissue regenerative medicine, where hydroxyapatite nanoparticles (HAPna) synthesised was added at concentration of 0.5 and 1mg/ml. They found that hMSCs were proliferated and osteogenic differentiation was promoted within the hydrogel(13). Hence, water states and water/polymer interactions within this material should be studied when development or modification in composition are needed. Water is an important for cells to maintain viable and proliferate, and water diffusivity is one the important factors

that need to be understood, due to it is related to diffusion of nutrients and waste removal during cell growth.

In this current study, water state and water/polymer interactions, during the dehydration and rehydration processes were investigated using Fourier transform infrared attenuated total reflectance (FTIR-ATR). Where two different ratios of HEMA (5 and 10 wt. %) were used to explore the influence of HEMA ratio on dehydration and rehydration kinetics and water state.

4.6.1 Dehydration study

Samples were synthesised as described in Chapter 2.2, 30µl of each formula was pipetted directly onto the ATR crystal which had been pre-set to 25˚C. Data collection was directly begun with 8 scans per spectrum at a resolution of 8cm^{-1} on a Thermo Nicolet Nexus instrument, using a series setup, a spectrum was taken automatically every 30 sec for 800m (13.3h). Dehydration process was monitored using FTIR-ATR, to investigate effect of incorporated HEMA into Poly (N-Isopropylacrylamide) based Laponite® injectable hydrogel. For simplicity, selections of spectra at different time points during drying of L-pNIPAM$_{90}$-co-HEMA$_{10}$ (1) have been chosen to demonstrate the monitoring of the drying of hydrogel samples in real time by following the decrease in intensity of the ν(OH) band between 3600-3100 cm^{-1}, and increasing intensity of the δ(NH) band at ~ 1550 cm^{-1} (Figure 4.11) associated with the polymer. In addition, there was a shift in δ(NH) band to lower wavenumber, indicating a reduction in the hydrogen bonding between water and polymer molecules (Figure 4.11).

Expansions of these spectra are shown in Figure 4.12 and 4.13, to emphasise the observable peak intensity and peak shifts changes during the drying process (Figure 4.12 and 4.13).

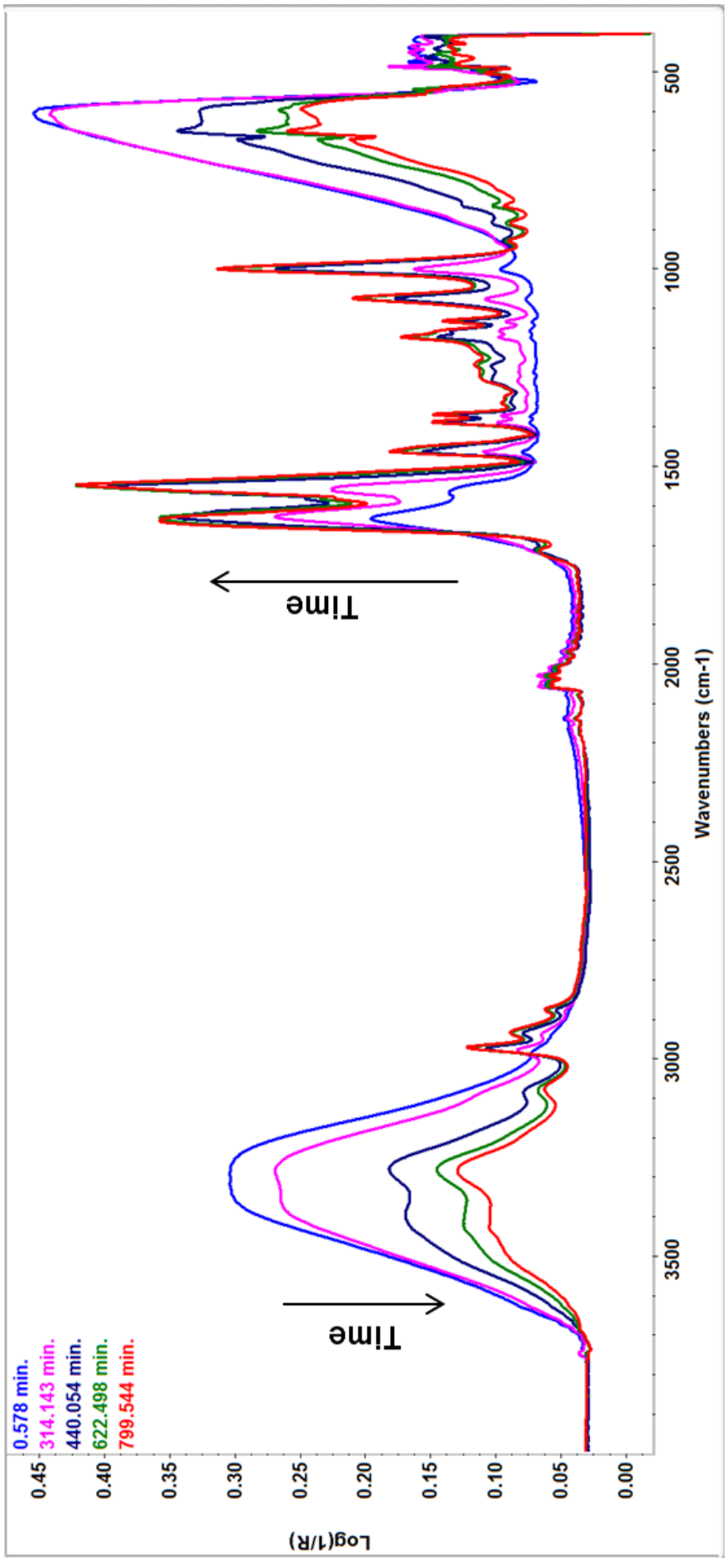

Figure 4.11: Full spectra of water evaporating from L-pNIPAM$_{90}$-co-HEMA$_{10}$ (1) hydrogel at 25˚C.

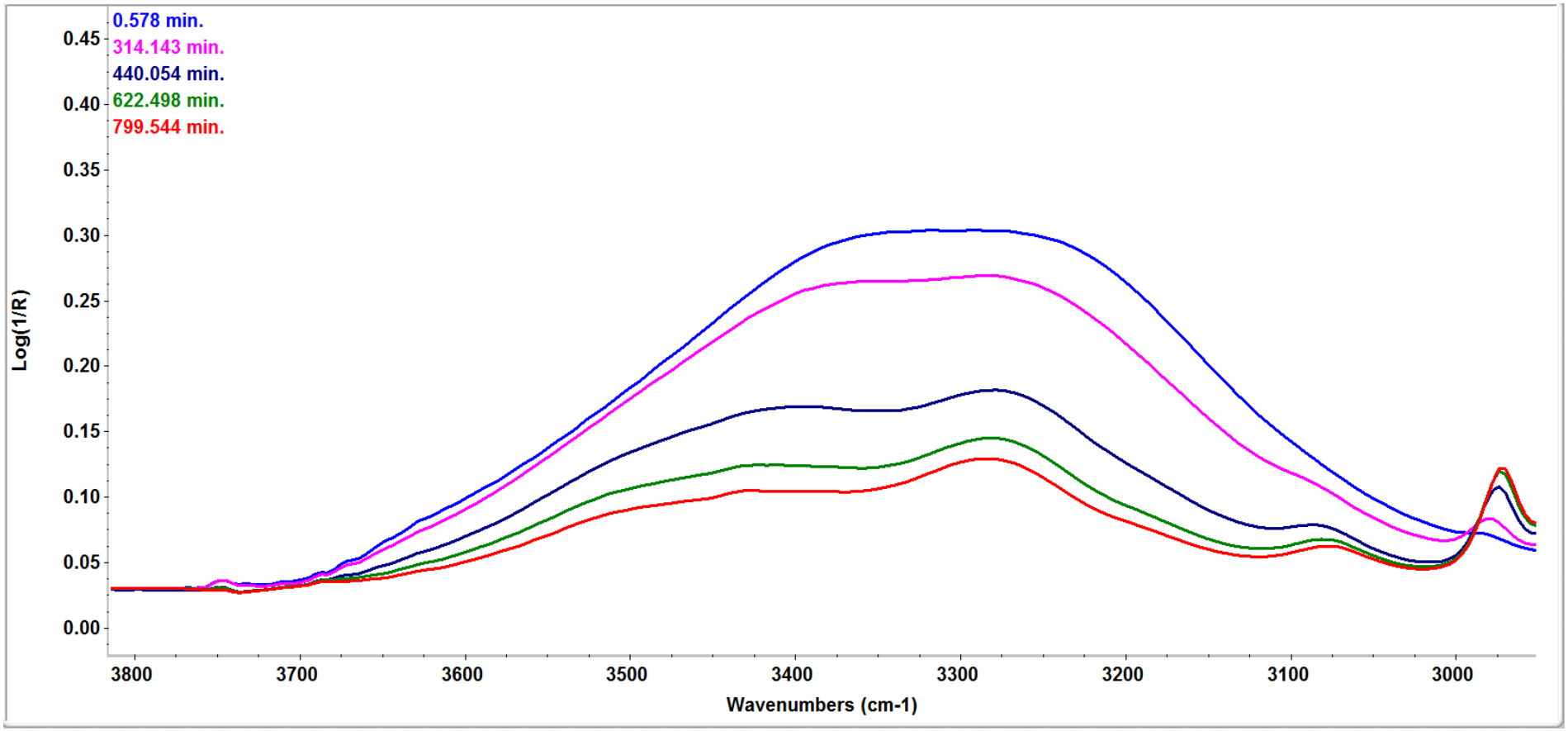

Figure 4.12: *v* (OH) (3700-300cm-1) taken during the drying of L-pNIPAM$_{90}$-co-HEMA$_{10}$ (1) hydrogel at 25˚C.

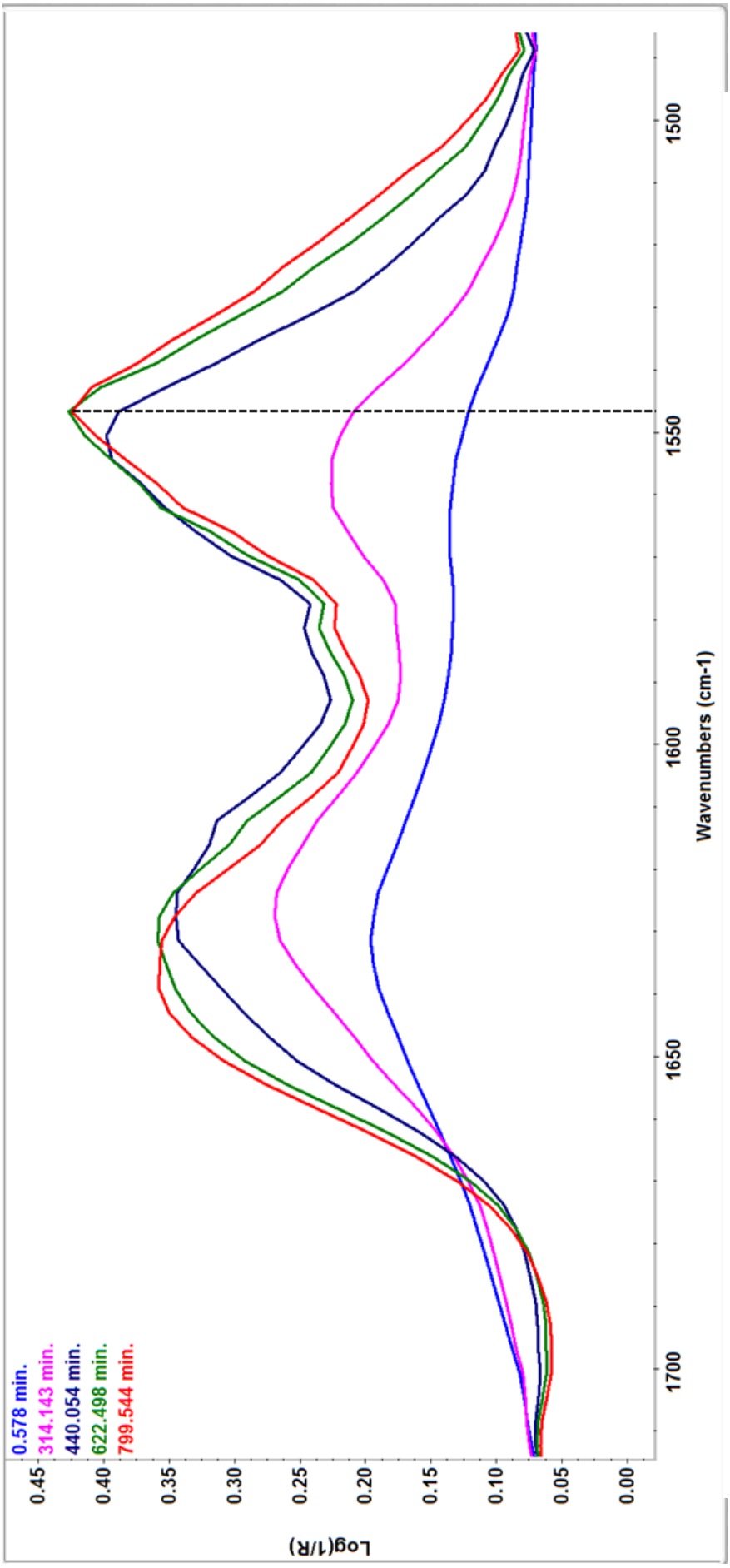

Figure 4.13: δ (NH) band (1550cm^{-1}) taken during the dehydrating of L-pNIPAM90-co-HEMA10 (1) hydrogel at 25˚C.

The intensity of ν(OH) band was plotted as a function of time for different ratios of HEMA incorporated into L-pNIPAM (Figure 4.14).Incorporation of HEMA into L-pNIPAM, was shown to decrease the dehydration rate, which is thought to be due to the increase in hydrophilic polymeric units which are able to interact with water, causing a delay in the drying process (Figure 4.14).

As there were no significance changes in the hydrogel morphology observed via SEM images, changes in the dehydration rate must solely be attributed to changes in the chemistry of the system and the increased hydrophilicity that incorporating HEMA has on the system. Here we observe that systematically increasing the HEMA content systematically retards the dehydration rate. This observation agrees with the work of George et al (23) who looked at the influence of HEMA content on the water diffusion within EMA-co-MOEP hydrogels.(22).

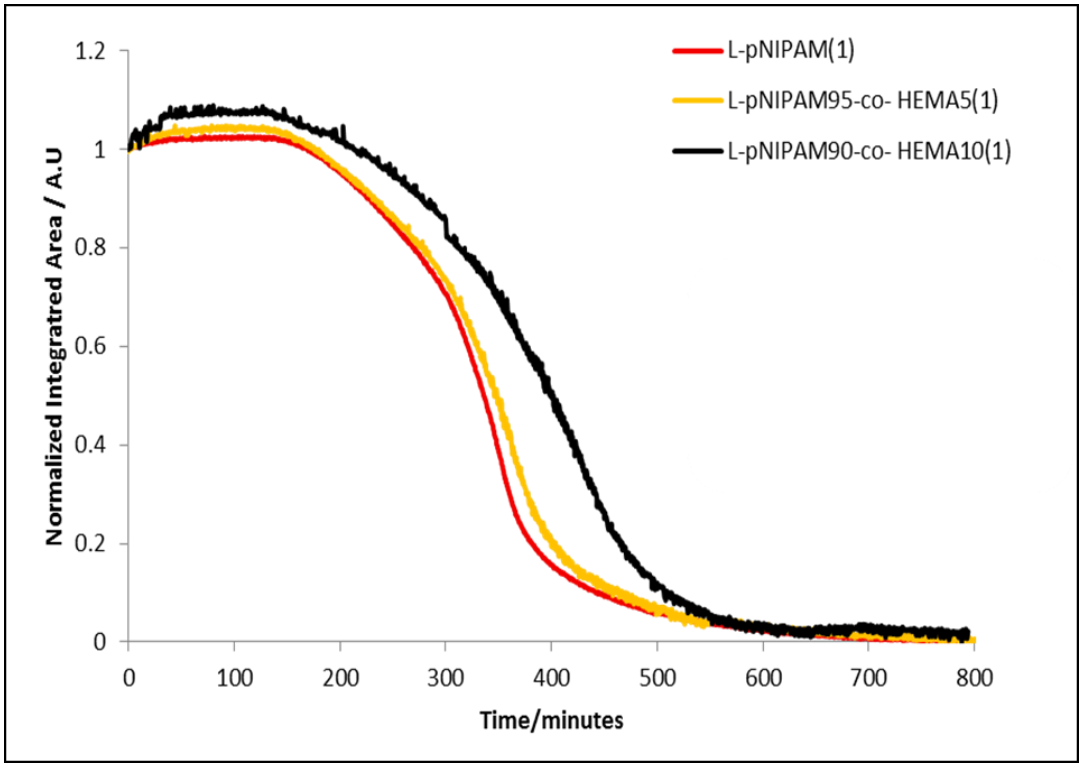

Figure 4.14: Water profiles for different HEMA concentrations hydrogels during dehydration.

The change in δ (NH) band position during water loss is plotted in Figure 4.15, and is a clear indication of a reduction of the number of H-bonds between polymeric chains and water as the water evaporated. The shifts in the δ(NH) band position are much more remarkable during the second phase of dehydration, suggesting bound water is being lost from the sample (Figure: 4 .15).

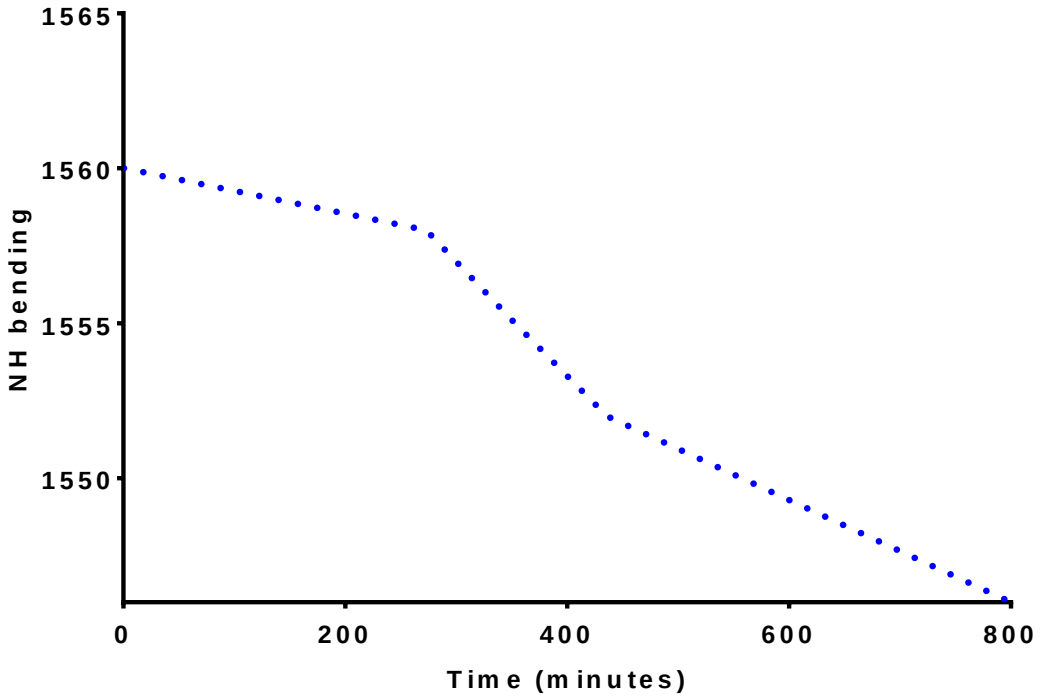

Figure 4.15: Shifts in δ (NH) band of L-pNIPAM$_{90}$-co-HEMA$_{10}$ (1) during dehydration.

To test the hypothesis that water was both free and bound within the hydrogels and that this is lost during dehydration process(23), Free and bound water, within L-pNIPAM-co-HEMA hydrogels, were approximated, using water profiles of different HEMA concentrations (Figure 4.14). Two different states of water can be seen, as shown in Chapter 3.6.1, where free and bound water fractions were calculated for each composition (Figure 4.16).

Incorporation of HEMA into L-pNIPAM hydrogel was shown to increase the bound water fraction, which is thought to be due to the increase hydrophilic polymeric units, which holds water longer. Where more hydrophilic polymeric units within hydrogel matrix, leads to greater bound water content(24).

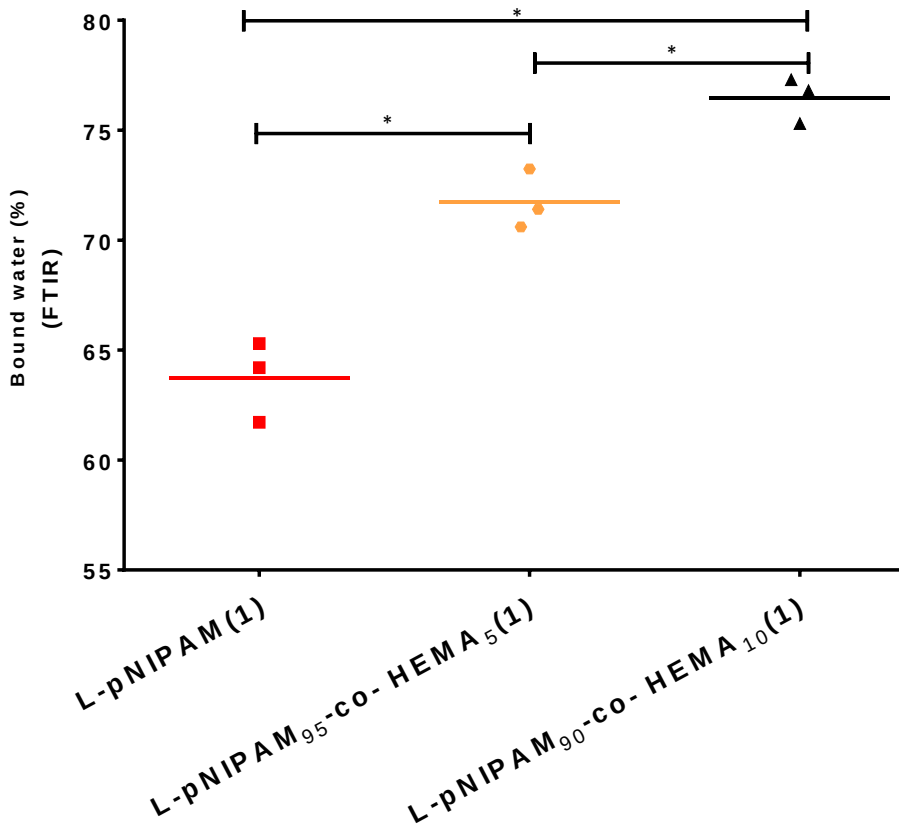

Figure 4.16: Bound water content of L-pNIPAM-co-HEMA with different HEMA concentrations, estimated using FTIR.

The state of water within L-pNIPAM hydrogels were verified using the 'gold standard' method of differential scanning calorimetry (DSC) with a good agreement observed between the two techniques (Figure: 4.17).

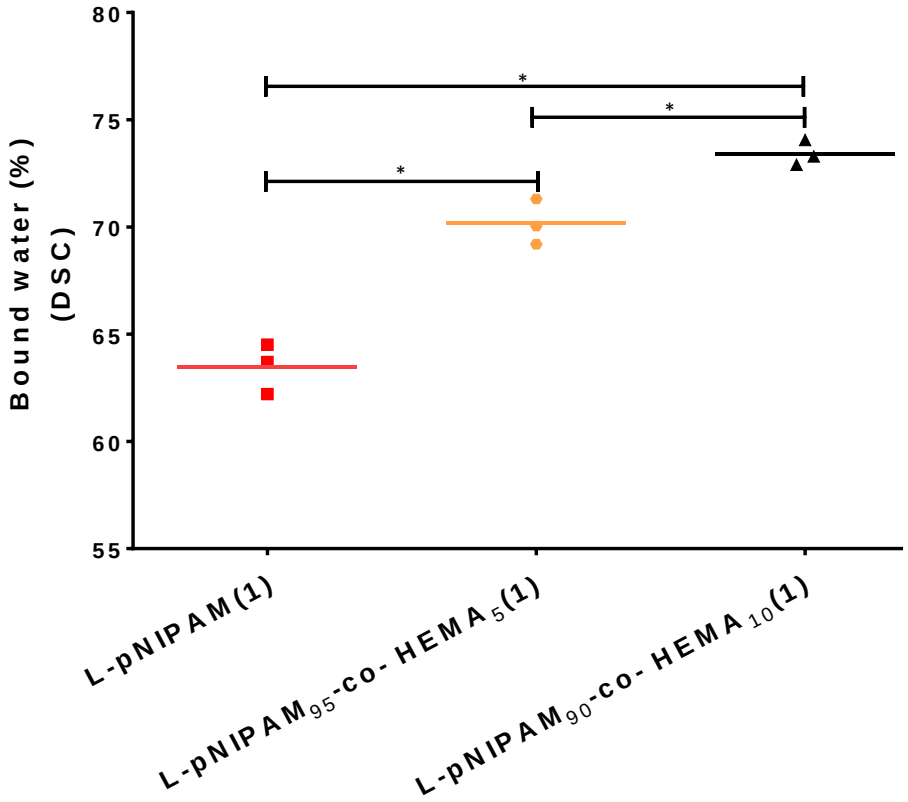

Figure 4.17: Bound water content of pNIPAM based Laponite® hydrogel with different HEMA concentrations, estimated using DSC. *=P<0.05.

4.6.2 Rehydration studies of L-pNIPAM-co-HEMA

Following complete dehydration, hydrogel samples were fully dried and adhered to the ATR crystal. A rehydration experiment was then performed by putting deionised water in contact with dried sample using liquid cell holder, with the same setting that used in dehydration experiment except using a shorter time (240m). Water absorption was monitored by FTIR-ATR, by observing ν(OH) band between 3600-3100 cm^{-1}, and δ (NH) at ~ 1550 cm^{-1} (Figure 4.17).

The intensity of ν(OH) band was increased with time as more water was absorbed by the sample (Figure 4.18). On other hand, the intensity of the δ(NH) band decreased as more water entered the sample, resulting in a reduction in the effective polymer concentration in the evanescent field (Figure 4.19). Moreover, a shift to higher wavenumber was observed in δ(NH) as more water entered, indicating more hydrogen bonding between polymer chains and water molecules (Figure 4.19).

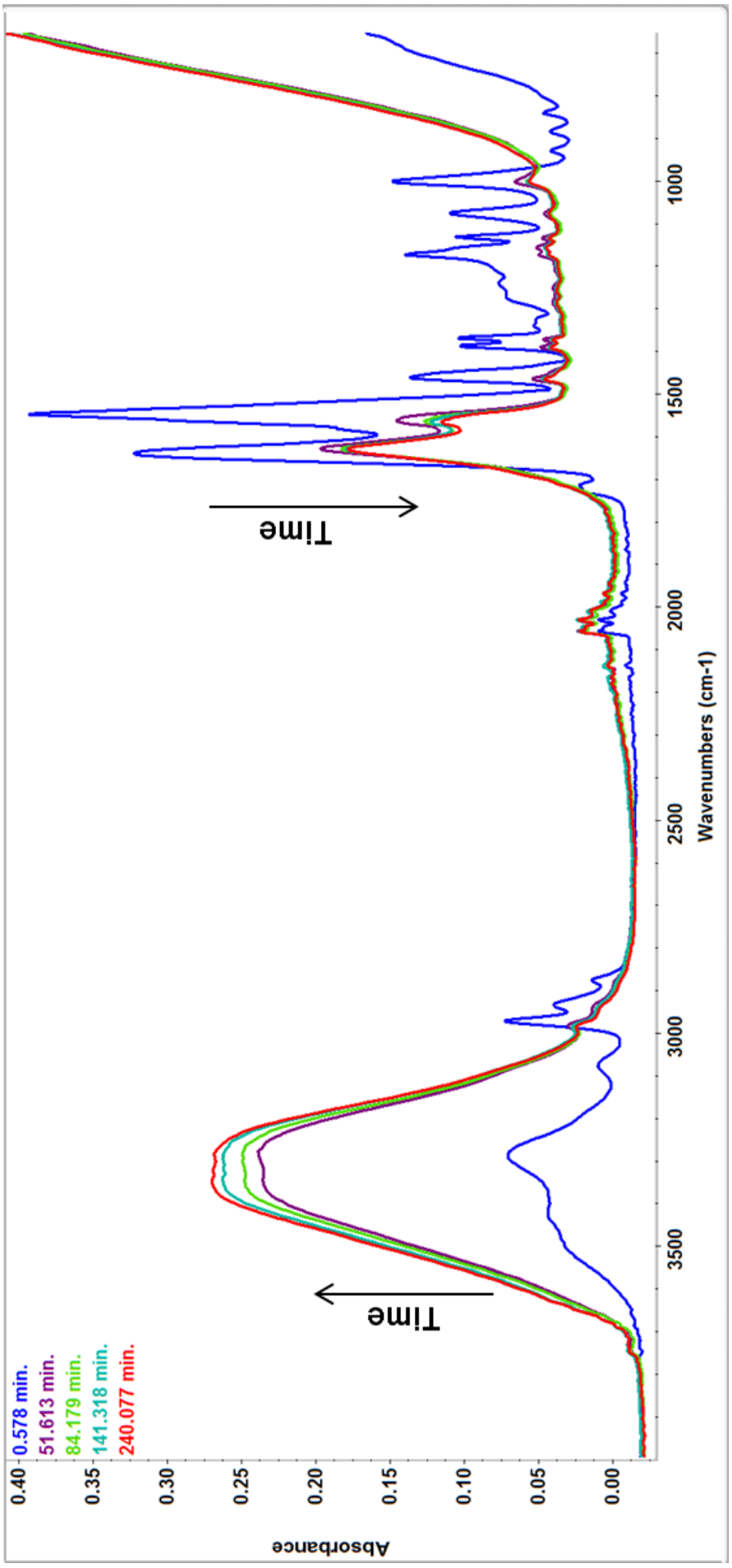

Figure 4.18: Full spectra of water evaporating from L-pNIPAM$_{90}$-co-HEMA$_{10}$ (1) hydrogel at 25˚C.

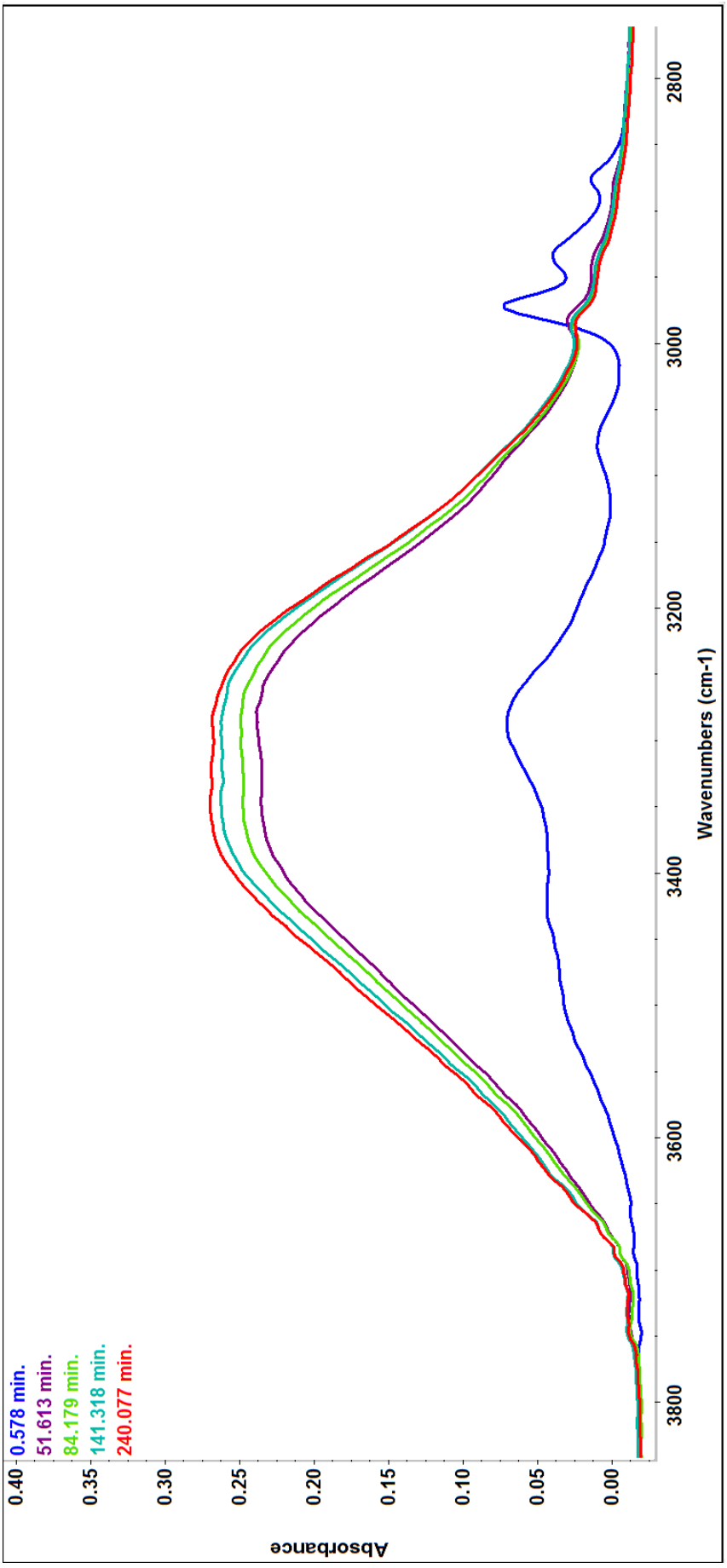

Figure 4.19: *v* (OH) (3700-300cm-1) taken during the rehydration of L-pNIPAM$_{90}$-co-HEMA$_{10}$ (1) hydrogel at 25˚C.

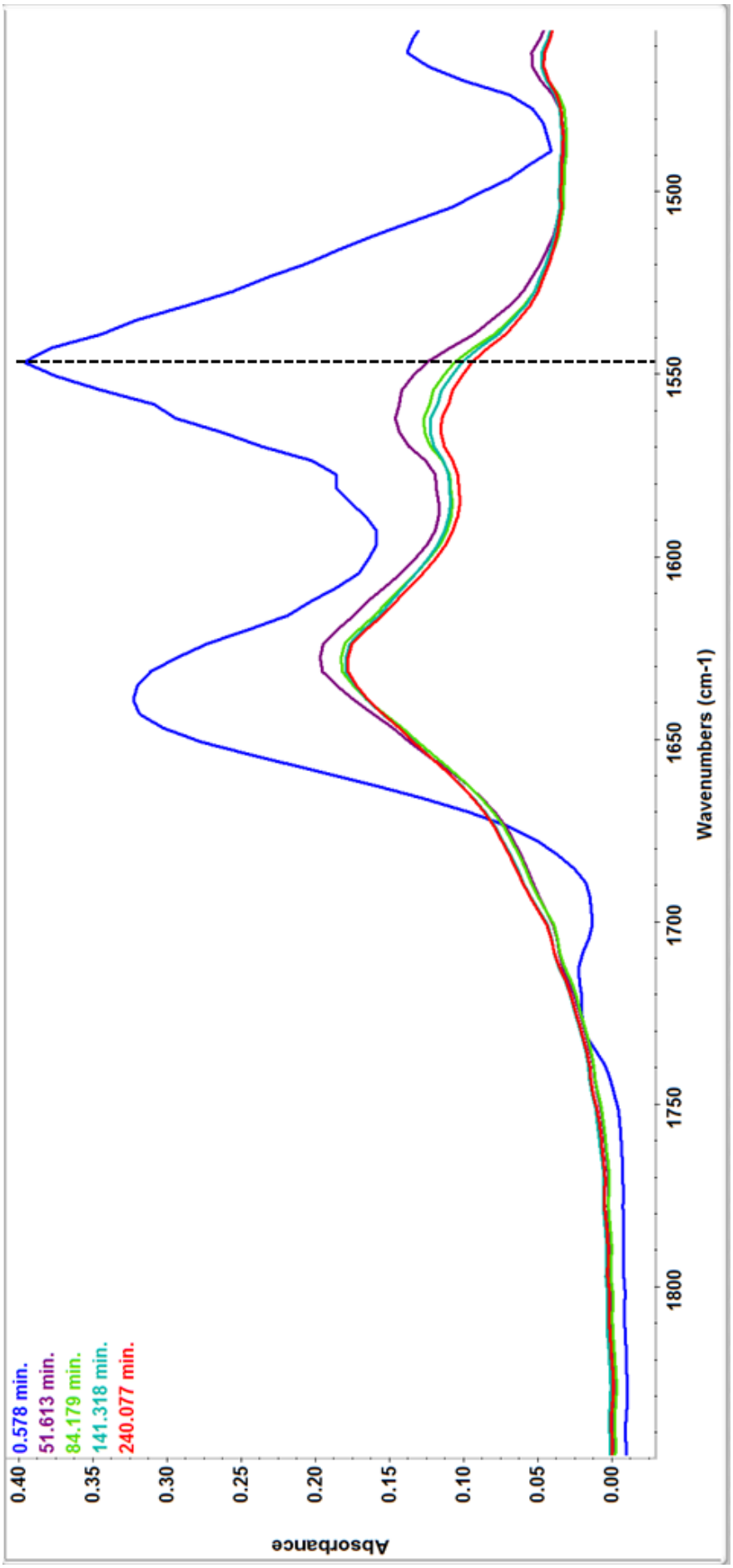

Figure 4.20: δ (NH) band (1550cm^{-1}) taken during the rehydrating of L-pNIPAM90-co-HEMA10 (1) hydrogel at 25˚C.

The intensity of ν(OH) band was plotted as a function of time for different HEMA concentrations hydrogels (Figure 4.20), to illustrate the influence of incorporation of HEMA as comonomer on rehydration rate. Incorporation of HEMA increased the rehydration rate systematically, ***despite of there were no significant differences in pore size when HEMA was added. This increase in rehydration rate was thought to be due to the increase in hydrophilic polymeric units which increased the hydrophilicity of the hydrogel.***

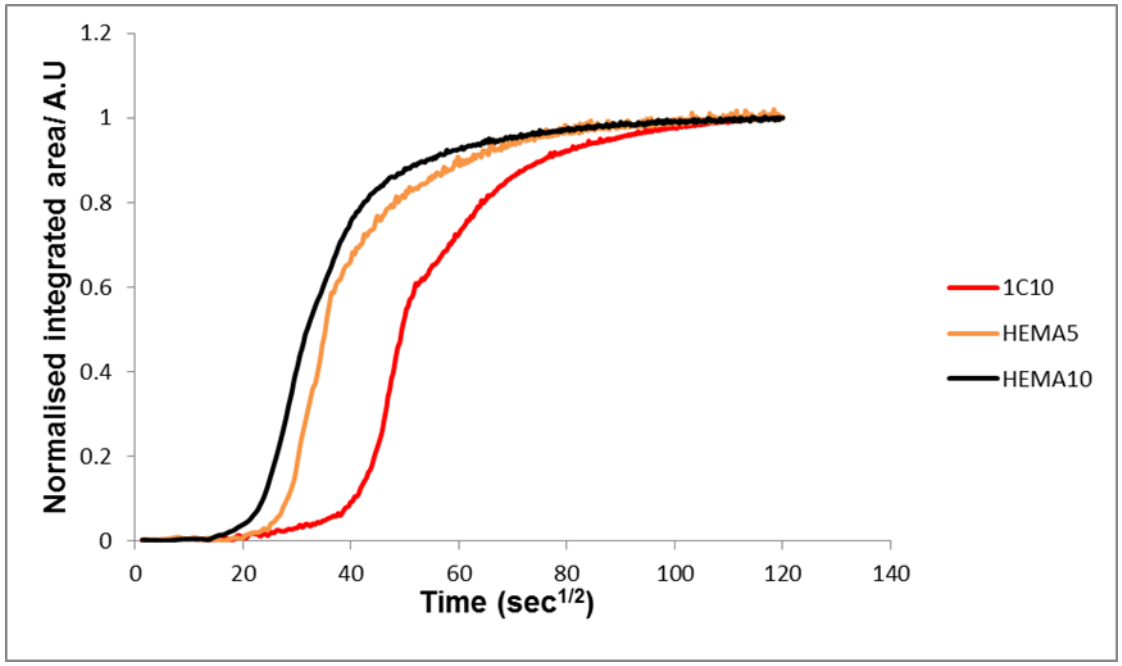

Figure 4.20: water profiles for different HEMA concentrations hydrogels during rehydration.

Position of the δ(NH) band was plotted as a function of time during rehydration, where a shift to higher wavenumber was observed over time, due to more hydrogen bonding between absorbed water and polymeric chains in the swollen hydrogel sample (Figure 4.21).

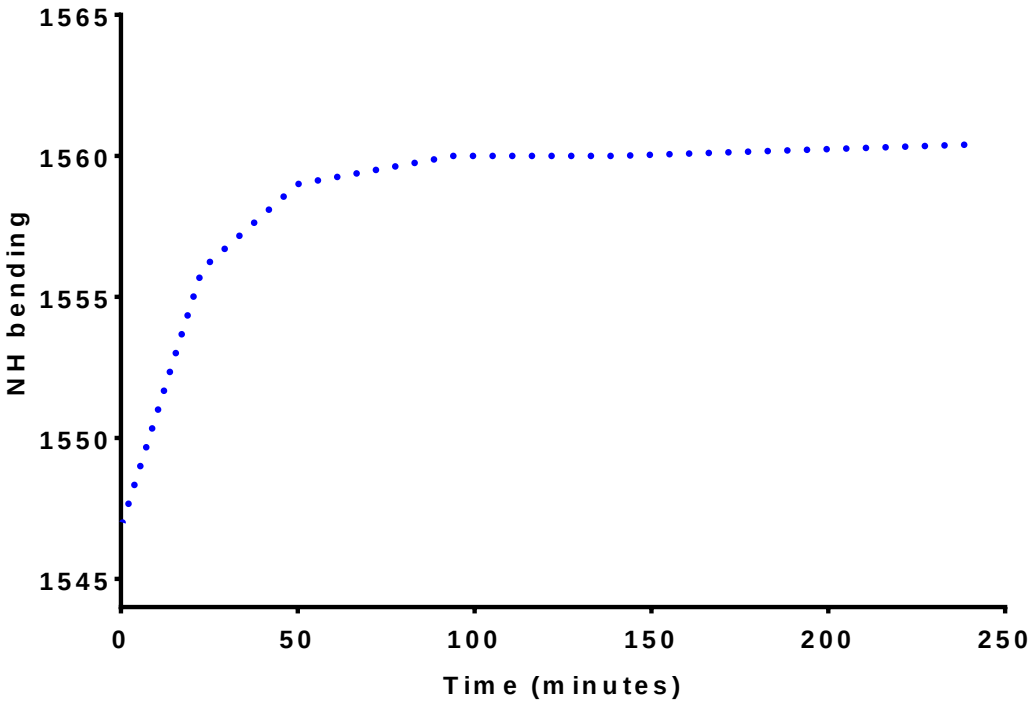

Figure 4.21: Shifts in δ (NH) band of L-pNIPAM$_{90}$-co-HEMA$_{10}$ (1) during rehydration.

The diffusion coefficient (D) of water through hydrogel samples with different HEMA concentrations, was calculated using to the Fieldson equation(25,26), as described in section 3.6.2.

Water diffusivity at 25˚C, through pNIPAM based Laponite® hydrogel during rehydration process was shown to be restricted by incorporating HEMA, where D value decreased when 5 wt. % HEMA was incorporated. However, further increase of HEMA concentration to 10 wt. %, resulted to slight increase of water diffusivity (Figure 4.22). The measured rate of the diffusion of water through pNIPAM based Laponite® hydrogel, was decreased at lowest concentration of HEMA, despite of hydrophilic nature of HEMA, where more hydrophilic network provides a greater force for water absorption into the matrix (22). It should however be noted that although the slope of the diffusion curve indicates that diffusion is slower in L-pNIPAM-co-HEMA than L-pNIPAM, diffusion finishes sooner, systematically with higher HEMA content as expected with a more hydrophilic system. The D value only relates to the slope of the linear portion, it is unclear if calculating D is informative here; perhaps time taken to reach equilibrium is more relevant.

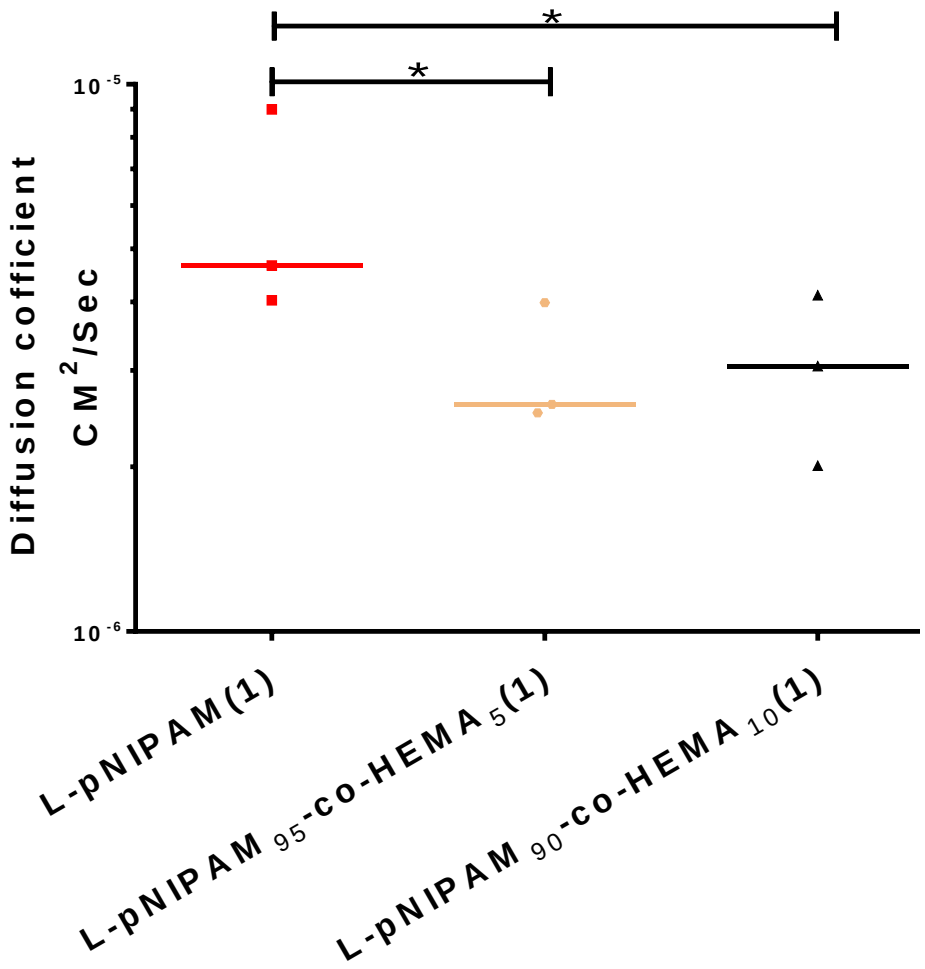

Figure 4.22: Diffusion coefficient of pNIPAM base d Laponite® hydrogel with different HEMA concentrations. *=P<0.05.

4.7 Influence on cell behaviour of incorporation of HEMA to pNIPAM based Laponite® hydrogel

Rat stem cells were used to investigate influence of incorporation of HEMA into pNIPAM based Laponite® injectable hydrogel, on cell viability within hydrogel structure. HEMA was incorporated at concentration of 5 and 10 wt. %. Alamar blue assay, as a measure of metabolic cell activity and thus the total number of viable cells, was assessed up to 7 days in culture (Figure 4.23). On day 0 significant decreases were observed in metabolic cell activity of the cells that cultured within hydrogels with HEMA compared to those without HEMA (Figure 4.23). Following 2 days in culture a reduction in metabolic cell activity, within all compositions that studied, which is a common phenomenon when cells are transferred from monolayer culture into 3D culture as their proliferation rates

slow(27). Following 7 days in culture cells cultured within hydrogels containing HEMA were significantly reduced compared to those hydrogels without HEMA (Figure 4.23). These data suggest that the incorporation of HEMA was detrimental to cell viability with decreased cell metabolism seen during culture (Figure 4.23). The L-pNIPAM hydrogel alone in the absence of HEMA has previously been shown to have excellent biocompatibility (13,21,28). Thorpe A. *et al* demonstrated pNIPAM based Laponite® hydrogel, promoted differentiation of mesenchymal stem cells (MSCs) to nucleus pulposus (NP) cells without additional growth factors(21). Similar results were obtained by Dosh R. *et al* for different type of cells, where pNIPAM based Laponite® hydrogel was utilised as a 3D culture model for human intestinal cells (28). This model system could be utilised as an alternative *in vitro* biomaterial in studies to investigate human intestinal problems or to explore possible intestinal drugs(28).

It is possibly that the L-pNIPAM-co-HEMA systems have not fully reacted causing some residue non-polymerised molecules being within the system that adversely affected cell viability within this material. The reason behind non-biocompatibility of pNIPAM based Laponite® injectable hydrogel when HEMA was incorporated required further investigation, but that was considered beyond the scope of this work.

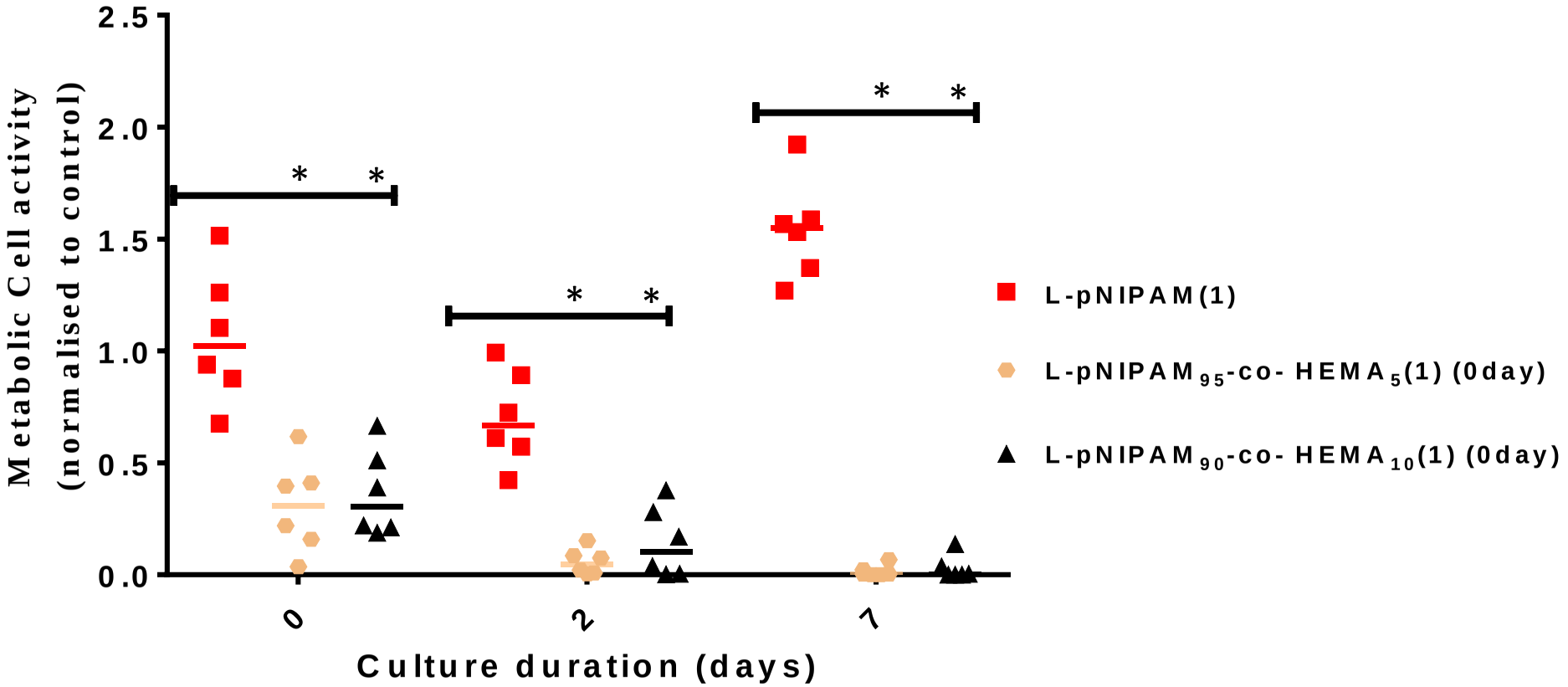

Figure 4.23: *In vitro* cell proliferation using Alamar blue of rat stem cells were cultured witin hydrogels containing different HEMA concnetrations,

4.7.1 Scanning electron microscopy investigation

Hydrogel samples with human mesenchymal stem cells (hMSC), cultured within their structures, either layered on hydrogel surfaces, or suspended into their structures, were analysed by SEM.

4.7.1.1 Scanning electron microscopy investigation of hMSC cells layered on hydrogel samples surface.

Scanning electron microscopy (SEM) was used to analyse cells cultures in layers for 2 weeks, on the surface of pNIPAM based Laponite® injectable hydrogel with 10wt. % HEMA incorporated. Cells spread on the surfaces of pNIPAM based Laponite® injectable hydrogel without HEMA incorporated, SEM images showed a reduction in the porosity of hydrogel, where cells covered the honeycomb like structure of hydrogel (Figure 4.24). In contrast, there was no evidence of cell growth on the surface of hydrogel containing HEMA (Figure 4.24). These results support those of the metabolic cell activity which showed decreased activity with time in culture suggesting toxcity to the cell.

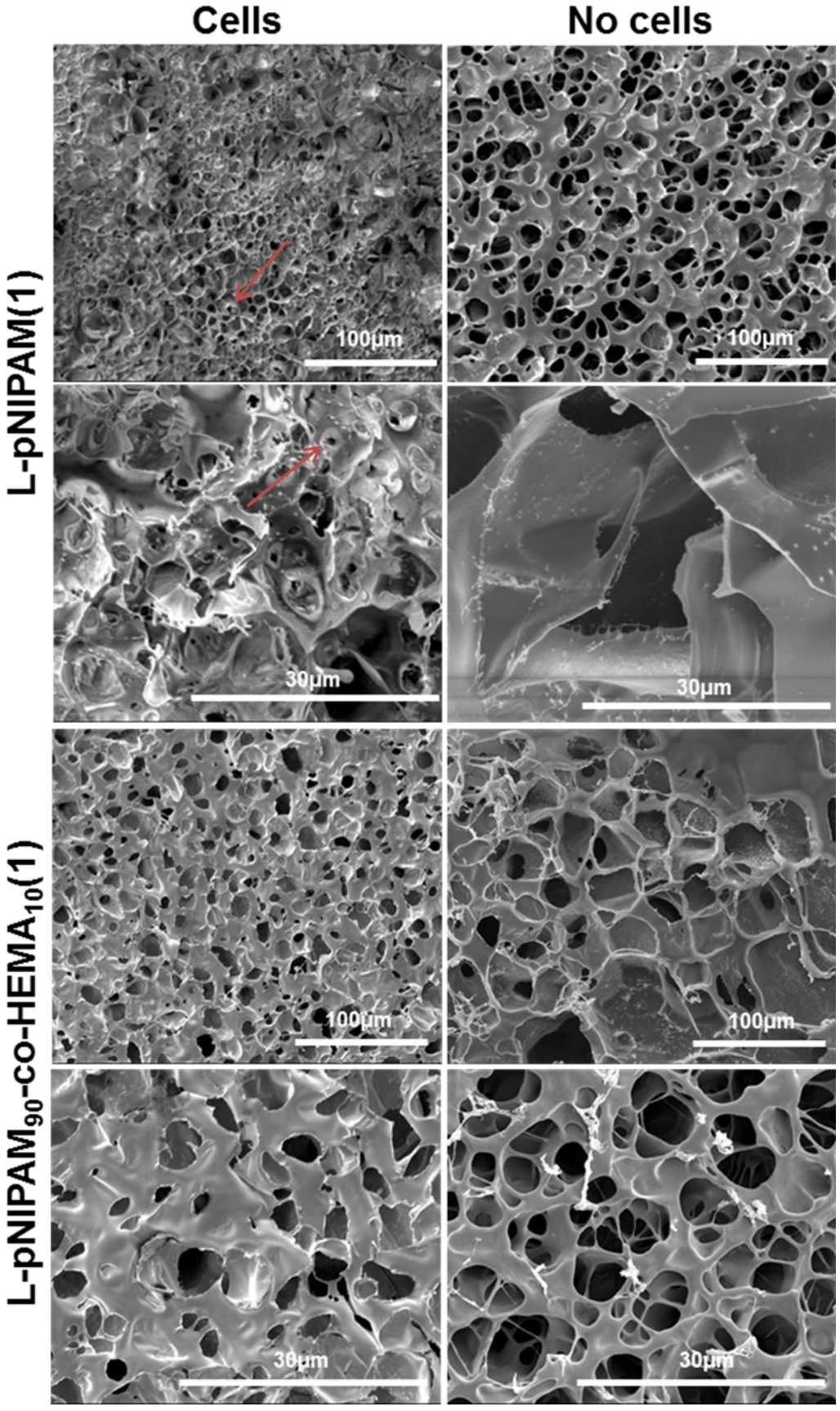

Figure 4.24: Scanning electron microscopy (SEM) of hMSC layered on hydrogel surfaces for 2 weeks and acellular hydrogels with and without HEMA incorporated. Red arrows show cells occupy the pores.

4.7.1.2 Scanning electron microscopy investigation of hMSC cells suspended in hydrogel.

Analysis of hydrogel samples with hMSC cells, cells suspended in the hydrogel prior to gelation was performed using SEM. Secondary electron images were captured at accelerating voltage of 5KV and magnifications ranging 1000x to 30000x were used. Images were visualised and compared with each relevant control image, to explore the effect of adding HEMA on cell behaviour within pNIPAM based Laponite® injectable hydrogel. Cells were shown to grow through the pores of hydrogel structure, when they suspended into pNIPAM based Laponite® hydrogel that did not contain HEMA. At higher magnification cells were observed to deposit matrix within the hydrogel structure, which reduced the pore size of interconnected channels of hydrogel (Figure 4.25). Contrary, cells suspended into hydrogels with HEMA incorporated were absent suggesting cell death which was confirmed by cell viability results (Figure 4.25). Zuwei M. *et al* synthesised thermally responsive injectable hydrogel, using copolymers formed by free radical of methacrylate polylactide (MAPLA), NIPAM and HEMA. They used hexane to precipitate the resulted copolymer and then copolymer was purified further by precipitation from THF into diethyl ether and vacuum dried, to obtain ~ 90% yields. They found that the synthesised hydrogel was biocompatible, where rat vascular smooth muscle cells were cultured within the hydrogel and metabolic cell activity was measured for cells within the hydrogel up to using RSMC assay. They conclude that thermally responsive hydrogel had no negative influence on the metabolic cell activity and number of live cells(29). Ryan L. *et al* have also purified 2-Hydroxyethyl methacrylate (HEMA)-based (co)polymers following its synthesised, to remove any non-polymerised units. They found that ~ 90% yields was achieved in their study(30). Together with the results shown in this study this suggests extensive clean-up is required to remove unpolymerised monomer to prevent toxicity effects. However a key attribute for clinical application of biomaterials is the ease of manufacture and thus if clean-up is not required this is preferable, suggesting HEMA co-polymers are not ideal materials as they require extensive clean up prior to use to ensure they do not induce toxic effects(31).

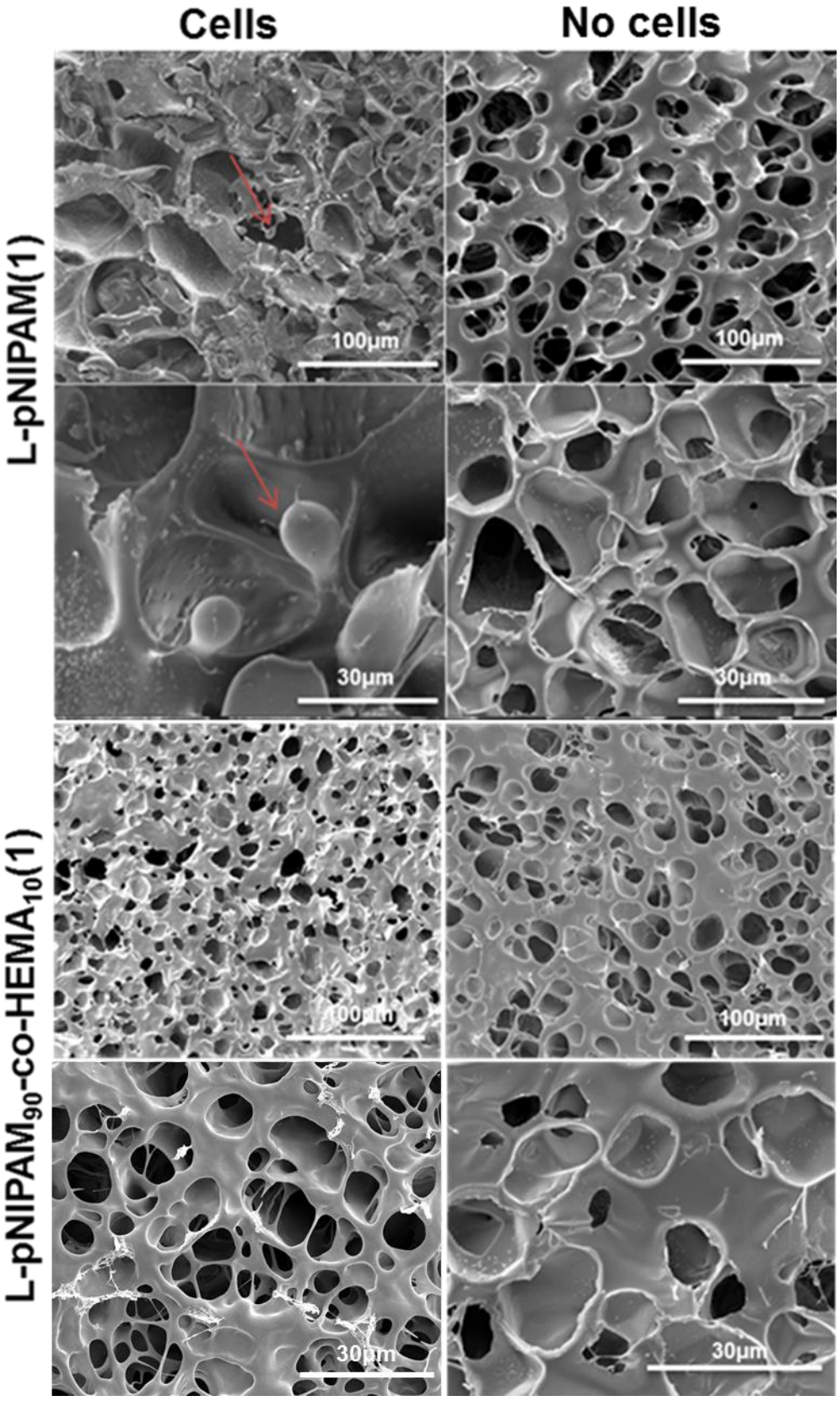

Figure 4.25: Scanning electron microscopy (SEM) of hMSC cells suspended into hydrogel for 2 weeks and acellular hydrogels with and without HEMA incorporated. Red arrows show cells within the pores.

4.8 Summary

In this chapter, the influence of incorporation of Poly (2-hydroxyethyl methacrylate) (pHEMA) on physical and mechanical properties of pNIPAM based Laponite® hydrogel, was studied. Thermoresponsive characteristic of pNIPAM based Laponite® was not affected by HEMA incorporation , where the lower critical solution temperature (LCST) was ~ 32˚C for all compositions suggesting that the thermal response of pNIPAM chains were not affected by HEMA incorporation and no copolymer chains were formed(16). No changes were observed in morphological properties of pNIPAM based Laponite® injectable hydrogel, except a slight increase in pore size when HEMA concentration increased to 10 wt. %, with an increase in heterogeneity seen in L-pNIPAM$_{90}$-co-HEMA$_{10}$ (1), this was thought to be due to an increase pHEMA molecules that formed within the hydrogel.

A significant decrease in stiffness of L-pNIPAM$_{90}$-co-HEMA$_{10}$ was seen compared to 5% wt and L-pNIPAM hydrogel alone. This decreased stiffness was thought to be related to the increase in pore size, and increase pHEMA within hydrogel matrix.

The swelling behaviour was affected by the incorporation of HEMA into L-pNIPAM hydrogel, where swelling ratio was higher when 10 wt. % of HEMA was added, this was thought to be due to hydrophilicity of pHEMA chains which elevated the rate of water absorption. In addition equilibrium water content was higher when HEMA incorporated. Deswelling was also decreased when HEMA was incorporated, which was thought to be due to pHEMA obstructed shrinkage rate of pNIPAM above its LCST. Therefore, maximum degree of deswelling was significantly decreased when HEMA was added.

Dehydration rate was decreased systematically when different HEMA concentrations were incorporated, due to ability of pHEMA chains to interact and bind with water molecules, caused delay in water lost. As expected bound water content was increased systematically and significantly as HEMA incorporated, due to increase hydrophilicity of overall hydrogel by adding HEMA.

Rehydration rate was increased steadily when HEMA incorporated, as a result of adding more hydrophilic polymeric units into the matrix. Diffusion coefficient of water through the hydrogel decreased as 5 wt. % HEMA was added, due to interaction that could happen between water molecules and pHEMA chains, as pHEMA is more hydrophilic than pNIPAM. However, when HEMA concentration went up to 10 wt. %, water diffusivity slightly increased as a result of increase in pore size happen in this composition.

Further investigation on how NIPAM and HEMA were polymerised, need to be done, to understand why cell viability showed to be adversely affected by adding HEMA into pNIPAM based Laponite® injectable hydrogel.

4.9 References

1. Haraguchi K, Farnworth R, Ohbayashi A, and Takehisa T. Compositional effects on mechanical properties of nanocomposite hydrogels composed of poly(N,N-dimethylacrylamide) and clay. Macromolecules. 2003;36(15):5732–5741.

2. Paula Andrade-Vivero 1, Elena Fernandez-Gabriel 1, Carmen Alvarez-Lorenzo 1 AC. Improving the Loading and Release of NSAIDs from pHEMA Hydrogels by Copolymerization with Functionalized Monomers. Journal of Pharmaceutical Science. 2007;96(4):802–813.

3. Ina G. US Patent (1970). (19).

4. Enzymes P. US Patent (1980) 54:62–66.

5. Obereigner B, Burešová, M, Vrána, A, and Kopeček J. Preparation of polymerizable derivatives of N-(4-aminobenzenesulfonyl)-N′-butylurea. In: 17th Prague Micro-symposium on Macromolecules. Prague: Institute of Macromolecular Chemistry Prague; 1977:77-81.

6. Obereigner B, Burešová M, Vrána A, Kopeček J. Preparation of polymerizable derivatives of N-(4-aminobenzenesulfonyl)-n′-butylurea. Journal of Polymer Science. 1979;66(1):41–52.

7. Ants Lääanea, Vladimír Chytrýb, Mati Hagaa, Peeter Sikka AA and JK. Covalent attachment of chymotrypsin to poly[N-(2-hydroxypropyl)methacrylamide]. Collection of Czechoslovak Chemical Communication. 1981;46(6):1466.

8. El-Din HMN. Characterization and Caffeine Release Properties of N-isopropylacrylamide/Hydroxypropyl Methacrylate Copolymer Hydrogel Synthesized by Gamma Radiation. Journal of Applied Polymer Science. 2011;119:577–585.

9. Mohammad M. Fares AAO. Lower Critical Solution Temperature Determination of Smart, Thermosensitive N–Isopropylacrylamide-alt-2–Hydroxyethyl Methacrylate Copolymers: Kinetics and Physical Properties. Journal of Applied Polymer Science. 2008;110:2815–2825.

10. Lanzalaco S, Armelin E. Poly(N-isopropylacrylamide) and Copolymers: A Review on Recent Progresses in Biomedical Applications. Gels. 2017;3(4):36.

11. Gan T, Zhang Y, Guan Y. In situ gelation of P(NIPAM-HEMA) microgel dispersion and its applications as injectable 3D cell scaffold. Biomacromolecules. 2009;10(6):1410–1415.

12. Yildiz B, Is B, Kis M. Thermoresponsive poly (N -isopropylacrylamide- co -acrylamide- co -2-hydroxyethyl methacrylate) hydrogels. Journal of Applied Polymer Science 2002;52:3–10.

13. Thorpe AA, Creasey S, Sammon C, Le Maitre CL. Hydroxyapatite nanoparticle injectable hydrogel scaffold to support osteogenic differentiation of human mesenchymal stem cells. European Journal of

Cells and Materials. 2016;32:1–23.

14. Tang S, Floy M, Bhandari R, Dziubla T, Hilt J. Development of Novel N-isopropylacrylamide (NIPAAm) Based Hydrogels with Varying Content of Chrysin Multiacrylate. Gels Journal. 2017;3(4):40-50.

15. Feil H, Bae YH, Feijen J, Kim SW. Effect of Comonomer Hydrophilicity and Ionization on the Lower Critical Solution Temperature of N-Isopropylacrylamide Copolymers. Macromolecules. 1993;26(10):2496–500.

16. Tuncel a. Preparation and Characterization of Thermoresponsive Isopropylacrylamide – Hydroxyethylmethacrylate. 1997;527–541.

17. Liu Y, Zhang K, Ma J, Vancso GJ. Thermoresponsive semi-IPN hydrogel microfibers from continuous fluidic processing with high elasticity and fast actuation. ACS Applied Materials Interfaces. 2017;9(1):901–8.

18. Potorac S, Popa M, Verestiuc L, Le Cerf D. New semi-IPN scaffolds based on HEMA and collagen modified with itaconic anhydride. Materials Letters. 2012;67(1):95–8.

19. Wang J, Wu W. Swelling behaviors, tensile properties and thermodynamic studies of water sorption of 2-hydroxyethyl methacrylate/epoxy methacrylate copolymeric hydrogels. Eurpean Polymer Journal. 2005;41(5):1143–1151.

20. Ngai T, Wu C, Chen Y. Effects of temperature and swelling on chain dynamics during the Sol-Gel transition. Macromolecules. 2004;37(3):987–993.

21. Thorpe AA, Dougill G, Vickers L, Reeves ND, Sammon C, Cooper G, et al. Thermally triggered hydrogel injection into bovine intervertebral disc tissue explants induces differentiation of mesenchymal stem cells and restores mechanical function. Acta Biomaterialia. 2017;54:212–226.

22. George KA, Wentrup-Byrne E, Hill David DJT, Whittaker AK. Investigation into the diffusion of water into HEMA-co-MOEP hydrogels. Biomacromolecules. 2004;5(4):1194–1199.

23. Sammon C, Mura C, Yarwood J, Everall N, Swart R, Hodge D. FTIR−ATR Studies of the Structure and Dynamics of Water Molecules in Polymeric Matrixes. A Comparison of PET and PVC. Journal of Physical Chemistry, Part B. 1998;102(18):3402–3411.

24. Hackl E V., Khutoryanskiy V V., Tiguman GMB, Ermolina I. Evaluation of water properties in HEA-HEMA hydrogels swollen in aqueous-PEG solutions using thermoanalytical techniques. Journal of Thermal Analysis and Calorimetry 2015;121(1):335–345.

25. Duda L. Molecular diffusion in polymeric systems. Pure and Applied Chemistry Journal. 1985;57(1):1681–1690.

26. Karimi M. Diffusion in Polymer Solids and Solutions. Mass Transfer in Chemical Engineering Process. 2011; 17-40

27. Thorpe AA, Dougill G, Vickers L, Reeves ND, Sammon C, and Cooper G,. Thermally triggered hydrogel injection into bovine intervertebral disc tissue explants induces differentiation of mesenchymal stem cells and restores mechanical function. Acta Biomaterialia. 2017;54:212–226.

28. Dosh RH, Essa A, Jordan-Mahy N, Sammon C, and Le Maitre CL. Use of hydrogel scaffolds to develop an in vitro 3D culture model of human intestinal epithelium. Acta Biomaterialia. 2017;62:128–143.

29. Ma Z, Nelson DM, Hong Y, and Wagner WR. Thermally responsive injectable hydrogel incorporating methacrylate-polylactide for hydrolytic lability. Biomacromolecules. 2010;11(7):1873–1881.

30. Longenecker R, Mu T, Hanna M, Burke NAD, Stöver HDH. Thermally responsive 2-hydroxyethyl methacrylate polymers: Soluble-insoluble and soluble-insoluble-soluble transitions. Macromolecules. 2011;44(22):8962–8971.

31. Peppas, Y, Huang, M, Torres-Lugo, J. H. Ward and JZ. Physicochemical Foundations and Structural Design of Hydrogels in Medicine and Biology. Annual Review. 2000;2:9–29.

Chapter - 5

Incorporation of hydroxypropyl methacrylate (HPMA) into L-pNIPAM hydrogel

5.1 Introduction

As described in the first chapter, hydrogels can be synthesised using one monomer (homopolymer hydrogel), or two comonomers (copolymer hydrogel) usually in conjunction with a crosslinker. However, incorporating different comonomers with varied concentrations impacts the physical, mechanical properties and suitability for different applications of the synthesised hydrogel(1,2). Therefore, when different comonomers are used, potential changes in hydrogel properties should be assessed.

The first use of hydroxypropyl methacrylate (HPMA) copolymers was in the early 1970s (3,4). Subsequently, work has focused on pharmaceutical applications of HPMA (5–7). Poly hydroxypropyl methacrylate (poly (HPMA)) was found to be suitable for pharmaceutical applications, due to its flexibility which was shown to be similar to soft tissue, in addition to its inherent hydrophilicity and biocompatibility(8) Therefore, it has been used for several pharmaceutical applications.

Injectable poly (HPMA) based hydrogel was used to deliver anticancer drugs(8). Copolymers have been incorporated to produce poly (HPMA) based hydrogels, to improve their pharmaceutical application; such as drug release(9,10). Marek *et al* synthesised HPMA based copolymer hydrogels, for drug delivery applications, using radical solution copolymerisation of hydroxypropyl methacrylate (HPMA) with N, O-dimethacryloyl hydroxylamine (DMHA). Hydrogel discs were immersed into anticancer drug solution, to allow drug loading. Subsequently, hydrogel discs loaded with drug were implanted into the right flanks of mice, directly after sterilization. They concluded that hydrogel facilitated the release the drug for at least 96 hours, and the release time can be controlled by changing crosslinking density(9).

Many studies have been conducted in the field of drug delivery, using HPMA as comonomer to prepare hydrogel carriers to deliver different types of drugs such as; insulin(11) and caffeine(12).

Vladimir *et al* synthesised hydrogels based on copolymer of N-(2-hydroxypropyl) methacrylamide and N-methacryloyldiglycyl p-nitrophenyl ester. They loaded the hydrogel with insulin, which covalently bound onto the

polymeric chains. The product was found to exhibit sustained insulin release(11).

Horia *et al* have prepared HPMA based copolymer hydrogels, with caffeine as a model drug by dissolving different ratios of HPMA and NIPAM in distilled water, and using N,N methylenebisacrylamide (MBAAm) as crosslinker. Polymerisation was carried out by gamma irradiation. They found that caffeine release can be varied, depending on the hydrogel chemical composition and pH(12).

More recently, there has been interest in using HPMA either as homopolymer or as copolymer hydrogel, to prepare hydrogel materials for tissue engineering applications(13,14). Pertici *et al* synthesised pHPMA based hydrogels by radical polymerization, and using divinyl as crosslinking agent. After polymerisation was finished the gel was washed with water to remove unreacted monomer units, and stored in distilled water at 4^{o}C. A small block of pHPMA hydrogel was implanted into the hemisected T10 rat spinal cord. They found that locomotor neurophysiological improvements were induced, after 14 weeks of implantation(14).

In many systems, HPMA hydrogels have been shown to either not be fully polymerised(14) or not injectable(9).

In the current study, fully injectable L-pNIPAM-co-HPMA was synthesised and characterised to investigate the influence of different comonomer ratios on the mechanical and physical properties. In addition, cell viability within the manufactured hydrogels was assessed and osteogenic differentiation was explored.

5.2 Synthesis of L-pNIPAM-co-HPMA with different pNIPAM/pHPMA ratios

All materials used and methods of hydrogel synthesis and experimental work were detailed in chapter two, section 2.2.

5.3 results and discussion

5.3.1 Influence of incorporation of hydroxypropyl methacrylate (HPMA) on lower critical solution temperature of L-pNIPAM-co-HPMA

L-pNIPAM hydrogels have been synthesised(15), and its composition adjusted to ensure a lower critical solution temperature of 37°C by incorporating N, N - dimethyl acrylamide (DMAc) which allowed it to meet medical application requirements (16). It is well known that, pNIPAM has an LCST at ~32 °C (17–19), but it can be modified to meet different applications requirements; such as tissue engineering. By adding more hydrophilic comonomer LCST of pNIPAM based hydrogels can be elevated, or reduced if more hydrophobic comonomer incorporated. HPMA and NIPAM are soluble in water and have hydrophilic groups to create miscible solutions, but HPMA has greater hydrophilicity (Figure 5.1).

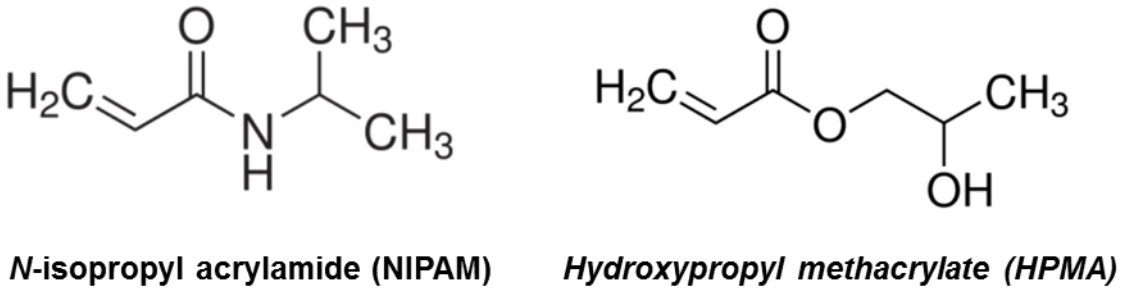

N*-isopropyl acrylamide (NIPAM)** ***Hydroxypropyl methacrylate (HPMA)

Figure 5.1: Chemical structures of N-isopropyl acrylamide (NIPAM) and hydroxypropyl methacrylate (HPMA).

As detailed in chapter 2, section 2.2; L-pNIPAM-co-HPMA hydrogel was synthesised, using HPMA ratio of 5, 10 and 17% of total monomers. However hydrogel contained 17% HPMA was found to be not completely liquid and injectable, due to the observation of small solid particles, hence only formulations contained 5 and 10 % were selected and subjected to further characterisation. Both formulations remained liquid after polymerisation reaction was complete and they could be stored for extended periods at 60°C without a detrimental impact on their performance. The LCST of synthesised L-pNIPAM-co-HPMA based Laponite® hydrogel was measured in triplicate using a digital

thermometer, where the LCST was determined as the point at which the sample no longer flowed.

The incorporation of a more hydrophilic comonomer into pNIPAM hydrogels has been shown to elevate the LCST from ~32 °C to ~37 °C (16,19). A thermally-induced LCST mechanism originates from phenomena occurring at the temperature above which the polymer becomes insoluble in aqueous media. It is the temperature at which coil-to-globule conformational changes of the polymer network occur, due to sufficient disruption of hydrogen bonding between the amide groups of the polymer and the water molecules, allowing hydrophobic interactions to form between the non-polar domains of the system, i.e. the solvent changes from “good” to “poor”(20–22). Generally if more hydrophilic components are incorporated into the amphiphilic polymer backbone, water acts as a good solvent at higher temperatures, hence the LCST is higher. Counterintuitively in L-pNIPAM-co-HPMA, adding more hydrophilic (HPMA) comonomer and following exactly the same procedure of hydrogel synthesis used to make L-pNIPAM, a reduction in the setting temperature, which is related to the LCST is observed, changing from ~32°C to ~27°C (Figure 5.2). We postulate that interactions between the pendent OH groups on the HPMA units and the Laponite® surface may mask the inherent hydrophilicity of the HPMA moieties.

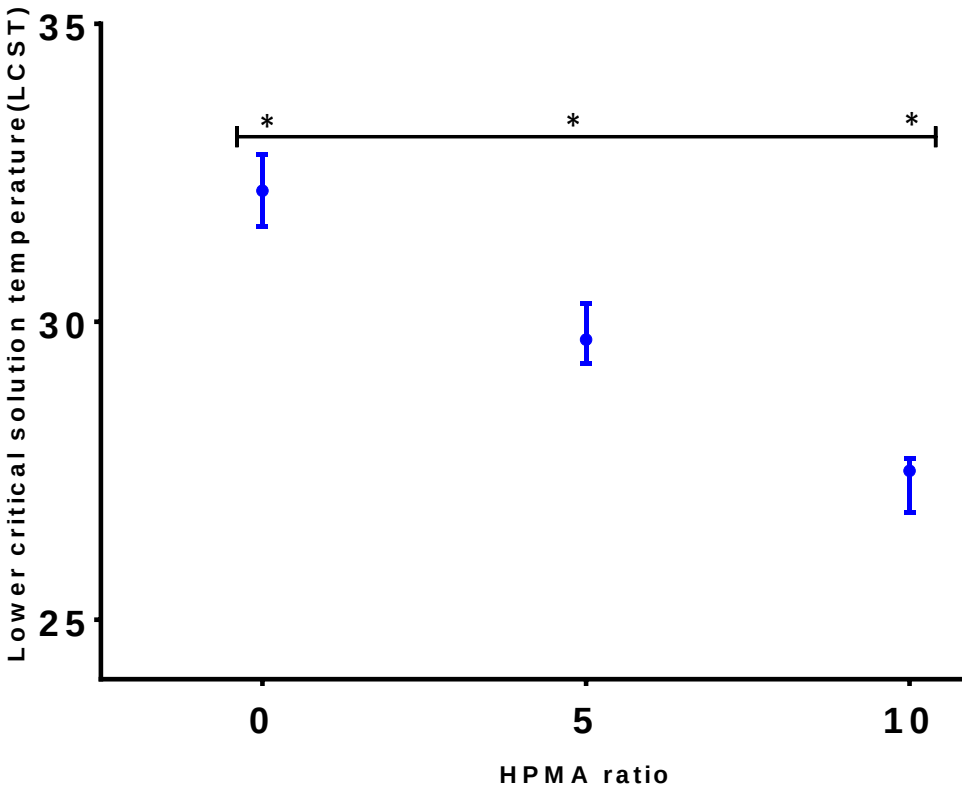

Figure 5.2: Lower critical solution temperature (LCST) of pNIPAM/HPMA based Laponite® hydrogel with different ratios of HPMA. n=3

5.3.2 Morphological study and pore size measurement of L-pNIPAM-co-HPMA hydrogels

The effect of incorporating HPMA on morphological and structural properties of L-pNIPAM-co-HPMA hydrogels was explored using scanning electron microscopy, to determine the pore sizes of different compositions and their heterogeneity (Figure 5.3). Six images of each composition was used to measure the pore sizes, and plotting pore size distribution of each composition allowed the comparison between systems and facilitated the elucidation of the influence of using HPMA as comonomer on the morphology (Figure 5.4).

An increase in average pore size when compared to L-pNIPAM for L-pNIPAM-co-HPMA was observed when 5wt. % of HPMA was incorporated (Figure 5.3). However, no further increase in hydrogel pore size when HPMA concentration increased to 10 wt. % (Figure 5.3).

Jiyuan *et al* have prepared hybrid hydrogels using peptide grafted with HPMA and N-(3-aminopropyl) methacrylamide; these are referred to as (MA-NH2) copolymers. Copolymerisation was performed using AIBN as the initiator, and

synthesised peptides were attached to the polymer backbone. They have revealed that, increased copolymer concentration from 0.1 to 5 wt. % changed the morphology of hydrogel from dense monoliths to porous sponge-like structures (23).

In L-pNIPAM-co-HPMA hydrogels system, it is also was found that incorporating HPMA as comonomer initially (up to 5 wt%) increased the average pore size (Figure 5.4). However, no further increase was observed when HPMA concentration was further increased to 10 wt. %.

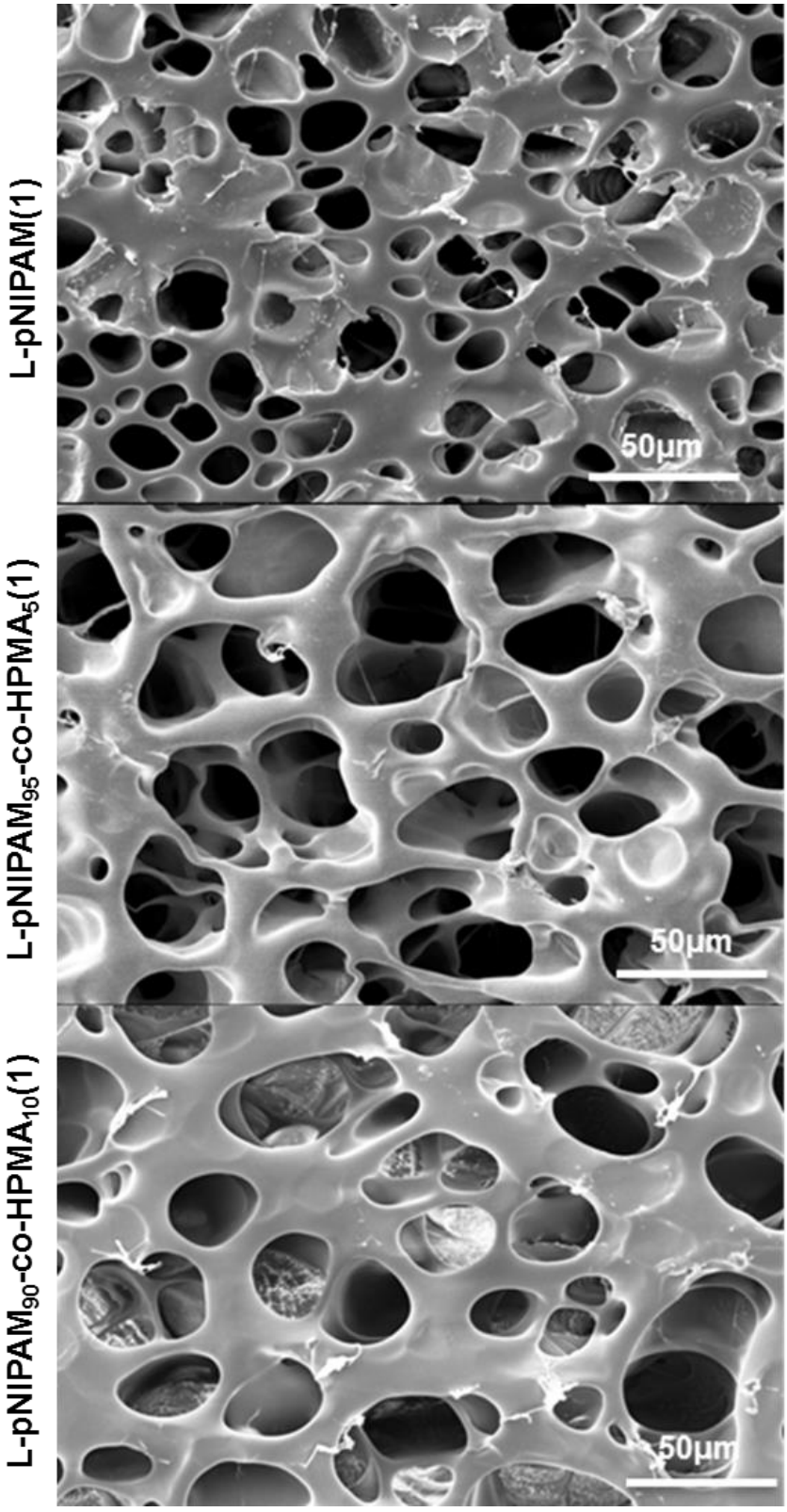

Figure 5.3: Scanning electron microscopy images of L-pNIPAM hydrogels with HPMA concentration of 5 and 10 wt. %. Scale bar 50 µm.

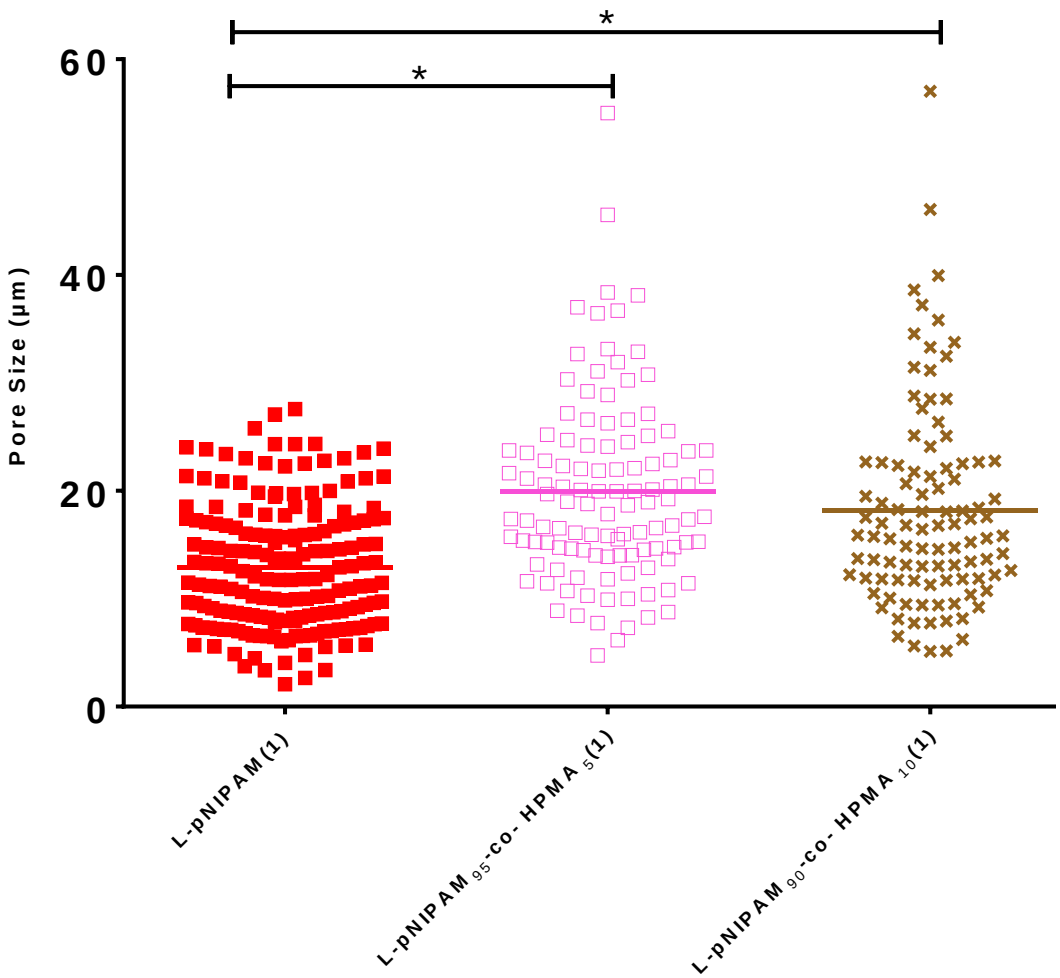

Figure 5.4: Statistical analysis of pore size of L-pNIPAM hydrogels with HPMA concentration of 5 and 10 wt. %. *= P<0.05

5.3.3 Dynamic Mechanical Analysis (DMA) frequency scan data of L-pNIPAM-co-HPMA

The viscoelastic behavior of L-pNIPAM-co-HPMA was studied using dynamic mechanical analysis, at a fixed frequency (10Hz) in compression mode. To determine influence of the NIPAM: HPMA ratio on mechanical properties of L-pNIPAM-co-HPMA hydrogels, six samples of each composition described in Table 5.1 were synthesised, and the storage modulus (E') was recorded for each. For all samples, E' did not increase as a function of increasing frequency (Figure 5.5). Therefore, 10 Hz was selected to compare potential differences in the mechanical properties between different compositions of hydrogel samples (Figure 5.6). L-PNIPAM$_{95}$-co-HPMA$_5$ was shown to decrease storage modulus significantly compared with L-pNIPAM (Figure 5.6). However, increasing the HPMA content did not decrease the storage modulus further.

Many researchers have linked morphological changes with mechanical properties of hydrogel materials (24,25). Where increasing the pore size of hydrogel materials decreases the mechanical properties and vice versa. Our interpretation of the influence of composition on mechanical properties in the current study is consistent with this concept.

Moreover, Lutz states that an increased concentration of hydrophobic comonomer leads to enhanced mechanical properties (26). Our findings contradict this, where incorporation of hydrophilic comonomer (HPMA) decreases mechanical strength significantly (Figure 5.6). One can only assume that this supposition is highly system dependent.

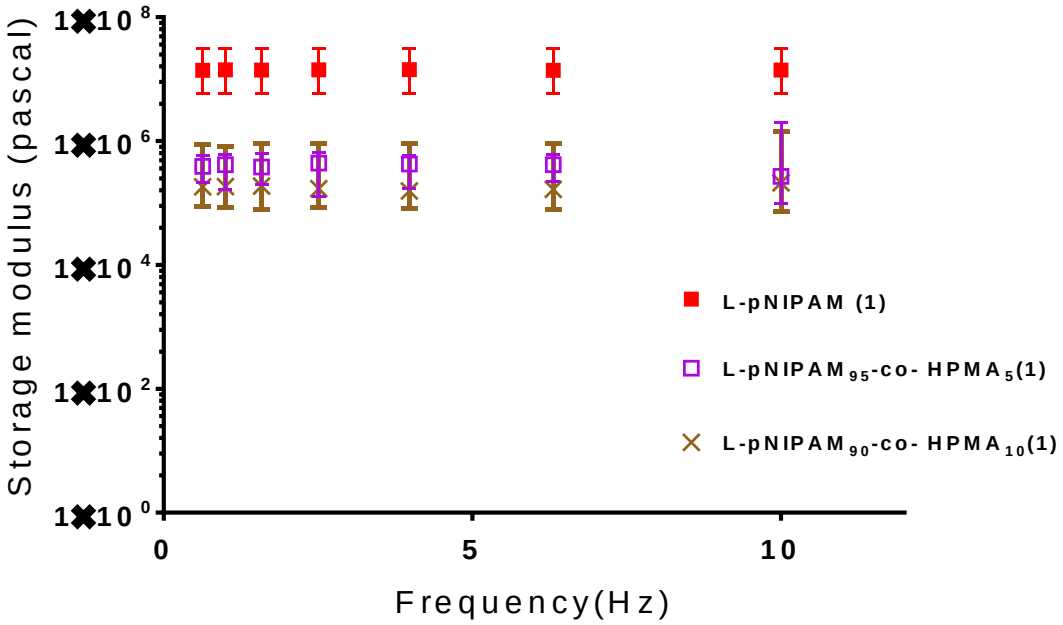

Figure 5.5: Dynamic Mechanical Analysis (E' values) of pNIPAM based Laponite® hydrogel with different HPMA concentrations.

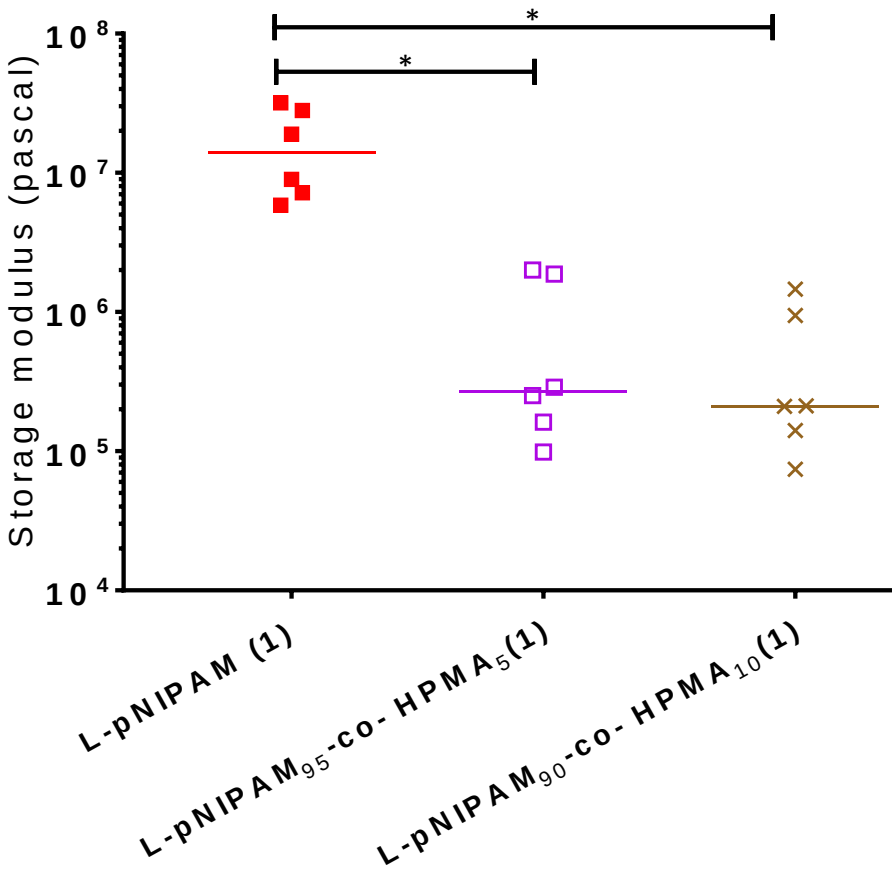

Figure 5.6: Influence of HPMA concentration on storage modulus determined by DMA in compression mode at 10Hz. *= P<0.05

5.3.4 Swelling and deswelling kinetics

5.3.4.1 Swelling kinetics

The influence of the composition of L-pNIPAM-co-HPMA on the swelling behaviour in distilled water at 25°C as a function of time up to 24 hours was investigated. The influence of the NIPAM/HPMA ratio on swelling ratio and maximum equilibrium swelling degree of L-pNIPAM-co-HPMA was determined as detailed in chapter 2, section 2.3.7. L-pNIPAM-co-HPMA displayed a higher degree of swelling than L-pNIPAM (Figure 5.7), due to the more hydrophilic character of HPMA compared to NIPAM. To obtain a more quantitative understanding, the maximum equilibrium degree of swelling was compared for both L-pNIPAM and L-pNIPAM-co-HPMA hydrogels, where L-pNIPAM-co-HPMA hydrogels were shown to possess a significantly higher equilibrium swelling degree after 24 hours (Figure 5.8).

Generally, hydrogels with more hydrophilic groups swell faster and reach a higher degree of swelling compared to the those containing more hydrophobic groups(27). Therefore, logically one supposes that more hydrophilic polymeric units (HPMA) attract more water molecules into the hydrogel structure, which enhances the swelling ratio of L-pNIPAM-co-HPMA (Figure 5.7). Furthermore, bigger pore sizes observed for these systems may also contribute to the maximum equilibrium swelling degree (Figure 5.8).

Interestingly, for L-pNIPAM$_{90}$-co-HPMA$_{10}$ (1) hydrogels, bigger pore sizes have been shown to slow the swelling rate as more time was needed for water to enter into the gel matrix and fill the pores(28).

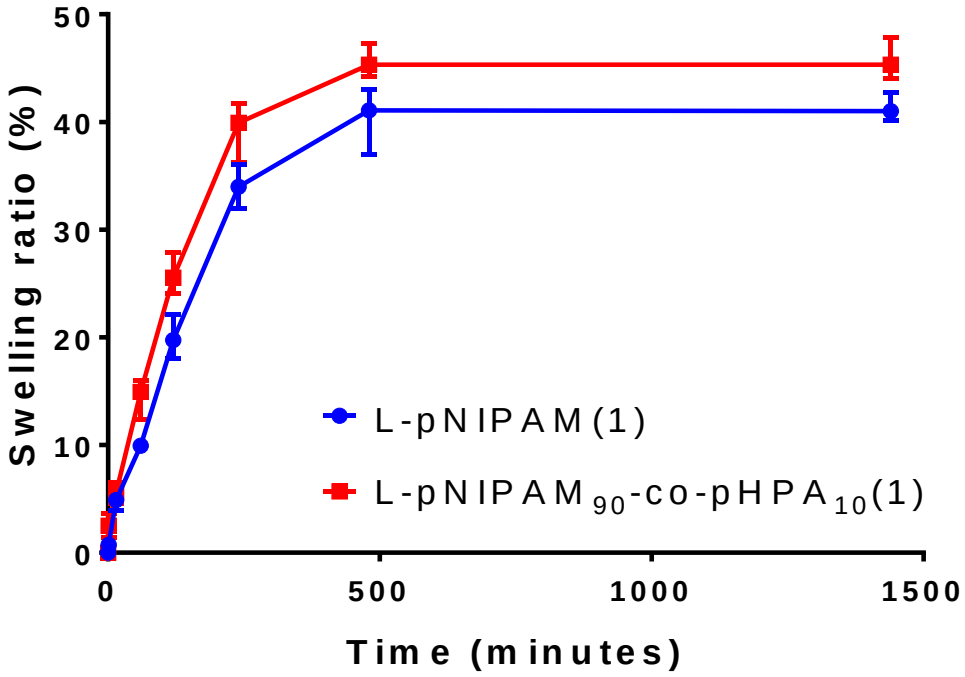

Figure 5.7: Swelling ratio of L-pNIPAM hydrogels with and without HPMA incorporated.

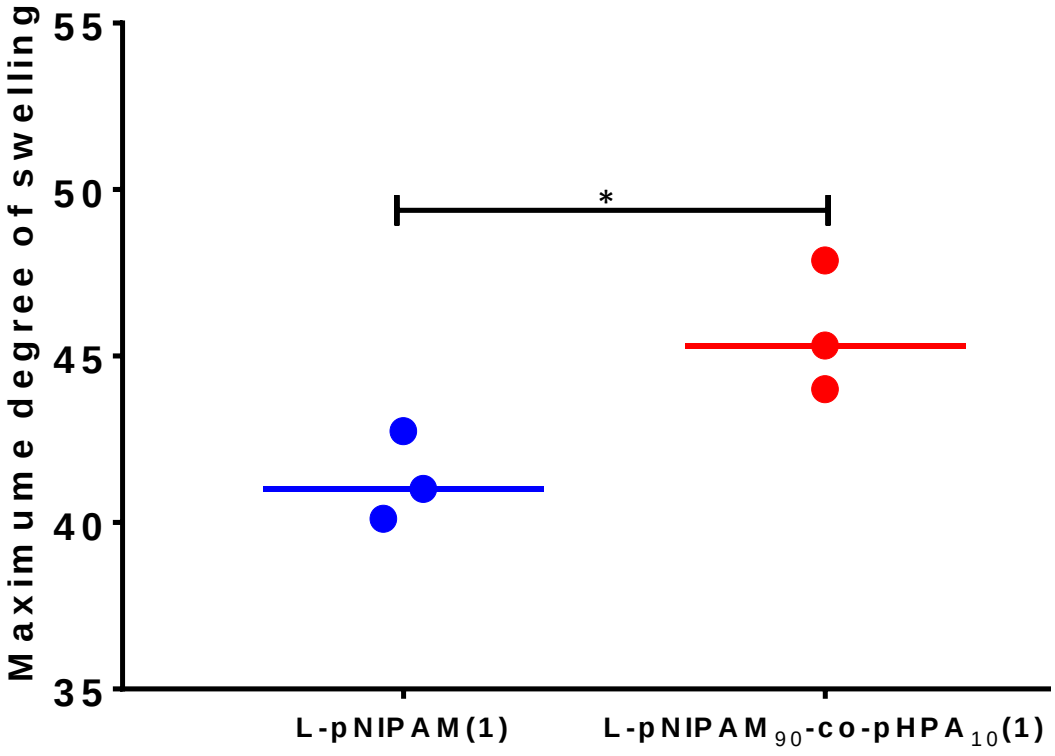

Figure 5.8: Equilibrium swelling degree of L-pNIPAM hydrogels with and without HPMA incorporated. *= P<0.05

5.3.4.2 Deswelling kinetics of L-pNIPAM-co-HPMA hydrogels

The deswelling behaviour of L-pNIPAM-co-HPMA hydrogels was observed when changing the temperature from 25°C to 62°C. As detailed in chapter 2, section 2.3.8. Briefly; 2 ml of hydrogel sample of each formulation was poured into graduated glass cylinder, and allowed to solidify for 10 minutes at room temperature. Thereafter, 2 ml of preheated deionised water was added into each cylinder at 62°C, and cylinders were kept at 62°C, and changes in hydrogel dimensions, during thermal challenge, were observed and recorded on a digital camera at different time intervals (Figure 5.9). Dimensional changes were measured from the captured images using ImageJ150 software.

The deswelling of a thermoresponsive hydrogel is a thermal response to the changes in the surrounding environment above the LCST of the polymer (29). Here, L-pNIPAM$_{90}$-co-HPMA$_{10}$, has lower proportion of thermally responsive component than L-pNIPAM, therefore its maximum deswelling was lower (Figure 5.10 and 5.11). However the rate of deswelling was faster due to the difference in pore size.

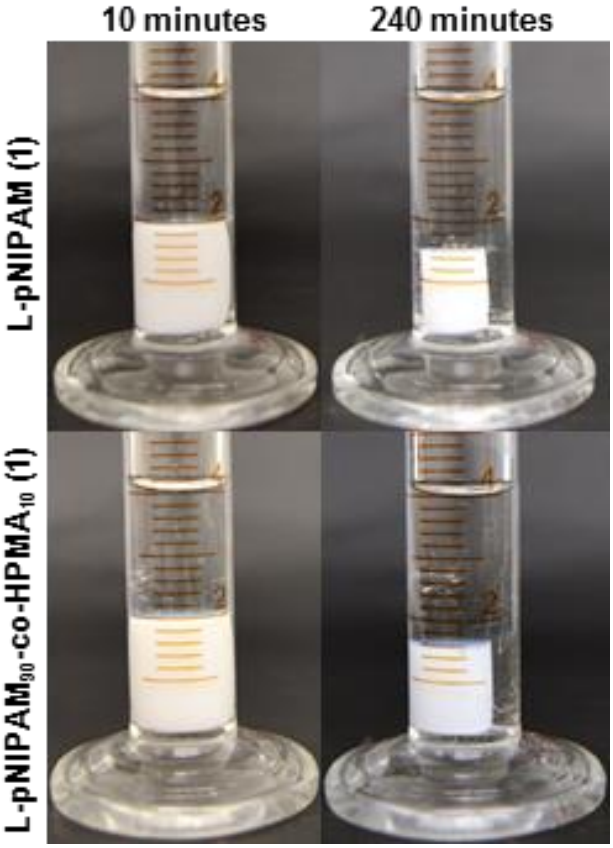

Figure 5.9: Photograph images showing different thermal response for L-pNIPAM (1) and L-pNIPAM$_{90}$-co-HPMA$_{10}$ (1) at 10 and 240 minutes. T=62°C.

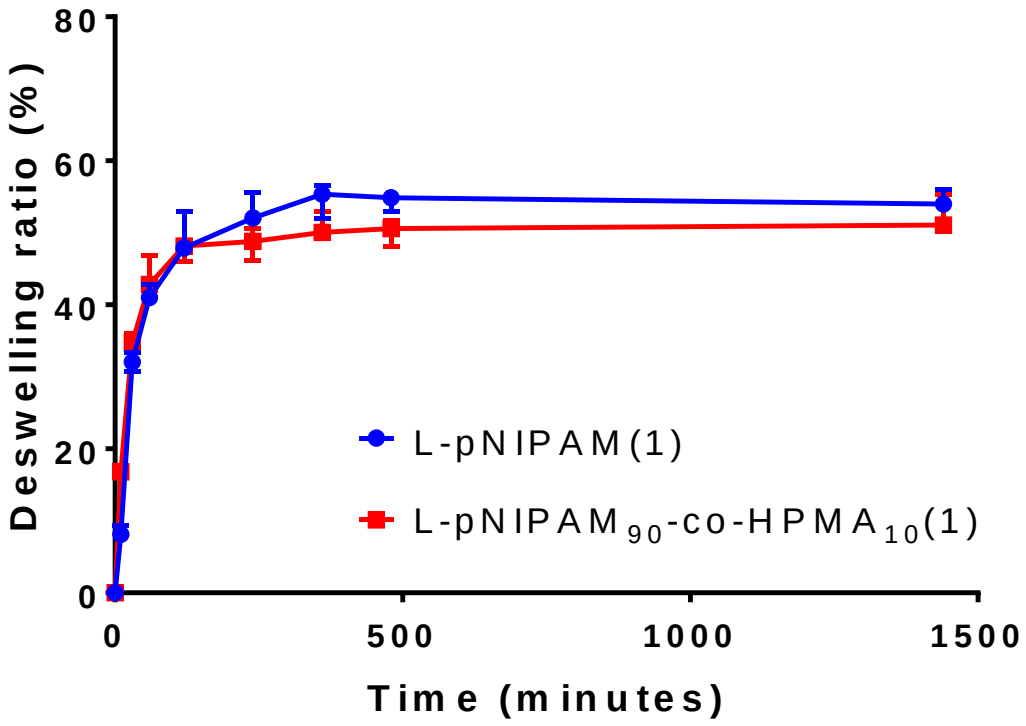

Figure 5.10: Deswelling ratio of L-pNIPAM hydrogels with and without HPMA incorporated.

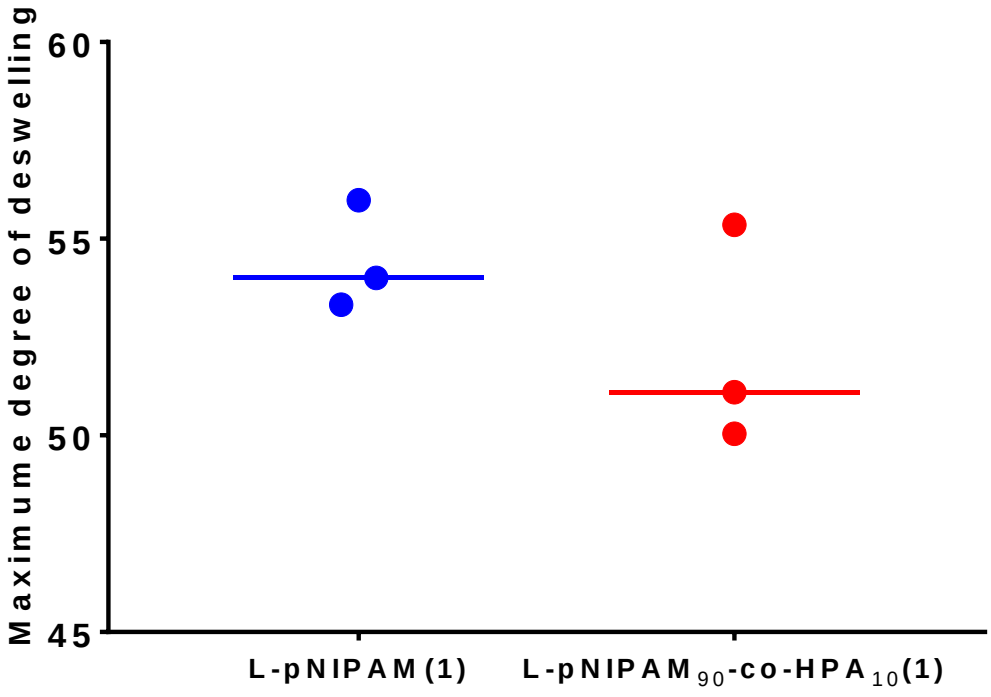

Figure 5.11: Maximum degree of deswelling of L-pNIPAM hydrogels with and without HPMA incorporated.

5.3.5 Contact angle measurements

As described in chapter 2, section 2.3.5, contact angle of L-pNIPAM-co-HPMA was measured on glass slides (Leica Microsystem Milton Keynes, UK). The influence of composition of liquid hydrogel on the contact angle on glass was investigated. When L-pNIPAM (1) was pipetted on the surface of the glass slide, the contact angle created between the hydrogel and the slide was measured and found to be ~ 47°. This value was found to decrease as HPMA was incorporated, i.e. the wettability of the glass surface was enhanced. The contact angle of L-pNIPAM$_{95}$-co-HPMA$_5$ (1) was recorded to be ~44° and a further reduction in contact angle was observed as HPMA concentration was increased, and the contact angle of L-pNIPAM$_{90}$-co-HPMA$_{10}$ (1) was ~ 39°. Four measurements were used for each formulation.

Therefore, increasing the concentration of HPMA was shown to decrease the contact angle, which effectively increased surface area of each L-pNIPAM-co-HPMA drop systematically (Figure 5.12). This finding has implications when the drying experiments are conducted.

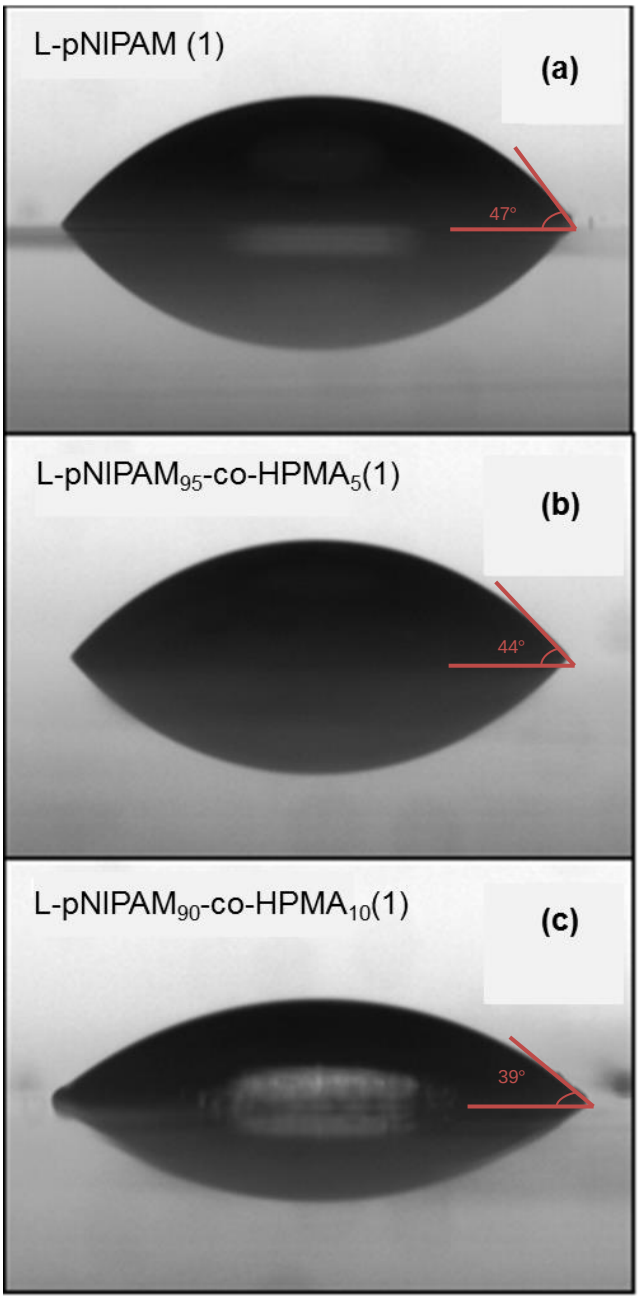

Figure 5.12: contact angle of pNIPAM based Laponite® hydrogel with various HPMA concentrations.

Water contact angle (WC) is an important characteristic for hydrogel materials that have potential biomedical applications, due to its correlation to many properties such as surface adhesion and biocompatibility. In addition, water contact angle is a standard measurement to represent surface wettability(30).

Incorporation of HPMA as comonomer into L-pNIPAM was shown to decrease water contact angle significantly. Increasing the HPMA concentration from 5 to 10 wt. % increased the wettability of the hydrogel (Figure 5.13), due to the increase in overall hydrophilicity as HPMA is more hydrophilic than NIPAM.

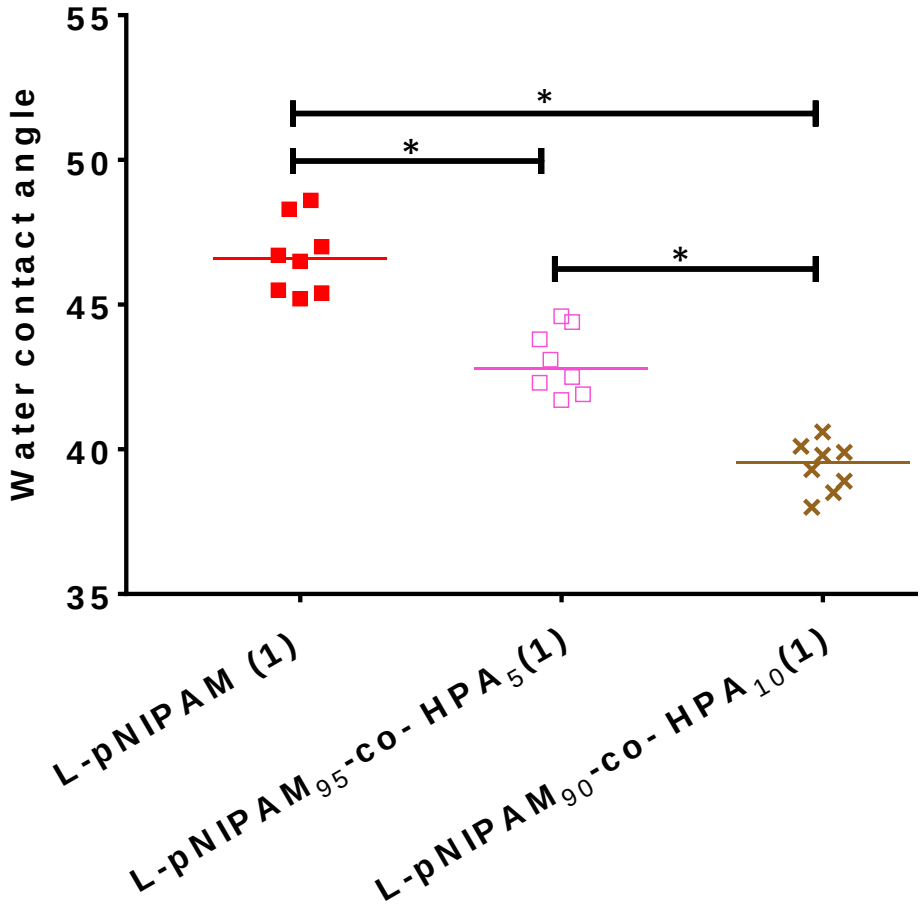

Figure 5.13: Water contact angle of pNIPAM based Laponite® hydrogel with various HPMA concentrations. *= P<0.05. n=4.

5.3.6 Water states and water/polymer interactions study

As previously mentioned, L-pNIPAM consists of 90 % water and has different potential of biomedical and tissue regeneration applications. Therefore, it is crucial to understand water behaviour within this material. In the current study water states, water/ polymer interactions and dehydration and rehydration behaviour, within L-pNIPAM-co-HPMA were studied.

5.3.7 Dehydration of L-pNIPMA-co-HPMA formulations

Fourier transform infrared attenuated total reflectance (FTIR-ATR) has proven its perfection and accuracy to investigate diffusion and sorption kinetics in polymeric materials (31,32). Fourier transform infrared attenuated total reflectance (FTIR-ATR) was used to monitor the dehydration process of L-pNIPAM and L-pNIPAM-co-HPMA, to explore the effect of HPMA as comonomer on dehydration behaviour of such materials.

Samples were synthesis as described in chapter two, section 2.2; 30µl of each formulation was pipetted directly onto the ATR crystal which had been pre-set to 25˚C. Data collection was immediately commenced with 8 scans per spectrum at a resolution of 8cm^{-1} on a Thermo Nicolet Nexus instrument, using a series setup, a spectrum was taken automatically every 30 sec for 800m (13.3h).

For clarity, selected spectra at different time intervals during drying of L-pNIPAM (1) have been displayed (Figure 5.14). This allows the monitoring of the drying of hydrogel samples in real time by following the decrease in intensity of the ν(OH) band, associated with water, between 3600-3100 cm^{-1}, and increase intensity of δ(NH) band at ~1550 cm^{-1} this band is also known as the amide III band and is indicative of the polymer concentration in the evanescent field. In addition, there was shift in δ(NH) band to lower wavenumber over time, this can be related to changes in the local environment of polymer chains and therefore be directly linked to hydrogen bonding between water and the polymer chains within the system.

Expansions of these data are shown in Figures 5.15 and 5.16, to highlight the observable peak intensity and peak shift changes during the drying process (Figure 5.15 and 5.16).

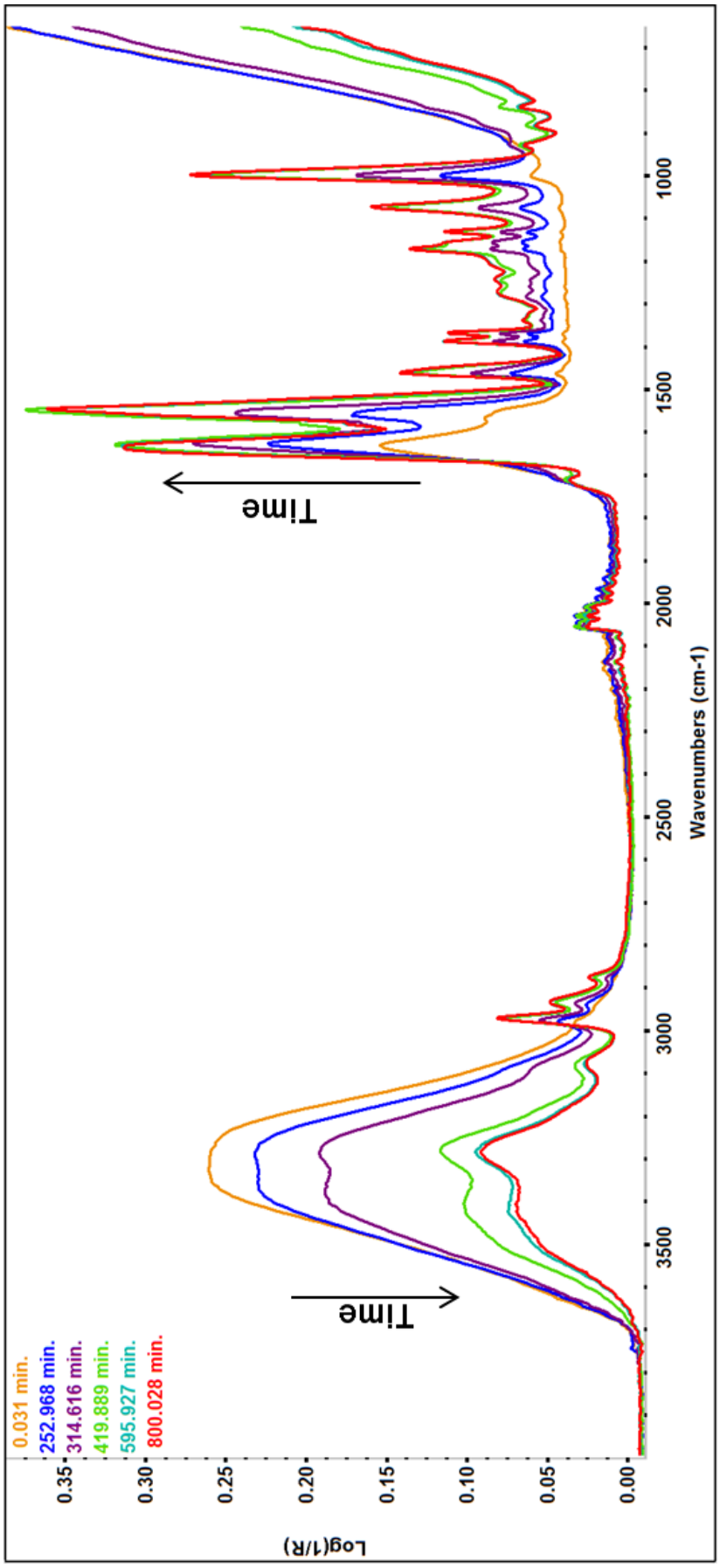

Figure 5.14: Full spectra of water dehydrating from L-pNIPAM$_{90}$-co-HPMA$_{10}$ (1) hydrogel at 25˚C.

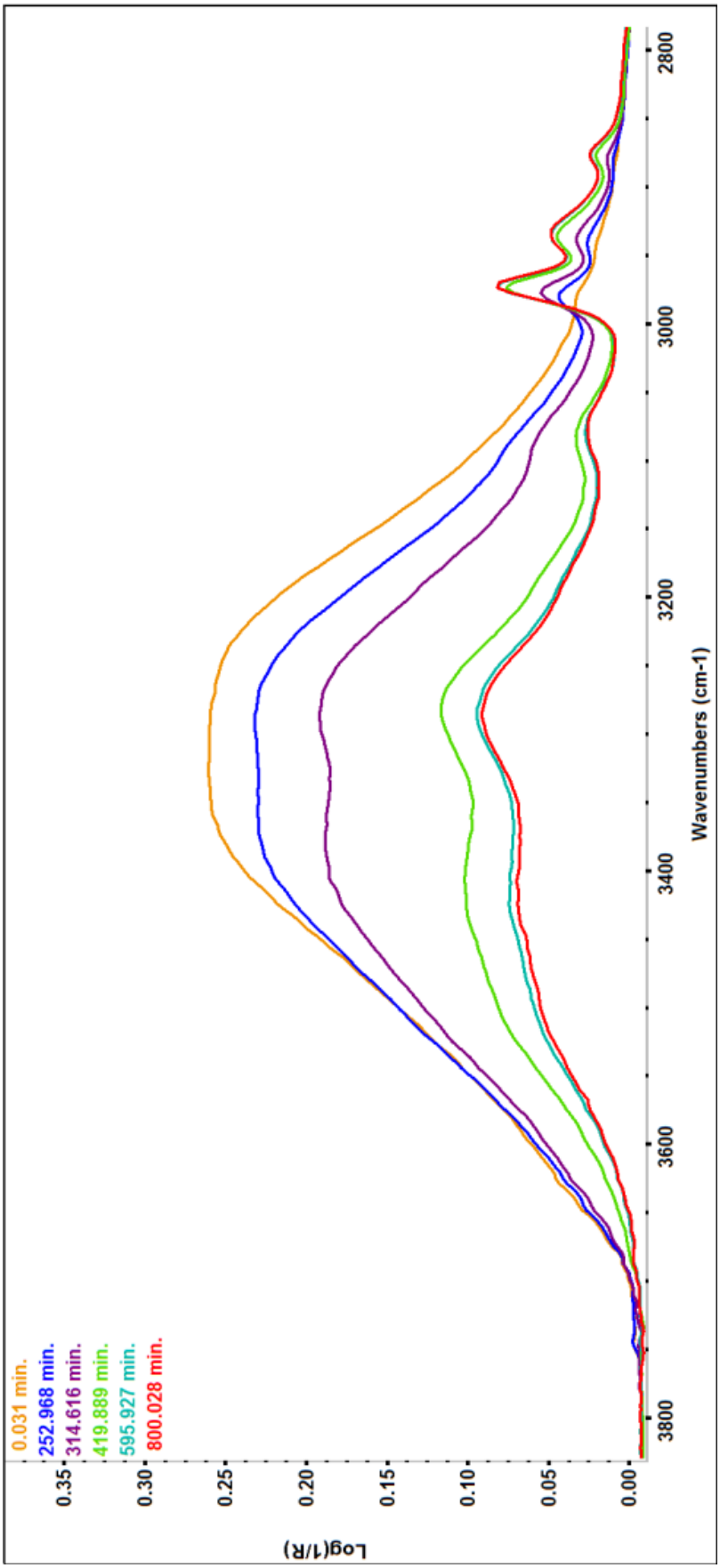

Figure 5.15: *v* (OH) (3700-300cm-1) taken during the drying of L-pNIPAM$_{90}$-co-HPMA$_{10}$ (1) hydrogel at 25˚C.

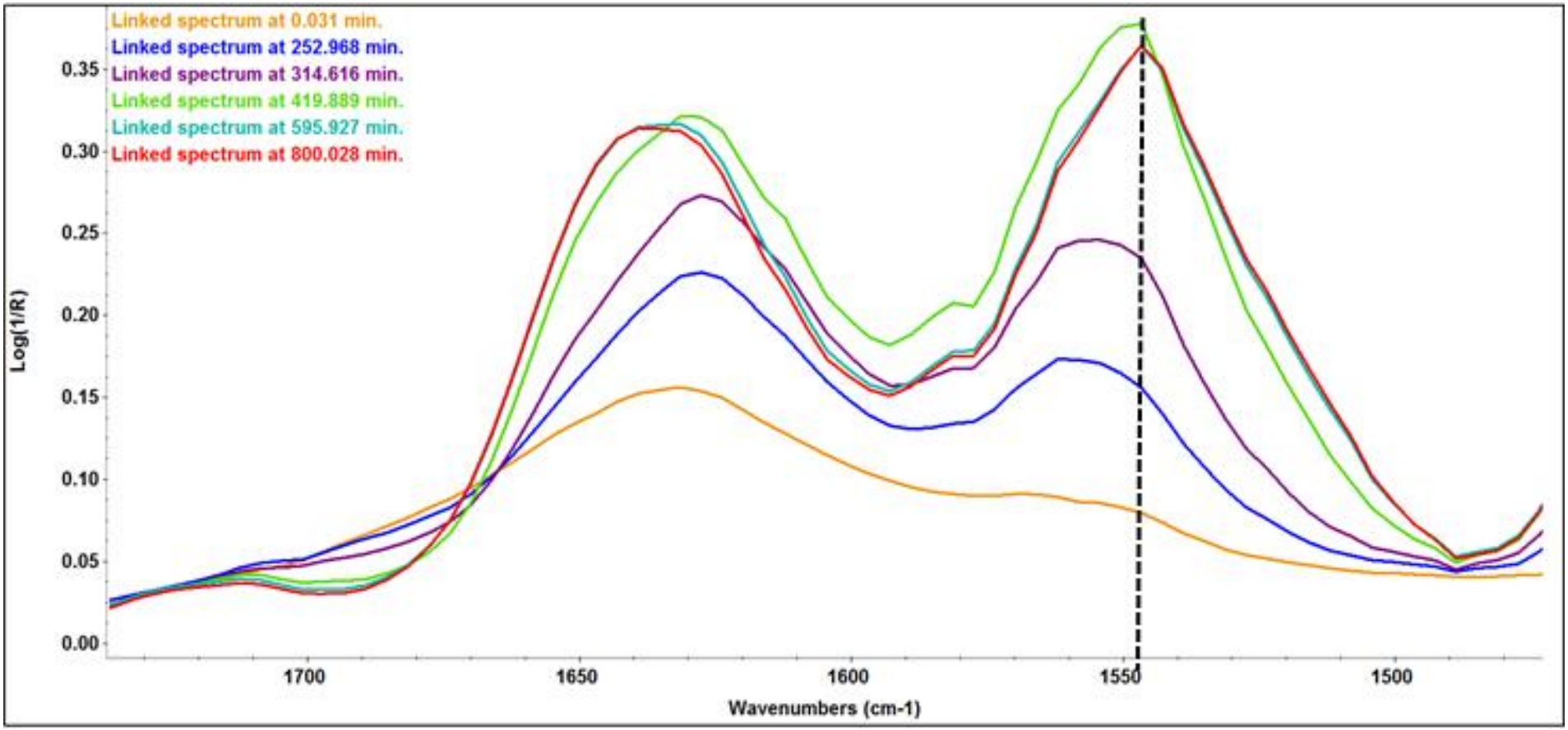

Figure 5.16: δ (NH) band (1550cm^{-1}) taken during the dehydrating of L-pNIPAM$_{90}$-co-HPMA$_{10}$ (1) hydrogel at 25˚C.

The intensity of the ν(OH) band was plotted as a function of time for different formulations of L-pNIPAM-co-HPMA (Figure 5.17) and this allows the influence of HPMA on dehydration rate to be illustrated.

The intensity of ν(OH) was observed to increase slightly at the beginning of the experiment, due to cooling of the hydrogel sample, from 50 to 25˚C, where ν(OH) changes as a function of temperature(33) (Figure 5.17). Following, the reduction in intensity was shown in two phases, where we speculate free water to evaporate firstly and bound water lost later (Figure 5.17).

Incorporation of HPMA was shown to retard the dehydration rate in the first instance, when 5 wt. % HPMA was incorporated, due to an increase in the hydrophilic polymeric molecules. However, when the HPMA concentration was increased to 10 wt. %, this reduction was less pronounced (Figure 5.17). This is observation is counterintuitive, as one would anticipate that increasing the more hydrophilic component would further decrease the dehydration rate. Investigations were then performed to determine if other factors were contributing to the dehydration rate. Contact angle measurements of the L-pNIPAM$_x$-coHPMA$_y$ series shows a systematic decrease in contact angle with increased HPMA content, meaning that the surface area of the hydrogel droplet increases with HPMA content as one might anticipate. As evaporation is a surface effect, one would anticipate that increasing the surface area of the liquid hydrogel droplet would accelerate the dehydration process. It is postulated that the incongruous dehydration profile for the pNIPAM$_{90}$-coHPMA$_{10}$ system is due to the competition between the increase in hydrophilicity retarding the dehydration rate and the increase in the surface area increasing the dehydration rate. In addition, pore size measurements showed an increase in pore size was observed when HPMA incorporated, which may also contribute to the dehydration mechanism.

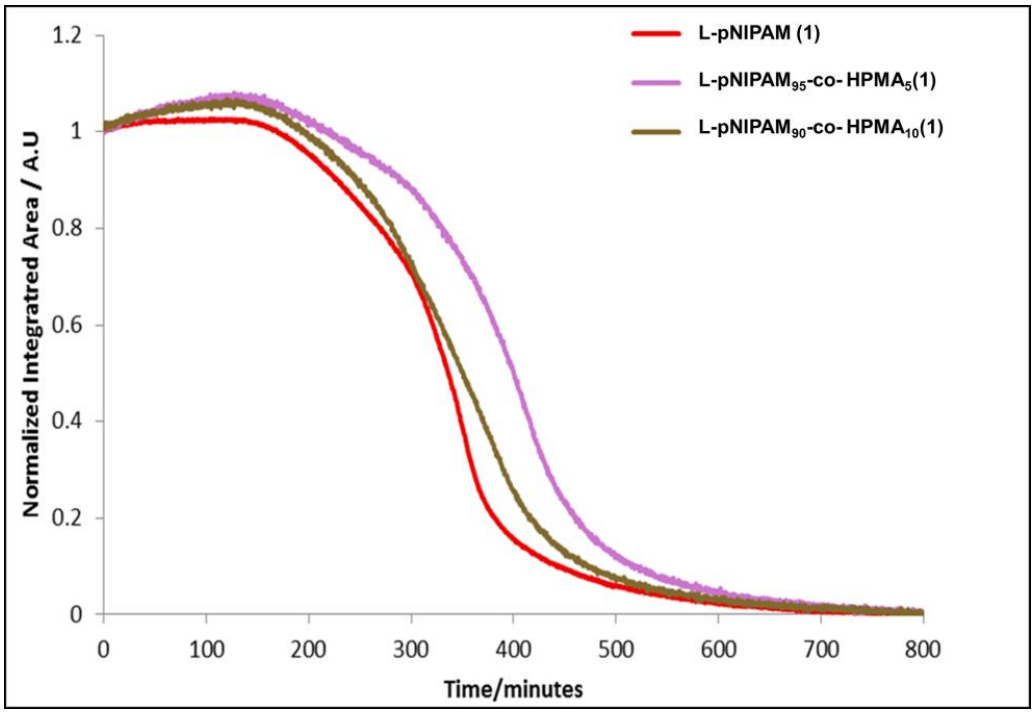

Figure 5.17: water profiles for different HPMA concentrations hydrogels during dehydration.

The change in δ(NH) band position of pNIPAM, which is a good indicator of hydrogen bonding, during water loss is plotted in Figure 5.18. This provides a clear indication of a reduction of the number of H-bonds between polymer chains and water as the water evaporated. The changes in δ(NH) band position are much more noticeable during the second phase of dehydration, where we hypothesize that bound water is being lost from the sample (Figure: 5.18).

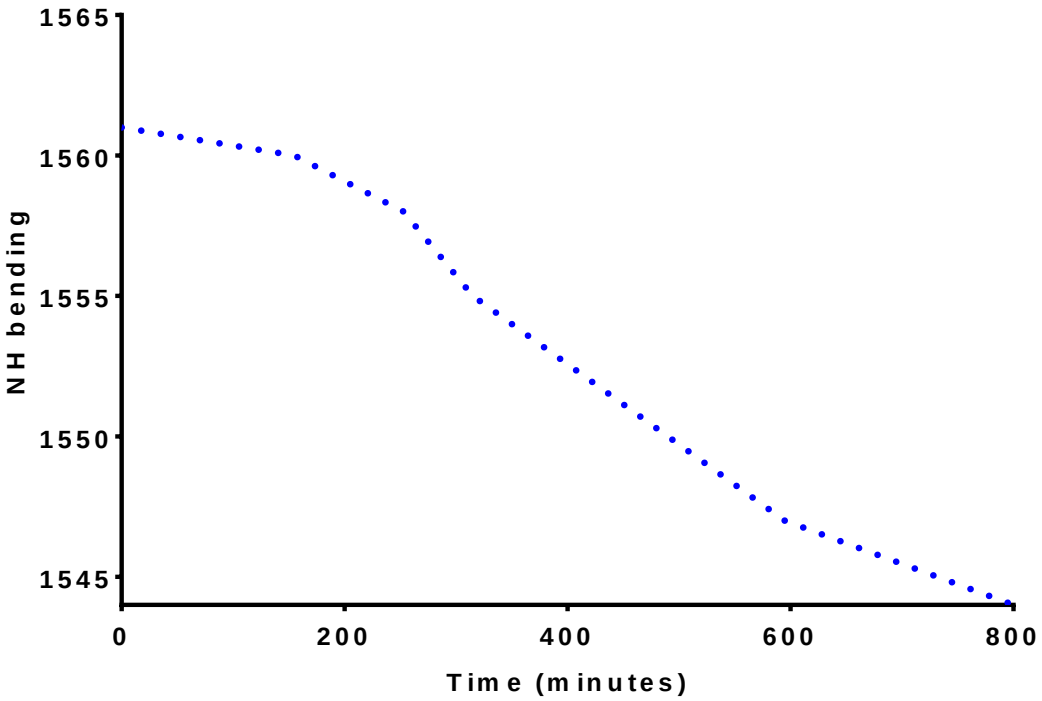

Figure 5.18: Shifts in δ (NH) band of L-pNIPAM$_{90}$-co-HPMA$_{10}$ (1) during dehydration.

Free and bound water concentrations were approximated, according to the hypothesis of water lost during the dehydration process(34), using polymer dehydration profiles for different hydrogel compositions (Figure 5.19). Two different phases of water can be observed, as shown in chapter 3. Bound and free water contents were calculated for each composition (Figure 5.19). Changing the HPMA content in L-pNIPAM-co-HPMA was shown to increase the so-called non-freezable water (bound water), due to an increase in the hydrophilic polymeric units that interact with water molecules within hydrogel structure. Despite the increase in pore size of L-pNIPAM-co-HPMA, with increased HPMA content, which one would expect to increase the free water fraction, increasing the hydrophilicity of L-pNIPAM-co-HPMA had a strong impact on the water state within the hydrogel. The state of water within the hydrogels was verified using the 'gold standard' method of differential scanning calorimetry (DSC) with a good agreement observed between the two methods (Figure: 5.20).

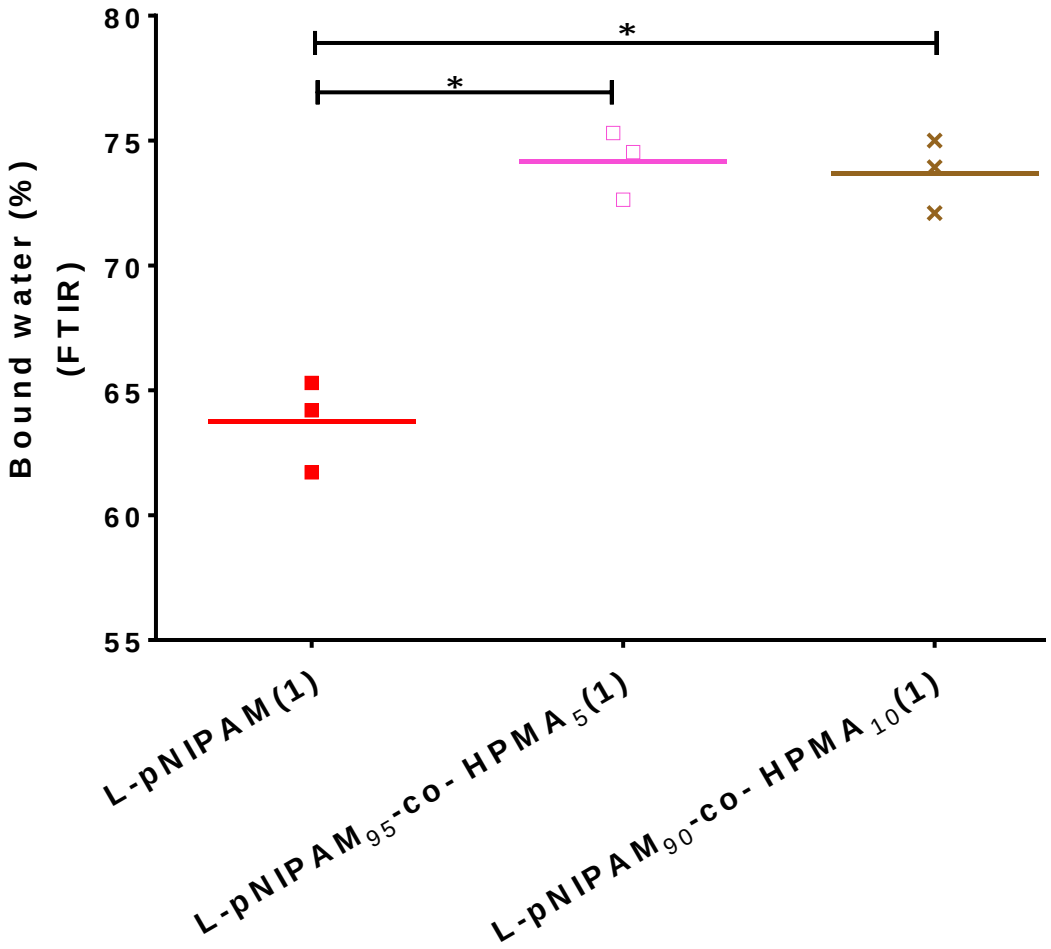

Figure 5.19: Bound water content of pNIPAM based Laponite® hydrogel with different HPMA concentrations, calculated using FTIR. *= P<0.05

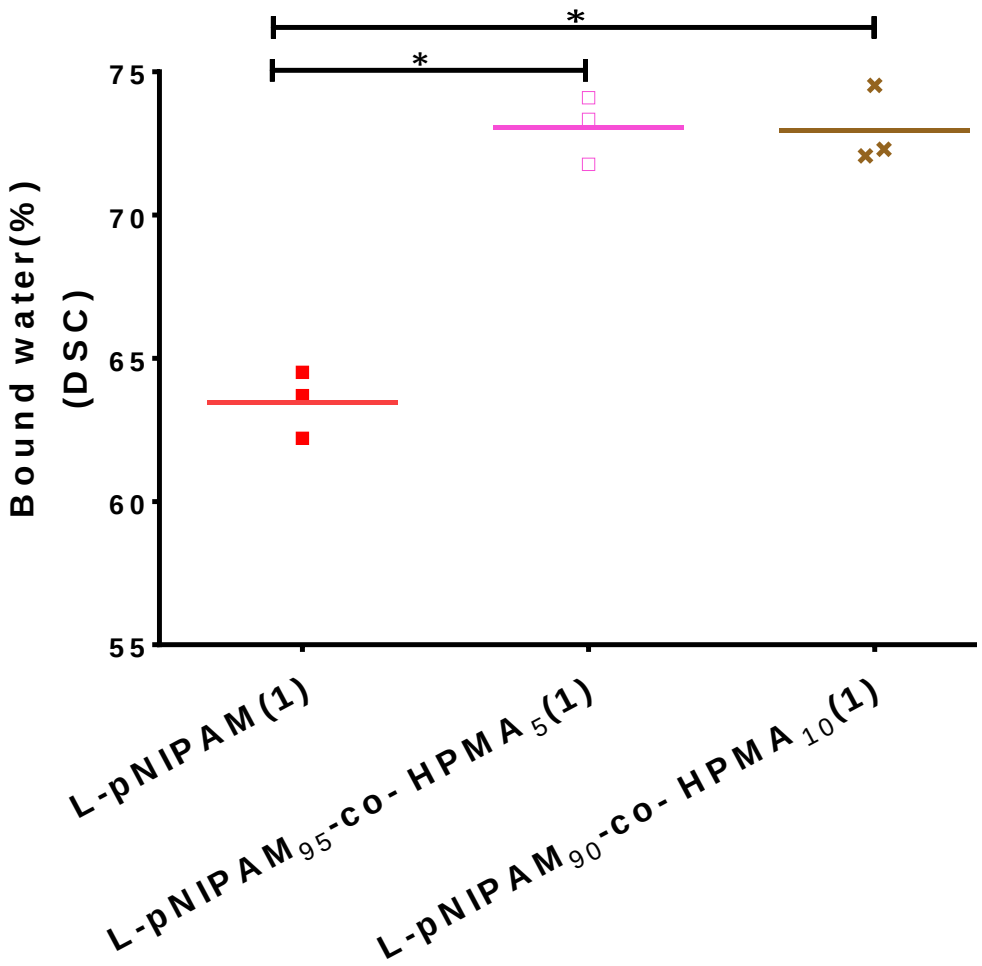

Figure 5.20: Bound water content of pNIPAM based Laponite® hydrogel with different HPMA concentrations, calculated using DSC. *= P<0.05

These findings were in good agreement with previous studies conducted by Mengfan *et al* (35), where they prepared a super macroporous poly (hydroxypropyl methacrylate) cryogel with HPMA concentrations of (5, 7, 8.5 and 9 v/v %), using N, N′-methylenebisacrylamide (MBAAm) as crosslinker and cryogelation method was applied at - 16°C (35,36). They have found that increasing the HPMA concentration increased the bound water fraction in pHPMA cryogel systematically.

5.3.8 Rehydration study

Directly after the dehydration experiment was finished with the dried hydrogel sample still in good contact with the ATR crystal. Rehydration studies were performed by placing deionised water (18MΩ) in contact with the sample using a liquid cell holder. FTIR data collection parameters used were the same as those used for the dehydration experiment, however a shorter total collection

time of 240 minutes was used. Water absorption was monitored by observing changes in the ν(OH) band between 3600-3100 cm^{-1} and δ(NH) (Figure 5.21). The intensity of ν(OH) band increased over time as more water entered the sample (Figure 5.22). Shifts in the δ(NH) band as a function of water content indicate changes in the hydrogen bonding between water molecules and polymeric chains over the course of the experiment (Figure 5.23).

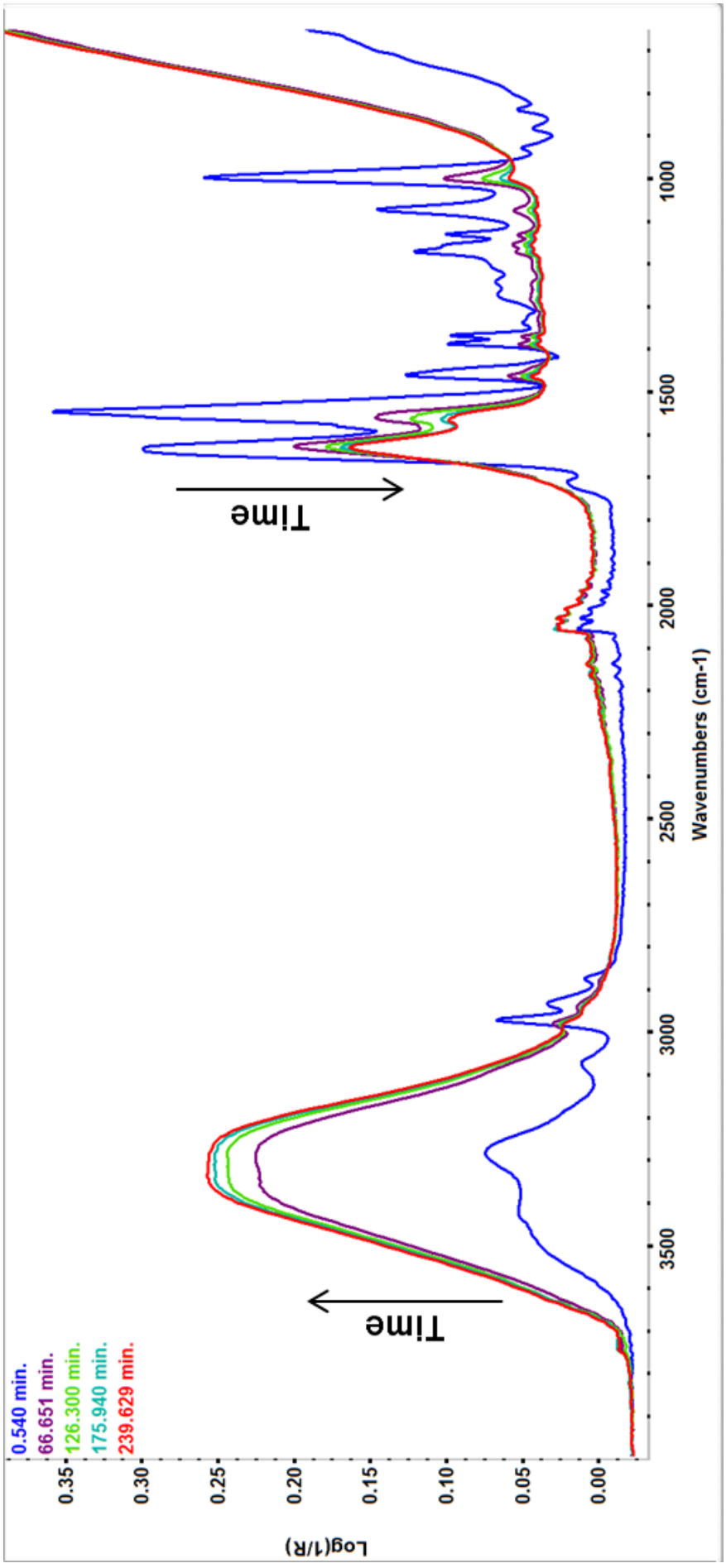

Figure 5.21: Full spectra of water absorbing into L-pNIPAM$_{90}$-co-HPMA$_{10}$ (1) hydrogel at 25˚C.

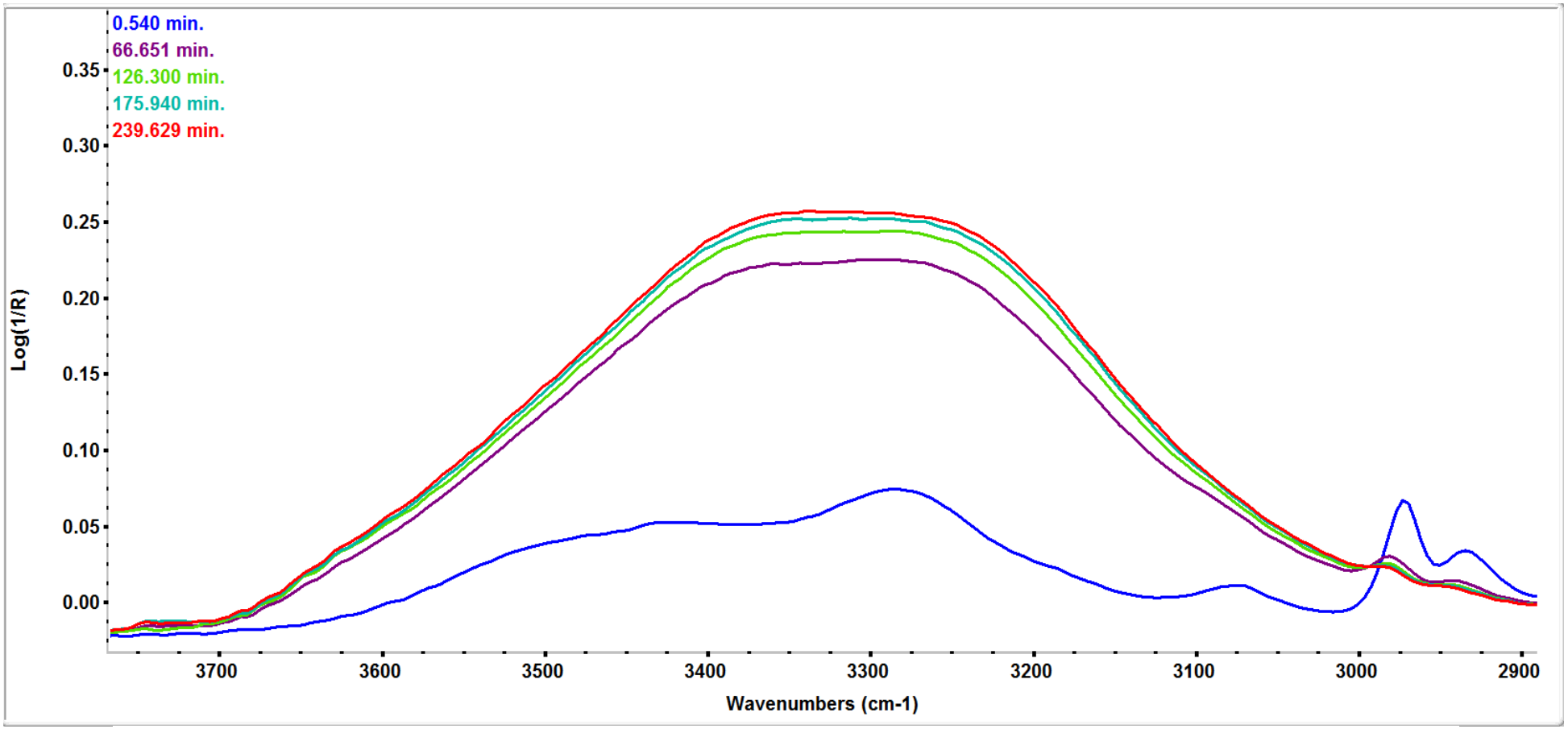

Figure 5.22: *v* (OH) (3700-300cm-1) taken during the rehydration of L-pNIPAM$_{90}$-co-HPMA$_{10}$ (1) hydrogel at 25˚C.

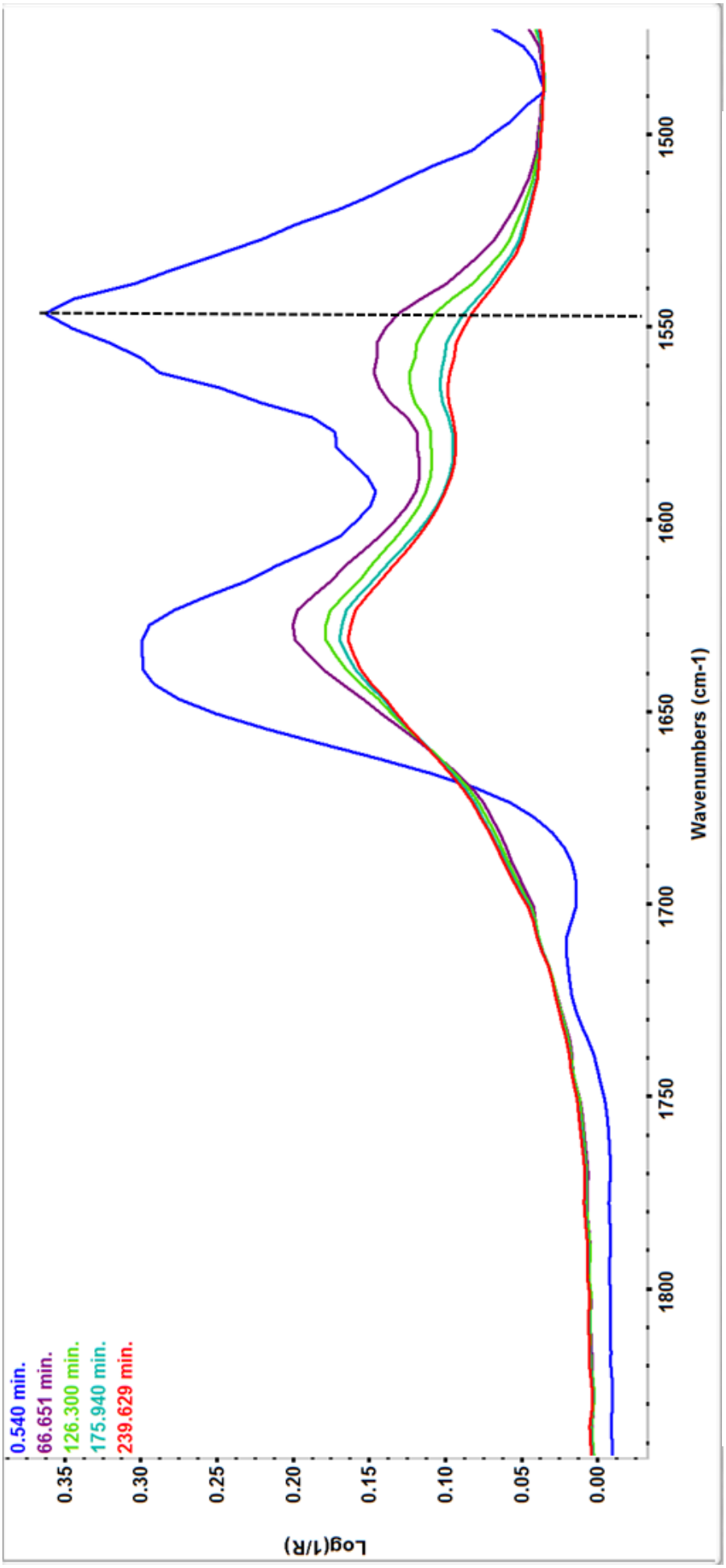

Figure 5.23: δ (NH) band (1550cm^{-1}) taken during the rehydrating of L-pNIPAM$_{90}$-co-HPMA$_{10}$ (1) hydrogel at 25˚C.

The intensity of ν(OH) band was plotted as a function of time for L-pNIPAM-co-HPMA with different HPMA concentrations(Figure 5.24). As the rehydration profile is a combination of the rate of hydration and the sample thickness, each experiment was plotted individually (organised by colour) to show the reproducibility of the experiment. Distinct 'banding' of each of the rehydration curves was observed. As can be seen, especially in the 10% HPMA system, there is some evidence of delamination during the rehydration experiment. With this in mind, careful selection of the linear portion of the rehydration profile before the point of delamination and no higher than 0.5 A.U, was used to calculate the diffusion coefficients for these data. The diffusion coefficient of water through hydrogel samples with different HPMA concentrations, was calculated according to Fieldson equation(37,38), as detailed in section 3.6.2.

Diffusion of water through L-pNIPAM-co-HPMA during the rehydration process was shown to be affected by the level of incorporated HPMA, where water diffusivity increased when HPMA was incorporated (Figure 5. 25), due to larger pore sizes and increased hydrophilicity of hydrogel, where more hydrophilic network leads to greater sorption of water(39). In addition, the decrease of hydrogel stiffness as HPMA concentration was increased could also affect the mobility of molecules through the sample. Calculation of the D values as a function of HPMA content shows a systematic and statistically significant increase in the rehydration rate. Incorporating HPMA was shown to increase the rehydration rate of L-pNIPAM, due to an increase in hydrophilicity, pore size and the flexibility of the polymer chains, as expected.

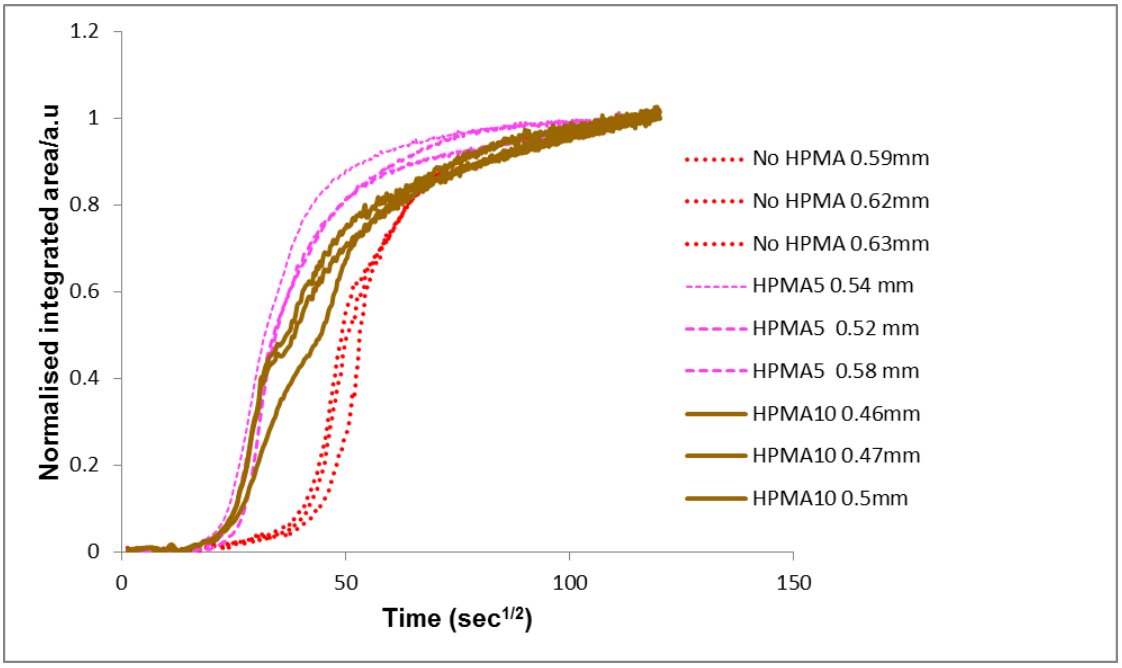

Figure 5.24: water profiles for different HPMA concentrations hydrogels during rehydration.

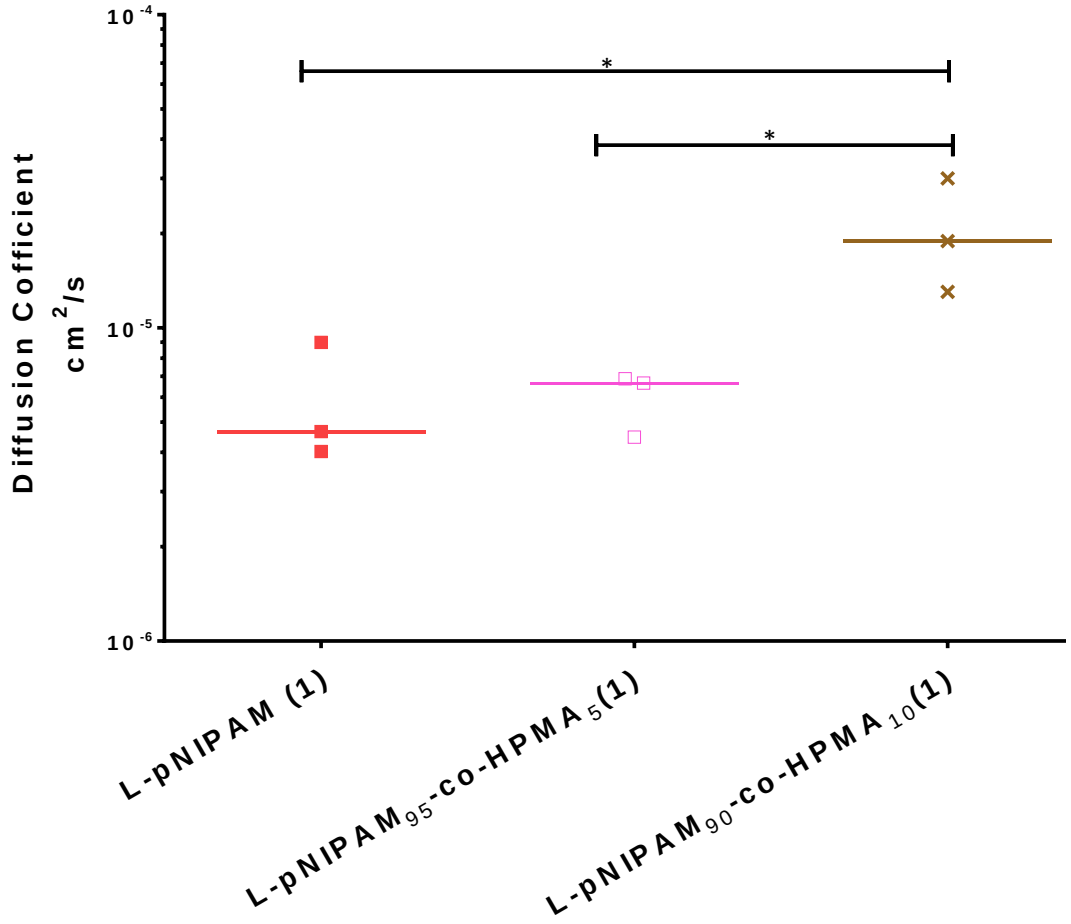

Figure 5.25: Diffusion coefficient of pNIPAM base d Laponite® hydrogel with different HPMA concentrations.

Observable shifts within the δ(NH) band of L-pNIPAM$_{90}$-co-HPMA$_{10}$ (1) during the rehydration process was plotted as a function of time, showing shifting to higher wavenumber as more water was absorbed by the sample and increasing the level of hydrogen bonding between polymeric chains and absorbed water in the swollen sample (Figure 5. 26).

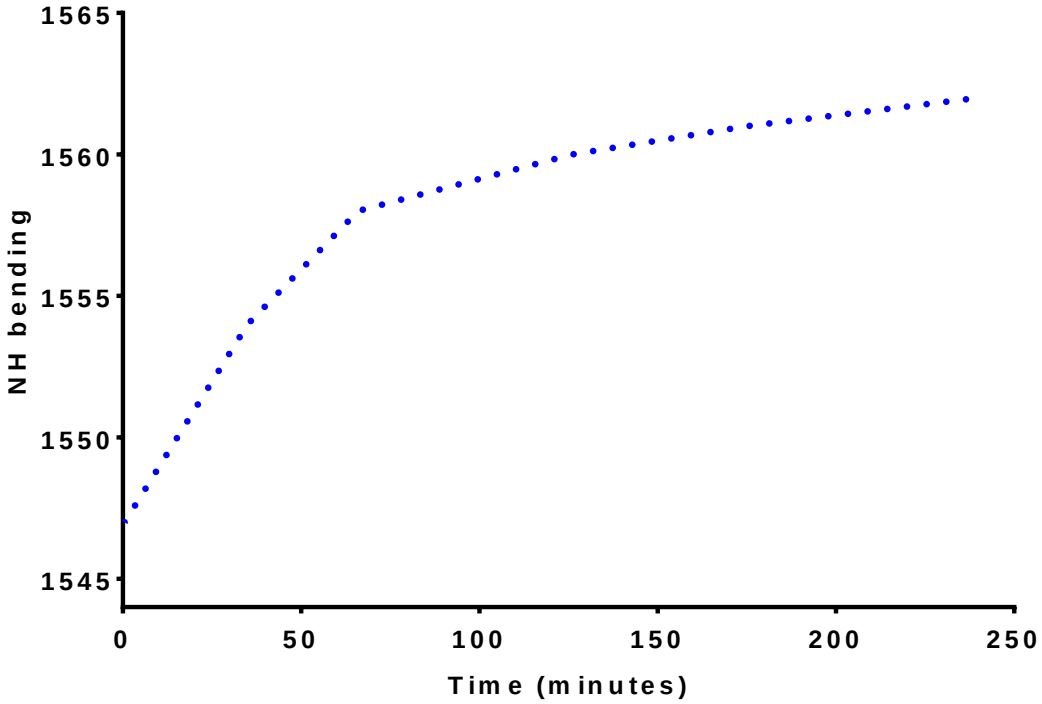

Figure 5.26: Shifts in δ (NH) band of L-pNIPAM$_{90}$-co-HPMA$_{10}$ (1) during rehydration.

5.3.9 Influence of HPMA on cell behaviour

Rat stem cells were used initially, to explore effects of adding HPMA on cell proliferation within pNIPAM based Laponite® injectable hydrogel. Where cytotoxicity where measured and number of live cells was estimated, using Alamar blue protocol. Verification was done using human mesenchymal stem cells (hMSC), by repeating exactly the same steps and using Alamar blue. Where metabolic cell activity was measured to hMSC within different pNIPAM based Laponite® injectable hydrogel with different HPMA concentrations. Both types of cells were cultured within the hydrogel, and metabolic cell activity level was assessed following 0, 2 and 7 days in culture.

5.3.9.1 Influence of HPMA on proliferation of rat stem cells

Rat stem cells were used to investigate the influence of adding HPMA on viability of cells within pNIPAM based Laponite® injectable hydrogel (Figure 5. 27). Significant differences in metabolic cell activity and number of live cells were detected on day 0 between hydrogel without HPMA incorporated and two other formulations that contain 5 and 10wt. % HPMA. An increase in the

metabolic activity indicating a potential increase in the number of live cells within hydrogels containing HPMA was observed (Figure 5. 27). All hydrogel formulations were shown to decrease metabolic cell activity from day 0 to day 2 (Figure 5. 27), which have been detected in many previous studies (16,40), due to change in cells environment. On day 7 metabolic cell activity and thus number of live cells were increased within all hydrogel composition that were investigated (Figure 5. 27). However, significant differences were observed in metabolic cell activity between L-pNIPAM$_{90}$-coHPMA$_{10}$ (1) and two other formulations (Figure 5.27). Demonstrating that, proliferation of the cells within L-pNIPAM$_{90}$-coHPMA$_{10}$ (1) was significantly more than other two formulations. Considering bigger pore size was shown as a result of incorporate HPMA and higher water diffusivity, which are important factors that affect the cells within material used as scaffold (41–43). Increase diffusivity of the water and molecules into hydrogel structure improves oxygen and nutrient supply to the cells and ease waste removal(43), which could be a reason for increased cell proliferation within this material. Therefore, increase in cells proliferation were seen at day 7 within L-pNIPAM$_{90}$-coHPMA$_{10}$ (1) that showed the biggest pore size and highest water diffusivity when compared to L-pNIPAM$_{95}$-coHPMA$_{5}$ (1) and L-pNIPAM (1). In addition, increase in bound water fraction within pNIPAM based Laponite® injectable hydrogel, as a result of adding HPMA was shown to decrease dehydration rate, which keep cells viable.

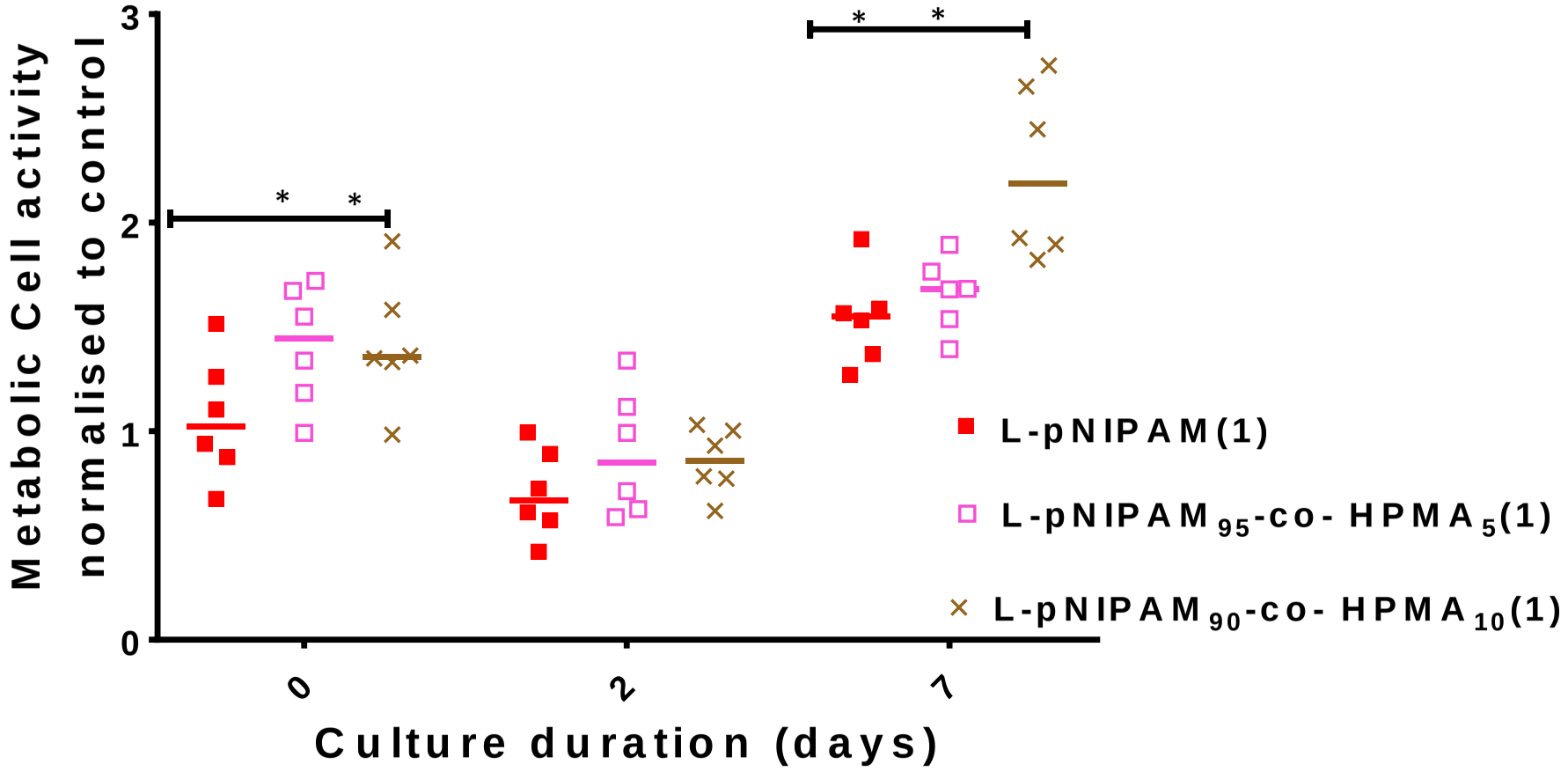

Figure 5.27: *In vitro* cell proliferation using Alamar blue assay of rat stem cells incorporated into pNIPAM based Laponite injectable hydrogel with different HPMA concentrations. *= P<0.05

5.3.9.2 Influence of HPMA on proliferation of hMSC cells

Human mesenchymal stem cells (hMSC) were used to verify the influence of incorporate HPMA into pNIPAM based Laponite® injectable hydrogel. Where Alamar blue protocol was used to investigate the effect of HPMA on human mesenchymal stem cell (hMSC) proliferation within pNIPAM based Laponite® injectable hydrogel. On day 0 all formulations showed similar metabolic cell activity for the cells cultured within hydrogels structures (figure 5.28). Day 2 was shown slight decrease in metabolic cell activity within all hydrogel formulations (Figure 5.28). Increase metabolic cell activity and number of live cells was observed within all formulations on day 7 of culture, and a significant difference was detected in the proliferation of the cells within pNIPAM based Laponite® injectable hydrogel that contain 10wt. % HPMA, when compared to the other formulations (Figure 5.28). These results confirmed the data show in rat stem cells.

Incorporation of HPMA was shown to enhance the number of live cells and proliferation up to 7 days in culture, due to enhancement in physical properties of pNIPAM based Laponite® injectable hydrogel, when HPMA was incorporated. Pore size of pNIPAM hydrogel was increased when HPMA incorporated, which increase spaces for more cells to occupy these interconnected pores. Also, hydrophilicity of the hydrogel increased as HPMA was added, which inhibited dehydration rate of pNIPAM based Laponite® injectable hydrogel, due to adding HPMA. On other hand, water diffusivity of pNIPAM based Laponite® injectable hydrogel increased, as HPMA incorporated, which increase nutrients absorption and oxygen permeability to the cells. Despite of decrease in mechanical strength as HPMA incorporated, which may adversely affect the cells within the hydrogel, but it is usually showed that culturing the cells within hydrogel material enhance mechanical strength of this material, due to cellular matrix that produced by the cells(16).

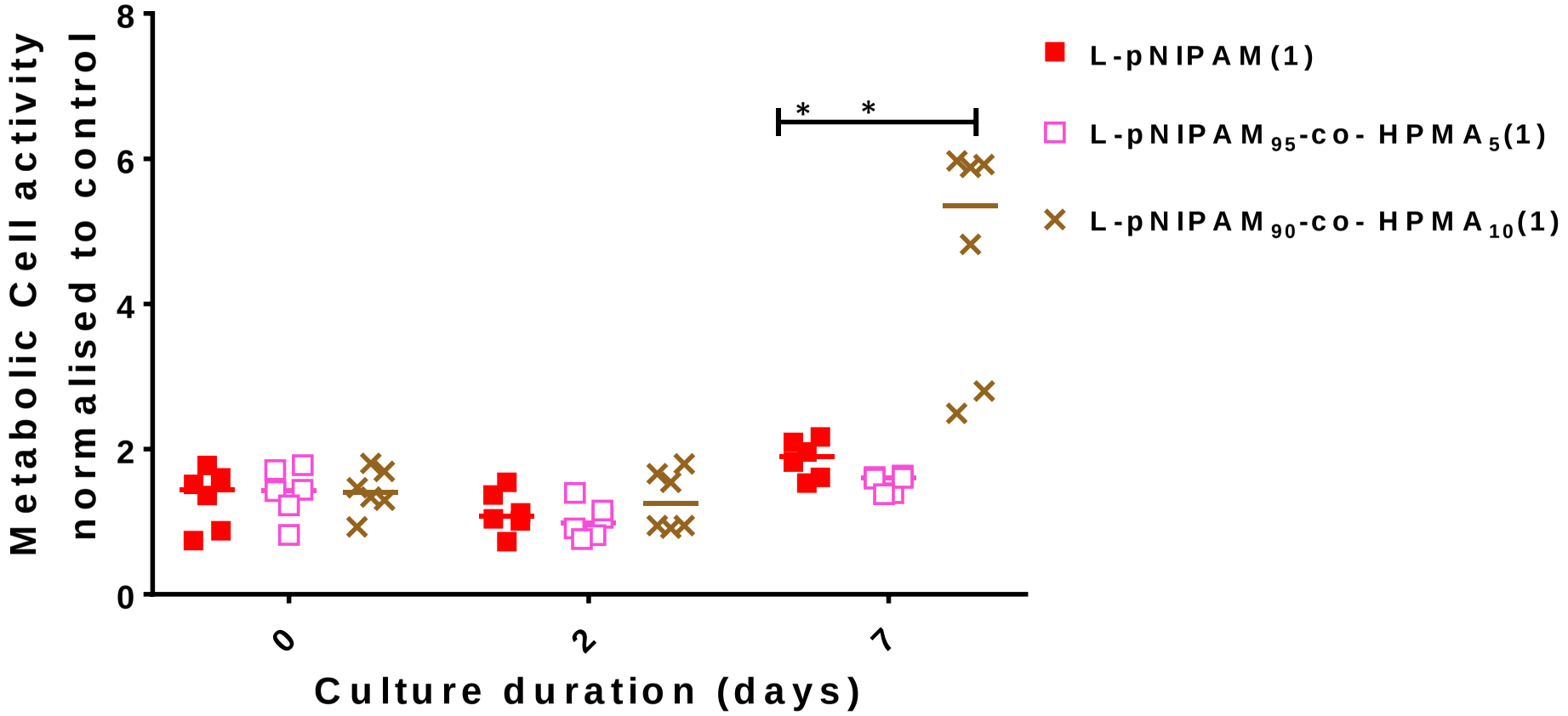

Figure 5.28: *In vitro* cell proliferation using Alamar blue assay of hMSC cells incorporated into pNIPAM based Laponite injectable hydrogel with different HPMA concentrations. *= P<0.05

5.3.9.3 Scanning electron microscopy investigation of human mesenchymal stem cells (hMSC) within pNIPAM based Laponite® injectable hydrogel

Scanning electron microscopy was used for further investigation of influence of adding HPMA on human mesenchymal stem cells (hMSC) cell proliferation, where cells were either layered on the surface of the hydrogel or encapsulated within and cultured up to 2 weeks.

5.3.9.3.1 Scanning electron microscopy investigation of human mesenchymal stem cells (hMSC) layered on hydrogel samples surface

Human mesenchymal stem cells (hMSC) were layered on the surface of the hydrogel to investigate the effect of adding HPMA on cell proliferation. SEM images showed cells filling the pores of honeycomb like structure of the hydrogel with and without HPMA, after 2 weeks in culture (Figure 5.29). However, L-pNIPAM$_{90}$-coHPMA$_{10}$ (1) demonstrated a dense matrix deposition which was thought to be extracellular matrix (Figure 5.29). Further magnification showed some spherical single cells occupying the pore size of L-pNIPAM (1), whereas extracellular matrix was observed within L-pNIPAM$_{90}$-coHPMA$_{10}$ (1) (Figure 5.29). These observations confirm our findings that obtained using Alamar blue protocol, where adding HPMA to pNIPAM based Laponite® injectable hydrogel enhance proliferation of the cells within this material, due to enhancement that shown in physical properties, when HPAM was added.

Anna K. *et al* explored the influence of mechanical stiffness and swelling behaviour of poly (ethylene glycol) (PEG) hydrogel on human mesenchymal stem cells (hMSCs) behaviour, where osteogenic differentiation was induced chemically using differentiation media contained adipogenic differentiation media or osteogenic differentiation media. They produced soft and stiff PEG hydrogel, with mechanical stiffness of 8-10 kpa and 50-60 kpa respectively, where the equilibrium swelling degree of the soft hydrogel formulations was twice that of stiff hydrogel. their results were demonstrated that human mesenchymal stem cells (hMSCs) cultured in soft hydrogel, were showed significantly higher alkaline phosphatase (alp) expression, and there was no significant differences in runx2 expression in both hydrogel stiffness(44).

Other study was conducted by Ciara *et al*, where collagen-glycosaminoglycan (CG) scaffold was produced by blending micro-fibrillar bovine tendon collagen

with chondroitin-6-sulphate, isolated from shark cartilage, in 0.05 M acetic acid. Scaffold pore size was varied with a range of 85 - 325μm, and pre-osteoblastic cell line (MC3T3-E1) was cultured within collagen based scaffold, to investigate influence of pore size on cell number and behaviour. They found that increase pore size of CG scaffold increased the number of live cells within its structure up to 7 days, where haemocytometer was used to count the live cell number in different CG scaffold with different pore size. In addition, cell adhesion was increased as pore size was increased, in the first 48 hours, which plays crucial rule in cell differentiation within the scaffold later on(45,46).

ShihJye T. investigated the effects of Injectable transglutaminase cross-linked gelatine (TG-Gel) on osteogenic differentiation of Mouse C2C12 myoblast cells. They produced different composition with different mechanical stiffness by changing the concentration of gelatine (3, 6 and 9%), where compression strength was ranging between 1.58 - 32.32 kpa, and porosity of 17 - 58.38 %. The results were showed that stiffer TG-Gel facilitated osteogenic differentiation, where Calcium deposition within 9% TG-Gel was increased significantly after two weeks in culture.

In the current study pNIPAM based Laponite® hydrogel was showed mechanical stiffness of ~ 10^4 kpa for hydrogel without HPMA incorporated, and 10^2 kpa when 10wt. % HPMA was incorporated, which much stiffer than (PEG) that used by Anna K. et al(44) and ShihJye T(47). In addition, adding HPMA was also showed increase in pore size and equilibrium swelling degree, which may explain the increase in cell density in hydrogel contained HPMA, due to increase the ability of the hydrogel to absorb nutrients.

Our findings were also demonstrated that adding HPMA increased the number of live cells within pNIPAM based Laponite® hydrogel, due to increase pore size from ~ 13 μm to ~18 μm as HPMA incorporated.

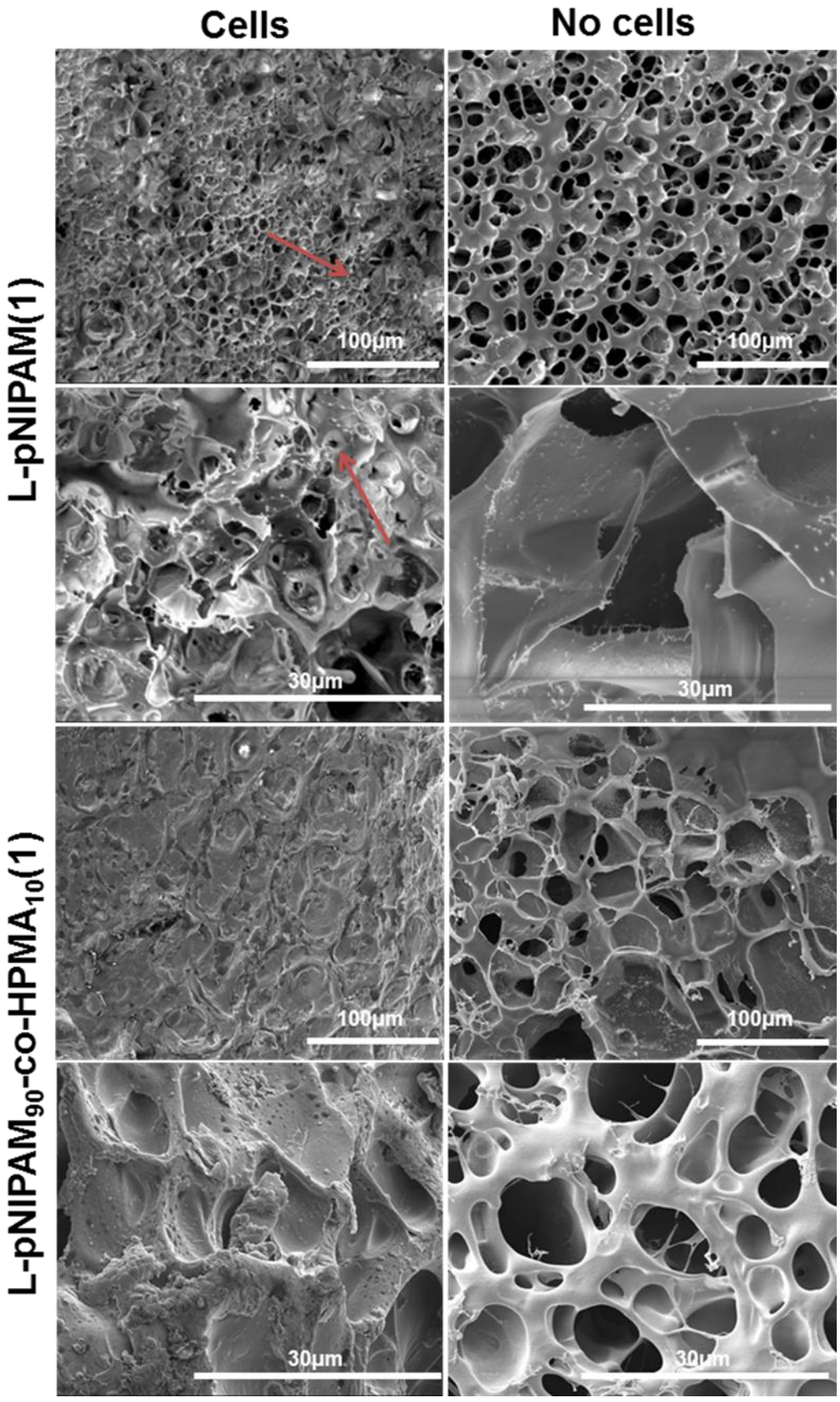

Figure 5.29: Scanning electron microscopy (SEM) of hMSC layered on hydrogel surface for 2 weeks and acellular hydrogels, with and without HPMA incorporated.

5.3.9.3.2 Scanning electron microscopy investigation of human mesenchymal stem cells (hMSC) suspended into hydrogel samples

Suspension of hMSC cells were mixed with liquid hydrogel at density of $1x10^6$ cells/ml and, after 2 weeks in culture samples were prepared as described in chapter two. SEM images were captured and analysed visually to explore effects of adding HPMA to pNIPAM based Laponite® injectable hydrogel, on the cells that suspended into the hydrogel structures. SEM images of broken hydrogel samples showed hMSC cells filled the interconnected pore structure of the hydrogel with different density (Figure 5.30). Where hydrogel without HPMA showed spherical shapes within the pores with limited matrix deposition, the materials were heterogeneous and cells didn't not appear to cover the whole surface (Figure 5.30), whereas hydrogel with HPMA incorporated showed very dense structure due to progressive increase in the number of the cells and matrix deposition covering its pore structure (Figure 5.30).

Scanning electron microscope observations were in agreement with the results obtained by Alamar blue assay, and give explanation of how the changes in hydrogel structures were impacted cell behaviour within pNIPAM based Laponite® injectable hydrogel. Proliferation of the cells was increased noticeably when HPMA was incorporated, due to enhancement that observed in the properties of the hydrogel when HPMA was added. Where dehydration rate was decreased and rehydration increased, bigger pore size was detected, smaller water contact angle was observed and higher water diffusivity within the hydrogel structure was observed. These improvements enhanced the proliferation of the cells within pNIPAM based Laponite® injectable hydrogel.

Better proliferation of hMSC cells was showed within pNIPAM based Laponite® injectable hydrogel with HPMA incorporated, and higher number of live cells within its structure. Therefore, further investigation was subjected to explore the ability of this material to enhance differentiation of hMSC cells.

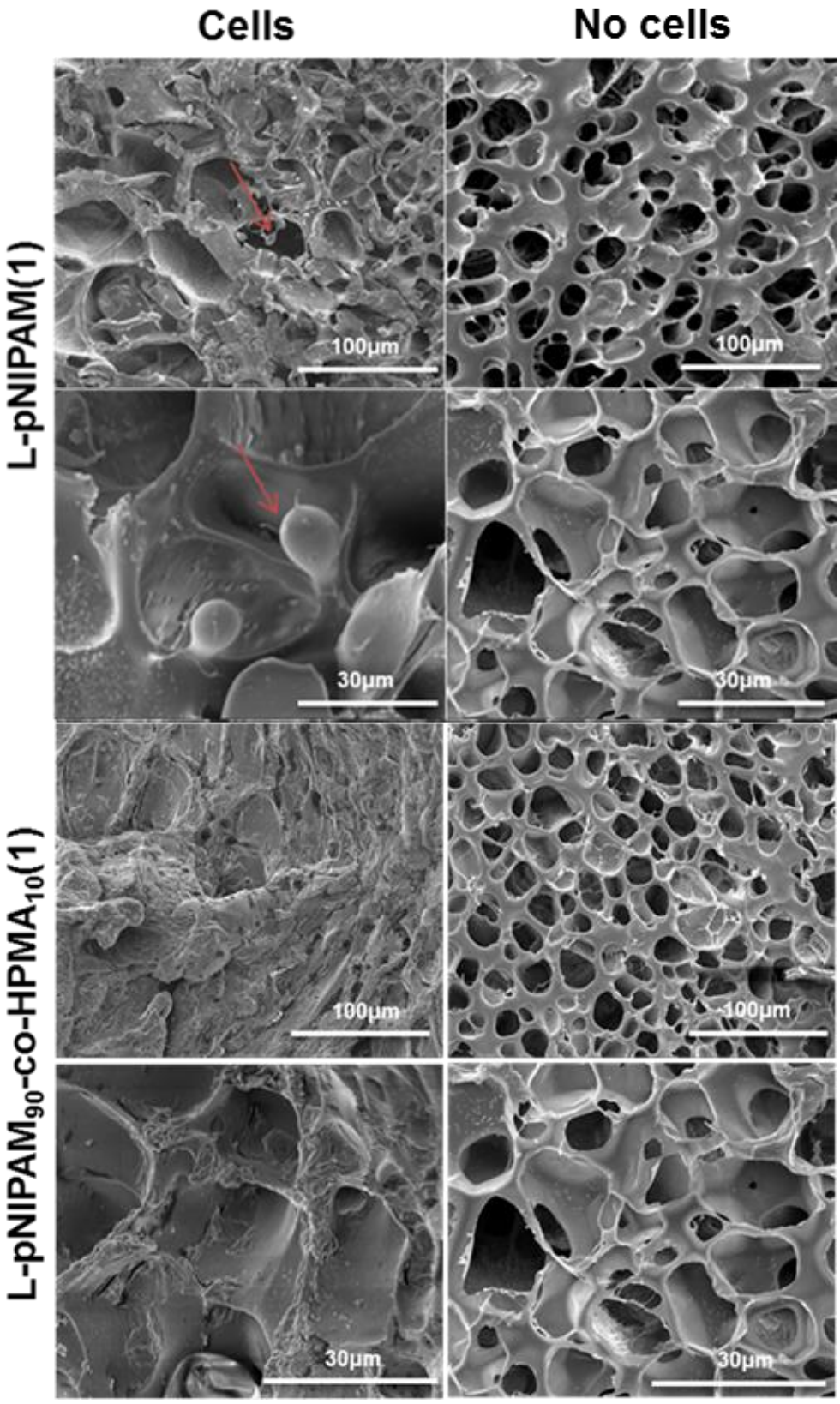

Figure 5.30: Scanning electron microscopy (SEM) of hMSC suspended into hydrogel for 2 weeks and acellular hydrogels, with and without HPMA incorporated.

5.4 Summary

In this chapter, the effects of adding hydroxypropyl methacrylate (HPMA) on physical, mechanical and cell viability of L-pNIPAM was investigated in depth. Where the thermal response of L-pNIPAM-co-HPMA was investigated, results showed that the lower critical solution temperature of pNIPAM hydrogel was significantly decreased as HPMA incorporated. Morphological studies showed that incorporating 5wt. % HPMA increased the average pore size of the hydrogel significantly. However, when HPMA concentration was doubled pore size of resulted hydrogel seemed to be slightly decreased when compared to 5 wt. % hydrogel. This reduction could be as a result of increase heterogeneity of the hydrogel as HPMA concentration increased. the viscoelastic behaviour of L-pNIPAM-co-HPMA was shown to be influenced by the level of HPMA, where significant decreases in storage modulus were recorded as HPMA was incorporated.

The swelling ratio of L-pNIPAM-co-HPMA was increased when HPMA incorporated, due to the increased pore size and a shorter period of time was needed for the swelling process to occur. Equilibrium swelling degree was increased due to increase pore size and increased chain mobility with HPMA incorporated.

The deswelling ratio was decreased as HPMA incorporated. Also, maximum degree of deswelling was reduced as HPMA was added.

Contact angle of dried hydrogel films on a glass slide surface was measured and results showed a decrease in contact angle. Water contact angle of L-pNIPAM-co-HPMA decreased as HPMA incorporated, due to the increase hydrophilicity.

Dehydration rate of L-pNIPAM-co-HPMA was decreased as 5wt. % of HPMA was incorporated, due to increased proportion of more hydrophilic polymeric units that were able to bind with water molecules within the hydrogel matrix. In addition bigger pore size makes dehydration faster. However, when the HPMA concentration doubled, dehydration rate was decreased, as a result of numerous factors; contact angle measurement of liquid hydrogels showed increase in surface area as HPMA concentration increased. Also, Pore size

measurements were showed increase in size which could lead to a faster dehydration rate.

Water states were calculated to investigate the influence of adding HPMA on bound and free water proportion in cast solutions. Bound water was proportionally increased when HPMA was incorporated.

Rehydration studies revealed that incorporation of 5wt. % HPMA elevated rehydration rate of L-pNIPAM-co-HPMA, due to the increase in pore size and elasticity of hydrogel when HPMA was added. However, when further HPMA was added a reduction in rehydration rate was observed due to increase hydrophilic polymeric units able to interact with absorbed water molecules, causing to retard rehydration process.

Water diffusivity through L-pNIPAM was increased as HPMA incorporated, due to bigger pore size.

Interestingly, adding HPMA to L-pNIPAM was found to enhance cell viability of hMSCs. The number of live cells was significantly increased ($P<0.05$) when HPMA was added, due to larger pores, which are occupied by cells. In addition, proliferation of hMSCs was better than in the hydrogel without HPMA, as a result of increase in diffusion coefficient when HPMA was added; hence more nutrients diffuse through the structure of L-pNIPAM-co-HPMA.

5.5 References

1. Haraguchi K, Farnworth R, Ohbayashi A, and Takehisa T. Compositional effects on mechanical properties of nanocomposite hydrogels composed of poly(N,N-dimethylacrylamide) and clay. Macromolecules. 2003;36(15):5732–5741.

2. Paula A, Elena F, and CarmenA. Improving the Loading and Release of NSAIDs from pHEMA Hydrogels by Copolymerization with Functionalized Monomers. Journal of Pharmaceutical Science. 2007;96(4):802–813.

3. Ina G. US Patent (1970). (19).

4. Enzymes P. US Patent (1980) 54.

5. Obereigner B, Burešová, M, Vrána, A, and Kopeček J,. Preparation of polymerizable derivatives of N-(4-aminobenzenesulfonyl)-N′-butylurea. In: 17th Prague Micro-symposium on Macromolecules. Prague: Institute of Macromolecular Chemistry Prague; 1977: 117-121.

6. Obereigner B, Burešová M, Vrána A, and Kopeček J. Preparation of polymerizable derivatives of N-(4-aminobenzenesulfonyl)-n′-butylurea. Journal of Polymer Science. 1979;66(1):41–52.

7. Ants L., Vladimír C., Mati H., Peeter S., and J. Covalent attachment of chymotrypsin to poly[N-(2-hydroxypropyl)methacrylamide]. Collection of Czechoslovak Chemical Communications. 1981;46(6):1466.

8. Whiteman K, Subr V, Ulbrich K, and Torchilin V. Poly(HPMA)-coated liposomes demonstrate prolonged circulation in mice. Journal of Liposome Research. 2001;11(2–3):153–64.

9. Šťastný M, Plocová D, Etrych T, Kovář M, Ulbrich K, and Íhová B,. HPMA-hydrogels containing cytostatic drugs: Kinetics of the drug release and in vivo efficacy. Journal of Controlled Release. 2002;81(1–2):101–111.

10. Peterson C, Shiah J, Sun Y, KopeČKovÁ P, Minko T, and Straight R,. HPMA Copolymer Delivery of Chemotherapy and Photodynamic Therapy in Ovarian Cancer. In: Polymer Drugs in the Clinical Stage. Springer, Boston, MA; 2003. p. 101–123.

11. Chytrý V, Vrána A, Kopeček J. Synthesis and activity of a polymer which contains insulin covalently bound on a copolymer of N-(2-hydroxypropyl)methacrylamide and N-methacryloyldiglycyl p-nitrophenyl ester. Macromolecular Chemical Physics. 1978;179(2):329–336.

12. El-Din HMN. Characterization and Caffeine Release Properties of N-isopropylacrylamide/Hydroxypropyl Methacrylate Copolymer Hydrogel Synthesized by Gamma Radiation. Journal of Applied Polymer Science. 2011;119:577–585.

13. Woerly S, Pinet E, De Robertis L, Bousmina M, Laroche G, Roitbackt T, et al. Heterogeneous PHPMA hydrogels for tissue repair and axonal regeneration in the injured spinal cord. Journal of Biomaterials Science,

Polym Edn. 1998;9(7):681–711.

14. Pertici V, Amendola J, Laurin J, Gigmes D, Madaschi L, Carelli S, *et al.* The Use of Poly(N-[2-Hydroxypropyl]-Methacrylamide) Hydrogel to Repair a T10 Spinal Cord Hemisection in Rat: A Behavioural, Electrophysiological and Anatomical Examination. American Society of Neurochemistry Journal. 2013;5(2): 149-166.

15. Boyes VL, Sammon C, Lemaitre C BC. UK Patent (2012).

16. Thorpe AA, Creasey S, Sammon C, and Le Maitre CL. Hydroxyapatite nanoparticle injectable hydrogel scaffold to support osteogenic differentiation of human mesenchymal stem cells. European Cells and Materials. 2016;32:1–23.

17. Gorelov A V., Du Chesne A, Dawson KA. Phase separation in dilute solutions of poly (N-isopropylacrylamide). Physica A Statistical Mechanics and its Applications. 1997;240(3–4):443–452.

18. Zhang XZ, Yang YY, Wang FJ, Chung TS. Thermosensitive poly(N-isopropylacrylamide-co-acrylic acid) hydrogels with expanded network structures and improved oscillating swelling-deswelling properties. Langmuir. 2002;18(6):2013–2018.

19. Tang S, Floy M, Bhandari R, Dziubla T, Hilt J. Development of Novel N-isopropylacrylamide (NIPAAm) Based Hydrogels with Varying Content of Chrysin Multiacrylate. Gels. 2017;3(4):40.

20. Baltes T, Garret-Flaudy F, Freitag R. Investigation of the LCST of polyacrylamides as a function of molecular parameters and the solvent composition. Journal of Polymer Science, part A: Polymer Chemistry. 1999;37(15):2977–2989.

21. Schild HG, Muthukumar M, Tirrell DA. Cononsolvency in Mixed Aqueous Solutions of Poly(N- isopropylacrylamide). Macromolecules. 1991;24(4):948–952.

22. Okada Y, Tanaka F. Cooperative hydration, chain collapse, and flat LCST behavior in aqueous poly(N-isopropylacrylamide) solutions. Macromolecules. 2005;38(10):4465–4471.

23. Vincent J., Modifying skin pigmentation – approaches through intrinsic biochemistry and exogenous agents. National Institutes of Health Journal. 2009;6(4):247–253.

24. Jang J, Seol YJ, Kim HJ, Kundu J, Kim SW, Cho DW. Effects of alginate hydrogel cross-linking density on mechanical and biological behaviors for tissue engineering. Journal of Mechanical Behaviour of Biomedical Materials. 2014;37:69–77.

25. Metz J, Gonnerman K, Chu A, Chu T-MG. Effect of crosslinking density on swelling and mechanical properties of PEGDA400/PCLTMA900 hydrogels. Biomedical Science Instrumentations. 2006;464:389–394.

26. Lutz PJ. Structural properties of poly(ether) macromonomer based

hydrogels. Polymer Bulletin. 2007;58(1):161–171.

27. Peppas NA, Bures P, Leobandung W, Ichikawa H. Hydrogels in pharmaceutical formulations. European Journal of Pharmaceutical Biopharmaceutics. 2000;50(1):27–46.

28. Chen J, Park H, Park K. Synthesis of superporous hydrogels: Hydrogels with fast swelling and superabsorbent properties. Journal of Biomedical Materials Research. 1999;44(1):53–62.

29. Burmistrova A, Richter M, Eisele M, Üzüm C, von Klitzing R. The effect of co-monomer content on the swelling/shrinking and mechanical behaviour of individually adsorbed PNIPAM microgel particles. Polymers (Basel). 2011;3(4):1575–1590.

30. Boulogne F, Ingremeau F, Limat L, Stone HA. Tuning the Receding Contact Angle on Hydrogels by Addition of Particles. Langmuir. 2016;32(22):5573–5579.

31. Boyes V. The Synthesis and development of novel, easily processable poly (N- Isopropylacrylamide) - based hydrogels. PhD.(Thesis). Shefffield Halam university. 2012.

32. Elabd YA, Baschetti MG, Barbari TA. Time-resolved Fourier transform infrared/attenuated total reflection spectroscopy for the measurement of molecular diffusion in polymers. Journal of Polymer Science, Part B. 2003;41(22):2794–2807.

33. Bajwa GS, Sammon C, Timmins P, Melia CD. Molecular and mechanical properties of hydroxypropyl methylcellulose solutions during the sol:gel transition. Journal of Polymer Science. 2009;50(19):4571–4576.

34. Sammon C, Mura C, Yarwood J, Everall N, Swart R, Hodge D. FTIR−ATR Studies of the Structure and Dynamics of Water Molecules in Polymeric Matrixes. A Comparison of PET and PVC. Journal of Physical Chemistry, Part B. 1998;102(18):3402–3411.

35. Zhai M, Ma F, Li J, Wan B, Yu N. Preparation and properties of cryogel based on poly(hydroxypropyl methacrylate). Journal of Biomaterials Science, Polymer edn . 2018;29(12):1401–1425.

36. Zhao Q, Sun J, Wu X, Lin Y. Macroporous double-network cryogels: Formation mechanism, enhanced mechanical strength and temperature/pH dual sensitivity. Soft Materials. 2011;7(9):4284–4293.

37. Duda L. Molecular diffusion in polymeric systems. 1985;57(1):1681–1690.

38. Karimi M. Diffusion in Polymer Solids and Solutions. Mass Transfer in Chemical Engineering Process. 2011:101-107.

39. George KA, Wentrup-Byrne E, Hill David DJT, Whittaker AK. Investigation into the diffusion of water into HEMA-co-MOEP hydrogels. Biomacromolecules. 2004;5(4):1194–1199.

40. Dosh RH, Essa A, Jordan-Mahy N, Sammon C, Le Maitre CL. Use of hydrogel scaffolds to develop an in vitro 3D culture model of human

intestinal epithelium. Acta Biomaterialia. 2017;62:128–143.

41. Annabi N, Mithieux SM, Weiss AS, Dehghani F. The fabrication of elastin-based hydrogels using high pressure CO2. Biomaterials. 2009;30(1):1–7.

42. Gan T, Guan Y, Zhang Y. Thermogelable PNIPAM microgel dispersion as 3D cell scaffold: Effect of syneresis. Journal of Materials Chemistry. 2010;20(28):5937–5944.

43. Mandal BB, Kundu SC. Cell proliferation and migration in silk fibroin 3D scaffolds. Biomaterials. 2009;30(15):2956–2965.

44. Whitehead AK, Barnett HH, Caldorera-Moore ME, Newman JJ. Poly (ethylene glycol) hydrogel elasticity influences human mesenchymal stem cell behavior. Regenerative Biomaterials. 2018;5(3):167–175.

45. Murphy CM, Haugh MG, O'Brien FJ. The effect of mean pore size on cell attachment, proliferation and migration in collagen-glycosaminoglycan scaffolds for bone tissue engineering. Biomaterials. 2010;31(3):461–466.

46. Anselme K. Osteoblast adhesion on biomaterials. Biomaterials. 2000;21(7):667–681.

47. Tan SJ, Fang JY, Yang Z, Nimni ME, and Han B. The synergetic effect of hydrogel stiffness and growth factor on osteogenic differentiation. Biomaterials. 2014;35(20):5294–5306.

Chapter - 6

Incorporation of hydroxyapatite nanoparticles into L-pNIPAM hydrogel

6.1 Introduction

Hydroxyapatite (HAp, Ca_{10} $(PO_4)_6(OH)_2$) exists naturally in bones and teeth as the main inorganic constituent. Thus, synthetic hydroxyapatite has attracted great attention by researchers to be studied as a potential bone substitute, due to its similarity to the natural material(1–3). Presently, synthetic hydroxyapatite has been broadly considered as a part of bionanocomposite materials, due to its applications in the biomedical field and new potential specific applications in bone repair (4). In the last decade hydroxyapatite was used as temporary scaffolds to give mechanical support for damaged tissues, until they have regenerated naturally. In addition, researchers have studied the possibility of adding hydroxyapatite nanoparticles to bioscaffold materials, to enhance mechanical properties(5) and to stimulate of osteogenic differentiation(6,7).

In the current work 0.5 mg/ml synthetic hydroxyapatite nanoparticle (HAPna) was incorporated into different formulations of pNIPAM based Laponite® injectable hydrogels, to induce osteogenic differentiation of human mesenchymal stem cells (hMSC)(7). Previously, Thorpe *et al* studied the influence of adding two different concentration of synthetic HAPna; they added 0.5 and 1mg/ml to L-pNIPAM-co-DMAc prior to incorporating hMSCs into the hydrogel. They found that the optimised concentration of HAPna was 0.5mg/ml, where adding 0.5mg/ml of HAPna to L-pNIPAM-co-DMAc was shown to enhance mechanical stiffness of the hydrogel as well as induced osteogenic differentiation of hMSCs.

In this chapter, the influence of adding synthetic hydroxyapatite on material behaviour and structure were assessed and investigated. In addition, the impact of HAPna on osteogenic differentiation of hMSC was explored.

6.2 Synthesis of pNIPAM based Laponite® hydrogel and incorporating hydroxyapatite nanoparticles

The procedure of hydrogel synthesis was given and detailed in Chapter 2.2.

Four different hydrogel compositions were used as follows: L-pNIPAM (0.5), L-pNIPAM (1), L-pNIPAM (1.5) and L-p$NIPAM_{90}$-co-HPA_{10} (1) and the exact composition of the hydrogels is given in Table 2.1. Once synthesised, the

hydrogel was cooled to 50°C and HAPna (<200 nm, 10wt. % in H_2O) (Sigma, Poole UK) was added to the hydrogel at concentration of 0.5mg/ml. Subsequently, hydrogel/HAPna mixture was homogenously mixed prior to use to ensure HAPna does not precipitated.

6.3 Morphological study and pore size measurements

The influence of incorporating hydroxyapatite nanoparticles on the morphology of pNIPAM based Laponite® hydrogels was explored using scanning electron microscopy. SEM images of different composition were used to investigate the possible changes in internal structure of hydrogel samples and pore size measurements (Figure 6.1). Six images of each composition were used to measure the pore size. The distribution of pore size measurements were plotted to demonstrate the effect of incorporating hydroxyapatite on the morphology of different compositions (Figure 6.2-6.5). No aggregates were observed within the explored compositions as shown in SEM images (Figure 6.1) indicating an homogeneous dispersion of hydroxyapatite nanoparticles, within the hydrogel structures.

Generally, the honeycomb like structure of the hydrogel was not changed, when HAPna was added, in all studied compositions. However a reduction in pore size was observed when HAPna was incorporated, especially in L-pNIPAM (1) and L-pNIPAM (1.5), where significant reduction in pore size of those two compositions was found (Figure 6.3 and 6.4). For L-pNIPAM (0.5) pore size was slightly decreased as HAPna was added (Figure 6.2).

Adding hydroxyapatite has also shown to change the interconnected structure, where the shape and distribution of pores were changed. However, no significant change in pore size of L-pNIPAM$_{90}$-co-HPMA$_{10}$ was observed (Figure 6.4).

These findings are in agreement with previous results shown by Akhilesh *et al*, in different hydrogel system. They have studied the effect of adding different concentrations (5, 10 and 15%) of hydroxyapatite to poly (ethylene glycol) hydrogel. They concluded that, hydroxyapatite nanoparticles decrease the pore

size in systematic manner, within the investigated concentrations of hydroxyapatite(8).

In current study, it is also has been found a reduction in hydrogel pore size of the hydrogel with higher crosslink density, when hydroxyapatite was incorporated, despite of using low concentration of hydroxyapatite. Furthermore, no aggregates were observed within the explored compositions as shown in SEM images (Figure 6.1) indicating that, homogeneous dispersion of hydroxyapatite nanoparticles, within the hydrogel structures.

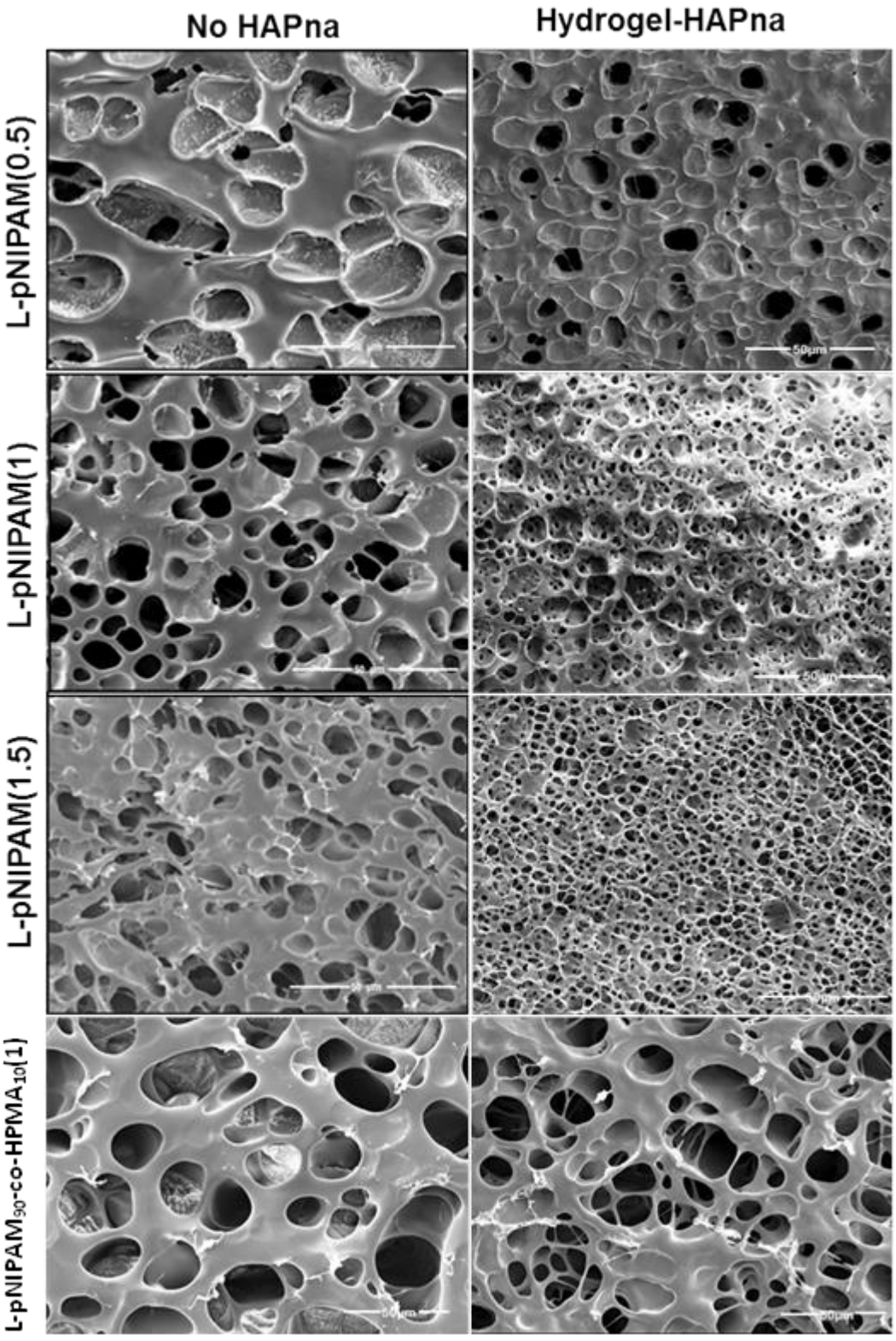

Figure 6.1: Scanning electron microscopy images of L-pNIPAM hydrogels with and without HAPna incorporated, illustrate the effect of HAPna on the morphology of pNIPAM based Laponite® hydrogel. Scale bars 50 μm, n=6.

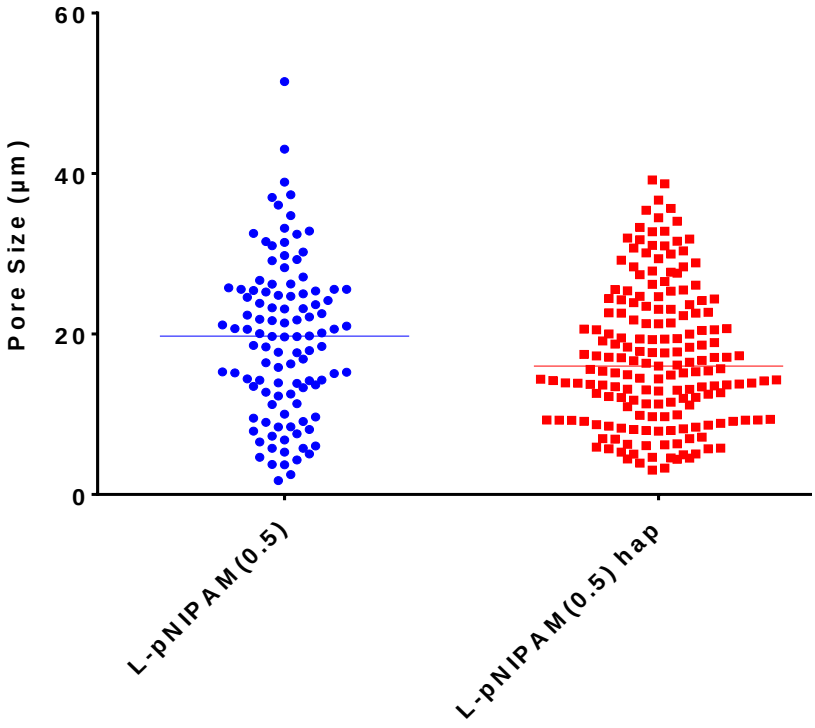

Figure 6.2: Pore size distribution of L-pNIPAM (0.5) with and without synthetic hydroxyapatite incorporated.

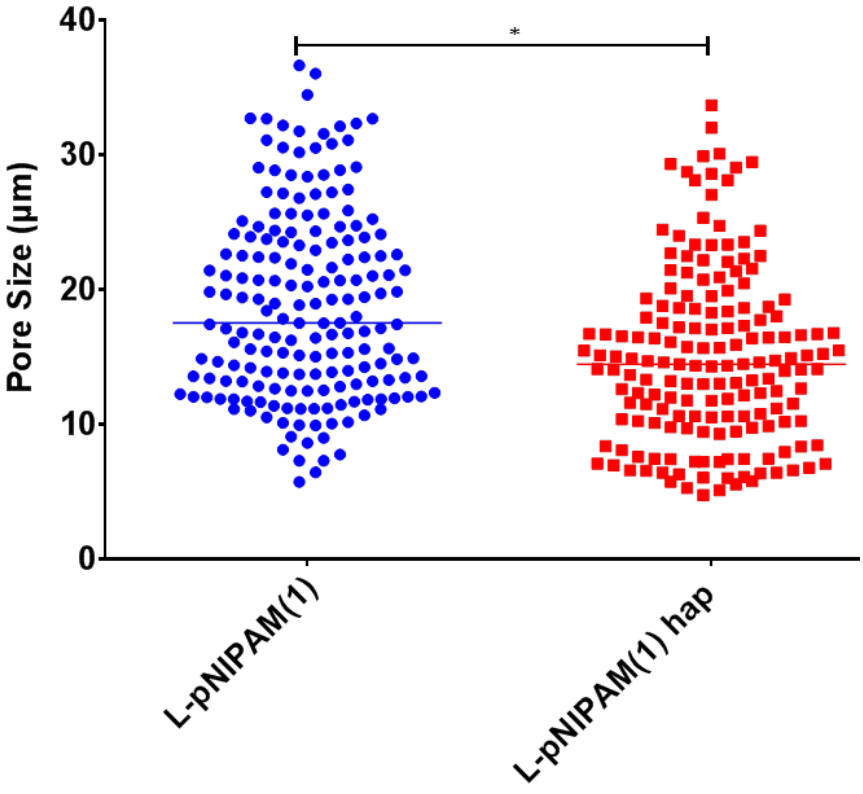

Figure 6.3: Pore size distribution of L-pNIPAM (1) with and without synthetic hydroxyapatite incorporated, showing statistical difference. *=P<0.05.

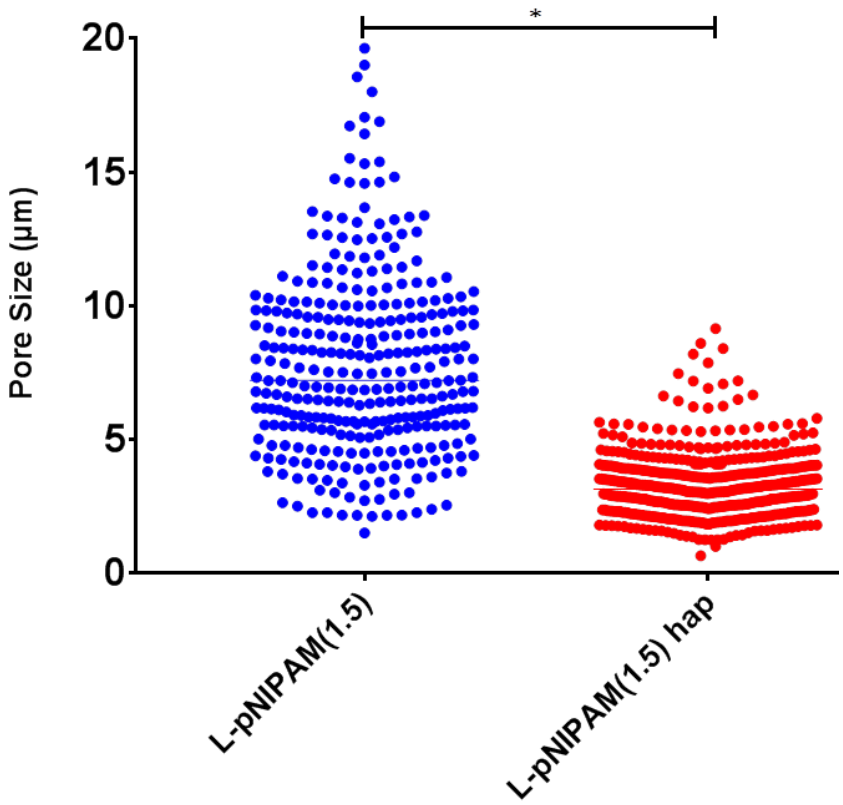

Figure 6.4: Pore size distribution of L-pNIPAM (1.5) with and without synthetic hydroxyapatite incorporated, showing statistical difference. *=P<0.05.

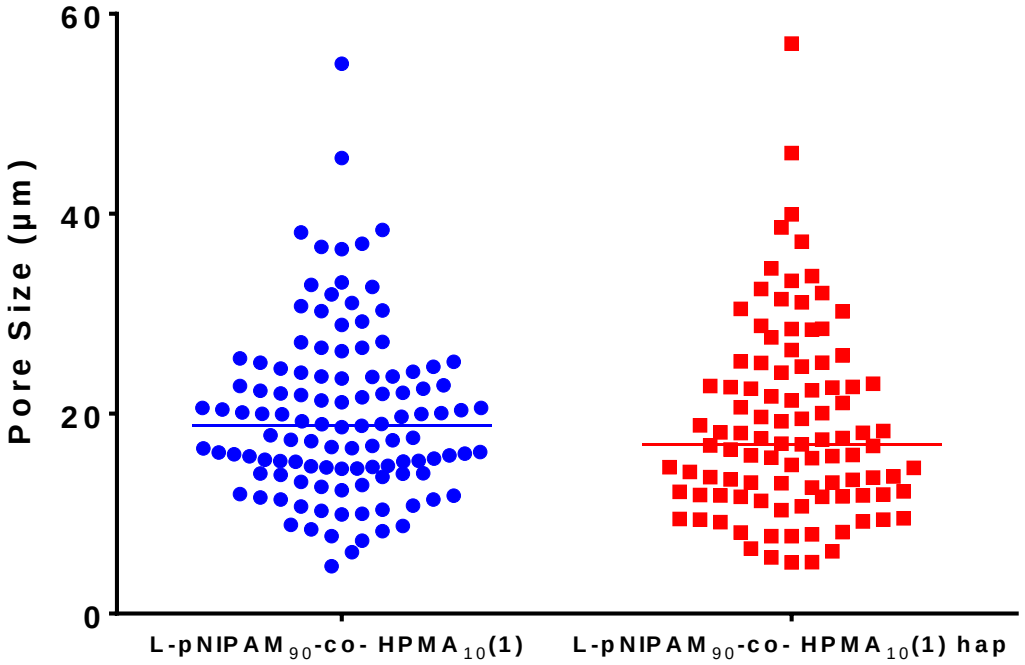

Figure 6.4: Pore size distribution of L-pNIPAM$_{90}$-co-HPMA$_{10}$ (1) with and without synthetic hydroxyapatite incorporated.

6.3 Mechanical properties

The storage modulus of pNIPAM based Laponite® hydrogels and hydroxyapatite nanoparticles - pNIPAM based Laponite® hydrogels was evaluated, using dynamic mechanical analysis in compression mode (using the parameters outlined in Chapter 2. section 2.1.

The effect of hydroxyapatite on mechanical properties of different compositions of pNIPAM based Laponite® hydrogel are shown in Figures 6.5 - 6.8. In general, the incorporation of HAPna increased the storage modulus of pNIPAM based Laponite® hydrogels for all studied compositions (Figure 6.5 - 6.8). However, there was no significant difference in the stiffness of (L-pNIPAM (0.5) as a result of adding 0.5mg/ml HAPna (Figure 6.5).

Significant increases in hydrogel stiffness were observed within two compositions (L-pNIPAM (1) and L-pNIPAM (1.5)), that contained the higher crosslink density (Figure 6.6 and 6.7). No significant difference in the mechanical stiffness of the hydrogel was observed when 0.5mg/ml of HAPna was added into L-pNIPAM$_{90}$-co-HPMA$_{10}$ (1) (Figure 6.8).

Nanoparticles can act as crosslinkers to the polymeric chains, which enhances the mechanical properties(9). In this study hydroxyapatite was added to L-pNIPAM hydrogels after the polymerisation reaction was finished, and no further heating was applied. We postulate that hydroxyapatite nanoparticles occupied the interstitial spaces within the structure of the hydrogel samples. As pore sizes of the studied hydrogels were shown to vary, before adding hydroxyapatite (particle size<200 nm), Therefore, the influence that hydroxyapatite has on the morphology and mechanical properties of the hydrogel is dependent on the original pore size. The influence of HAPna incorporation was limited on the hydrogel with bigger pore size (Figure 6.5 and 6.8).

Synthesised hydroxyapatite has been found to influence the mechanical properties of different hydrogel systems. Akhilesh *et al* showed that adding hydroxyapatite into poly (ethylene glycol) hydrogels increased tensile and compression strengths, and both tensile and compression moduli increased systematically with increased hydroxyapatite concentrations within the studied limits (5, 10 and 15%)(8).

Jiang *et al*. have used hydroxyapatite nanowires (HANWs), to enhance the mechanical properties of sodium alginate hydrogel materials. They concluded that incorporation of HANWs was shown to enhance both tensile and compression moduli in a systematic manner(10).

Furthermore, Thorpe *et al*, demonstrated increased hydroxyapatite nanoparticle (HAPna) concentration from 0.5 to 1mg/ml increased the storage modulus of pNIPAM/DMAc based Laponite® hydrogels (7).

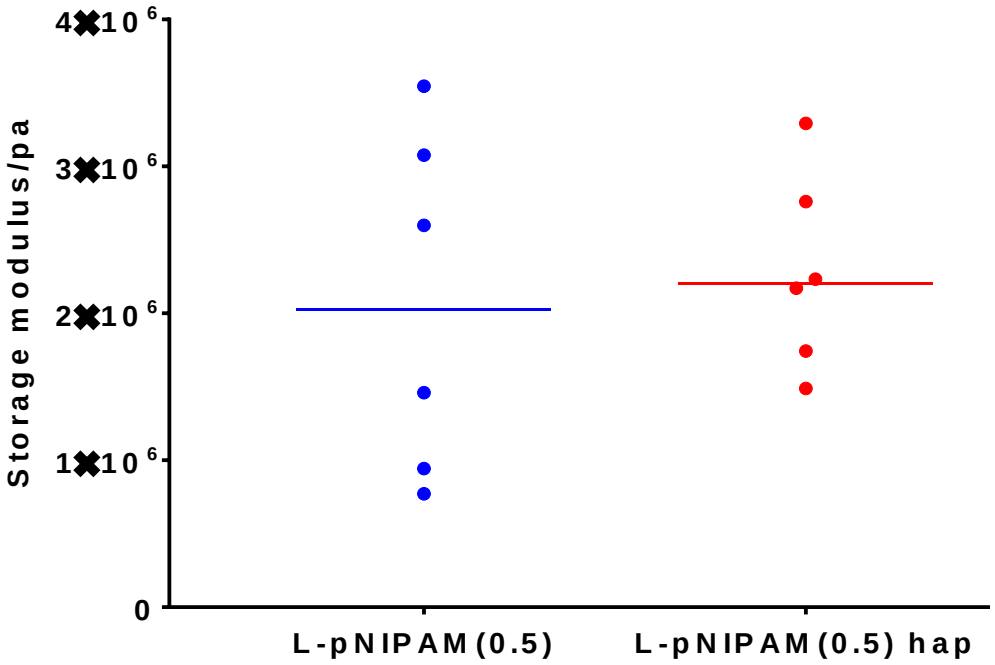

Figure 6.5: Storage modulus of L-pNIPAM (0.5) with and without synthetic hydroxyapatite incorporated. *=P<0.05.

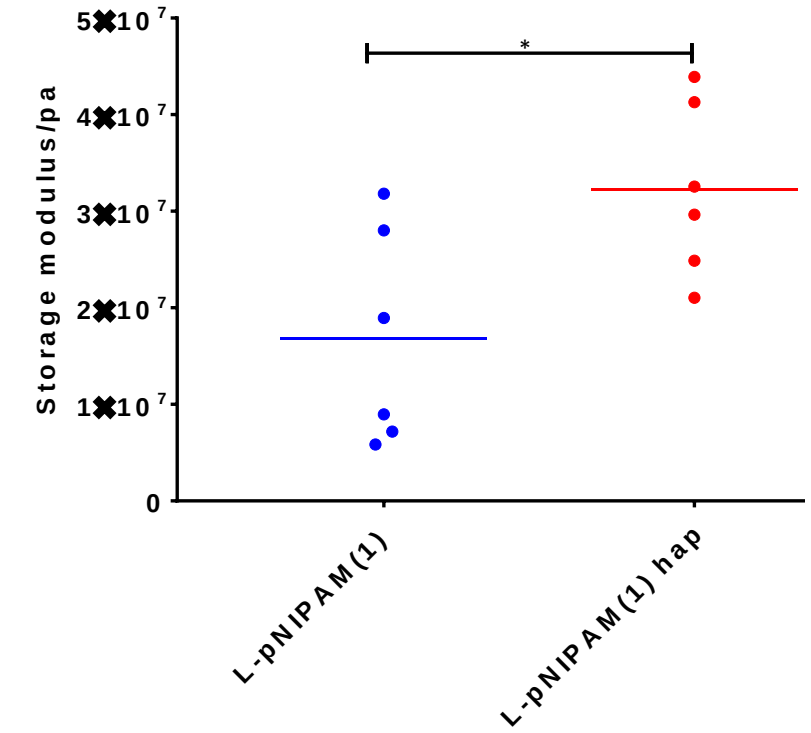

Figure 6.6: Storage modulus of L-pNIPAM (1) with and without synthetic hydroxyapatite incorporated, showing statistical difference. *=P<0.05.

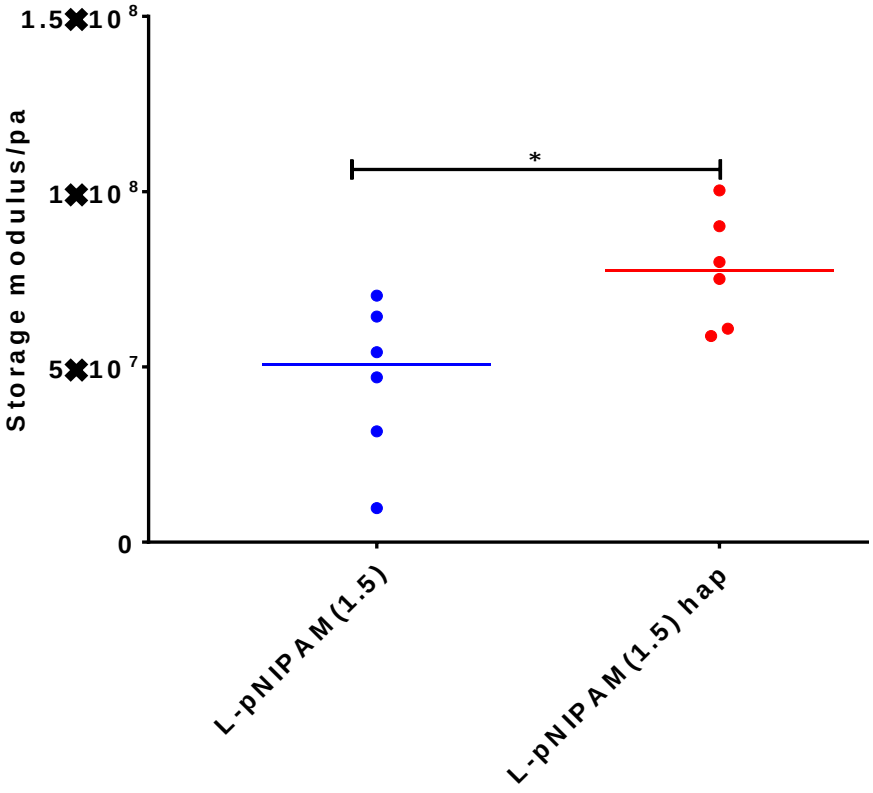

Figure 6.7: Storage modulus of L-pNIPAM (1.5) with and without synthetic hydroxyapatite incorporated, showing statistical difference. *=P<0.05

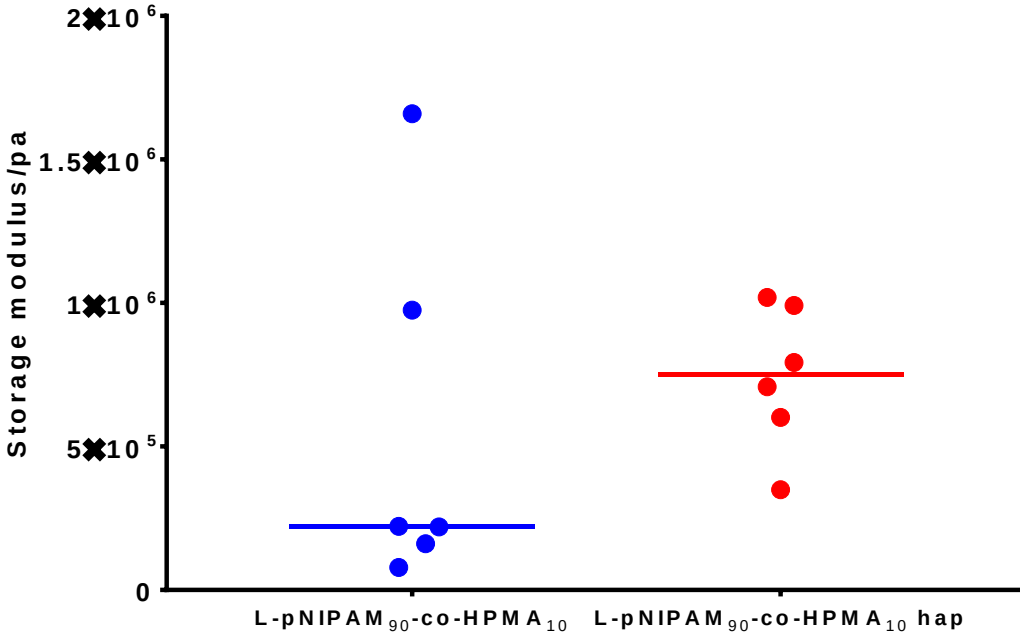

Figure 6.8: Storage modulus of L-pNIPAM$_{90}$-co-HPMA$_{10}$ (1) with and without synthetic hydroxyapatite incorporated.

By adding extra water to the system, when 10% HAPna/water suspension was incorporated, we may expect a negative impact on mechanical strength of L-pNIPAM hydrogels. Therefore, a calculation of the change in water fraction was done as follows:

Density of HAPna = 1.038 g/ml (11), 0.5mg HAPna suspension was added.

$$Volume\ (ml) = \frac{mass(g)}{Density(\frac{g}{ml})} \qquad (6.1)$$

$$Volume\ (ml) = \frac{0.0005g}{1.038(\frac{g}{ml})} = = \ 0.0004817\text{ml} \qquad (6.2)$$

0.0004817ml of HAPna dispersion contains 0.000434 ml water (90%).

This shows that the water content of the hydrogel will slightly increase upon the addition of the HAPna suspension, which would have a negative impact on the mechanical strength. However, here we have shown that this effect is dramatically offset by the influence that the HAPna have on mechanical properties. We propose that the HAPna supplements the crosslinking effect of the Laponite® and this manifests itself as an increase in the mechanical strength of the hydrogels coupled with a reduction in the median pore size.

6.4 swelling behaviour

The swelling ratio of different compositions of L-pNIPAM as-synthesised and with HAPna incorporated at a concentration of 0.5mg/ml, was performed in distilled water at 25°C for up to 24 hours, to explore the influence of HAPna on the swelling behaviour.

The swelling ratio of L-pNIPAM (0.5) with and without HAPna is illustrated in figure 6.9, demonstrating the influence of adding HAPna on swelling ratio of the hydrogel, where swelling ratio was reduced as HAPna was incorporated. Also, the equilibrium swelling degree of L-pNIPAM (0.5) was slightly decreased when HAPna was added (Figure 6.9). The swelling ratio of L-pNIPAM (1) was shown to be noticeably affected by adding HAPna, and therefore equilibrium swelling degree of L-pNIPAM (1) was significantly reduced (Figure 6.10). A significant reduction in swelling ratio was found when HAPna was added to L-pNIPAM (1.5) (Figure 6.11), and equilibrium swelling degree was decreased dramatically (Figure 6.12). Limited impact was recorded, when HAPna was added to L-$pNIPAM_{90}$-co-$HPMA_{10}$ (1), on both swelling ratio and equilibrium swelling degree (Figure 6.13 and 14).

The observation that hydrogels with HAPna incorporated have lower swelling ratio than as-synthesised hydrogels, is most likely to be due to a more rigid hydrogel structure. Furthermore, hydrogel based HAPna were shown to have lower values of equilibrium swelling ratio (ESR), most probably due to a reduction in the median pore size as HAPna was added.

Zhiyong *et al*, have studied the effects of the incorporation of hydroxyapatite on tough polyacrylamide (PAAm) hydrogels. They added HAP at a concentration of 29 and 39 wt. %. Demonstrating that addition of HAPna decreased the swelling ratio and ESR of these hydrogels in (PBS). Also, increasing HAP concentration from 29 to 39 wt. % was shown to decrease both swelling ratio and ESR further (16).

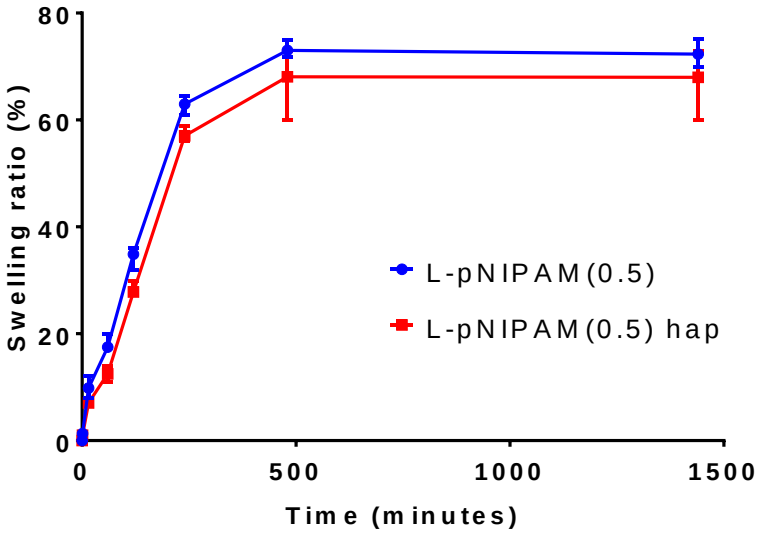

Figure 6.9: Swelling ratio of L-pNIPAM (0.5) with and without synthetic hydroxyapatite incorporated.

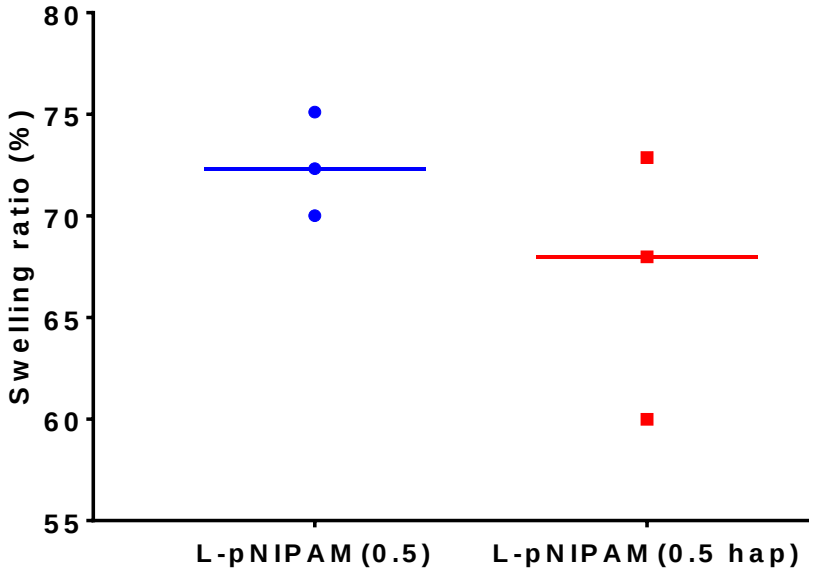

Figure 6.10: Equilibrium swelling degree of L-pNIPAM (0.5) with and without synthetic hydroxyapatite incorporated.

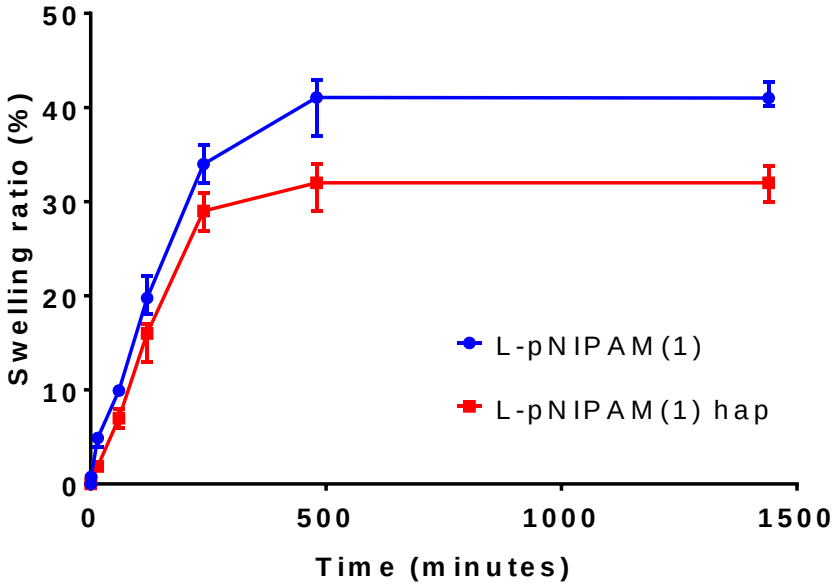

Figure 6.11: Swelling ratio of L-pNIPAM (1) with and without synthetic hydroxyapatite incorporated.

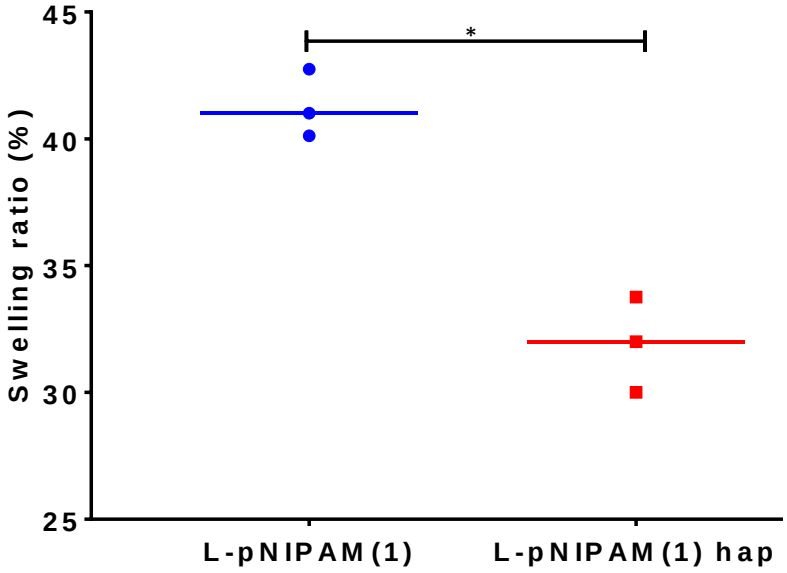

Figure 6.12: Equilibrium swelling degree of L-pNIPAM (1) with and without synthetic hydroxyapatite incorporated, show significant difference. *=P<0.05.

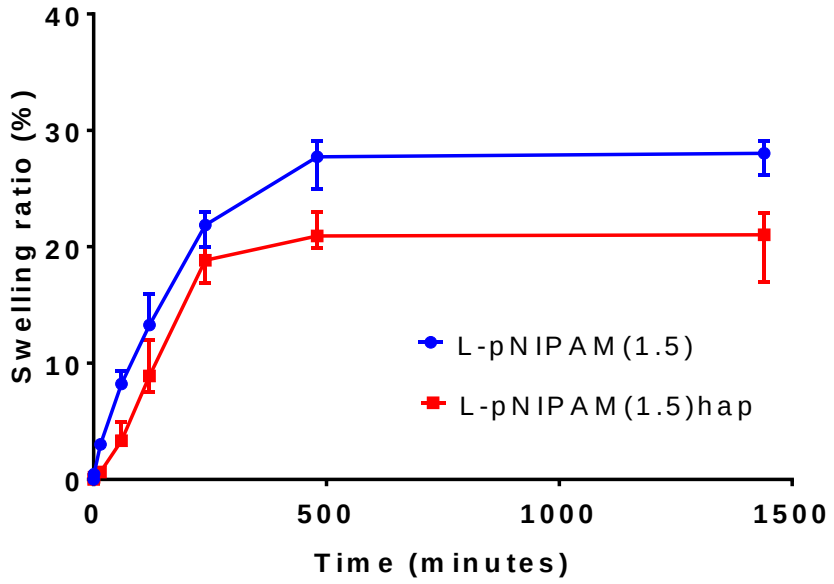

Figure 6.13: Swelling ratio of L-pNIPAM (1.5) with and without synthetic hydroxyapatite incorporated.

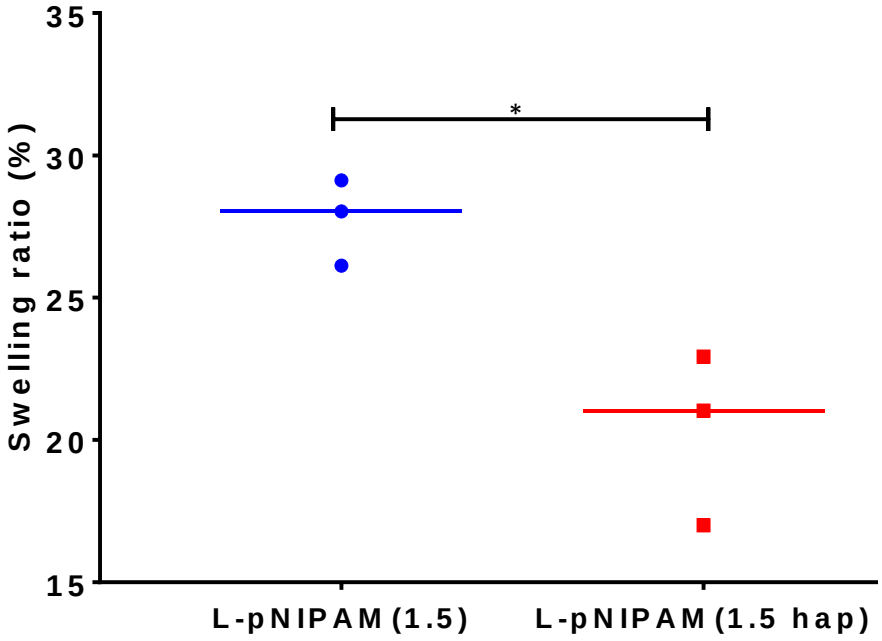

Figure 6.14: Equilibrium swelling degree of L-pNIPAM (1.5) with and without synthetic hydroxyapatite incorporated, show significant difference. *=P<0.05

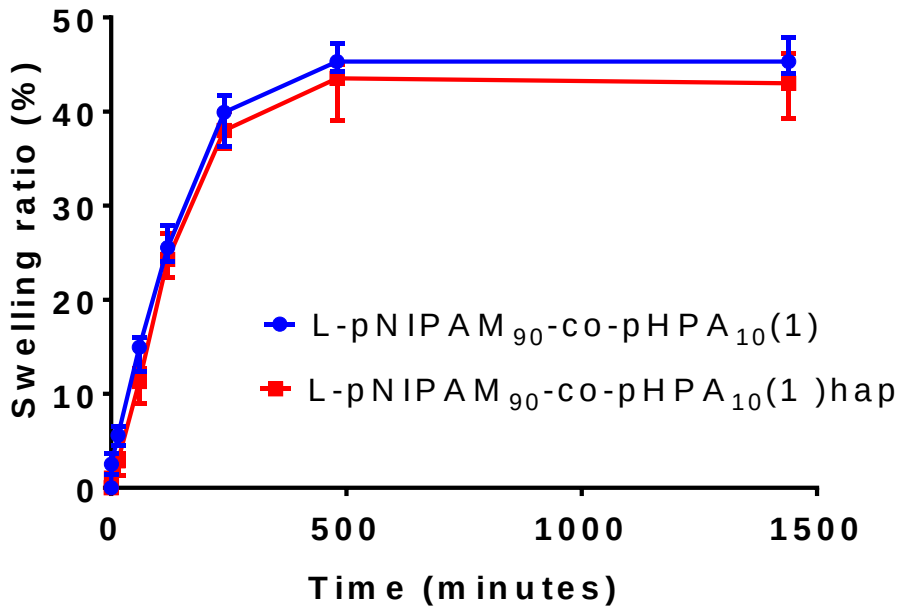

Figure 6.15: Swelling ratio of L-pNIPAM$_{90}$-co-HPMA$_{10}$ (1) with and without synthetic hydroxyapatite incorporated.

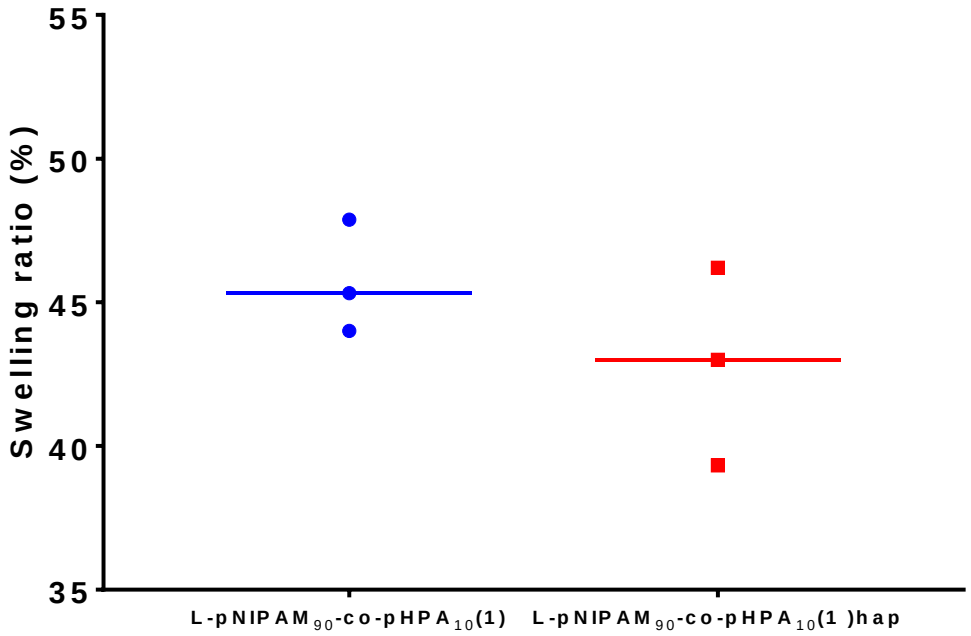

Figure 6.16: Equilibrium swelling degree of L-pNIPAM$_{90}$-co-HPMA$_{10}$ (1) with and without synthetic hydroxyapatite incorporated.

6.5 Deswelling

Since L-pNIPAM hydrogels, are thermoresponsive hydrogels, that possess sol-gel transition around its lower critical solution temperature (LCST), as mentioned in chapter 1, section 1.4. Therefore, deswelling kinetics as a response to changes in temperature was performed, to investigate influence of adding HAPna on thermoresponsive behaviour of pNIPAM based Laponite® injectable hydrogels. Temperature was elevated from 25 to 62 °C and shrinkage as a response to thermal changes was measured as detailed in Chapter 2.2.

The deswelling ratio of hydrogels can be impacted by multiple factors; including the lower critical solution temperature (LCST), the stiffness and the pore size. The hydrogel stiffness could affect the mobility of the polymer chains within the internal structure, where more rigid networks may result in a slower deswelling ratio. Bigger or smaller pore sizes could affect the deswelling equilibrium degree, as smaller pore sizes lead to lower deswelling equilibrium degree and vice versa.

Deswelling ratio of L-pNIPAM (0.5) was reduced when HAPna was incorporated (Figure 6.17), specifically after the first hour, when the hydrogel with HAPna incorporated became more likely to achieve the maximum deswelling degree. The maximum degree of deswelling was decreased as HAPna was added (Figure 6.18).

Incorporation of HAPna into L-pNIPAM (1) was shown to decrease the deswelling ratio (Figure 6.19) and significantly reduced the maximum degree of deswelling for L-pNIPAM (1) (Figure 6.20).

The highest crosslink density L-pNIPAM (1.5) hydrogel also showed the lowest deswelling ratio when HAPna was incorporated, and a longer time was needed to reach the maximum degree of deswelling (Figure 6.21). The maximum degree of deswelling in this composition was dramatically decreased (Figure 6.22).

Incorporation of HAPna into $pNIPAM_{90}$-co-$HPMA_{10}$ (1) was found to slightly affect both deswelling ratio and maximum degree of deswelling (Figure 6.23 and 24). However, the deswelling rate was observed to be noticeably affected,

where $pNIPAM_{90}$-co-$HPMA_{10}$ (1) possessed very different deswelling rate as HAPna was incorporated (Figure 6.23).

In the current study, we have found that incorporation of HAPna decreased deswelling ratio and equilibrium deswelling degree in all pNIPAM based Laponite® hydrogel samples studied. The most obvious deswelling restriction was found in 1 and 1.5 wt. % crosslink density hydrogels, where equilibrium deswelling degree was significantly lower in hydrogel with HAPna incorporated than as - synthesised hydrogels (Figure 6.20 and 6.22).

Z. Guifu *et al*, have investigated the influence of laminated hydroxypatite on chitosan (CS) hydrogels used for pharmacutical applications, with a range of different HAP concentrations (1, 2 and 3 wt. %). They found that HAP decreased deswelling rate which is a positive impact for CS-HA hydrogels used in slow drug release(17). In this current study it was also found HAPna reduced the deswelling ratio and maximum degree of deswelling, despite using very low concntrations of synthetic HAPna.

The deswelling of L-pNIPAM hydrogels, as a thermal response was restricted when HAPna incorporated, due to changes in structure and mechanical strength. Smaller pore size and rigid structure would result in slower deswelling rate, as seen when HAPna was incorporated into L-pNIPAM (1.5).

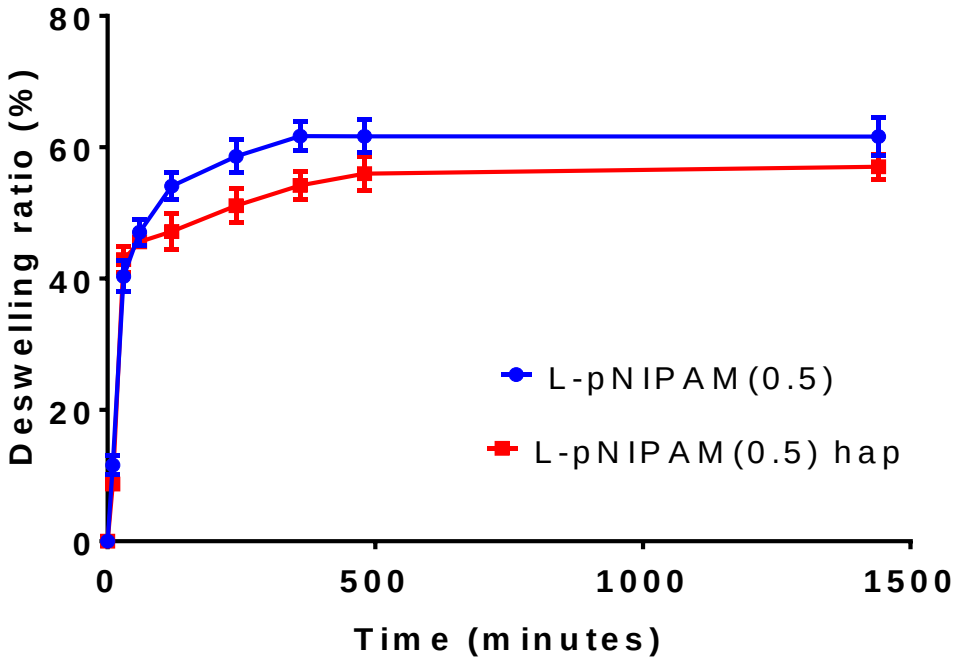

Figure 6.17: Deswelling ratio of L-pNIPAM (0.5) with and without synthetic hydroxyapatite incorporated.

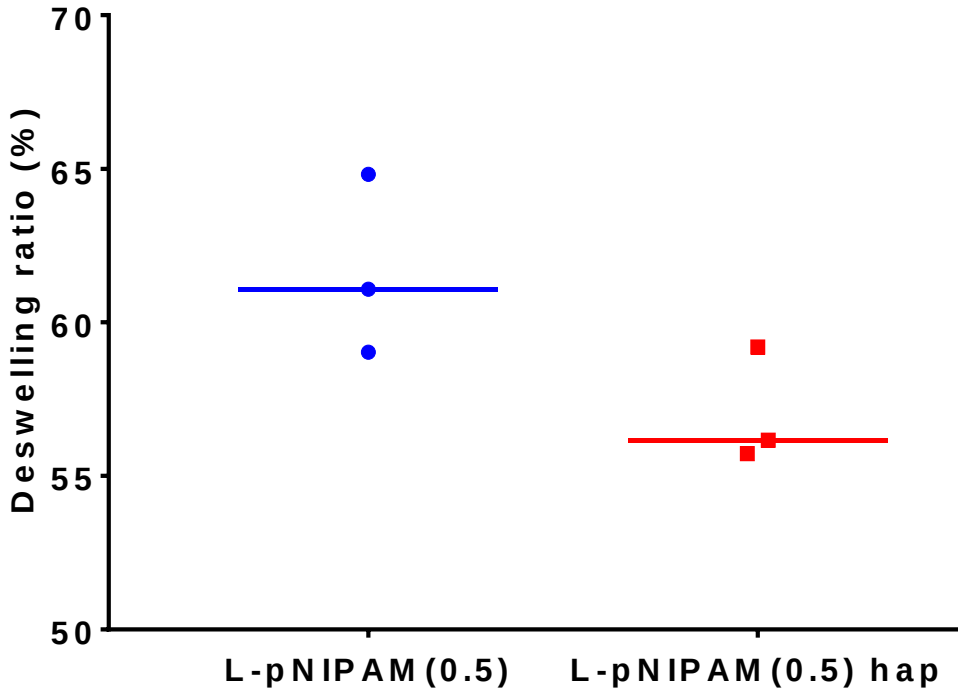

Figure 6.18: Equilibrium deswelling degree of L-pNIPAM (0.5) with and without synthetic hydroxyapatite incorporated.

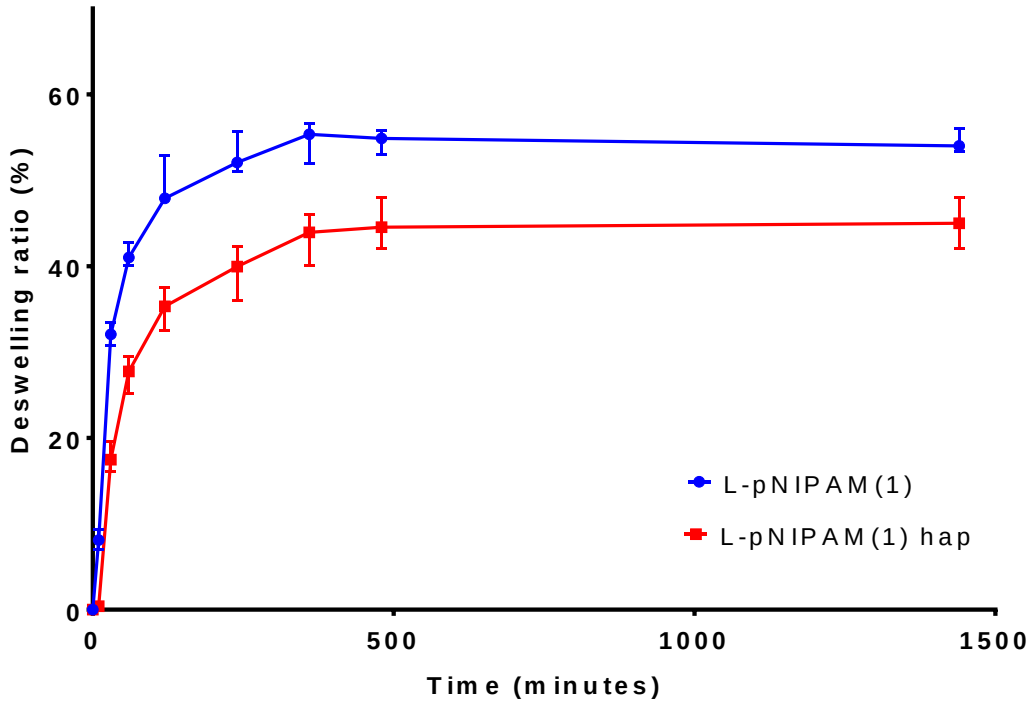

Figure 6.19: Deswelling ratio of L-pNIPAM (1) with and without synthetic hydroxyapatite incorporated.

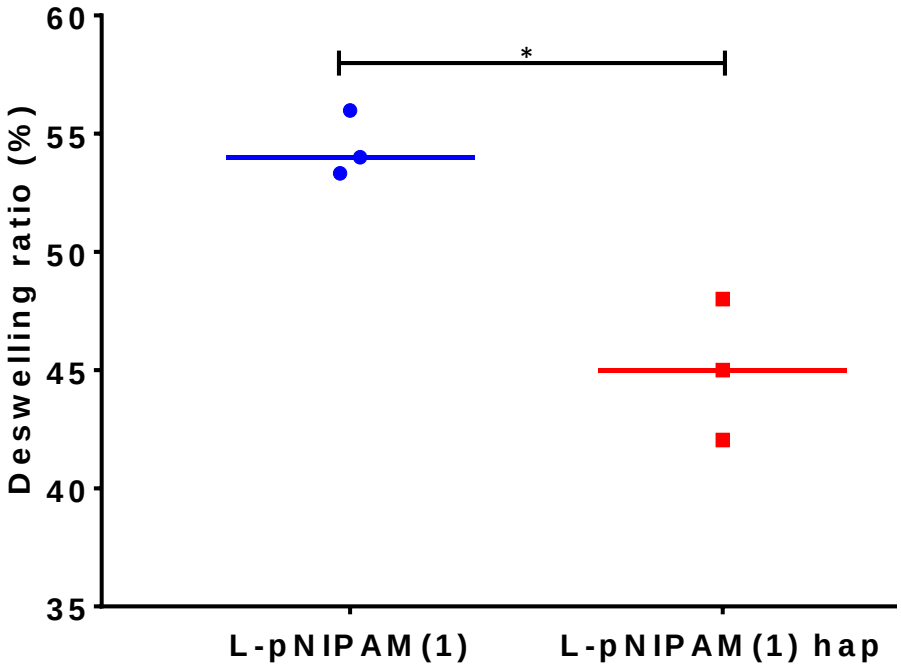

Figure 6.20: Equilibrium deswelling degree of L-pNIPAM (1) with and without synthetic hydroxyapatite incorporated, showing statistical difference. *=P<0.05

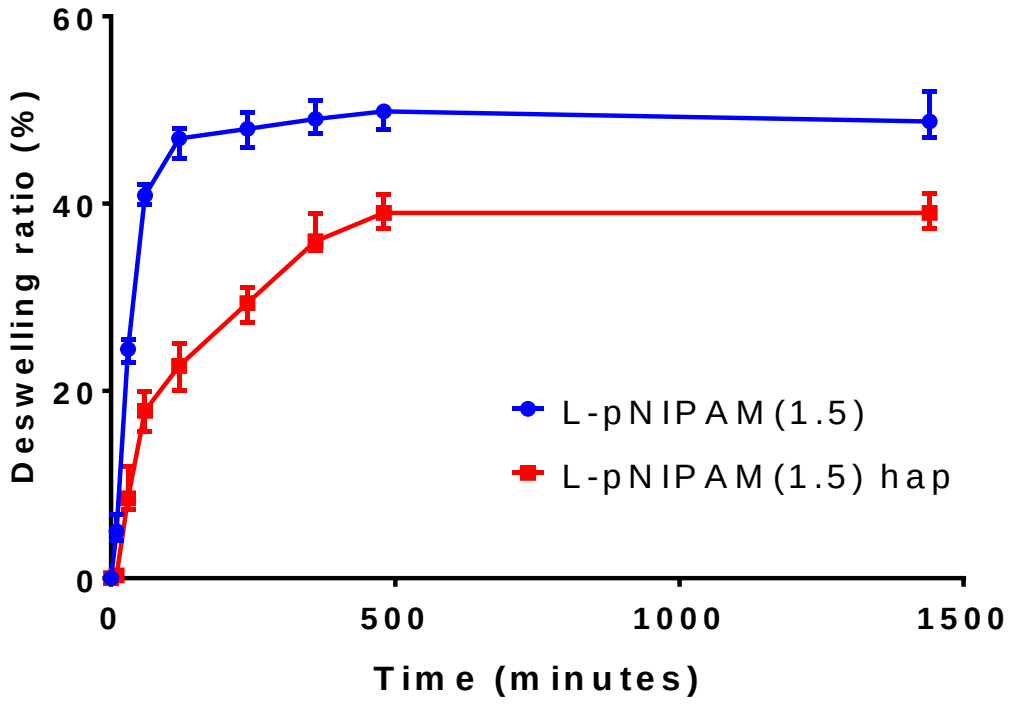

Figure 6.21: Deswelling ratio of L-pNIPAM (1.5) with and without synthetic hydroxyapatite incorporated.

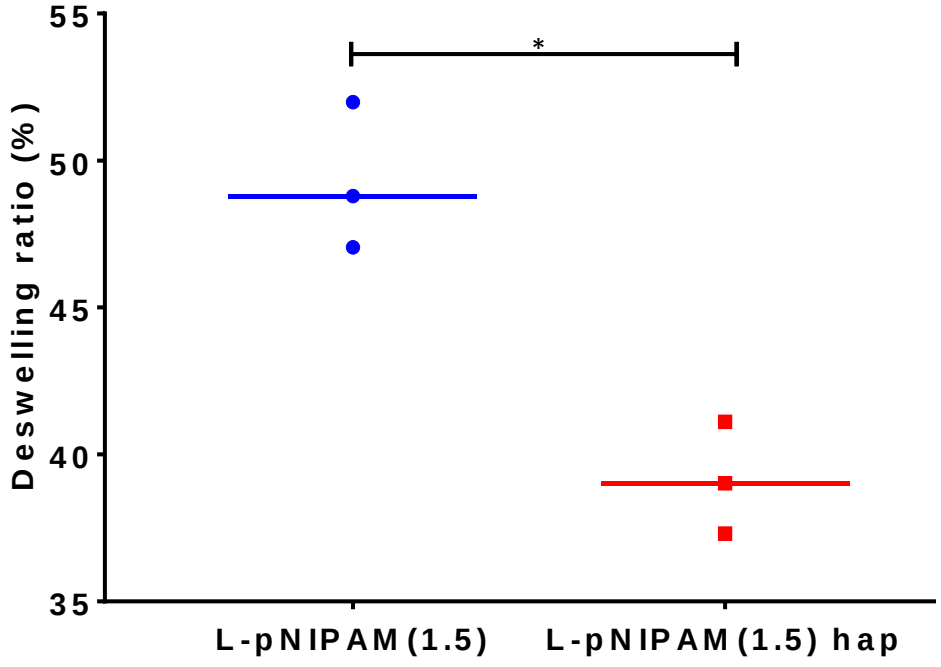

Figure 6.22: Equilibrium deswelling degree of L-pNIPAM (1.5) with and without synthetic hydroxyapatite incorporated, showing statistical difference. *=P<0.05.

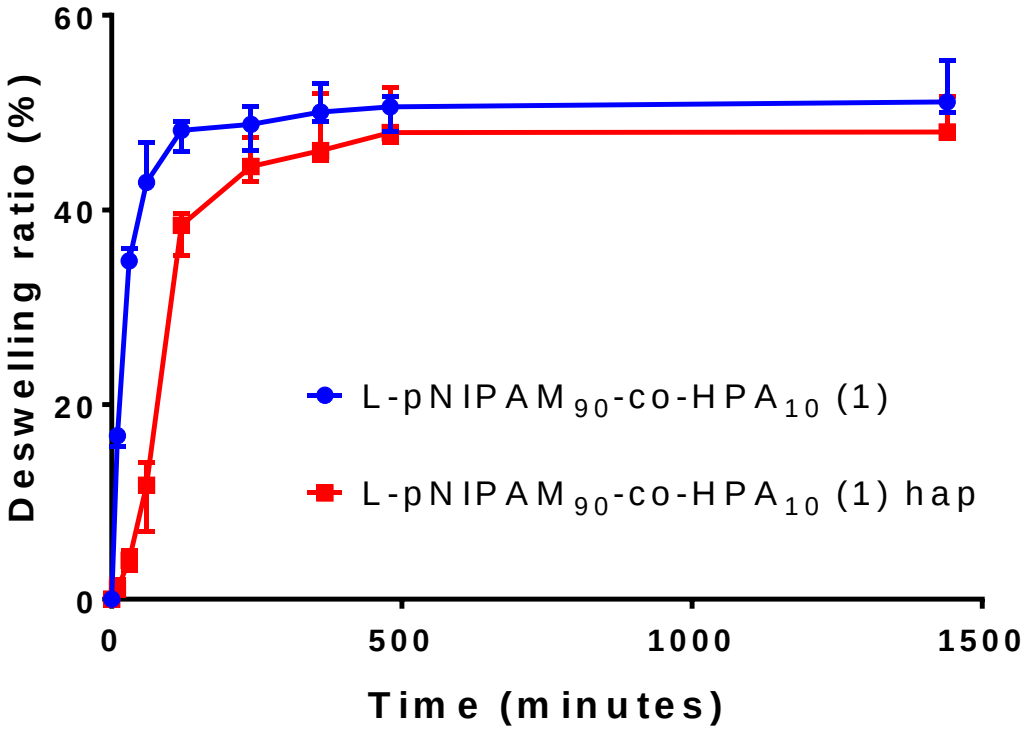

Figure 6.23: Deswelling ratio of L-pNIPAM90-co-HPA10 (1) with and without synthetic hydroxyapatite incorporated.

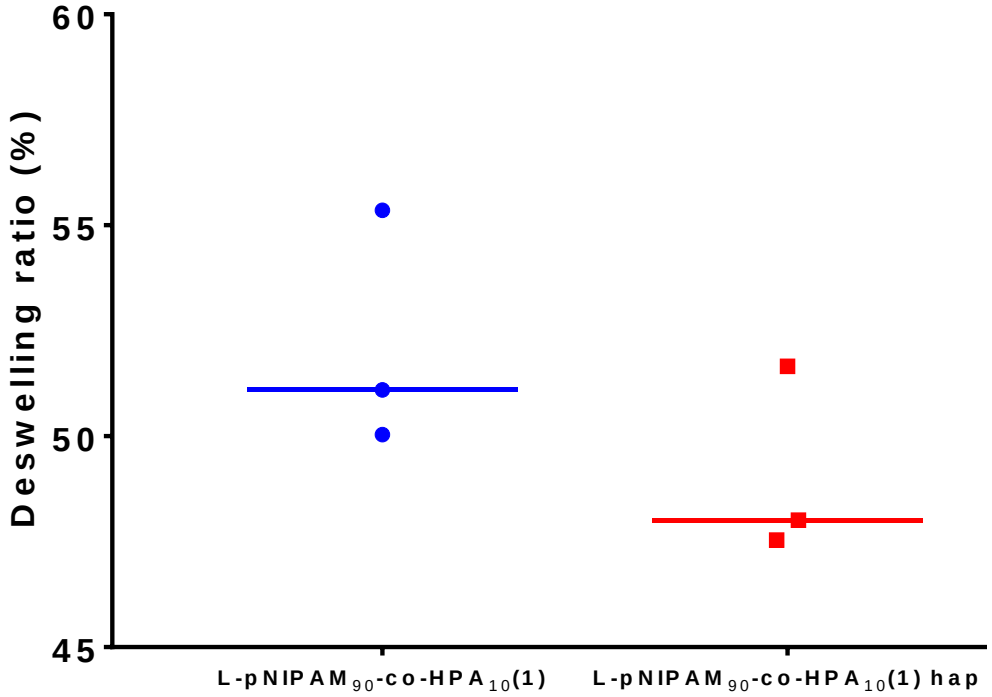

Figure 6.24: Equilibrium deswelling degree of L-pNIPAM90-co-HPA10 (1) with and without synthetic hydroxyapatite incorporated. n=3.

6.6 influence of incorporate of hydroxyapatite on cell behaviour

Two compositions of L-pNIPAM hydrogels were selected, for further studies based on the results obtained from Alamar blue staining and SEM images for both cells suspended into and layered on different compositions. L-pNIPAM$_{90}$-co-HPA$_{10}$ (1) and L-pNIPAM (1) exhibited the highest number of live cells; hence further investigations were needed to explore the ability of these compositions to induce osteogenic differentiation of human mesenchymal stem cells (hMSC).

Synthesised hydroxyapatite nanoparticles (HAPna) were incorporated into two compositions of L-pNIPAM hydrogel, to promote osteogenic differentiation of human mesenchymal stem cells (hMSC). Thorpe A. *et al* (2016) found that by incorporating of HAPna into L-pNIPAM-co-DMAC hydrogel, bone differentiation markers and collagen deposition were induced within 48 h, and calcium deposition was increased with time in culture(7). Thorpe. *et al.* (2016) investigated two concentrations of synthesised HAPna (0.5 and 1mg/ml), where the optimum concentration was 0.5mg/ml and 1mg/ml was found to be cytotoxic. Therefore, in this study 0.5mg/ml HAPna was incorporated into the selected two compositions of L- pNIPAM hydrogel (L-pNIPAM$_{90}$-co-HPA$_{10}$ (1) and L-pNIPAM (1)), to promote osteogenic differentiation of human mesenchymal stem cells (hMSC). HAPna was incorporated prior to gelation, and mixed homogeneously to avoid precipitation of HAPna.

6.6.1 Scanning electron microscopy investigation

Scanning electron microscopy images of hMSC cells cultured within the selected compositions of L-pNIPAM. Culture durations of 2 days, 2 and 4 weeks were used to explore the morphology of hydrogels following incorporation of hMSC cells. SEM images at a range of magnifications were captured to investigate the differences between the morphology and density of hMSC cells within pNIPAM based Laponite® hydrogel, to explore the influence of incorporation of 0.5mg/ml HAPna on cell behaviour.

Following two days in culture within all hydrogels investigated, SEM images demonstrated cells occupying the interconnected structure of the hydrogels (Figure 6.25 and 26). L-pNIPAM (1) without HAPna incorporated displayed single cells with spherical shape occupying the pores of the hydrogel;

extracellular matrix material was also seen within the hydrogel (Figure 6.25). When HAPna was incorporated into L-pNIPAM (1) and after two days in culture cell density within hydrogel structure was increased, compared to the hydrogel without HAPna incorporated (Figure 6.25).

L-pNIPAM$_{90}$-co-HPMA$_{10}$ (1) showed a denser structure than L-pNIPAM (1), where more single cells were observed within hydrogel, which appeared to be closer together than seen in L-pNIPAM (1). Following 2 days, the interconnected porous structure of L-pNIPAM$_{90}$-co-HPMA$_{10}$ (1) hydrogel was completely filled (Figure 6.26).

Incorporation of HAPna into L-pNIPAM$_{90}$-co-HPMA$_{10}$ (1) appeared to increase the deposition of extracellular matrix within the hydrogel, where no single cells could be observed in this composition following 2 days in culture (Figure 6.26).

Incorporation of HAPna into L-pNIPAM hydrogels increased the number of viable cells within the hydrogel matrix, in both L-pNIPAM (1) and L-pNIPAM$_{90}$-co-HPMA$_{10}$ (1), this could be as a result of the increased hydrogel stiffness following incorporation of HAPna. Extracellular matrix deposition was increased as HAPna was incorporated.

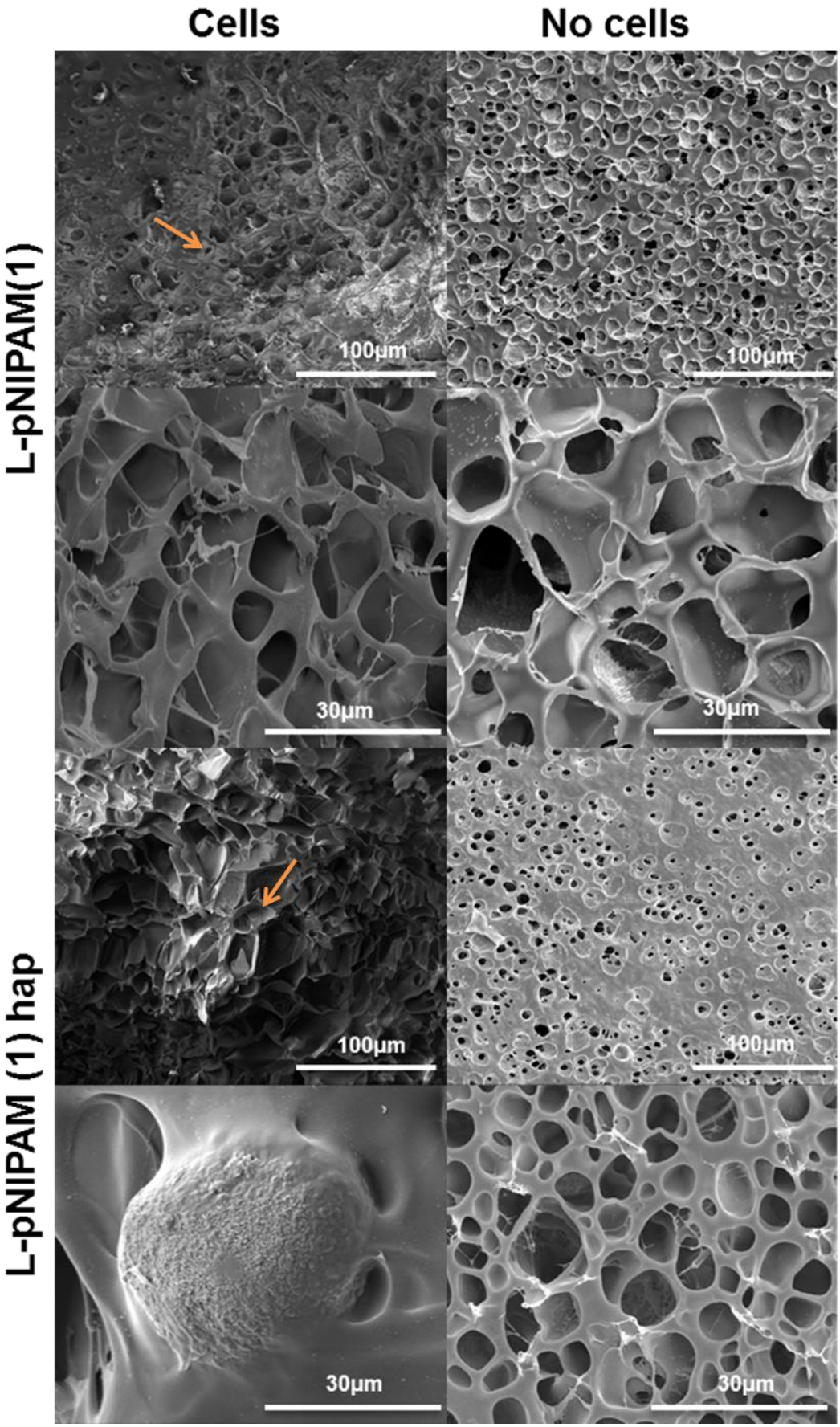

Figure 6.25: Scanning electron microscopy (SEM) of hMSC and acellular L-pNIPAM (1) hydrogel with and without 0.5mg/ml HAPna, following 2 days in culture. Scale bare 30 and 100 µm.

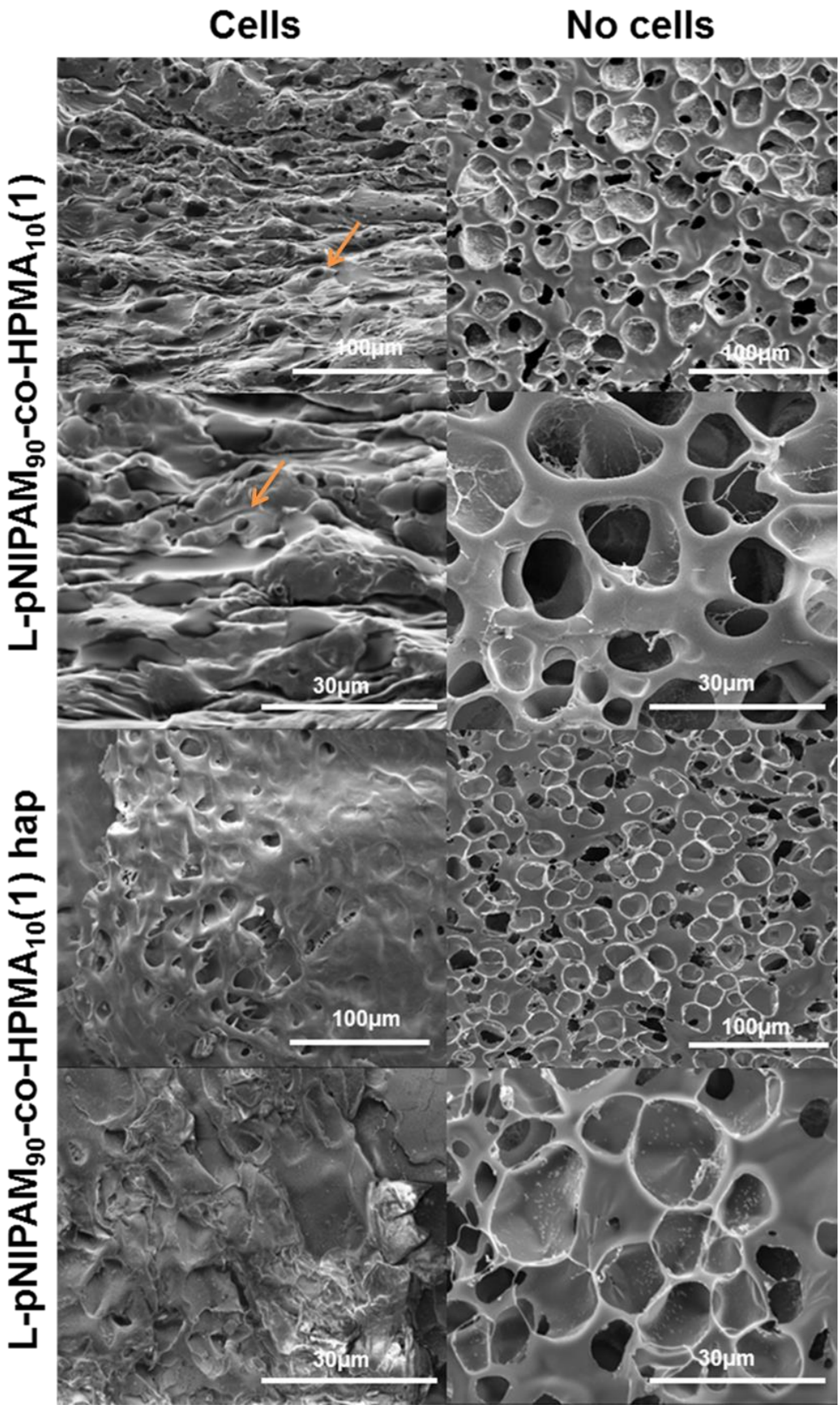

Figure 6.26: Scanning electron microscopy (SEM) of hMSC and acellular L-pNIPAM$_{90}$-co-HPMA$_{10}$ (1) hydrogel with and without 0.5mg/ml HAPna, following 2 days in culture. Scale bare 30 and 100 µm.

Following two weeks in culture, L-pNIPAM (1) showed an increase cellular material and deposition of extracellular matrix (Figure 6.27), whilst hydrogels containing HAPna displayed denser matrix deposition and following 2 weeks no observable pores were seen (Figure 6.27).

Cells cultured within L-pNIPAM$_{90}$-co-HPMA$_{10}$ (1) for two weeks produced a dense extracellular matrix, which filled nearly all the pores. The matrix density was further enhanced by the incorporation of HAPna (Figure 6.28).

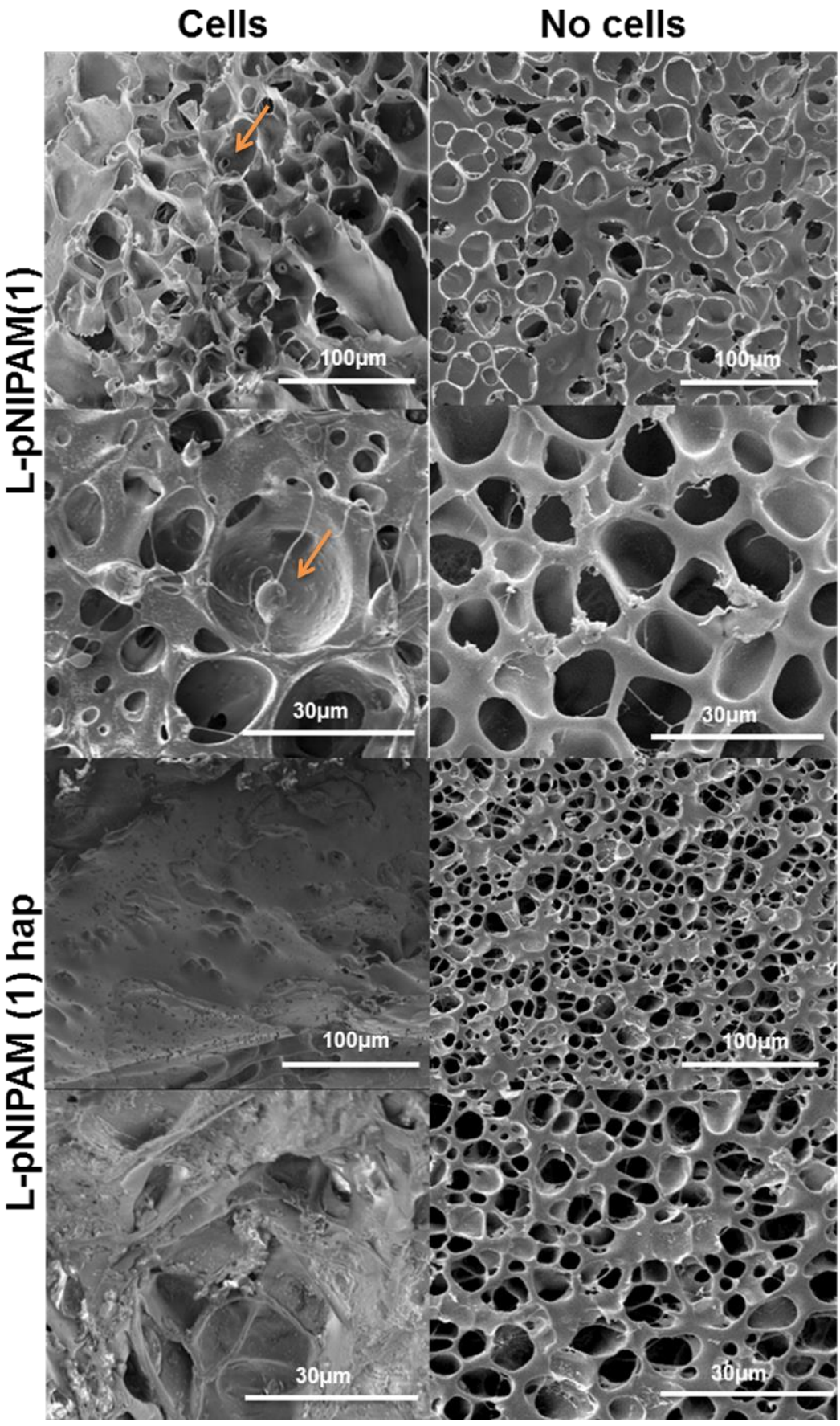

Figure 6.27: Scanning electron microscopy (SEM) of hMSC and acellular L-pNIPAM (1) hydrogel with and without 0.5mg/ml HAPna, following 2 weeks in culture. Scale bare 30 and 100 µm.

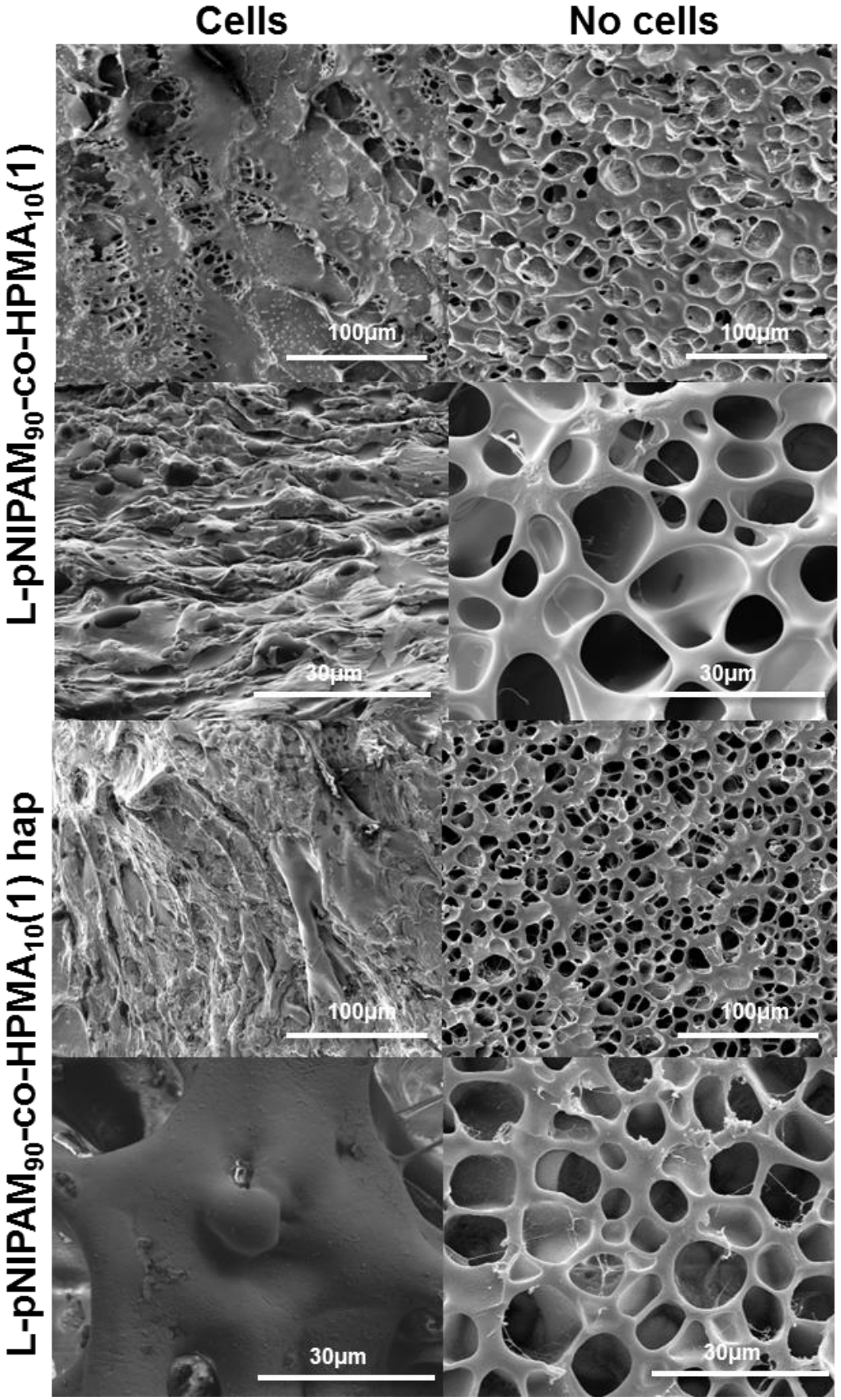

Figure 6.28: Scanning electron microscopy (SEM) of hMSC and acellular L-pNIPAM$_{90}$-co-HPMA$_{10}$ (1) hydrogel with and without 0.5mg/ml HAPna, following 2 weeks in culture. Scale bare 30 and 100 µm.

SEM images of hMSC cultured within pNIPAM based Laponite® injectable hydrogel for four weeks, showed a progressive increase in the structural density of the hydrogel (Figure 6.29 and 30). However, the morphology of hMSC hydrogel was dependant on the composition, where L-pNIPAM (1) displayed an even coating, whereas incorporation of HAPna resulted in an undulating surface, which might be due to cellular differentiation (Figure 6.29).

For cells cultured within L-pNIPAM$_{90}$-co-HPMA$_{10}$ (1) structure, SEM images were showed similar morphology for hMSC hydrogel with and without HAPna incorporated (Figure 6.30). In other words, cells produced similar shape of extracellular matrix, hence further investigations are required to explore type of cells, that produced by differentiation of hMSC within different hydrogel composition. Therefore histological and immunohistochemistry investigations were conducted to identify the composition of the extracellular matrix that was produced within different compositions of L-pNIPAM hydrogels.

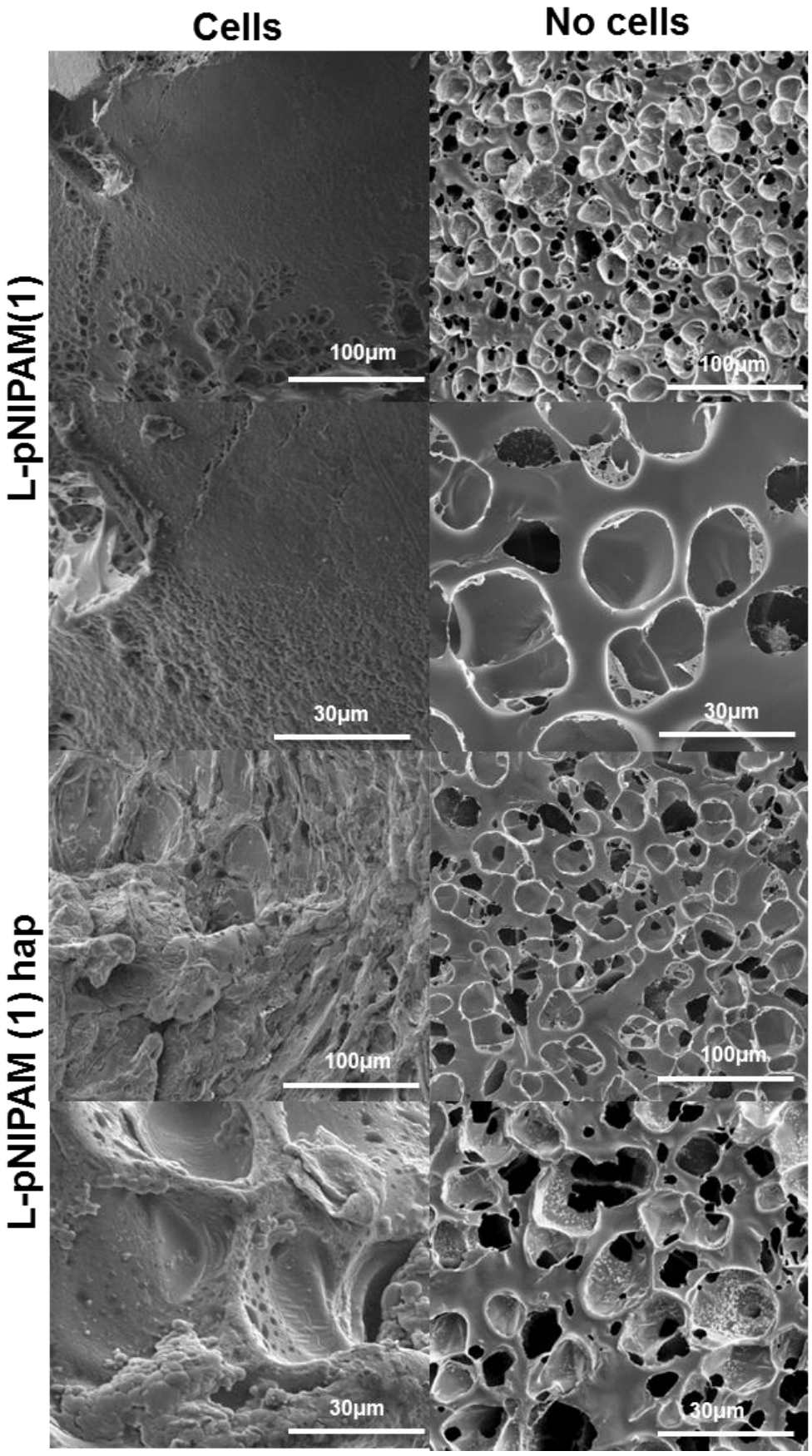

Figure 6.29: Scanning electron microscopy (SEM) of hMSC and acellular L-pNIPAM (1) hydrogel with and without 0.5mg/ml HAPna, following 4 weeks in culture. Scale bare 30 and 100 µm.

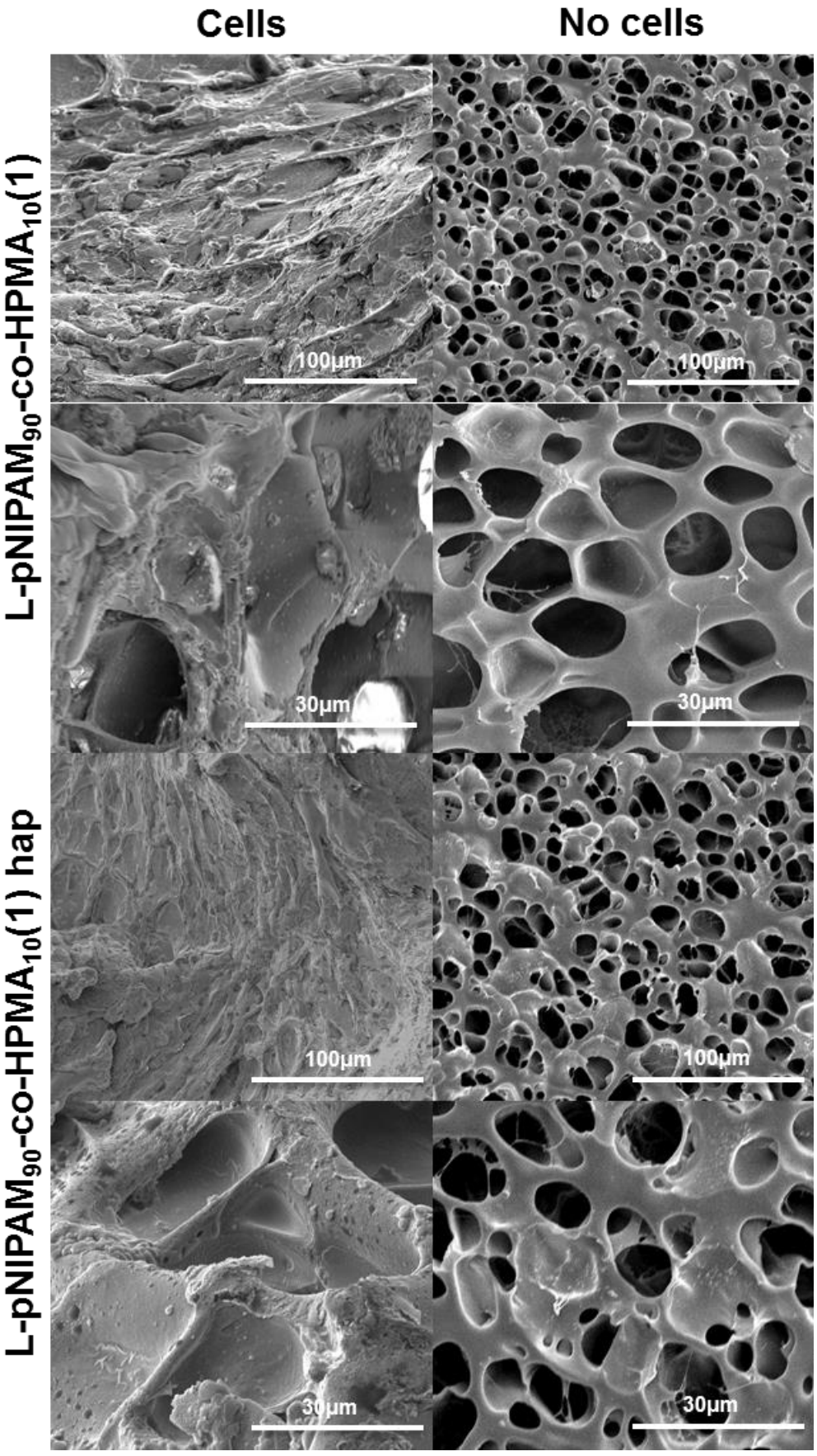

Figure 6.30: Scanning electron microscopy (SEM) of hMSC and acellular L-pNIPAM90-co-HPMA10 (1) hydrogel with and without 0.5mg/ml HAPna, following 4 weeks in culture. Scale bare 30 and 100 µm.

6.6.2 Histological assessment of cellular matrix within the hydrogel

6.6.2.1 Morphology of Live cells within hydrogel

General morphology of hMSC cultured within different hydrogel compositions were assessed using haematoxylin & eosin (H&E). Cells were detected within the hydrogel at all time points, where cells increased with time in culture (Figure 6.31). However, the highest number of observed cells was detected within L-pNIPAM$_{90}$-co-HPMA$_{10}$ (1) and L-pNIPAM$_{90}$-co-HPMA$_{10}$ HAP (1), which were confirmed by metabolic cell activity measurement and SEM. As mentioned previously, an increase in number of cells in L-pNIPAM$_{90}$-co-HPMA$_{10}$ (1) and L-pNIPAM$_{90}$-co-HPMA$_{10}$ HAP (1) could be due to increased pore size or altered mechanical properties when HPMA was incorporated.

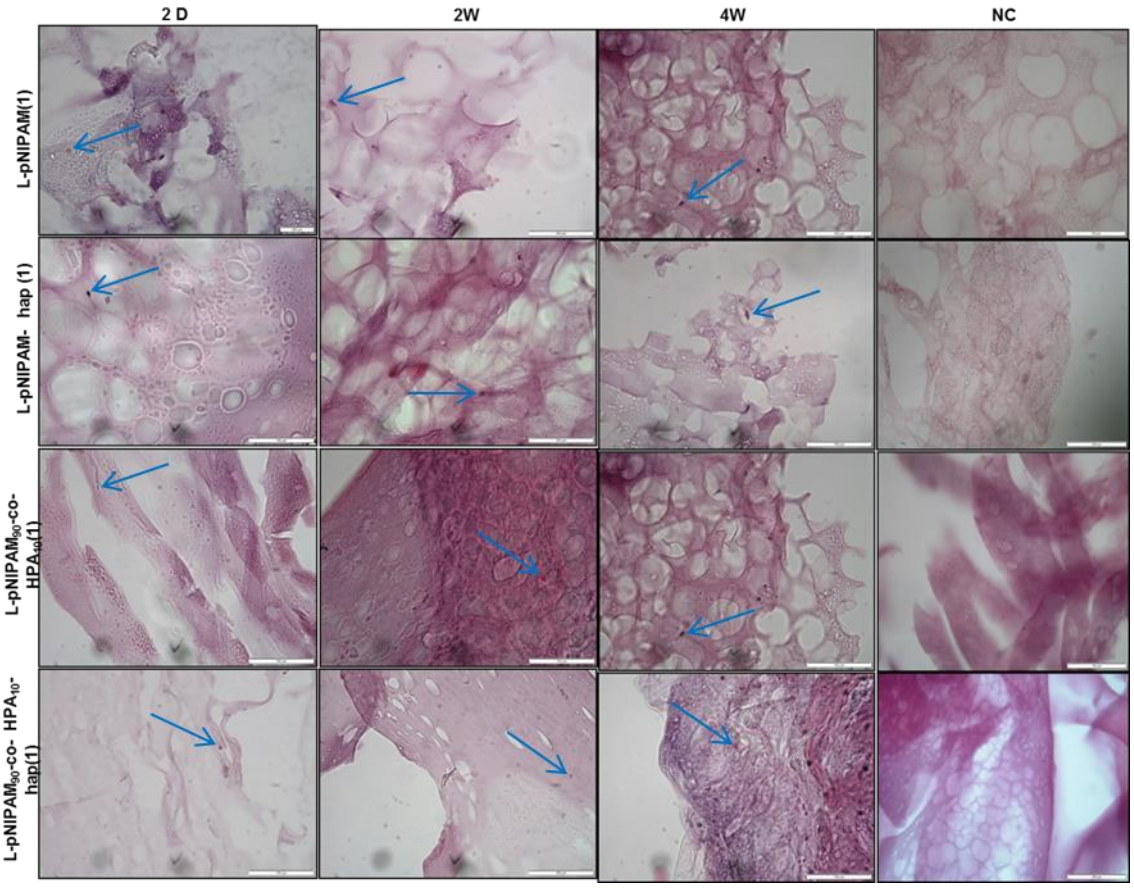

Figure 6.31: Histological stains: Haematoxylin and Eosin (H&E) for cell morphology, following 2 days, 2 and 4 weeks. Scale bare 100 µm.

6.6.2.2 Histological evaluation of proteoglycan deposition within Hydrogels

Proteoglycan is one of the main components of cartilage which in bone forming from osteochondrial ossification is an important intermediary extracellular matrix (18,19). In this study Alcian blue (AB) was used to histologically stain for proteoglycan deposition, as described in chapter two. Areas of blue staining were observed within hydrogel matrix on all hydrogel samples (Figure 6.32). Proteoglycan deposition was detected within cultures from 2 days to 4 weeks; especially within hydrogels containing HAPna (Figure 6.32).

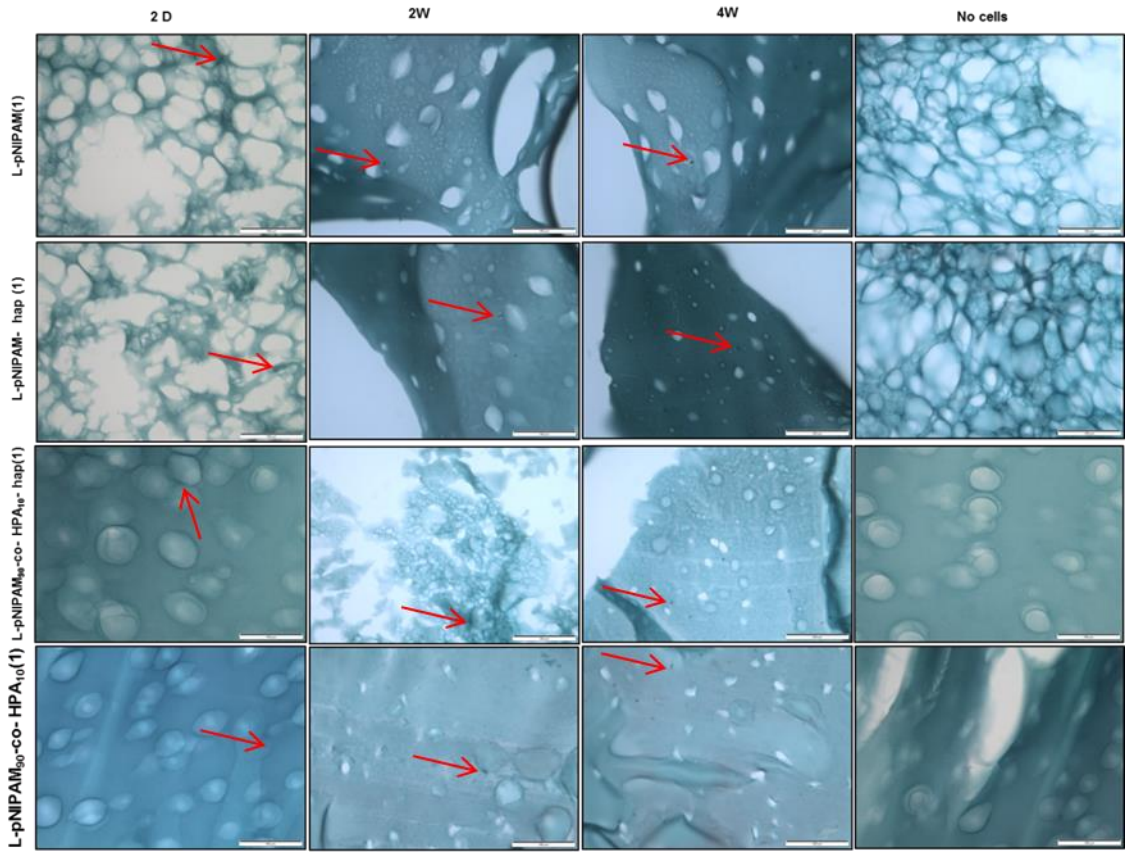

Figure 6.32: Histological stains: Alcian Blue (AB) for proteoglycans, following 2 days, 2 and 4 weeks. Scale bare 100 µm.

6.6.2.3 Evaluation of calcium deposition within Hydrogel matrix

Calcium is one of the main minerals that construct bone tissue; hence calcium deposition was selected in this study to be assessed as a sign of bone differentiation and mineralisation. Alizarin red was used to stain calcium deposition within extracellular matrix, where hMSC hydrogels were stained as detailed in chapter two, section 2.5.3. Calcium deposition was seen in L-pNIPAM$_{90}$-co-HPMA$_{10}$ (1) and L-pNIPAM (1), with levels increasing following incorporation of HAPna (Figure 6.33). Calcium deposition was observed within L- pNIPAM$_{90}$-co-HPMA$_{10}$ (1) even without HAPna incorporated, following 2 days in culture (Figure 6.33), which could possibly be as a result of bigger pore size that cells can grow and proliferate within, and change in mechanical properties when HPMA was added. Whilst, calcium deposition within L- pNIPAM (1) was only observable following 2 weeks in culture (Figure 6.33).

Interestingly, calcium deposition was detected in acellular hydrogels contained HAPna, which could possibly be due to containing synthesised HAPna which could act as a focal deposition point for calcium within the culture media. Therefore, further investigation was needed to determine if this was the case. Raman spectroscopy was used to determine if samples contained free calcium or calcium phosphate. However, unfortunately limited sample was available from 4 µm section available that results were inconclusive.

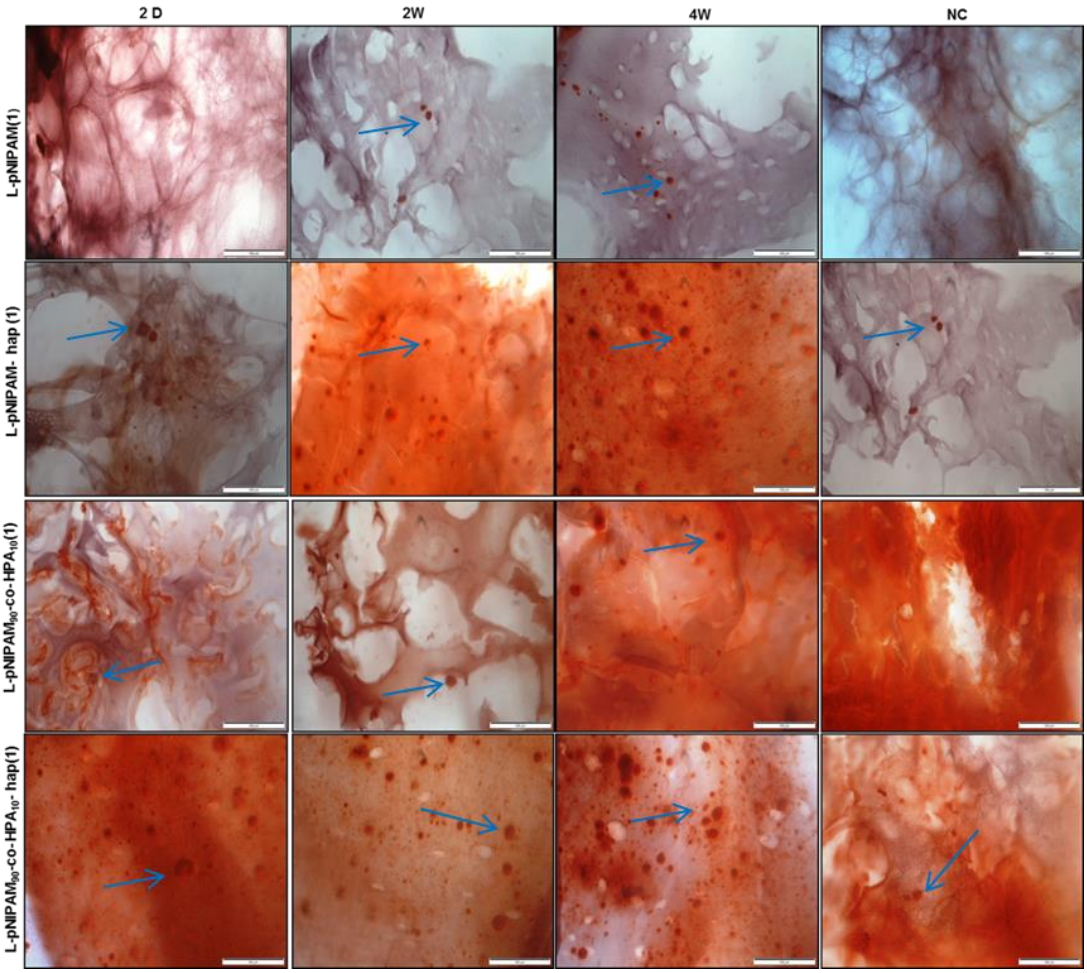

Figure 6.33: Histological stains: Alizarin red for calcium deposition, following 2 days, 2 and 4 weeks. Scale bare 100 µm.

6.6.2.4 Evaluation of collagen deposition within Hydrogel matrix

Collagen is the main organic component of bone, and gives the flexibility to the bones to resistant fracture during daily activities. In this work, collagen deposition within extracellular matrix was selected as one of the main signs for potential osteoblast differentiation. Masson's trichrome was used as described in chapter two, section 2.5.3, to stain collagen deposition within hMSC hydrogels. Collagen deposition was observed within all compositions of pNIPAM based Laponite® hydrogel, with increased in deposition intensity as HAPna incorporated (Figure 6.34). Surprisingly, positive staining was detected in no cell control as HAPna was incorporated (Figure 6.34).

For hydrogels that do not contained HAPna, collagen deposition was observable in both L-pNIPAM$_{90}$-co-HPMA$_{10}$ (1) and L-pNIPAM (1) with increased in deposition as a result of adding HPMA, due to increase in pore size which leaded to significant increase in the number of live cells ($P<0.05$).

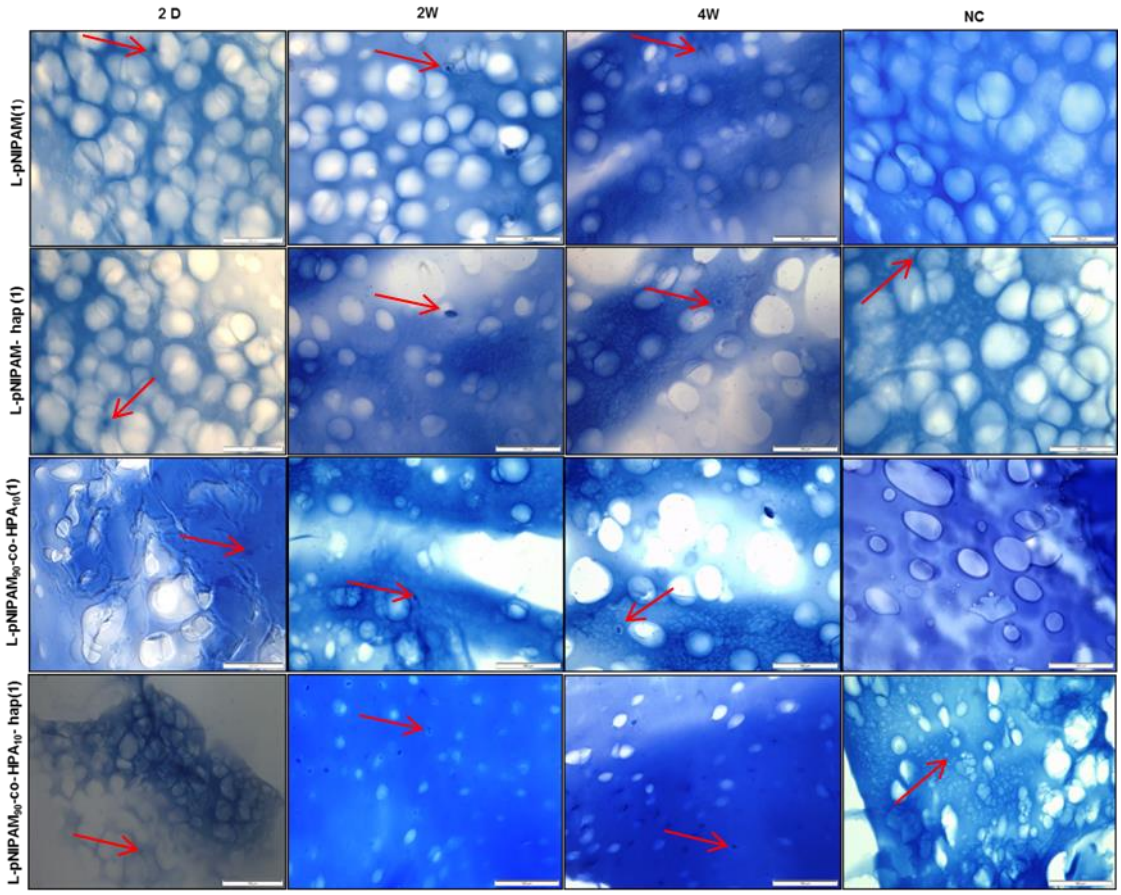

Figure 6.34: Histological stains: Masson's trichrome for collagen deposition, following 2 days, 2 and 4 weeks (arrows indicate collagen deposition). Scale bare 100 µm.

6.6.3 Immunohistochemical evaluation

Immunohistochemistry was used to determine expression of cell matrix markers collagen type I and osteopontin along with the marker of apoptosis caspase 3 to determine cell viability.

6.6.3.1 Evaluation of dead and live cells within hydrogels

Caspase3 is an executer caspase involved in induction of apotosis. Caspase 3 is activated by caspase8 and caspase9 the initiator caspases(20). Thus, caspase 3 was utilised to determine induction of apoptosis within hydrogels as a proxi measure of cell death.

Generally, the highest number of live cells was found within L-pNIPAM$_{90}$-co-HPMA$_{10}$ (1), with or without HAPna (Figure 6.35). These findings verified metabolic cell activity results and SEM observations. In addition, incorporate of 0.5mg/ml HAPna was found not to reduce the number of live cells within the hydrogel, which was demonstrated in a previous study(7,21).

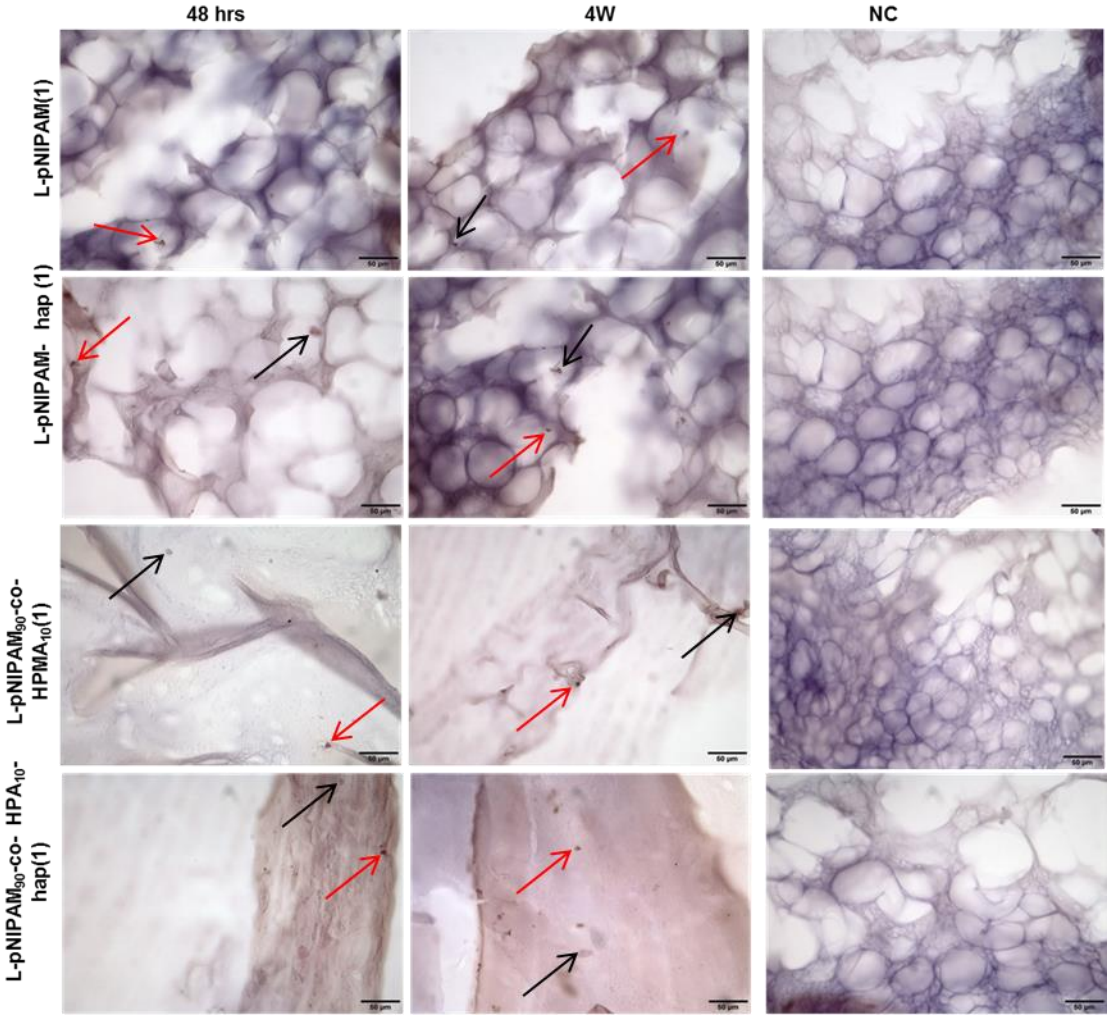

Figure 6.35: Immunohistochemical detection of caspase 3 marker for live and dead cells, following 2 days and 4 weeks (red arrows indicate negative stained cells, and black arrows indicate positive stained cells). Scale bare 50 µm.

6.6.3.2 Evaluation of collagen expression

As mentioned in section 6.6.2.4 collagen is the main organic component of the bones, hence further investigation was performed in this study to specifically verify synthesis of collagen matrix, within the hydrogel, which was done histologically using Masson's trichrome. Collagen type I was selected for immunohistochemistry (IHC) investigation for 2 days and 4 weeks in culture as the main collagen type found in bone (22).

In L-pNIPAM$_{90}$-co-HPMA$_{10}$ (1) and L-pNIPAM$_{90}$-co-HPMA$_{10}$ hap (1), collagen type I was found to be highly expressed by hMSCs harvested directly from monolayer culture (~99%), following by significant decrease ($p<0.05$), in the number of immunopositive cells detected after 2 days in culture (Figure 6.36).

For L-pNIPAM (1) low level of collagen type I was found to be expressed, after 2 days in culture with further reduction in positive cells after 4 weeks (Figure 6.36).

However, when HAPna was incorporated into L-pNIPAM (1) an increase in immunopositive cells was observed (~58%), after four weeks in culture, with a significant decrease in number of cells displaying immunopositivity for collagen type I following the first two days (Figure 6.36).

A noticeable increase in immunopositive cells, when hMSCs was incorporated into the hydrogel containing HPMA, when compared to the hydrogel that did not contain HPMA. Interestingly, L-pNIPAM$_{90}$-co-HPMA$_{10}$ (1) was showed to enhance the number of immunopositive cells, either with or without HAPna incorporated. However, more matrix staining for collagen type I was seen when HAPna was incorporated (Figure 6.36).

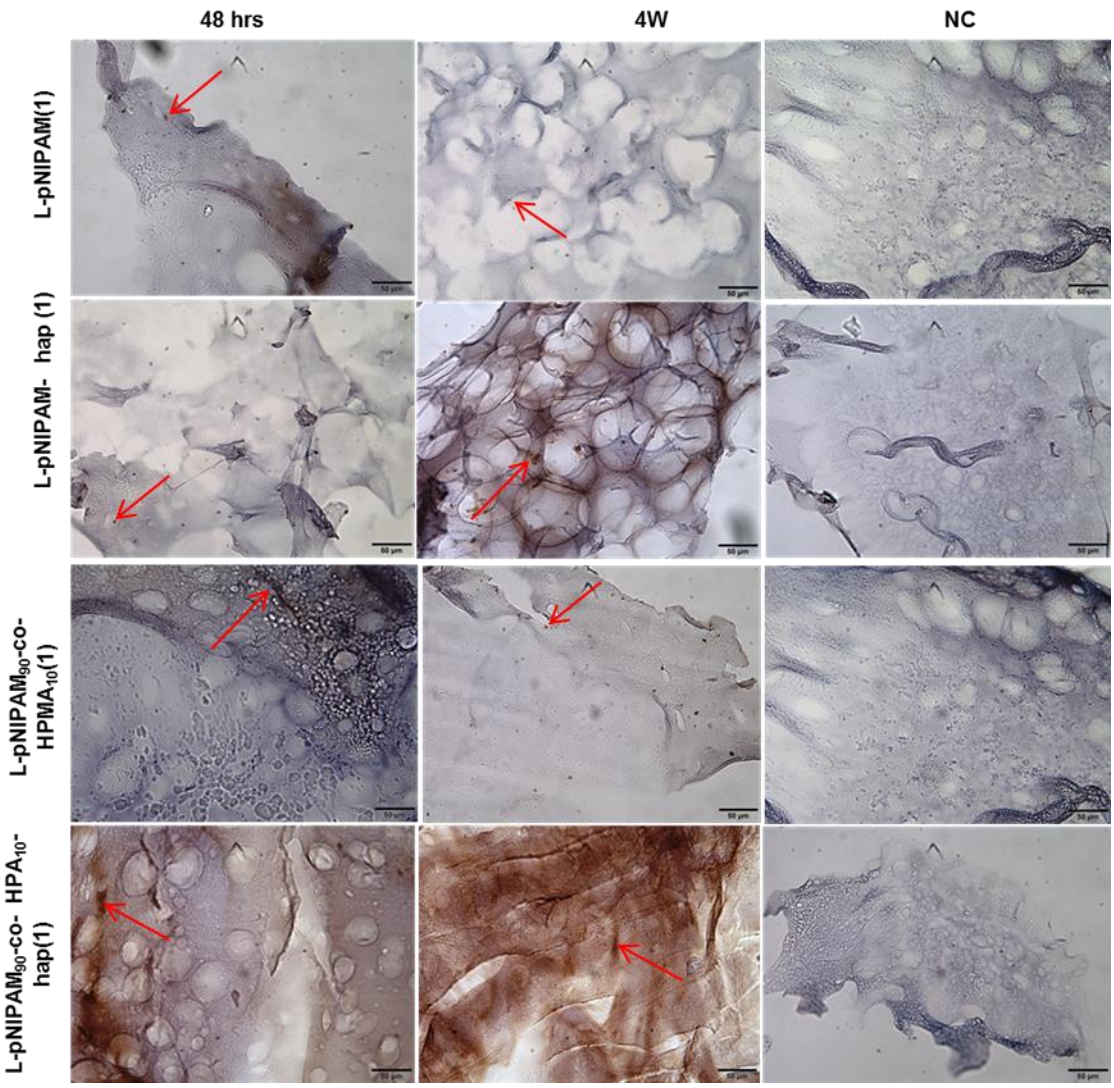

Figure 6.36: Immunohistochemical detection of collagen type I marker for collagen, following 2 days and 4 weeks (arrows indicate stained collagen). Scale bare 50 μm.

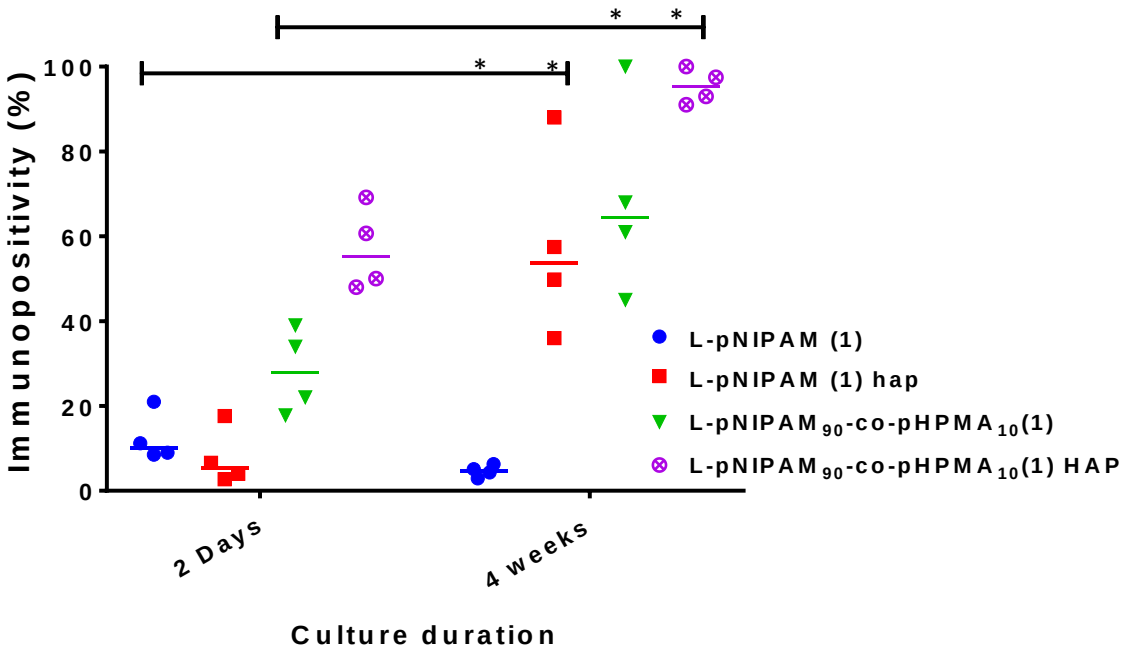

Figure 6.37: Percentages of Collagen type I immunopositivity following 2 days and 4 weeks (*=p ≤ 0.05).

6.6.3.3 Evaluation of osteopontin expression

Natural bone consists of organic and inorganic components, organic matrix of bones consist of multiple components, one of which osteopontin which is responsible of cell binding protein(23). Also, Osteopontin is a marker of the late phase of mature osteogenesis(7).

In the current work osteopontin was selected for immunohistochemistry (IHC) investigation to assess the osteogenic differentiation capacity of hMSCs cultured in different compositions of L-pNIPAM hydrogels. In all studied compositions of the hydrogel, osteopontin was shown to be expressed by significantly increased number of hMSCs ($p<0.05$) (Figure 6.39) after 4 weeks in culture, except in cells cultured in L-pNIPAM (1), where osteopontin was shown to be expressed by a high number of cells following 2 days in culture, before a significant reduction was detected ($p<0.05$) in the expression, after 4 weeks (Figure 6.38).

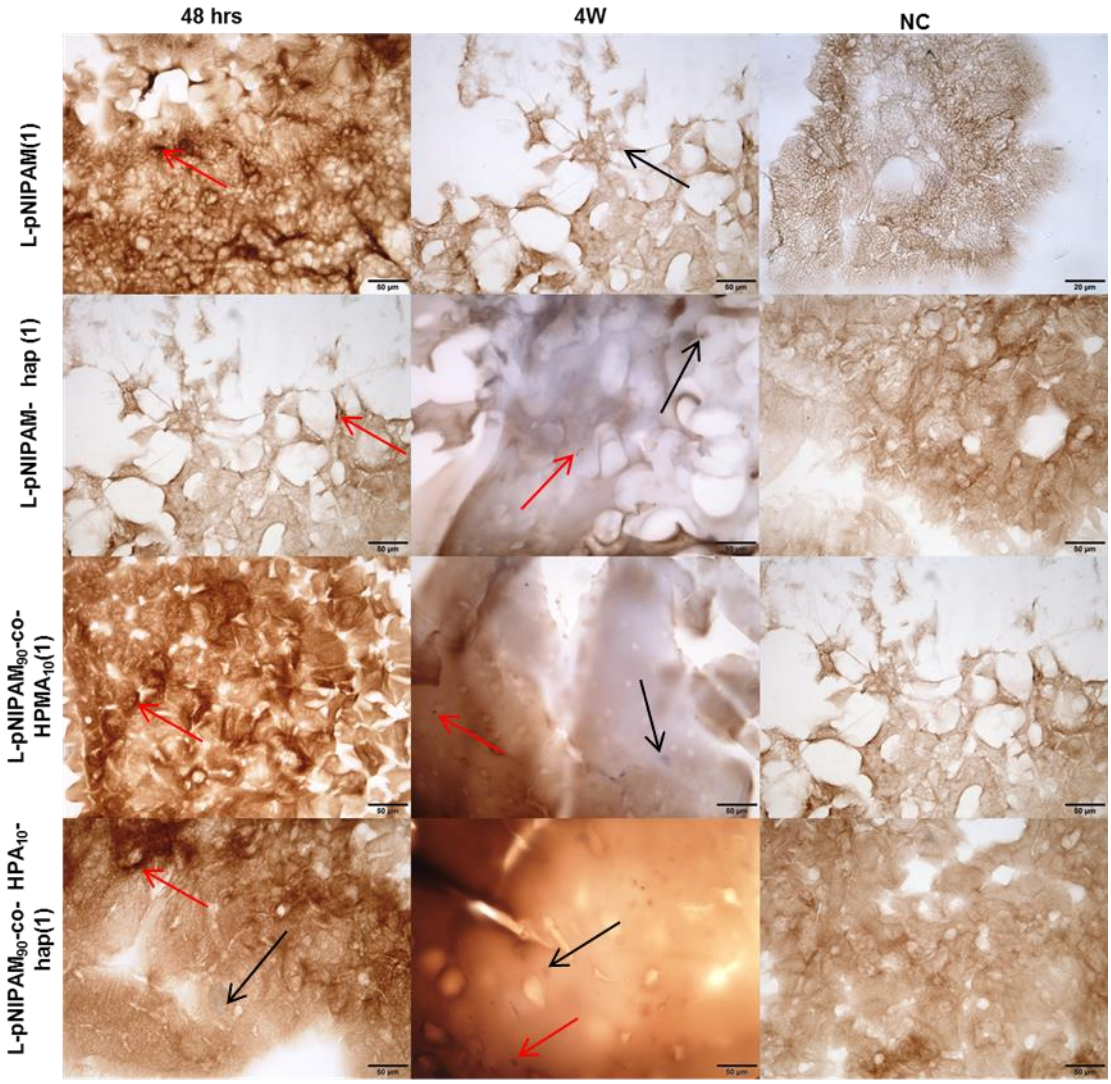

Figure 6.37: Immunohistochemical detection of osteopontin marker for osteopontin, following 2 days and 4 weeks (black arrows indicate positive stained cells and red arrows indicate negative stained cells).Scale bare 50 μm.

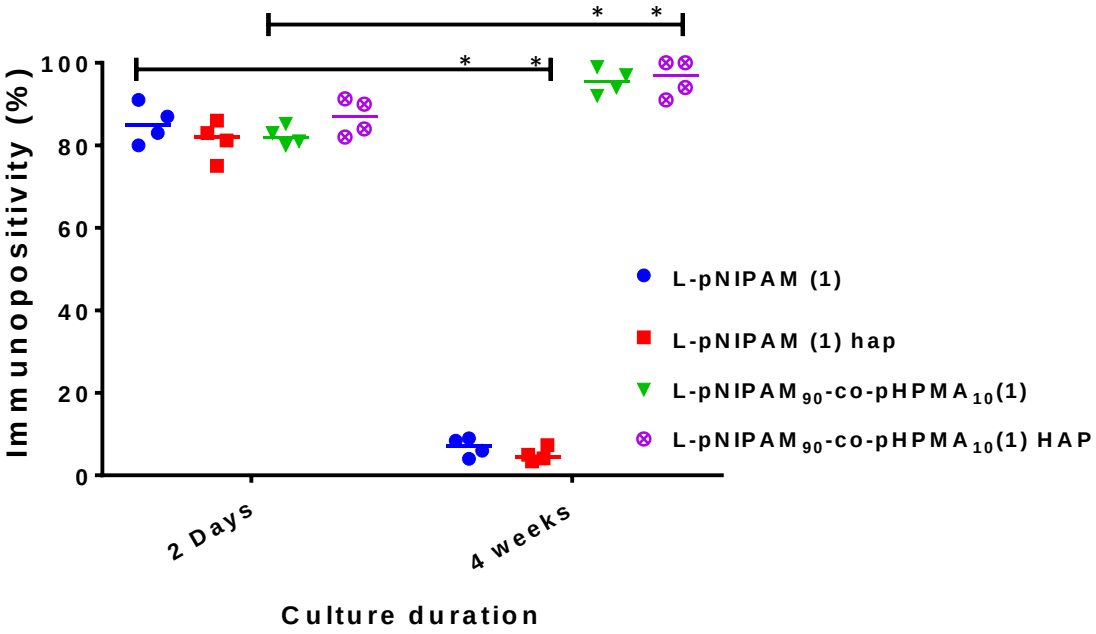

Figure 6.38: Percentages of osteopontin immunopositivity following 2 days and 4 weeks (*=p ≤ 0.05).

In the current study, incorporation of HAPna enhanced osteogenic differentiation of human mesenchymal stem cells (hMSC). Where, histological investigation was performed to assess the matrix deposition of calcium, collagen and proteoglycan. In addition, immunohistochemical evaluation for collagen, osteopontin and caspase 3 were performed to verify the histological findings.

The obtained results are in agreement with previous results conducted in the field of tissue engineering and bone repair(21,24). Dhivya *et al* studied the influence of adding HAPna to chitosan composite hydrogel; which was shown to have potential for use as a scaffold for bone repair. They found that, adding HAPna to the hydrogel enhanced osteoblast differentiation of hMSCs under osteogenic conditions *in vitro*, where bone regeneration was accelerated(25).

6.7 Summary

Adding hydroxyapatite nanoparticles was affected physical and mechanical properties of L-pNIPAM hydrogels. Morphology of the hydrogel changed and pore sizes generally decreased when HAPna incorporated. The microporous structure of the hydrogels was filled by HAPna of <200 nm particle size. Therefore, the influence of these particles on the pore size of different hydrogel compositions was depending on the original pore size of those compositions as synthesised (without HAPna), and considering the small amount of HAPna that added (0.5mg/ml) . Where, the lowest impact on the pore size was observed in both L-pNIPAM (0.5) and L-pNIPAM$_{90}$-co-HPA$_{10}$ (1) that have bigger pore size.

The mechanical strength of pNIPAM based Laponite® hydrogel increased by incorporation of HAPna, due to enhancements of the crosslinking which enhances the mechanical strength. Although the water content of hydrogel samples was slightly increased by adding HAPna suspension, which may adversely impact the mechanical strength of hydrogel in the first instance. However, nanoparticles enhanced hydrogel stiffness significantly in L-pNIPAM (1) and L-pNIPAM (1.5).

Swelling and deswelling ratio were restricted when HAPna incorporated, as a result of stiffer hydrogel networks formed and the mineral nature of HAPna.

Equilibrium degree of swelling and deswelling were influenced by adding HAPna, due to changes that happen in pore size and the stiffness of L-pNIPAM hydrogel.

Incorporation of HAPna enhanced osteoblast differentiation of hMSCs up to 4 weeks, where histological and immunohistochemistry investigation showed the ability of L-pNIPAM hydrogels, with HAPna incorporated, to induce osteogenic differentiation of hMSCs.

Finally, the positive enhancement of the incorporation of HAPna to hydrogel materials has been reported in many studies; improving mechanical strength and promoting osteogenic differentiation of human mesenchymal stem cells (MSCs). These findings support the supposition that the incorporation of HAPna should be considered as an important factor of changing properties and behaviour of hydrogels.

6.8 References

1. Turon P, del Valle L, Alemán C, and Puiggalí J. Biodegradable and Biocompatible Systems Based on Hydroxyapatite Nanoparticles. Applied Science. 2017;7(1):60.

2. Dorozhkin S V. Calcium orthophosphate bioceramics. Ceramics International Journal. 2015;(41): 13913–13966.

3. Wahl DA, and Czernuszka JT. Collagen-hydroxyapatite composites for hard tissue repair. European Journal of Cells and Materials. 2006;11:43–56.

4. Habraken W, Habibovic P, Epple M, and Bohner M. Calcium phosphates in biomedical applications: Materials Today Journal. 2016;19(2):69–87.

5. Sinha A, Das G, Kumar Sharma B, Prabahan Roy R, Kumar Pramanick A, Nayar S. Poly(vinyl alcohol)-hydroxyapatite biomimetic scaffold for tissue regeneration. Materials Science and Engineering Chemistry. 2007;27(1):70–74.

6. Patel M, Patel KJ, Caccamese JF, Coletti DP, Sauk JJ, Fisher JP. Characterization of cyclic acetal hydroxyapatite nanocomposites for craniofacial tissue engineering. Journal of Biomedical Materials Research - Part A. 2010;94(2):408–418.

7. Thorpe AA, Creasey S, Sammon C, and Le Maitre CL. Hydroxyapatite nanoparticle injectable hydrogel scaffold to support osteogenic differentiation of human mesenchymal stem cells. European Journal of Cells and Materials. 2016;32:1–23.

8. Gaharwar AK, Dammu SA, Canter JM, Wu CJ, Schmidt G. Highly extensible, tough, and elastomeric nanocomposite hydrogels from poly(ethylene glycol) and hydroxyapatite nanoparticles. Biomacromolecules. 2011;12(5):1641–1650.

9. Haraguchi, K., Takehisa K. Nanocomposite hydrogels: A unique organic-inorganic network structure with extraordinary mechanical, optical, and swelling/de-swelling properties. Advanced Materials. 2002;14(16):1120–1124.

10. Jiang YY, Zhu YJ, Li H, Zhang YG, Shen YQ, Sun TW, *et al.* Preparation and enhanced mechanical properties of hybrid hydrogels comprising ultralong hydroxyapatite nanowires and sodium alginate. Journal of Colloid Interface Science. 2017;497:266–275.

11. Safety Data Sheet for synthesis hydroxyapatite nano particles. SIGMA-ALDRICH. 2018;(1907):1–6.

12. Haraguchi K, Li HJ. Mechanical properties and structure of polymer-clay nanocomposite gels with high clay content. Macromolecules. 2006;39(5):1898–1905.

13. Hoffman AS. Hydrogels for biomedical applications. Advanced Drug Delivery Review . 2012;64(SUPPL.):18–23.

14. Dogu Y, Okay O,. Swelling-deswelling kinetics of poly(N-isopropylacrylamide) hydrogels formed in PEG solutions. Journal of Applied Polymer Science. 2006;99(1):37–44.

15. Ren H, Zhu M, Haraguchi K. Characteristic Swelling-Deswelling of Polymer / Clay Nanocomposite Gels. 2011;8516–8526.

16. Li Z, Su Y, Xie B, Wang H, Wen T, He C, et al. A tough hydrogel-hydroxyapatite bone-like composite fabricated in situ by the electrophoresis approach. Journal of Materials and Chemistry, Part B. 2013;1(12):1755–1764.

17. Zuo Guifu, Lun Huidong, Gao Guijing SY. The Microstructure and Swelling Properties of Laminated HAp/CS Hydrogels. Advanced Maderials Research. 2013;750.

18. Cs-Szabo G, Ragasa-San Juan D, Turumella V, Masuda K, Thonar EJ, An HS. Changes in mRNA and protein levels of proteoglycans of the anulus fibrosus and nucleus pulposus during intervertebral disc degeneration. The Spine Journal. 2002;27(20):2212–2219.

19. Lamoureux F, Baud'huin M, Duplomb L, Heymann D, Rédini F. Proteoglycans: Key partners in bone cell biology. Bioessays Journal. 2007;29(8):758–771.

20. Hirsch T, Xiang J, Chao DT, Korsmeyer SJ, Scaife JF, Colell A, *et al.* Caspases : Enemies Within. 1998;281(August):1307–1312.

21. Nilsson KG, Kärrholm J, Carlsson L, Dalén T. Hydroxyapatite coating versus cemented fixation of the tibial component in total knee arthroplasty: prospective randomized comparison of hydroxyapatite-coated and cemented tibial components with 5-year follow-up using radiostereometry. Journal of Arthroplasty. 1999;14(1):9–20.

22. Henriksen K, Karsdal MA. Type I Collagen. Biochemistry of Collagens, Laminins and Elastin: Structure, Function and Biomarkers. Elsevier Inc.; 2016. 1-11.

23. Obaton AF, Fain J, Djemaï M, Meinel D, Léonard F, Mahé E, et al. In vivo XCT bone characterization of lattice structured implants fabricated by additive manufacturing. 2017;3(8).

24. Hendriks J, Riesle J, Blitterswijk CA van. Development of porous chitosan–gelatin/hydroxyapatite composite scaffolds for hard tissue-engineering applications. Journal of Tissue Engineering and Regenerative Medicine. 2010;4(7):524–531.

25. Dhivya S, Saravanan S, Sastry TP, Selvamurugan N. Nanohydroxyapatite-reinforced chitosan composite hydrogel for bone tissue repair in vitro and in vivo. Journal of Nanobiotechnology. 2015;13(1):1–13.

Chapter - 7

Conclusions and Future Work

This thesis aimed to explore the influence of the chemical composition of pNIPAM based Laponite® hydrogels on physical and mechanical properties. Moreover how the composition can be adjusted to improve the characteristic properties enhancing cell viability within the hydrogel structure, with the goal to use them as scaffold in dental applications. The work looked in detail at the effect of copolymer nature/chemistry and crosslink density on the properties of these hydrogels, and how this could impact the cell viability and behaviour within their structures. The Thesis was comprised of four results chapters (Chapters 3, 4, 5 and 6).

In chapter 3 the influence of the change of crosslink density, across a small range (0.5 -1.5 wt. %) on physical and mechanical properties of L-pNIPAM was investigated and the implication of changes in hydrogel properties on cell viability and behaviour were explored. SEM data was able to show that an increase in crosslink density significantly reduced the measured pore size and DMA in compression mode showed significantly increased mechanical stiffness.

The reduction in pore size was also shown to significantly impact the swelling and deswelling ratios. Coupled to this, the final equilibrium swelling degree and maximum deswelling degree were dramatically reduced in systematic manner, with increased crosslink density.

Dehydration and rehydration rates were systematically decreased by increasing crosslink density, due to a combination of the reduction in pore size and changes in the mechanical properties, most notably stiffness. Additionally, changes in the hydrogel morphology were shown to change the physical water state and water diffusivity as a function of crosslink densities. Both FTIR and DSC measurements showed that more bound water was present at higher crosslink densities, due to the reduction in pore size leading to a sterically closer proximity of the water to the hydrophilic groups on the polymer backbone. There was a good correlation between the measurements of bound water using DSC and ATR-FTIR, with ATR-FTIR being used in this manner for the first time.

Changes in crosslink density were also shown to affect cell viability within this material, with cell viability decreasing with increased crosslink density.

Chapter 4 was concerned with the concept of incorporating the comonomer HEMA into L-pNIPAM hydrogels to make injectable systems with different properties to those of L-pNIPAM described in Chapter 3. For these compositions the Laponite® concentration was kept at 1% by weight.

For copolymer compositions with a HEMA concentration above 10% the final reacted hydrogel was heterogeneous in nature and did not remain as a stable colloidal suspension. Increasing the HEMA concentration in L-pNIPAM$_{95}$-co-HEMA$_5$ and L-pNIPAM$_{90}$-co-HEMA$_{10}$ had no impact on the measured setting temperature (believed to be linked to the LCST) compared to L-pNIPAM, which was somewhat counterintuitive, as the perceived wisdom is that increasing the hydrophilicity of an amphiphilic copolymer system should raise the LCST. It was postulated that the pendant OH groups on the HEMA units could be interacting with the polar groups of the Laponite® platelets effectively shielding their hydrophilicity in the colloidal suspension and negating the anticipated impact on the setting temperature. When the sample gels to form a hydrogel film, these hydrophilic groups are then available for interaction with the hydrating media.

SEM studies showed no statistically significant change in the pore size as a function of HEMA concentration. However, increasing HEMA was found to reduce mechanical stiffness once 10% of HEMA was incorporated; there was no difference in the mechanical properties of L-PNIPAM and L-pNIPAM$_{95}$-co-HEMA$_5$.

Increasing the HEMA content did have an impact on the rates of hydration and dehydration due to the enhanced hydrophilicity of the hydrogel as expected. The dehydration rate was retarded with increased HEMA content and the rehydration rate at 25 ˚C was elevated. Incorporation of HEMA into L-pNIPAM hydrogel was shown to systematically increase the bound water fraction, which is thought to be due to the increase in the number of hydrophilic polymeric units.

Most importantly, biocompatibility of L-pNIPAM-co-HEMA hydrogel was negatively affected. Hydrogels containing HEMA were shown to be toxic to the cells cultured within them structures after 2 weeks.

Chapter 5 related to the incorporation of HPMA as a comonomer into L-pNIPAM hydrogels. Incorporation of HPMA into L-pNIPAM resulted in a fully injectable L-pNIPAM-co-HPMA with excellent biocompatibility, as demonstrated by cell viability studies, detailed in chapter 5, section 5.3.9, where enhancement to cell viability and proliferation of hMSCs was observed.

Using HPMA as comonomer in L-pNIPAM-co-HPMA was shown to increase the pore size (SEM) with increased HPMA content. Increased HPMA content also significantly reduced the measured mechanical stiffness determined using DMA. The swelling ratio was reduced and equilibrium swelling degree significantly increased, with increased HPMA content, most likely due to the reduction in thermo-responsive component in the copolymer.

The setting temperature, which is related to the coil to globule transition and therefore the LCST, was found to reduce significantly by adding HPMA, which is counterintuitive as many studies report an increase in the measured LCST with increased HPMA content. Once more we postulate that interactions between the pendent OH groups and the Laponite® surface may mask the inherent hydrophilicity of the HPMA moieties.

Interesting findings were observed when dehydration and rehydration behaviours were monitored; where competition between multiple factors was detected, such as; hydrophilicity, sample surface area, mechanical stiffness and pore size. However, overall adding HPMA enhanced hydrophilicity of pNIPAM based Laponite® injectable hydrogel as dehydration rate decreased initially at 5% HPMA content, but was increased at 10% HPMA content. Rehydration rates followed a more logical trend and were shown to increase as HPMA was added. The changes in physical and mechanical properties of L-pNIPAM-co-HPMA hydrogels when HPMA was incorporated, lead to enhancements of cell viability and increased proliferation of hMSCs.

Characterisation of L-pNIPAM hydrogels following incorporation of 0.5mg/ml HAPna were presented in Chapter 6. HAPna was added to induce osteogenic differentiation of hMSC; however the incorporation of HAPna also enhanced the mechanical stiffness of L-pNIPAM, by decreasing the pore size of the honeycomb like structure. Cell metabolic activity was increased, suggesting increased proliferation of hMSC was increased when HPMA was incorporated.

Histological staining and immunohistochemistry of matrix depositions were performed to investigate type of cells within different formulations of L-pNIPAM hydrogels. The results showed an increase in calcium and collagen deposition when HPMA was incorporated, and further increases in those matrixes were observed as 0.5mg/ml HAPna incorporated.

The adding of HPMA played an important role in enhancing cell viability and increase matrix deposition indicating bone differentiation. Those findings could be beneficial to help in cleft palates, where the injection of hydrogel with stem cells could result in growing of the palatal bone of cleft margins. However, further investigations are needed to find out the suitability of this material to be applied in different dental applications.

7.1 Future Work

The work included in this thesis highlights the range of injectable hydrogels it is possible to produce based around the L-pNIPAM motif. There are several areas that could be expanded in the future.

The mechanical properties of hydrogels are known to change as cells grow within them and deposit matrix, cells are also known to take their cues from mechanical stimuli. It would be valuable to look at the changes in the viscoelastic behaviour of pNIPAM hydrogels as a function of chemical composition (selecting compositions from chapters 3, 5 and 6) with cells contained within them *in situ* over a period of several weeks. The lab has fairly recently acquired a Bose electro-force system, which allows the monitoring of viscoelastic behaviour during cell culture. Cells can be maintained within the mechanical loading unit and physiologically relevant loads can be programmed into the system. It would then be feasible to explore the influence of cells proliferation on mechanical properties of different chemical composition of pNIPAM hydrogels and also look at the influence of different mechanical stimuli (under-loading, over-loading and idealised-loading) on cell viability, proliferation and differentiation.

In this work dehydration and rehydration behaviour studies were conducted at temperatures below the LCST of L-pNIPAM. It would be interesting to repeat

this study at 37 ˚C, to simulate the human body environment. It would also be interesting to perform these studies well above the LCST. It would also, be interesting to optimise the experimental steps to perform these studies to try and eliminate potential variations in the measurements, such as; designing and manufacturing a confined cell holder to generate samples with the same thickness.

It would be interesting to look at the influence that the nature of the hydrating medium has on the swelling behaviour of these materials, for example looking at salts within the Hofmeister series or using simulated physiological fluids at 37 ˚C. There is a body of literature indicating that changes in the hydrating medium can influence the LCST. Other studies in the group have shown that samples left immersed in SBS show enhancements in the mechanical properties and robustness of L-pNIPAM-co-DMAC, a 37^{o}C setting injectable hydrogel. It would be interesting to see the influence that salts may play on the mechanical properties of HAPna L-pNIPAM hydrogels.

Rheological data could be generated for different formulations, as this an important property to study for injectable materials. It would be interesting to investigate the influence of chemical composition on the viscosity of pNIPAM hydrogels, as generally low viscosity hydrogels are preferred. It would be interesting to see the influence that T has on viscosity. Ultimately, viscosity measurements could be used as additional way to measure LCST, rather than being measured manually using a digital thermometer.

Non injectable formulations of L-pNIPAM based hydrogels, with higher >2% crosslink density and lower water contents, could possibly be used in different biomedical applications as implant pieces for tougher tissue types in the human body or as *in vitro* 3D culture models. Further investigations need to be performed to characterise these formulations, characterising their mechanical properties and cell viability.

Further investigation for formulations of pNIPAM hydrogels containing HEMA, are needed, to understand the reason behind the toxicity that was observed when hMSCs were cultured within them. There are various characterisation tools that could be used, for example real time ATR-FTIR; where double bonds

can be monitored during the polymerisation reaction. Other tools such as DSC may be able to ascertain the presence or otherwise of reactive monomer.

L-pNIPAM-co-HPMA hydrogel showed improvements such as; surface wettability, bigger pore size and faster rehydration than L-pNIPAM. These improvements enhanced cell viability and proliferation of hMSCs when cultured within its structure. Therefore long term viability and differentiation studies could be used in addition to immunohistochemistry assessment. Protein expression markers of late stage of chondrocyte hypertrophy, such as collagen type X. Osteogenic differentiation markers such as runx2 and osteopontin would be monitored to verify our findings that indicated an increase in cell viability of hMSCs within this material.

The influence of adding HPMA into pNIPAM hydrogels on the LCST of L-pNIPAM-co-HPMA, was found to be unexpected compared with results reported in the literature. Generally when more hydrophilic comonomer is added, this elevates LCST of pNIPAM hydrogels. However, in these pNIPAM based Laponite® hydrogel systems the LCST was reduced when HPMA was added. Therefore, extensive investigation should be performed to understand the different mechanism by which these hydrogels are forming. It may be useful to conduct experiments looking at polymerisation and setting using DLS and other scattering techniques.